

**Synthesis and biological testing of potential
anti-tuberculosis drugs targeting
the β -ketoacyl ACP synthase**

Dissertation zur Erlangung des
naturwissenschaftlichen Doktorgrades der
Julius-Maximilians-Universität Würzburg

vorgelegt von

Diana Kešetovič

aus Příbram

Würzburg 2016

**Synthesis and biological testing of potential
anti-tuberculosis drugs targeting
the β -ketoacyl ACP synthase**

Dissertation zur Erlangung des
naturwissenschaftlichen Doktorgrades der
Julius-Maximilians-Universität Würzburg

vorgelegt von

Diana Kešetovič

aus Příbram

Würzburg 2016

Eingereicht am:.....

bei der Fakultät für Chemie und Pharmazie

Gutachter der schriftlichen Arbeit

1. Gutachter: Prof. Dr. Ulrike Holzgrabe

2. Gutachter:

Prüfer des öffentlichen Promotionskolloquiums

1. Prüfer: Prof. Dr. Ulrike Holzgrabe

2. Prüfer:

3. Prüfer:

Datum des öffentlichen Promotionskolloquiums:.....

Doktorurkunde ausgehändigt am:.....

Die vorliegende Arbeit wurde am Institut für Pharmazie und Lebensmittelchemie der Bayerischen Julius-Maximilians-Universität unter der Anleitung von

Frau Prof. Dr. Ulrike Holzgrabe

angefertigt.

Danksagung

“Art is I, science is we“ – Claude Bernard

An dieser Stelle möchte ich meine Dankbarkeit ausdrücken, die letzten Worte in meiner Arbeit schreiben zu dürfen. Daher möchte ich mich bei allen Personen, unter deren Einfluss oder Mitwirkung ich diesen Punkt erreicht habe, bedanken.

Als Erstes möchte ich mich herzlich bei Frau Prof. Dr. Ulrike Holzgrabe für die freundliche Aufnahme in ihren Arbeitskreis und das in mich gesetzte Vertrauen bedanken. Ihre Anregungen, Unterstützung, Hinweise und Geduld habe ich sehr geschätzt.

Natürlich wäre meine Arbeit nicht ohne finanzielle Unterstützung machbar gewesen; ich bin deshalb der Deutschen Forschungsgemeinschaft (SFB 630) sowie den Stipendienprogrammen Erasmus und DAAD, die meinen Aufenthalt an der Universität Würzburg ermöglicht haben, sehr verpflichtet. Dafür, dass ich gerade nach Würzburg kam, bin ich Herrn Prof. Dr. Martin Doležal aus Hradec Králové in Tschechien dankbar, denn ohne den von ihm übermittelten Kontakt wäre mein Weg ganz anders gewesen.

Da mein Dissertationsthema in einem mehr oder weniger engen Zusammenhang mit den Arbeiten von Dr. Christine Topf, Dr. Benjamin Schaefer (AK Prof. Sotriffer), Dr. Johannes Schiebel (AK Prof Kisker) und Vanessa Schlag stand, möchte ich mich bei ihnen für die von ihnen erhaltenen Modellstrukturen (Christine, Benny), die ersten Aktivitätsmessungen meiner Produkte (Christine) und die Bereitstellung des KasA-Enzyms (Christine, Johannes, Vanessa) bedanken. Vanessa danke ich zusätzlich für die Zusammenarbeit an der Optimierung der Fluoreszenz-Assay-Methode. Ein besonderer Dank gilt Dr. Kanishk Kapilashrami aus der Stony Brook University, NY, für seine wertvollen Verbesserungstipps bezüglich des Assays und für die Testung einiger unserer Verbindungen im Labor von Prof. Dr. Peter Tonge. Weiterhin möchte ich mich bei Benjamin Merget (AK Prof. Sotriffer) für sein nettes Engagement in der Erstellung der „R“-Software-Vorlage für meine Berechnungen und für die Auswertung der mykobakteriellen Membrane-Gängigkeit von meinen Produkten mit Hilfe des MycPermCheck Programms bedanken. Für die ergänzende Docking-Studie, durchgeführt unter der Leitung von Prof. Dr. Christoph Sotriffer, danke ich Maximilian Kuhn, der mir dabei zur Seite stand.

Im Rahmen des SFB 630 wurden auch die Aktivitäten auf den ganzen Zellen von *Mycobacterium tuberculosis* bestimmt. Mein Dank gilt daher Frau Svetlana Sologub, die meine Produkte im Labor von Dr. Tobias Ölschläger getestet hat. Für die Durchführung weiterer antimikrobieller Testungen bedanke ich mich herzlich bei Frau Dr. Heike Bruhn und ihrem Team.

Herrn Dr. Krzysztof Radacki und Dr. Alexander Damme danke ich sehr für die erhaltenen Kristallstrukturen und ihre Hilfsbereitschaft bei deren Auswertung.

Für die NMR-spektroskopischen Messungen meiner Produkte möchte ich mich insbesondere bei Ines Schmidt, Florian Seufert, Regina Messerer, Dr. Johannes Wiest, Dr. Christina Juli, Dr. Christine Topf, Dr. Eberhard Heller, Dr. Georg Hiltensperger, Dr. Maximilian Tischer, Dr. Christian Markl und Dr. Curd Schollmayer bedanken. Dr. Petra Kapková danke ich für ihre Unterstützung bei den MS-Messungen.

Meinen AK-Kollegen bin ich vor allem dafür dankbar, dass sie sich für mich die Zeit genommen haben, sei es wegen der Nutzung von sämtlichen Instrumenten oder wegen entstandenen alltäglichen Laborproblemen. Mein besonderer Dank gilt Dr. Maximilian Tischer, Dr. Eberhard Heller, Dr. Johannes Wiest und Dr. Georg Hiltensperger. Natürlich möchte ich mich auch bei allen meinen damaligen Labor-Kollegen Christina, Christine, Max, Michi, Georg, Christian, Ines und Flo, und bei unseren Laborantinnen Lina und Anna für ihre Beiträge zu einem friedlichen Arbeitsklima herzlich bedanken. Für die ständige Hilfsbereitschaft in Sachen der Bürokratie bedanke ich mich bei Frau Möhler und Frau Ebner aus dem Sekretariat des Instituts. Für die Unterstützung bei sämtlichen technischen Problemen danke ich Herrn Dr. Bernd Reyer und Dr. Jens Schmitz.

Dr. Max Kurlbaum, Dr. Klaus Uhlenhut, Dr. Maximilian Tischer, Dr. Stephanie Bank, Dr. Frederic Vollmers, Melanie Mulek, Dr. David Ilko und Daniel Schuster, mit denen ich das Praktikum vom 5. Semester (Biochemie) unter der Leitung von Frau Prof. Dr. Petra Högger betreut habe, danke ich für die freundliche und entspannte Atmosphäre während und nach den Arbeitszeiten. Ebenso dankbar bin ich für die schönen Wanderungen und netten Abende, die ich im Arbeitskreis Holzgrabe erleben durfte.

Schließlich danke ich meiner Familie – vor allem meiner Mutti, Oma und Bruder – und meinen Freunden für die liebevolle Unterstützung.

Table of contents

Table of contents

1	Introduction	1
1.1	Tuberculosis	1
1.1.1	Etiology and pathology of the disease	2
1.1.2	Tuberculosis worldwide	3
1.2	The anti-tuberculosis therapy	4
1.2.1	First-line anti-tuberculosis drugs	4
1.2.2	Second-line antituberculosis drugs	6
1.2.3	Third-line antituberculosis drugs	10
1.2.4	Recently introduced novel drugs	10
1.2.5	Treatment regimens	11
1.3	The mycobacterial cell wall biosynthesis as an attractive drug target	13
1.3.1	The mycobacterial cell wall	13
1.3.2	Fatty acids biosynthesis	14
1.4	The β-ketoacyl-ACP synthase “KasA”	17
1.4.1	The catalytic mechanism of KasA	17
1.4.2	Inhibitors of the KasA catalytic activity	19
2	Aims & objectives	24
3	Synthesis	26
3.1	Synthesis of the chromone derivatives	27
3.1.1	Synthesis of chromone-2-carboxylic acid	27
3.1.2	Synthesis of chromone-2-carboxamides	28
3.1.3	Synthesis of 6-nitrochromone-2-carboxylic acid	30
3.1.4	Synthesis of 6-nitrochromone-2-carboxamides	31
3.1.5	Synthesis of the succinamic acids	32
3.1.6	Synthesis of 2-(4-hydroxy-3,5-dimethylbenzoyl)-4 <i>H</i> -chromene-4-ones 13 and 14	34
3.1.7	Synthesis of 4-((2-(4-hydroxy-3,5-dimethylbenzoyl)-4-oxo-4 <i>H</i> -chromen-6-yl)amino)-4-oxobutanoic acid 16	34
3.1.8	Synthesis of <i>N</i> -benzyl-6-(4-(4-methylpiperazin-1-yl)-4-oxobutanamido)-4-oxo-4 <i>H</i> -chromene-2-carboxamide 17	35
3.1.9	Synthesis of methyl malonyl ester-amides of chromone-2-carboxylic acid 18a and 18b	36
3.1.10	Synthesis of 2-((2-bromophenyl)carbamoyl)- <i>N,N,N</i> -trimethyl-4-oxo-4 <i>H</i> -chromene-6-aminium triiodone 19	36
3.2	Synthesis of the pyrimidine derivatives	37
3.2.1	Synthesis of pyrimidin-2-amines 21a-e	38
3.2.2	Synthesis of pyrimidin-2-ols 22a-e	39
3.2.3	Synthesis of ethyl 6-methyl-2-oxo-4-phenyl-1,2,3,4-tetrahydropyrimidine-5-carboxylate 23	39
3.3	NMR Spectroscopy	40
3.3.1	NMR Spectroscopy of the chromone derivatives	40
3.3.2	NMR Spectroscopy of the pyrimidine derivatives	47
4	Biological testing	49
4.1	KasA direct binding assay	49

Table of contents

4.1.1	Introduction.....	49
4.1.2	Methods.....	50
4.1.3	Results.....	52
4.1.4	Discussion and prospects	59
4.2	Inhibition activity testing on the whole cells of <i>M. tuberculosis</i>.....	61
4.2.1	Results.....	62
4.2.2	Discussion	64
4.3	Anti-infective screening.....	66
4.4	The assay interference potential of chromones.....	67
4.5	Solubility problems.....	70
4.5.1	Introduction.....	70
4.5.2	Crystal structure and packing of selected chromone derivatives	71
4.5.3	Solubilization assays.....	79
4.6	Docking of compound 9i into the KasA binding pocket.....	86
4.6.1	Introduction.....	86
4.6.2	Docking results	87
4.6.3	Discussion	89
5	Summary	91
6	Zusammenfassung	95
7	Experimental section	99
7.1	General Methods.....	99
7.1.1	Measuring devices.....	99
7.1.2	Chromatography.....	100
7.1.3	Chemicals.....	100
7.1.4	Software	101
7.2	Synthesis	101
7.2.1	Synthesis of 4-oxo-4 <i>H</i> -chromene-2-carboxylic acid 2	101
7.2.2	Synthesis of 4-oxo-4 <i>H</i> -chromene-2-carboxamides 3a–p and 4a– k	102
7.2.3	Synthesis of 4-oxo-4 <i>H</i> -chromene-2-carboxylic acid amides 7a–c	113
7.2.4	Synthesis of 6-nitro-4-oxo-4 <i>H</i> -chromene-2-carboxylic acid 8	115
7.2.5	Synthesis of 6-nitro-4-oxo-4 <i>H</i> -chromene-2-carboxamides 9a–j	115
7.2.6	Synthesis of 4-oxo-4 <i>H</i> -chromen-6-yl-aminobutanoic acids 12a–i	121
7.2.7	Synthesis of 2-(4-hydroxy-3,5-dimethylbenzoyl)-4 <i>H</i> -chromen-4-ones 13 and 14.....	126
7.2.8	Synthesis of 4-((2-(4-hydroxy-3,5-dimethylbenzoyl)-4-oxo-4 <i>H</i> -chromen-6-yl)amino)-4-oxobutanoic acid 16.....	127
7.2.9	Synthesis of <i>N</i> -benzyl-6-(4-(4-methylpiperazin-1-yl)-4-oxobutanamido)-4-oxo-4 <i>H</i> -chromene-2-carboxamide 17	128
7.2.10	Synthesis of methyl 3-((-4-oxo-4 <i>H</i> -chromen-6-yl)amino)-3-oxopropanoates 18a and 18b	129
7.2.11	Synthesis of 2-((2-bromophenyl)carbonyl)- <i>N,N,N</i> -trimethyl-4-oxo-4 <i>H</i> -chromen-6-aminium triiodone 19.....	131
7.2.12	Synthesis of ethyl 6-methyl-2-oxo-4-phenyl-1,2,3,4-tetrahydropyrimidine-5-carboxylate 23.....	131
7.2.13	Synthesis of pyrimidin-2-amines 21a–e.....	132
7.2.14	Synthesis of pyrimidine-2-ols 22a–e.....	134

Table of contents

7.3	Additional analytical experiments.....	136
7.3.1	Crystal analysis	136
7.3.2	LogP and peak purity determination	137
7.3.3	Content determination of compound 9d.....	139
7.4	Solubilization assays	141
7.4.1	Screening on suitable solubilizing agents among cyclodextrins	141
7.4.2	Experiments on complexation by means of UV spectroscopy.....	142
7.5	KasA binding assay	143
7.5.1	Assay conditions	143
7.5.2	Sample details	143
7.6	Whole cell inhibition activity testing.....	143
7.6.1	Assay conditions and method	143
7.6.2	Sample details	144
7.7	Anti-infective screening.....	144
7.8	Docking.....	145
8	Appendix.....	147
8.1	Poster presentations related to the thesis	147
8.2	List of abbreviations	148
9	Bibliography.....	151

1 Introduction

1.1 Tuberculosis

In 1882, *Mycobacterium tuberculosis*, the causative agent of tuberculosis (TB), was discovered by Dr. Robert Koch. He identified the new bacilli of “extremely small structures” after the use of a special staining technique. He also observed, that the bacteria frequently “lie within tissue cells” and described the very slow growth of mycobacterial cell culture on a solidified blood serum as being “seen by the naked eye in the second week after seeding”.¹

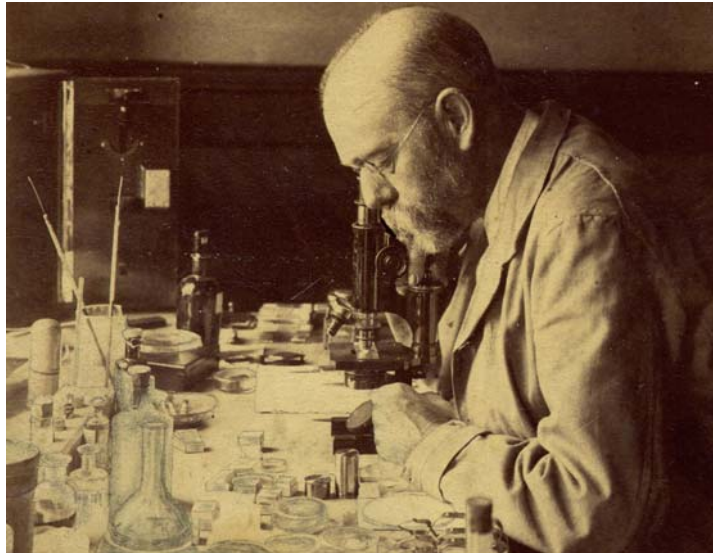


*Fig. 1 Dr. Robert Koch**

Since his discovery, significant advances in understanding the biology and immunology of *Mycobacterium tuberculosis* have been achieved. The whole genome sequence determination of the best-characterized strain H37Rv, reported in 1998 by Cole *et al.*², brought new challenges for TB drug research and development. Nevertheless, despite all the achievements in the prophylaxis (BCG vaccine) and chemotherapy treatment, tuberculosis remains the most deadly bacterial infection of today’s world.

* reprinted with kind permission from Dr. A. Pawliczek, Humboldt University of Berlin, University Archiv, “Sammlung Koch”

Introduction

1.1.1 Etiology and pathology of the disease

Mycobacterium tuberculosis is a Gram-positive bacillus with 2 – 6 µm in length. As a human intracellular pathogen, it is related to *Mycobacterium leprae*, the etiologic agent of leprosy or Hansen's disease. All mycobacteria possess an extremely resistant cell wall, which cannot be Gram-stained. Therefore, their visualization is achieved through staining with lipid-soluble dyes such as carbol fuchsin.³

M. tuberculosis affects mostly the lungs causing pulmonary tuberculosis. It is spread by inhalation of droplet nuclei containing as few as 1 – 3 bacilli, expelled from individuals with active TB through sneezing or coughing.⁵ In the alveoli, bacteria are taken up by lung macrophages, that protect them from the host's humoral immune response (complement and antibodies). Inside the phagosome, *M. tuberculosis* obstructs its destruction, as it prevents 1) the fusion between phagosome and digestive enzymes-containing lysosome, 2) oxidative burst through neutralization of toxic oxygen species, and 3) the antigen presentation to the helper T lymphocytes. These protective mechanisms enable its slow replication within macrophages and result in progression of **primary tuberculosis**, when the first pathological features, the **granulomas** (or "tubercles"), are formed. These encasements of fibrous tissue infiltrated by lymphocytes that surround live but non-contagious bacilli, are consequence of a cell-mediated chronic inflammatory immune response. A subsequent calcification of the damaged tissue prevents bacterial growth by limiting their access to essential nutrients. Tuberculosis can be held in its latent form for many years, until the host's immune response weakens. Then, the granulomas break down and the dormant tubercle bacilli reactivate. This process is accompanied by the typical clinical signs and symptoms of the disease, such as severe coughing, bloody sputum, fatigue, weight loss, night sweats and pale skin (hence the name "white plague").^{3,6}

Fortunately, there is a high natural resistance against *M. tuberculosis*, as the active disease develops in only 5 – 10 % cases during two years after initial infection. Thus, in the vast majority of cases, there are no clinical symptoms.⁷ The risk of disease outbreak rises at individuals with deficient cell-mediated immunity, such as people suffering from HIV infection or diabetes (29 times and 3 times, respectively).^{5,6} Generally, all immunocompromising conditions, whether due to chemotherapy, malnutrition, smoking or other factors, increase the risk for progression to active disease. In cases of suppressed immunity, mycobacteria can spread outside the lungs causing extrapulmonary tuberculosis lesions in any tissue of the body.

Introduction

1.1.2 Tuberculosis worldwide

The recent WHO Global Tuberculosis Report⁸ claims, there were about 9.6 million new active TB cases in 2014, estimated 12 % of them were HIV-positive. Nearly 1.2 million deaths resulted from the disease. Tuberculosis is alongside with AIDS the most deadly infection worldwide. The main TB burden lies stably in low- and middle-income countries. Especially in Sub-Saharan Africa, the highest rates of deaths relative to population and the most cases of HIV coinfection are reported. Since the “white plague” pandemic in Europe in the 19th and mid-20th centuries had been overcome, there was only a meagre interest on TB control in developing countries. Recently, tuberculosis has gained a worldwide attention mainly due to the rise of the global AIDS pandemic, travel boom and immigration. In 1993, tuberculosis was declared a global public health emergency. The “STOP TB initiative”, established by the WHO as a global platform for tuberculosis care, introduced a control strategy, so called **Directly Observed Treatment, Short-course** (DOTS), based on the following principles⁹:

- Funding commitment by national governments to assure available and effective treatment
- TB case detection through bacteriology including drug susceptibility testing
- Standardized and supervised treatment in accordance with the current guidelines¹⁰
- Effective and available drug supply logistics and administration
- Monitoring and evaluation of treatment outcomes

Implementation of these principles, evaluated in the Global Tuberculosis Report⁸, has already shown a positive impact on tuberculosis research and control:

- Mortality rate has declined by 47 % since 1990
- Estimated 43 million lives were saved owing to expanded TB care (effective diagnosis and treatment between 2000 and 2014)
- Access to antiretroviral therapy (ART) has been improved (in 2014, 77 % of the HIV-coinfected TB patients were started on ART)
- New diagnosis methods, *e.g.* the DNA-based rapid molecular diagnosis test Xpert MTB/RIF¹¹, and new anti-TB drugs (see *Chap. 1.2.4*) were introduced
- 15 Vaccine candidates are currently in clinical trials

Introduction

The vast majority of TB cases is curable, if treated according to the WHO guidelines.¹⁰ Nevertheless, due to the long-lasting regimens and high pill burden, the adherence to therapy is rather low, and thus treatment supervision is essential. Inadequate and unsupervised treatment in the past resulted in the emergence of multidrug-resistant strains of *M. tuberculosis*. Drug resistance has become the most feared cause of treatment failure and represent one of the main challenges in TB drug development. Various types of emerging resistant strains are described in the following chapter.

1.2 The anti-tuberculosis therapy

The slow growth of *M. tuberculosis* (doubling time about 24 hours), its dormancy inside macrophages and complex, hardly-permeable cell envelope are major features contributing to the chronic nature of the disease.² Therefore, an effective therapy requires a long-lasting drug administration. Since monotherapy leads to rapid development of drug-resistant strains, only combination therapy should be used (see *Chap. 1.2.5*). Single drug is administered exclusively under the terms of isoniazid preventive therapy mostly in HIV-positive patients.¹² Current anti-tuberculosis agents can be classified according to their priority and experience of use in three main groups: first-, second- and third-line drugs.¹⁶

1.2.1 First-line anti-tuberculosis drugs

Among the most potent first-line anti-tuberculosis agents belong isoniazid, rifampicin, pyrazinamide, ethambutol, rifapentin and rifabutin. The first four drugs have been used for decades starting with the introduction of isoniazid in the 1950's. The latter two rifamycin derivatives have been approved since the 1990's. All mentioned first-line drugs can be administered orally due to their lipophilic character.

1.2.1.1 Isoniazid (*Inh/H*)

Isoniazid (*Fig. 2*), the hydrazide of isonicotinic acid, represents a high effective bactericidal agent against replicating bacilli. In mycobacteria, isoniazid is transformed into its active form, isonicotinic acyl-NADH, which inhibits InhA, the NADH-dependent enoyl acyl carrier protein reductase, a key enzyme in the synthesis of mycolic acids, essential for the integrity of mycobacterial cell wall (see *Chap. 1.3.2.1*). Mycobacteria can develop resistance to isoniazid by increased expression of InhA or by mutations restricting the enzyme's affinity to NADH.^{10,13}

Introduction

1.2.1.2 *Pyrazinamide (Pza/Z)*

A synthetic analog of nicotinamide is converted to its active form, pyrazinoic acid, by mycobacterial nicotinamidase. Mutants lacking nicotinamidase activity develop resistance to pyrazinamide. The mechanism of action is still unclear. It is proposed that pyrazinoic acid inhibits the mycobacterial fatty acid synthase (FAS) I enzyme system, essential for the synthesis of mycolic acids.¹⁴ Another discussed mode of action is the disruption of membrane potential at acidic pH or inhibition of translation after binding to S1 component of 30S ribosomal subunit.^{15,16} Pyrazinamide (**Fig. 2**) is a weak bactericidal agent. Nevertheless, due to its sterilizing activity in acidic conditions inside the macrophages or in inflamed tissue, it has ability to shorten the treatment duration and prevent the risk of relapse.¹⁰

1.2.1.3 *Rifampicin (Rif/R)*

A semisynthetic derivative of rifamycin, a complex macrocyclic antibiotic, inhibits the DNA-dependent-RNA-polymerase, which is responsible for the DNA transcription. Rifampicin (**Fig. 2**) is a bactericidal agent possessing a potent sterilizing effect against *M. tuberculosis*, *i.e.*, it destroys even the non-replicating dormant bacilli in both, cellular and extracellular locations. Mycobacteria can develop resistance through conformational change of the active site on the β -unit of the RNA polymerase, hindering thus the inhibitor binding.^{10,14}

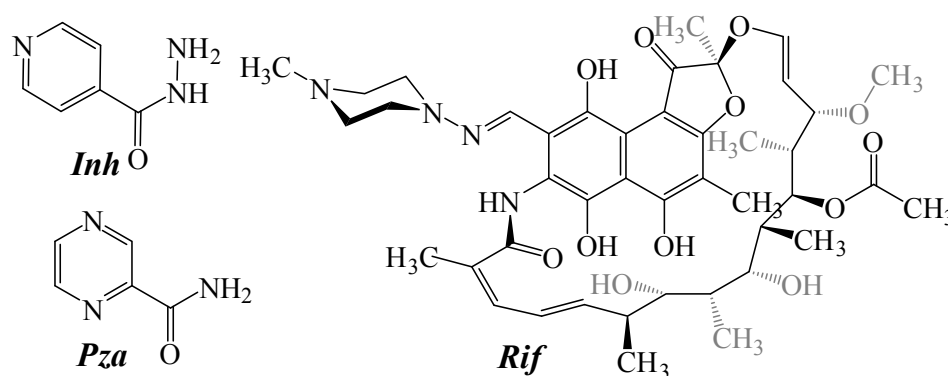


Fig. 2 Structures of isoniazid, pyrazinamide and rifampicin

1.2.1.4 *Rifapentin (Rpt/P) and rifabutin (Rfb)*

New rifamycin derivatives, rifapentin and rifabutin (**Fig. 3**), possess longer plasma half-life, achieve better exposure, and thus have the potential to shorten treatment duration. Compared to rifampicin, their hepatotoxic potential is decreased. Despite their induction of the hepatic enzyme system CYP3A4, they show less drug interactions than rifampicin (especially with ART).^{14,16}

Introduction

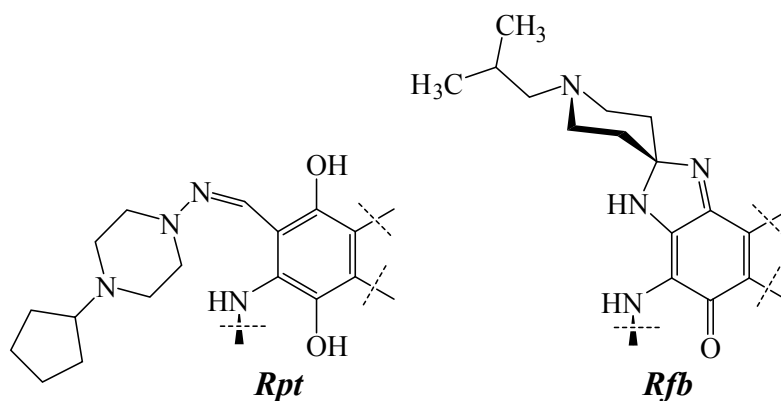


Fig. 3 Modified structural moieties of the new rifamycins (compare **Fig. 2**)

1.2.1.5 Ethambutol (Emb/E)

A synthetic *S,S*-enantiomer of 1,2-ethanediamine derivative is bacteriostatic against replicating mycobacteria. It obstructs the formation of cell wall through inhibition of arabinosyl transferase, an enzyme responsible for the synthesis of essential membrane components arabinogalactan and lipoarabinomannans.¹⁴

Ethambutol (**Fig. 4**) is used in combination with other drugs to prevent or postpone the emergence of resistant strains. The main adverse effects are hepatotoxicity and optic neuritis.¹⁰

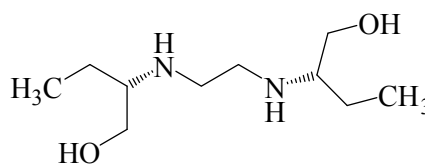


Fig. 4 Structure of ethambutol

1.2.2 Second-line antituberculosis drugs

Second-line drugs are reserved for treatment of multidrug-resistant tuberculosis and can be classified according to their descending priority into three groups: 1) injectable aminoglycosides and polypeptides, 2) fluoroquinolones, and 3) other orally-administered drugs.

1.2.2.1 Injectable aminoglycosides and polypeptides

Parenteral administration is required due to their polar character.

1.2.2.1.1 Aminoglycosides

Antitubercular aminoglycosides are broad-spectrum antibiotics isolated from *Streptomyces* species. The structure consists of a basic aglycon moiety, and mono- or disaccharides attached by glycosidic bonds. In bacteria, they bind on the ribosomal 16S-rRNA and thus inhibit

Introduction

protein synthesis interfering with the binding of aminoacyl-tRNA to the ribosomal 30S-subunit. Aminoglycosides are bacteriostatic against *M. tuberculosis*. Their therapeutic use is limited by nephro- and ototoxicity.¹⁴ **Streptomycin** (Stm/S, *Fig. 5*) was introduced in the 1940's as the first antitubercular agent. **Kanamycin** (Km) and **amikacin** (Amk) are reserved for treatment of rifampicin- and isoniazid-resistant *M. tuberculosis* strains.

1.2.2.1.2 Polypeptides

Capreomycin (Cm) and **viomycin** (Vim), also termed tuberactinomycins, are cyclic basic polypeptide antibiotics isolated from *Streptomyces* species. Like aminoglycosides, they inhibit protein synthesis and possess bacteriostatic activity. The mode of action affects both ribosomal subunits and is unique among the ribosome-targeting antibiotics. Tuberactinomycins bind to the intersubunit bridge B2a, formed by interaction between 23S and 16S of rRNA, and thus prevent the translocation of the ribosome along the mRNA. Aminoglycosides and tuberactinomycins share limited selectivity, that leads to mistranslation in mammalian mitochondrial ribosomes, and the correlating adverse effects: oto- and nephrotoxicity.¹⁷

1.2.2.2 Fluoroquinolones

Fluoroquinolones are synthetic broad-spectrum antibacterial agents possessing a fluor atom in position 6 of the quinoline ring. They exhibit bactericidal properties, targeting DNA-gyrase and topoisomerase IV, which are responsible for unlinking of the double strand DNA during replication. Antitubercular fluoroquinolones can be administered either orally or parenterally. They include the second- and third-generation fluoroquinolones: **ciprofloxacin** (Cfx), **ofloxacin** (Ofx) and **levofloxacin** (Lfx), as well as the most effective fourth-generation fluoroquinolones: **moxifloxacin** (Mfx, *Fig. 5*) and **gatifloxacin** (Gfx). Treatment regimens containing the latter two drugs have shown a potential to shorten the TB therapy and are currently in Phase III clinical trials.^{14,16}

Introduction

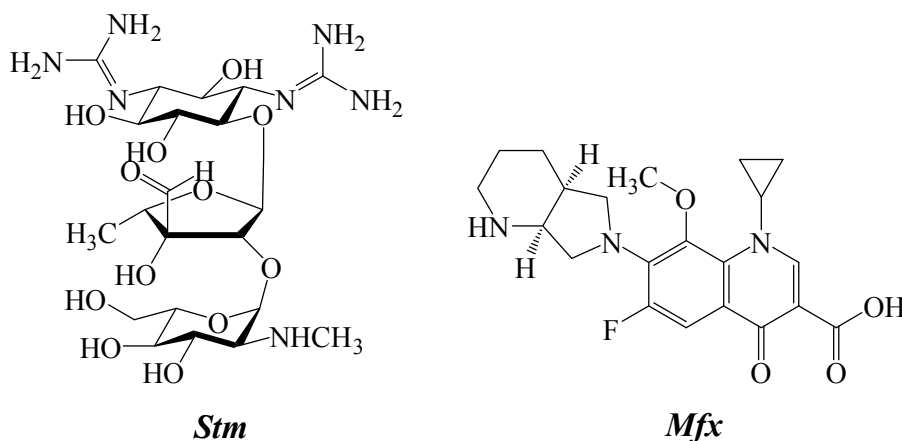


Fig. 5 Structures of streptomycin and moxifloxacin

1.2.2.3 Other orally-administered drugs

With an exception of the antibiotic cycloserine, all the following “alternative anti-tuberculosis drugs” are of synthetic origin, mostly possessing a bacteriostatic activity. They include derivatives of various structures: oxazolidinones (linezolid), isoxazolidinones (cycloserine, terizidone), thionamides (ethionamide, prothionamide), *para*-aminosalicylic acid and thioacetazone.

1.2.2.3.1 Oxazolidinones

1,3-Oxazolidinone derivatives represent a new chemical class of antibacterial agents. They inhibit the initial phase of protein synthesis by binding to 23S-rRNA of the 50S ribosomal subunit. Supposed mode of action is the inhibition of ribosomal peptidyltransferase center, which catalyzes the peptide-bond formation and peptide release. Due to the novel target, there is no cross-resistance between oxazolidinones and other ribosome-targeting agents. Though, resistant strains can emerge in consequence of alteration of the enzyme active site.^{14,18}

The most known representative is **linezolid** (Lzd, **Fig. 6**). Only the 5-*S*-enantiomer is effective. Its use is limited by a high rate of side effects: anaemia, peripheral and optic neuropathy.^{14,18}

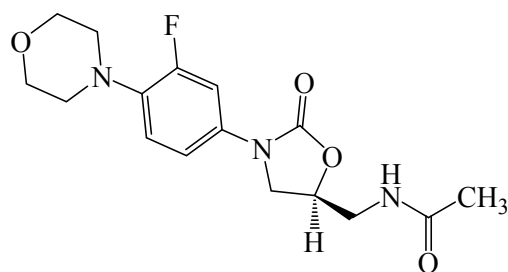


Fig. 6 Structure of linezolid

Introduction

1.2.2.3.2 Isoxazolidinones

Cycloserine and terizidone contain 1,2-oxazolidinone (isoxazolidinone) ring. **Cycloserine** (Dcs, *Fig. 7*) is an antibiotic produced by several *Streptomyces* species, but can be synthesized from the amino acid *D*-serine. It interrupts the synthesis of the cell wall component peptidoglycan by inhibition of the *D*-alanine-racemase and ligase. Overproduction of *D*-alanine leads to drug resistance. The main adverse effect is neurotoxicity. **Terizidone** (Trd) is a structural analog of cycloserine with improved tolerability.^{14,16}

1.2.2.3.3 Thionamides

Both representatives, **ethionamide** (Eto, *Fig. 7*) and **prothionamide** (Pto), are structurally related to isoniazid and share the same mode of action affecting the synthesis of mycolic acids. They have thus bactericidal properties. The bioactivation mechanism differs from isoniazid, alterations of the isoniazid-activating enzyme KatG (catalase-peroxidase) therefore do not induce drug resistance. Nevertheless, there is a cross resistance with isoniazid associated with *InhA* mutations.¹⁹

1.2.2.3.4 Para-aminosalicylic acid and thioacetazone

Para-aminosalicylic acid (Pas) was one of the first antitubercular agents. In the treatment regimen, it was later replaced by ethambutol, while in developing countries thioacetazone was used, due to its lower costs. *Para*-aminosalicylic acid is a prodrug targeting dihydrofolate reductase, an enzyme involved in the biosynthesis of nucleotides. The most common adverse effects are of gastrointestinal character. Chronic use can induce hypothyroidism and hepatitis.^{10,16,18}

Thioacetazone (Thz, *Fig. 7*), also called thiosemicarbazone, is an obsolete tuberculostatic drug that inhibits the mycolic acid synthesis. Due to its severe adverse effects (especially the cutaneous hypersensitivity called Stevens-Johnson syndrom), it can not be administered to HIV-positive patients.²⁰

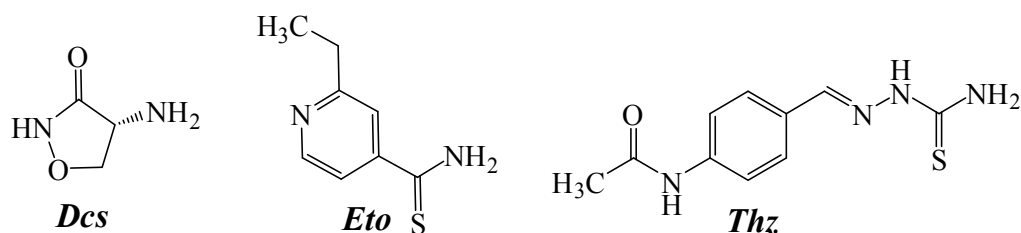


Fig. 7 Other second-line anti-TB drugs: Structures of D-cycloserine, ethionamide and thioacetazone

Introduction

1.2.3 Third-line antituberculosis drugs

This group includes only “re-purposed drugs”, *i.e.*, drugs that have been developed for the treatment of other infections than tuberculosis, such as the anti-leprotic clofazimine (Cfz) or broad-spectrum antibacterial agents: amoxicillin combined with β -lactamase inhibitor – clavulanate (Amx/Clv), imipenem combined with dehydropeptidase inhibitor – cilastatin (Ipm/Cln), or clarithromycin (Clr). They are not recommended for routine use in drug resistant TB treatment, due to their unclear efficacy.^{16,10}

1.2.4 Recently introduced novel drugs

The WHO Global tuberculosis report⁸ states, there are currently eight new or re-purposed anti-TB drugs in the late phases of clinical development. From 2012 to 2013, two new drugs have been approved for the treatment of multidrug-resistant tuberculosis under specific conditions: bedaquiline and delamanid. Since 2014, pretomanid has been approved as a part of novel treatment regimens.²¹

1.2.4.1 *Bedaquiline (former TMC-207)*

Bedaquiline (*Fig. 8*) is a diarylquinoline derivative with a unique mode of action targeting the proton pump of the ATP synthase, that affects the main source of energy of *M. tuberculosis*. The bactericidal agent is well tolerated, as the human mitochondrial ATP synthase is markedly less sensitive.¹⁶

1.2.4.2 *Delamanid (former OPC-67683) and pretomanid (former PA-824)*

Delamanid, a nitro-dihydro-imidazooxazole derivative, and pretomanid, a nitro-imidazo-oxazine derivative (*Fig. 8*), are prodrugs activated, similarly as metronidazole, by a nitroreductase. The proposed mode of action is the inhibition of mycolic acids biosynthesis. The observed activity is expected to result from oxidative damage by released nitrosyl radical. The main adverse effect is cardiotoxicity.¹⁶

Introduction

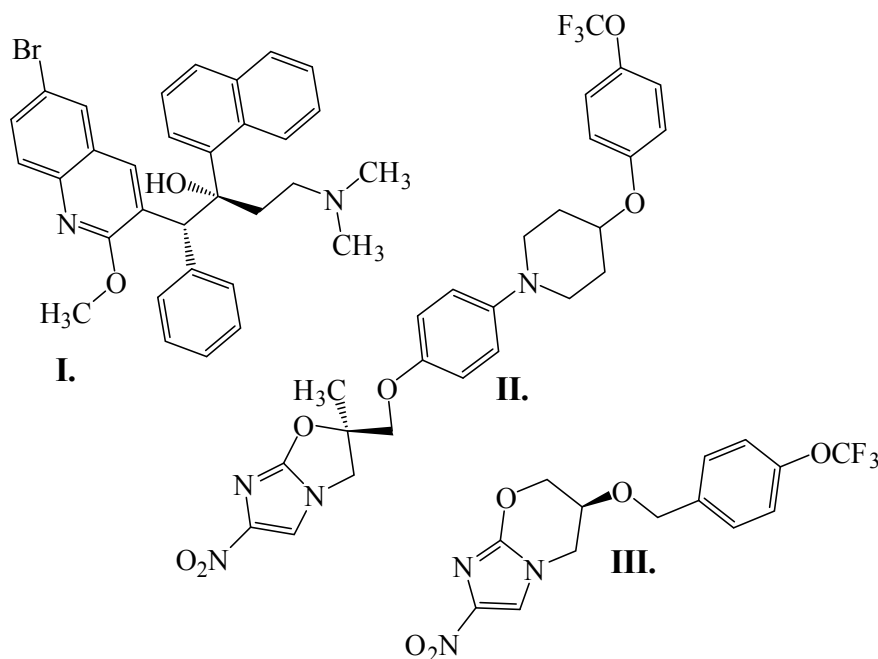


Fig. 8 Structures of bedaquiline (I), delamanid (II) and pretomanid (III)

1.2.5 Treatment regimens

Early after the introduction of the first anti-TB agents, resistant strains of *M. tuberculosis* were observed, if patients were treated with monotherapy. Since then, multi-drug regimens became an essential part of TB treatment. Currently, either standard or individualized regimens are used in the therapy of both, drug-susceptible and drug-resistant tuberculosis.^{10,18}

1.2.5.1 Standard treatment regimens for drug-susceptible tuberculosis

There are two main treatment regimens:

- **New patient-regimen**, abbreviated as **2HRZE/4HR**, consists of two months of intensive four drug treatment including the first-line drugs, isoniazid, rifampicin, pyrazinamide and ethambutol, and followed by a continuation phase of four months with isoniazid and rifampicin only. Optimal dose interval is daily, as the administration three-times weekly is associated with flu-like symptoms and a higher risk of treatment failure.
- **Retreatment regimen**: As recurrent tuberculosis patients are much more prone to develop drug resistance, prolonged treatment and addition of streptomycin, according to the scheme **2HRZES/1HRZE/5HRE**, is recommended.¹⁰

Introduction

1.2.5.2 *Treatment regimens for multidrug-resistant tuberculosis*

Treatment of multidrug-resistant tuberculosis is optimally based on the results of drug susceptibility testing (DST). Generally, there are three main kinds of resistant strains:

- **Multidrug-resistant tuberculosis (MDR-TB)** is caused by mycobacteria, that show resistance to, at least, isoniazid and rifampicin, the most potent first-line drugs, and forms approximately 5 % of all TB cases. This prevalence is apparently increased in HIV-positive individuals. More than a half of the global MDR-TB burden lies in only three countries: India, China and the Russian Federation. The relapse rate is high, as only 48 % of those infected are successfully treated.^{6,22} **MDR-TB treatment regimens** have a duration of 18 – 24 months, including 8 months of an intensive treatment and 12 months of a continuation phase. The used combination of first- and second-line drugs should include at least four effective drugs (remaining first-line drugs and bactericidal second-line drugs: *e.g.* kanamycin, ofloxacin, protionamide).¹⁰
- **Extensively drug-resistant tuberculosis (XDR-TB)** is caused by strains resistant to isoniazid, rifampicin and the most effective second-line drugs: fluoroquinolones and injectable agents. Approximately 9 % of all MDR-TB cases are XDR-TB. Only 22 % of XDR-TB patients involved in a cohort study were successfully cured.²² **Treatment regimens** require the use of third-line anti-TB drugs. The therapy is associated with increased adverse effects and higher costs.
- **Totally drug-resistant tuberculosis (TDR-TB)** is caused by strains resistant to all first- and second-line drugs and represent nowadays a nearly untreatable infection.¹⁶

1.2.5.3 *Special treatment regimens*

Apart from individual multidrug-resistant TB regimens based on the DST results, there are further patient conditions that require a special attention, such as HIV coinfection, chronic liver disease, renal failure, malnutrition, pregnancy or lactation.¹⁰

1.2.5.4 *Novel treatment regimens*

Two novel treatment regimens, including the recently introduced drugs, bedaquiline and pretomanid, are currently being tested in Phase II and Phase III clinical trials. They both promise to increase the efficacy and efficiency of MDR-TB therapy.

Introduction

- **Bedaquiline/pretomanid/pyrazinamide (BPaZ) regimen** has a potential to reduce the duration of TB therapy to three months and can be administered orally.
- **Pretomanid/moxifloxacin/pyrazinamide (PaMZ) regimen** is expected to shorten the treatment to four months and consequently shows minimal interactions with ART, improving thus the options for HIV-coinfected TB patients.²³

1.3 The mycobacterial cell wall biosynthesis as an attractive drug target

1.3.1 The mycobacterial cell wall

The complex cell wall is a feature responsible for the mycobacterial resistance to most chemotherapeutics. Its highly lipophilic structure is unique among living cells, since it provides protection not only from osmotic pressure and mechanical forces, but also from the harsh conditions inside the macrophages, where mycobacteria resist to acidic, oxidative and enzymatic degradation processes. The cell wall surrounds the plasma membrane and consists of an inner and an outer layer (see *Fig. 9*). The **inner compartment** includes three layers, peptidoglycan (or murein), arabinogalactan and mycolic acids, attached covalently to each other and directed from plasma membrane outward. The structure of **peptidoglycan** (PG) is unique for bacteria. It is a rigid material that maintains the rod shape of mycobacteria and provides them protection from osmotic pressure. It is composed of repeating strands of *N*-acetylglucosamine linked to *N*-acetylmuramic acid, extensively cross-linked by peptide bridge of *L*-alanyl-*D*-iso-glutaminy-*meso*-diaminopimelic acid. **Arabinogalactan** (AG) is a large polysaccharide anchoring the mycolic acids to the peptidoglycan layer by a covalent phosphoryl-*N*-acetylglucosaminosyl-rhamnosyl linkage. **Mycolic acids** are the components most responsible for the cell wall impermeability. Each molecule of mycolic acid is formed by 60 – 90 carbon atoms and consists of a long β -hydroxyl- and a short α -alkyl-fatty acid chain. A majority of the fatty acid chains is covalently linked to arabinogalactan through ester bond. The mycolic acid layer, also termed mycomembrane, is intercalated by free lipids and proteins of the **outer compartment**, including several key virulence factors, responsible for the mycobacterial resistance to macrophage killing functions, such as the capsule-forming glycolipids lipoarabinomannan (downregulates the oxidative burst and neutralizes toxic oxygen species) and dimycolyl trehalose, also termed “cord factor” (prevents fusion between fagosome and lysosome).^{4,24}

Introduction

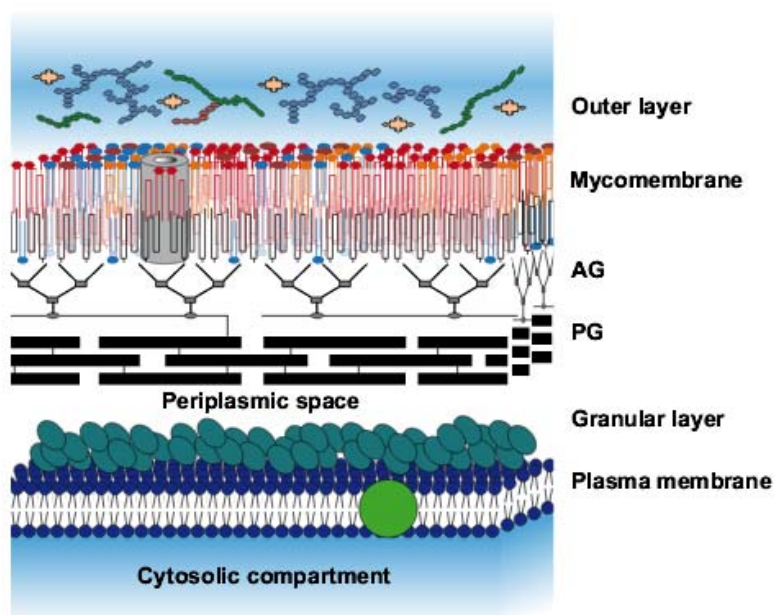


Fig. 9 A schematic illustration of the mycobacterial cell wall[†]

The cell wall biosynthesis is essential for mycobacterial survival and represents thus an excellent target for current (e.g. Inh, Emb, Eto, Pto, Dcs, Trd, Thz) and future anti-tuberculosis agents. Several key enzymes involved in the mycobacterial fatty acid synthesis but absent in mammalian/human cells are described in the following chapter.

1.3.2 Fatty acids biosynthesis

Mycobacterial fatty acids (FA), precursors for the synthesis of mycolic acids, are produced by two different means (see *Fig. 11*). The first is through a single, multifunctional polypeptide known as fatty acid synthase type I (FAS-I) or “**associated FAS system**“. This complex is also present in eukaryotic cells and is able to synthesize fatty acids *de novo*. The final products are fatty acid acyl coenzyme A (CoA) derivatives possessing 16 – 18 and 24 – 26 carbon atoms, respectively. The longer fatty acid derivatives form the α -alkyl branch of the final mycolic acids. The shorter fatty acid derivatives are further elongated to form the longer chain of mycolic acid, termed meromycolate, containing up to 56 carbon atoms. This process occurs in the second, “**dissociated FAS system**“ (FAS-II). FAS type II is specific for bacteria and comprises a complex of freestanding enzymes that each accomplish an individual step in the elongation cycle. A structural distinction of FAS-II enzymes from their FAS-I counterparts predestines them to play a crucial role as attractive drug targets. Especially the

[†] Reprinted from Chemistry and Biology, 21, Marrakchi, H., Laneelle, M.-A., Daffe, M., Mycolic Acids: Structures, Biosynthesis, and Beyond, Pages 67 – 85, Copyright (2014), with permission from Elsevier

Introduction

elongating enzymes MabA, InhA, HadAB and KasA (see *Chap. 1.3.2.1*) are the key regulators of fatty acid synthesis.^{24,25}

The mycolic acid synthesis is then concluded by a Claisen condensation of the α -alkyl branch with the modified and activated meromycolate, catalyzed by polyketide synthase Pks13. Finally, the produced unsaturated mycolate is reduced and linked to arabinogalactan or trehalose via ester bond.²⁵

1.3.2.1 *FAS type II*

Unlike other bacterial FAS-II enzyme systems, the mycobacterial FAS-II pathway is incapable of *de novo* synthesis of fatty acids from acetyl coenzyme A. Instead, the C₁₆₋₁₈ acyl CoA primers, generated by FAS-I, are used. In the following elongation cycles, the fatty acyl intermediates are covalently bound to a small highly acidic **acyl carrier protein** (ACP, AcpM stands for “mycobacterial ACP“), transferring them from enzyme to enzyme through the hydrophilic cytosol. The activated AcpM is analogous to CoA (*Fig. 10*) in FAS-I system. Both carriers contain a free sulfhydryl group in a 4'-phosphopantetheine prosthetic group, which forms thioesters with the intermediates.^{24,25}

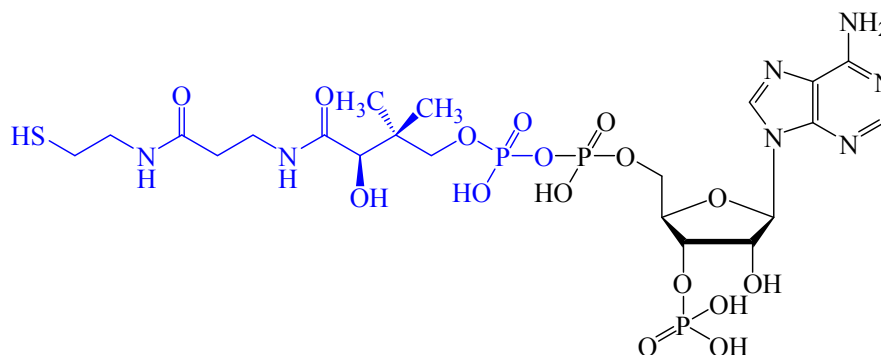


Fig. 10 Structure of Coenzyme A (with the 4'-phosphopantetheine moiety marked blue)

The first enzyme of fatty acid biosynthesis is acetyl-CoA carboxylase that catalyzes the carboxylation of acetyl-CoA to produce malonyl-CoA. Further steps are illustrated on the top of *Fig. 11*. The malonyl group is transferred to AcpM by malonyl-CoA:ACP transacylase (**FabD**) to form malonyl-AcpM.

Introduction

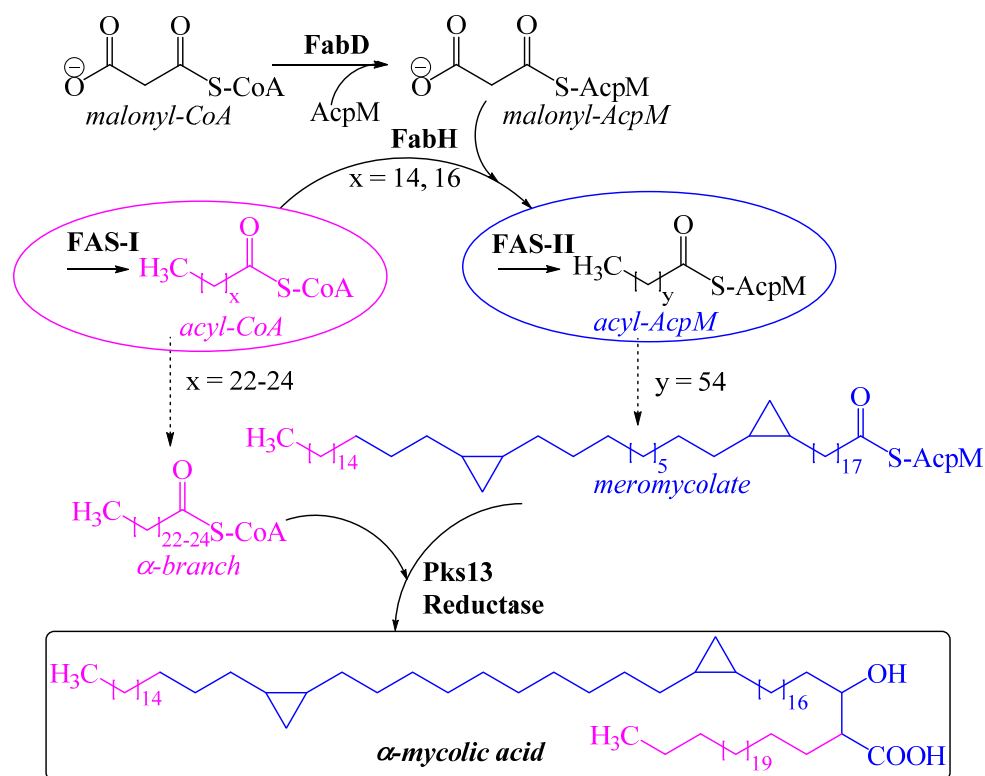


Fig. 11 Mycolic acid biosynthesis in mycobacteria. **On the top:** Transfer of the malonyl group to AcpM (mycobacterial acyl carrier protein) by malonyl-CoA:ACP transacylase (**FabD**) to form malonyl-AcpM. **In the centre:** Biosynthesis of the FAS-I products and condensation of the C₁₆₋₁₈ acyl-CoA primers with malonyl-AcpM by β -ketoacyl-ACP-synthase III (**FabH**) to form β -ketoacyl-AcpM. Further elongation is performed in the FAS-II enzymatic system to yield the full-length meromycolate. **At the bottom:** condensation of the meromycolate with the C₂₂₋₂₄ acyl-CoA products from the FAS-I by polyketide synthase **Pks13** to form the final product - mycolic acid. (Scheme modified according to Bhatt et al.²⁴)

A Claisen condensation with acyl-CoA (the FAS-I intermediate) by β -ketoacyl-ACP-synthase III (**FabH**) produces β -ketoacyl-AcpM. This intermediate enters the first elongation cycle (a detail of the FAS-II cycle is depicted in **Fig. 12**) beginning with the reduction of the β -keto group to a hydroxyl group by the NADPH-dependent β -ketoacyl-ACP-reductase (**MabA**). Next, water is removed by the β -hydroxyacyl-ACP dehydratase (**HadAB/BC**), forming a *trans*-2-enoyl-AcpM. The final step in the cycle is the reduction of the double bond in the enoyl intermediate by the NADH-dependent *trans*-2-enoyl-ACP reductase (**InhA**, the target of isoniazid) to form an acyl-AcpM. Subsequent cycles of elongation are started by the condensation of acyl-AcpM with malonyl-ACP by either β -ketoacyl-ACP synthase I or II (**KasA** or **KasB**), elongating the acyl-AcpM by further two carbons to form a β -ketoacyl-AcpM.^{25,26}

Introduction

1.3.2.2 *KasA as a key regulator of the FAS-II pathway*

The elongating enzymes KasA and KasB share 67 % of sequence identity, but they differ in substrate specificity. Whereas the first synthase catalyzes the Claisen condensation between malonyl-ACP and the growing acyl-ACP in the initial rounds of elongation, the latter synthase participates in subsequent rounds extending the chain to the full-length meromycolate. KasA is therefore a key enzyme in mycobacterial FAS-II system. Its depletion restrains markedly the mycolic acid biosynthesis and induces bacterial lysis. In comparison, reduction in the KasB levels decreases the virulence of mycobacteria without affecting their viability.^{24,25}

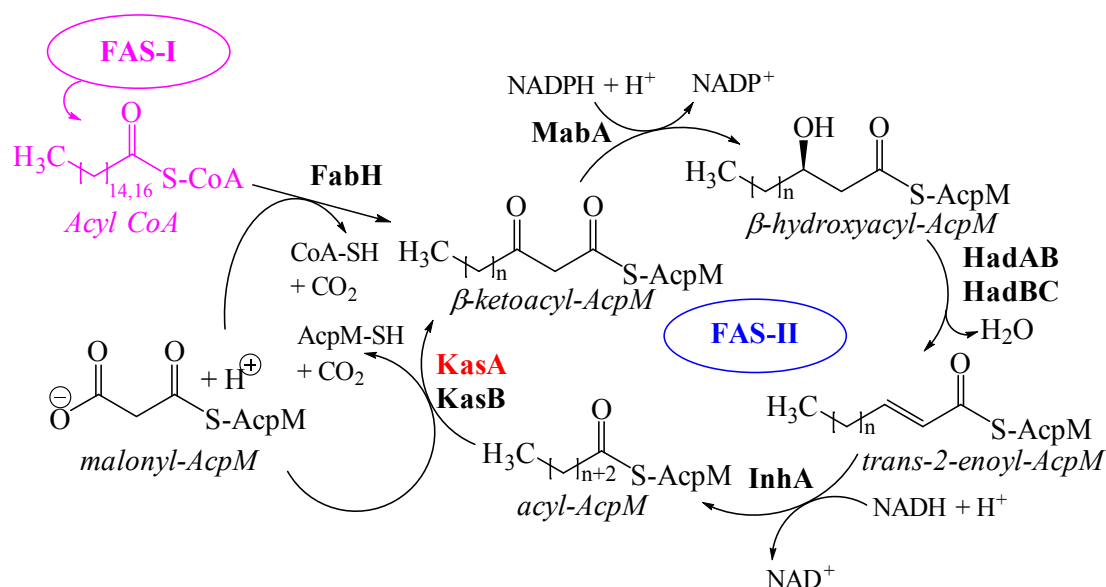


Fig. 12 FAS-II synthetic pathway in *M. tuberculosis*. First, malonyl-AcpM is condensed with the C_{16-18} acyl-CoA primer from FAS-I by β -ketoacyl-ACP-synthase III (**FabH**) to β -ketoacyl-AcpM. The first elongation step in the FAS-II cycle is the reduction of the β -keto group to a hydroxyl group by the NADPH-dependent β -ketoacyl-ACP-reductase (**MabA**). Dehydration of the product by the β -hydroxyacyl-ACP dehydratase (**HadAB/BC**) yields the *trans*-2-enoyl-AcpM. The final step, reduction of the double bond in the enoyl intermediate is carried out by the NADH-dependent *trans*-2-enoyl-ACP reductase (**InhA**) to form an acyl-AcpM. In the subsequent cycles, the malonyl-ACP is condensed with acyl-AcpM by β -ketoacyl-ACP synthase I or II (**KasA** or **KasB**). In each cycle, two carbon units are added to the growing acyl chain. (Scheme modified according to Schiebel et al.²⁷)

1.4 The β -ketoacyl-ACP synthase “KasA”

1.4.1 The catalytic mechanism of KasA

β -Ketoacyl synthases and polyketide synthases, both involved in the biosynthetic pathways FAS-I and FAS-II, are constituents of the thiolase superfamily. A common feature of these enzymes is the reactive cysteine, temporarily acylated in the catalytic cycle. Whereas the β -ketoacyl synthase III (**FabH** in *M. tuberculosis*) binds the acyl-CoA substrates, the

Introduction

β -ketoacyl synthases I and II (KasA and KasB in *M. tuberculosis*) and the polyketide synthase Pks13 (catalyzing the last condensation step in the biosynthesis of mycolic acids) are ACP-dependent.²⁸ Similarly as the majority of the enzymes of the thiolase superfamily, KasA is a homodimer, possessing two active sites capable of substrate binding. Each active site is divided in two halves: a half-site for acyl-AcpM and another half-site to bind malonyl-AcpM. A carbon-carbon bond formation between the two substrates is catalyzed via a Claisen condensation mechanism that occurs in the following steps:

1. **Acyl transfer:** A nucleophilic attack of the KasA cystein residue (Cys-171) on the carbonyl carbon of acyl-AcpM, facilitated by an oxyanion hole formed by the amide groups of Cys-171 and Phe-404 (*Fig. 13*), yields the acyl-enzyme intermediate and free AcpM.²⁹

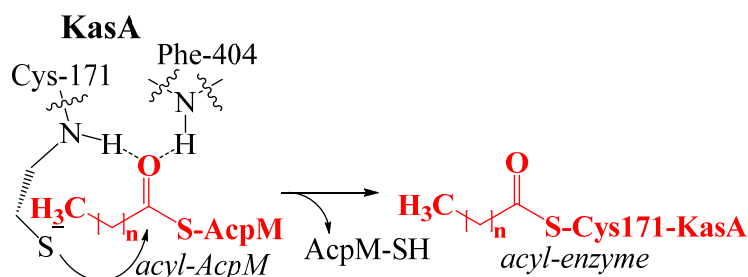


Fig. 13 Acyl transfer from ACP to KasA*

2. **Decarboxylation** of the second substrate, malonyl-AcpM, followed by a **carbanion formation** is facilitated by hydrogen bonds between the thioester carbonyl and two conserved histidines (His-311 and His-345, see *Fig. 14*). Also, the side chain of a conserved Phe-237 destabilizes the malonate anion, promoting the decarboxylation reaction.^{29,30}
3. **Condensation** of the carbanion with the carbonyl carbon of the enzyme bound acyl primer yields β -ketoacyl-AcpM and free enzyme.²⁹

* Scheme modified according to Machutta *et al.*²⁹

Introduction

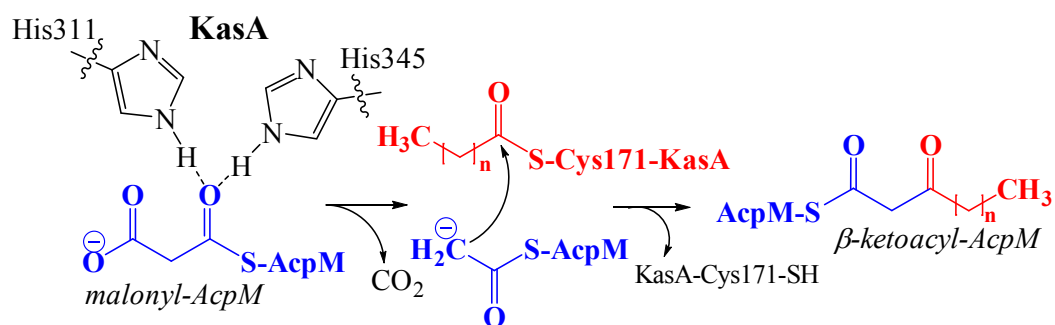


Fig. 14 Decarboxylation of malonyl-AcpM followed by condensation with the enzyme-bound acyl**

1.4.2 Inhibitors of the KasA catalytic activity

Three natural products are known to inhibit KasA: platensimycin, cerulenin and thiolactomycin.

1.4.2.1 Platensimycin

Platensimycin (**Fig. 15**) was isolated from *Streptomyces platensis* as a secondary metabolite possessing antimicrobial activity against Gram-positive bacteria, including methicillin- and vancomycin-resistant strains (MRSA, VRE). The inhibitory activity against KasA and KasB *in vitro* was described by Brown *et al.*³¹ The assessed IC₅₀ values were 4.53 and 9.51 μM, respectively.

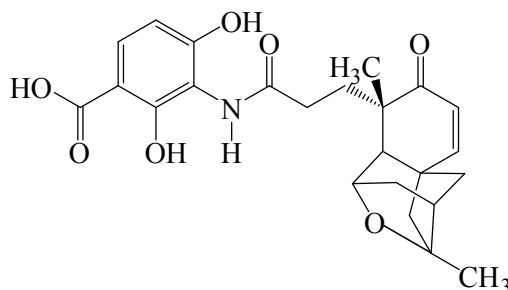


Fig. 15 Structure of platensimycin

The binding mechanism was elucidated on the previously reported crystal structure of platensimycin in complex with FabF, a KasB homolog from *Escherichia coli*.³² Platensimycin binds preferably to the acyl-enzyme intermediate and occupies the binding site for malonyl substrate. A low mammalian cell toxicity of platensimycin (IC₅₀ > 1000 μg/ml in a HeLa cytotoxicity assay^{32,31}) underlines its potential as a lead compound for novel drug design. Simplified platensimycin analogs, preserving only the key structural features (carboxyl, amide and the side chain enone) based on the known interactions with FabF, have recently been developed by Plesch *et al.*³³

** Scheme modified according to Machutta *et al.*²⁹

Introduction

1.4.2.2 Cerulenin

Cerulenin, isolated from *Cephalosporium caerulens*, inhibits the fatty acid synthesis in various strains of bacteria, fungi and yeasts. Due to its unselective character, it also inhibits the condensation reaction by the mammalian FAS-I system, and possesses thus certain antineoplastic activity. Additionally, its capability of reducing food intake and body weight in mice and the inhibitory activity of its analogs on efflux pumps in drug-resistant *Candida albicans* strains have been described.^{26,34} In mycobacteria, cerulenin irreversibly inhibits Kas I and Kas II, as it forms a covalent adduct with the active site cysteine. The thoroughly studied binding mechanism was derived from the reported crystal structure of cerulenin with FabB³⁰, the KasA homolog from *E. coli*. After opening of the cerulenin oxirane ring, a covalent bond is formed between the C2 carbon and the active site cysteine (Cys-163). The amide oxygen of cerulenin interacts via hydrogen bonds with the active site histidines (His-298 and His-333). The position of the former oxirane oxygen is stabilized by two hydrogen bonds with Phe-392 and Cys-163. Finally, the aliphatic chain of cerulenin fills the active site deep hydrophobic pocket.

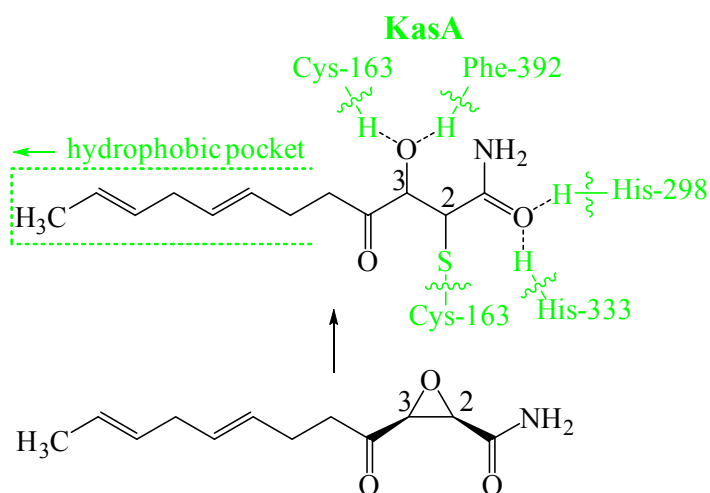


Fig. 16 Structure of cerulenin and its interactions with FabB (on the top, FabB marked green). Scheme modified according to Price et al.³⁰

The affinity for FabB is higher than for FabF (the Kas B homolog) and considerably higher in comparison to the initial Kas III synthase FabH, which is only poorly inhibited due to the lack of hydrophobic pocket in the active site. Cerulenin imitates the condensation transition state (see Fig. 16, compare Fig. 13, Fig. 14). The former oxirane oxygen atom mimics the substrate thioester carbonyl oxygen in the oxanion hole and the cerulenin amide oxygen imitates the carbonyl oxygen of the incoming malonyl group. Finally, the acyl chain of cerulenin replaces the acyl enzyme intermediate.³⁰

Introduction

Despite the strong inhibition of FabB ($IC_{50} = 3 \mu M$)³⁰, cerulenin is not an appropriate drug candidate, due to its unselective inhibitory mechanism (inhibition of FAS-I).

1.4.2.3 *Thiolactomycin*

Thiolactomycin (TLM, *Fig. 17*) is a unique thiolactone-based molecule produced by *Nocardia* species. It possesses antibacterial activity against both Gram-positive and Gram-negative strains. In mycobacteria, it reversibly inhibits FAS-II ketoacyl synthases. Its affinity to the FAS-I counterparts is considerably lower.

The antibiotic is effective against bacterial infections of urinary tract and peritoneal cavity and shows low toxicity in mice. Additionally, TLM also inhibits the growth of *Plasmodium falciparum* and trypanosoma.^{26,30}

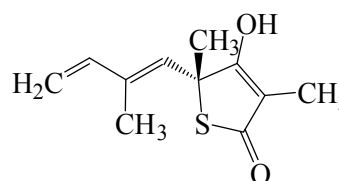


Fig. 17 Structure of (5R)-thiolactomycin

TLM is a promising lead compound for the development of FAS-II inhibitors. It exhibits a higher selectivity for KasA than KasB ($IC_{50} = 20$ and $90 \mu M$, respectively).³⁶ In KasA, TLM preferentially binds to the acyl-enzyme intermediate, imitating the malonyl substrate. The first crystal structure of TLM in complex with the free enzyme (“wild-type KasA”) and its acyl-enzyme mimic C171Q (catalytic cysteine replaced by glutamine) was reported by Luckner *et al.*³⁵

1.4.2.3.1 The TLM-KasA binding mechanism

TLM mimics malonyl binding to KasA, as described by Luckner *et al.*³⁵ Both methyl groups on the thiolactone ring are positioned in two hydrophobic pockets formed by the proline, glycine and phenylalanine residues Pro-280, Gly-318, Phe-402 and Phe-237. The isoprenoid moiety is intercalated between two peptide bonds, alanine Ala-279 and proline Pro-280, and glycine Gly-403 and phenylalanine Phe-404, respectively. Its tail is directed to an extended lipophilic pocket, where the position is further stabilized by two water molecules. The thiolactone oxygen is connected by two strong hydrogen bonds to the active site histidines (His-311 and His-345), pretending the binding of thioester carbonyl oxygen of malonyl-AcpM (see *Fig. 18*, compare *Fig. 14*). The binding mechanism of TLM in KasA is analogous to the previously reported TLM-FabB complex³⁰, apart from the different active site

Introduction

phenylalanine conformation. In FabB, the Phe-392 residue assumes always an “open conformation“ (before and after TLM binding), *i.e.*, its aromatic ring lies almost perpendicular to the thiolactone ring of TLM, whereas in KasA, the corresponding Phe-404 is constantly situated in a “closed conformation“, *i.e.*, parallel to the thiolactone ring. Particularly interesting is the phenyl position in the KasA mutant C171Q, that mimics the bound acyl substrate, since Phe-404 assumes an “open conformation“. This observation has lead to a presumption, that Phe-404 rotates after binding of the acyl substrate adopting thus an energetically favourable edge-to-face arrangement with the thiolactone ring.³⁵

This conformational change can explain the slow-onset inhibition mechanism ($t_{1/2}$ of the activated enzyme-inhibitor complex: 14 min) observed for TLM and C171Q KasA mutant by Machutta *et al.*²⁹ Their kinetic assay also confirmed the presumption, that TLM binds preferentially to the acyl-enzyme form of KasA (IC_{50} for the wild-type KasA: 242 μ M, IC_{50} for the KasA-TLM complex after preincubation with palmitoyl-AcpM substrate: 19 μ M).²⁹

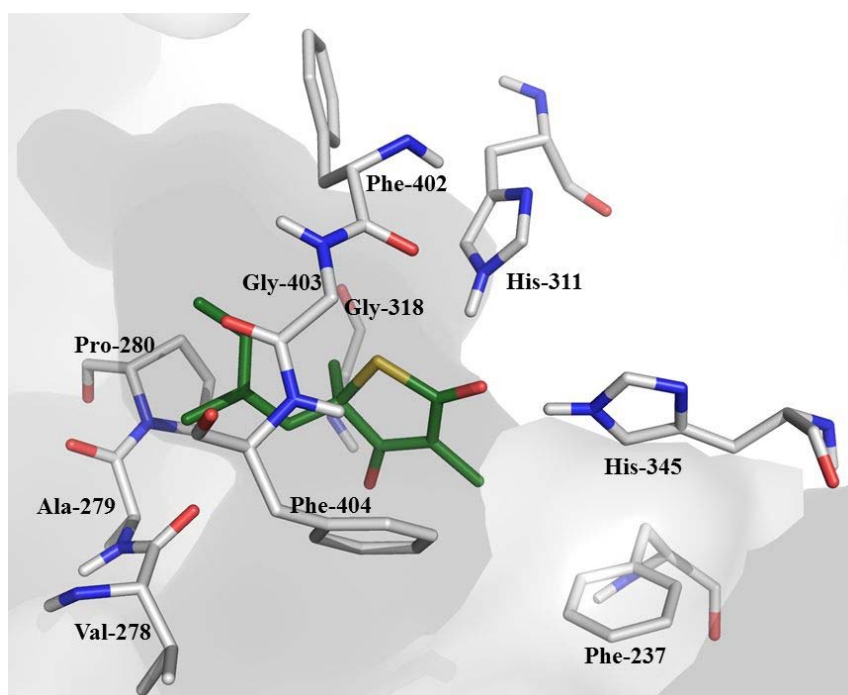


Fig. 18 Crystal structure of KasA-TLM complex showing TLM as a green backbone in the centre and selected active site amino acids. The thiolactone oxygen forms hydrogen bonds with His-311 and His-345. In front of TLM: Phe-404 in a “closed conformation”. Non-polar hydrogens have been omitted.^{††}

^{††} KasA structure downloaded from PDB <http://www.rcsb.org>, 2wge, Luckner *et al.*³⁵

Introduction

1.4.2.3.2 TLM analogs

The first structure-activity relationships in a series of TLM analogs were investigated by Kremer *et al.*³⁷ The observed increase in MIC values on *M. tuberculosis* H37Rv correlated with increased hydrophobicity of the TLM side chain via a varied length or saturation of the double bonds.

Based on the observed higher affinity of TLM for the acyl-enzyme intermediate, a detailed study of conformational changes in the active site of KasA was performed by Schiebel *et al.*²⁷ The evaluation of enzyme affinity was supported by crystal analysis data. The involved TLM analogs, substituted in position 3 of the thiolactone ring, were designed to mimic the two KasA substrates, acyl- and malonyl-AcpM. The affinity of the most potent inhibitor of the investigated series, possessing a trifluoromethyl-carbonyl moiety in position 3, was increased due to an additional hydrogen bond formation between the fluorine atom and the hydroxyl groups of the threonine residues Thr-313 and Thr-315.²⁷

Within their dissertation theses, Schaefer³⁸ and Topf³⁹ developed a TLM-based pharmacophore model, which was then applied in the virtual screening of a modified ZINC database¹²². The *in silico* evaluation yielded potential KasA inhibitors of various structures: *e.g.* isatine-, uracil- and benzoxazolinone derivatives. Among the best hits with the highest anticipated enzyme affinity were also the chromone- and pyrimidinone-based compounds presented here.

In conclusion, TLM represents a promising lead compound in the development of novel antimycobacterial agents. It exhibits a synergistic FAS-II inhibitory activity with the first-line drug isoniazid, but not a cross-resistance.³⁷ Therefore, the next improvement of TLM analogs may lead to novel drug candidates combating the multidrug-resistant *M. tuberculosis* strains.

2 Aims & objectives

In search for potential KasA inhibitors, compounds of an optimized ZINC database³⁸ were submitted to virtual screening based on the TLM pharmacophore model designed in the research group of Prof. Sotriffer* by Dr. B. Schaefer³⁸ and Dr. C. Topf³⁹ taking account of the known crystal structure of the KasA-TLM complex³⁵. Selected screening hits were synthesized in the research group of Prof. Holzgrabe* by Dr. Topf who began testing their activity *in vitro* to derive correlations between experimental and the *in silico* predicted affinity constants. Simultaneously, several compound libraries have been prepared by structural variation of the hits. The first task within this work was the synthesis of the chromone-based compound GS-71³⁹ and its structural modification. The docking pose of this hit in the KasA active site is shown in *Fig. 19*.

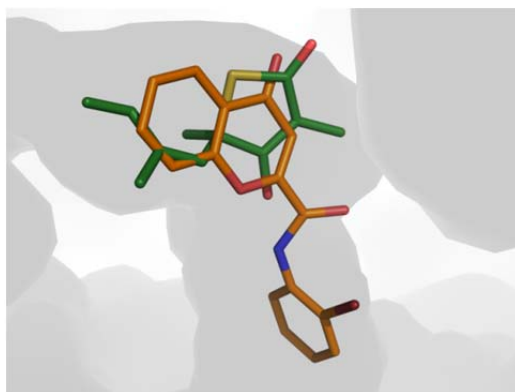


Fig. 19 Overlap of TLM (green backbone) and the docking pose of **GS-71** (orange) - created by Dr. C. Topf³⁹, reused with kind permission from Prof. Sotriffer. Hydrogens have been omitted.

A key structural element is the oxo group of the chromone ring, which is oriented toward His-311 and His-345 replacing thus the thiolactone ring oxygen as a dual hydrogen bond acceptor. The γ -pyrone ring of the chromone moiety resembles the thiolactone ring of TLM due to its vinylogous acid character with delocalized π -electrons between the both oxygen atoms. The aromatic amide residue does not head toward the large hydrophobic pocket, contrarily, it is directed to the active site entrance for malonyl-ACP. The benzene ring of the chromone moiety is positioned at the entrance of the hydrophobic pocket. The predicted affinity constant is with $\text{pK}_i = 5.85$ in the same (micromolar) range as the value for TLM ($\text{pK}_i = 4.84$; GOLD4.0, SFCscore)³⁹. In spite of the different arrangement of structure **GS-71**, an easy opportunity to create a compound library by substitution of the amide residue and the

* Institute of Pharmacy and Food Chemistry, University of Würzburg

Aims & objectives

low preliminary affinity constant ($K_D = 42 \mu\text{M}$), assessed meanwhile in the binding assay, favoured this hit for further variations.

Since the vast majority of the newly synthesized chromone-2-carboxamides precipitated in the testing buffer, the consequent aim was to solubilize these hydrophobic products. The inefficient attempts to improve the compound solubility by means of cyclodextrin complex formation were discontinued and the next work focused on structural modification of the hydrophobic chromone ring by insertion of polar groups. The synthesis of the **GS-71** analogs with a succinamidyl residue in position 6 of the chromone ring was supported by promising preliminary binding data (e.g. for **12b**, $K_D = 38 \mu\text{M}$).

The next aim within the synthesis consisted in variation of another hit, a pyrimidinone derivative **VS-8**³⁸. The obtained docking pose of this compound in the KasA active site can be seen in *Fig. 20*. The predicted affinity of **VS-8** to KasA is with $\text{pK}_i = 5.42$ comparable to TLM ($\text{pK}_i 5.56$; FlexX, SFCscore).³⁸

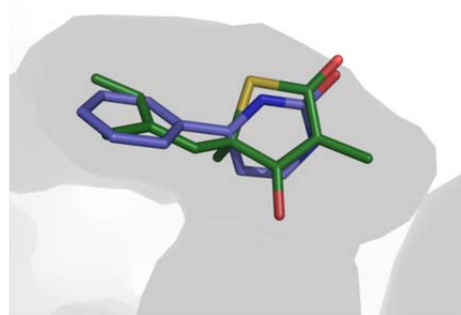


Fig. 20 *Overlap of TLM (green backbone) and the docking pose of VS-8 (blue) - created by Dr. B. Schaefer³⁸, reused with kind permission from Prof. Sotriffer.*

The pyrimidinone ring oxygen acts as the dual hydrogen bond acceptor, whereas the phenyl residue heads toward the large hydrophobic pocket, occupied in the case of TLM by the isoprenoid chain. The intention of further variation of compound **VS-8** was abandoned due to autofluorescence, detected to some degree in most of the synthesized derivatives, as it interfered with the activity evaluation performed in the fluorescence-based assay.

Meanwhile, the attention was drawn to the binding assay, introduced and performed by Dr. Topf. The relative narrow range of the obtained affinity constants together with the lacking correlations between predicted and experimental values arose a question of reliability of the assay method. Therefore, the aim focused on method optimization, in order to acquire more accurate data. An essential feature affecting the drug-like properties of the compounds is their capability to permeate the mycobacterial membrane. Hence, an important part of this work was the evaluation of the *in vivo* inhibitory activity tested on *M. tuberculosis* within the SFB 630 and the confrontation of the acquired data with the *in silico* predicted values of probability of the membrane permeation (MycPermCheck⁸⁴).

3 Synthesis

The synthesis focused on variation of the two virtual screening hits, **GS-71**³⁹ and **VS-8**³⁸ (see *Fig. 21*).

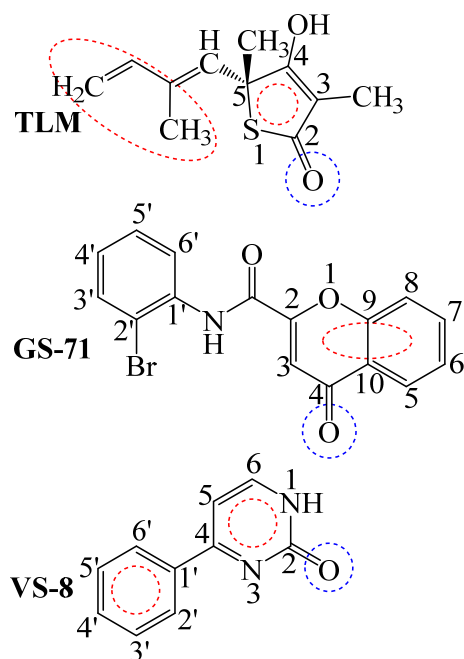


Fig. 21 Model structures **GS-71**³⁹ and **VS-8**³⁸ based on the **TLM** pharmacophore model. Dashed circles represent the overlapping essential structural features for the interaction with *KasA*: blue – H-bond acceptors, red – hydrophobic interactions.

First, the chromone derivative **GS-71** (here designated as **3b**) was modified in the amide part of the molecule, in order to investigate the effect of this moiety on the binding affinity. Toward preparing hydrophobic compounds with enhanced permeation through the mycobacterial membrane, halogen-, methyl- and methoxy-substituted anilines were prioritized. Subsequently, aniline was replaced by heterocyclic amine and methylene units were inserted between the amide nitrogen and the substituted benzene ring (syntheses of **3a-p** and **4a-k**). Additionally, a series of phenolic amides was prepared (syntheses of **7a-c**).

Finally, the model structure was varied in the linker feature, replacing the amide bond by a keto group, in order to examine the difference in the binding constants (synthesis of **13** and **14**). Since the majority of the obtained products precipitated during the course of biological testing performed in DMSO/buffer medium, a polar succinyl group was added to the chromone ring (see syntheses of succinamic acids **12a-i** and **16**). The first reaction intermediates, 6-nitro-substituted derivatives **9a-j**, were also characterized and tested, and several of them exhibited the highest activity among the tested chromones. The succinyl chain was further varied by an additional amide bond in case of compound **17**. Trimethylammonium salt **19** was prepared as a water-soluble analog of compound **GS-71** suitable for the biochemical assay. The synthesis of succinamic acids was supported by promising preliminary results obtained from the whole cell testing, which turned out to be false positive

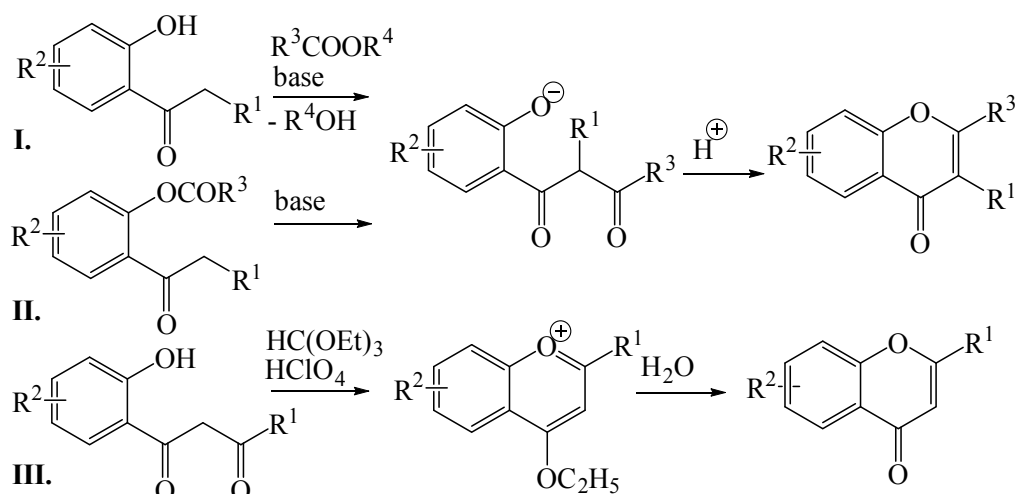
Synthesis

in a subsequent control study. The methyl malonyl esters **18a-b** were synthesized with the aim of maintaining the capability of permeation through the mycobacterial membrane.

The pyrimidinone derivative **VS-8** (here designated as **22a**) was varied by a substitution with methyl, *tert*-butyl and aryl in positions 4, 5 and 6. The reaction intermediates, pyrimidin-2-amines, were prepared in excess amounts to be evaluated as well (see the syntheses of **21a-e** and **22a-e**). Unfortunately, several compounds of the series displayed autofluorescence, and thus their enzyme affinity could not be evaluated. Additionally, a synthesis of the hydrophilic 1,3-dihydropyrimidinone **23** was performed.

3.1 Synthesis of the chromone derivatives

There are several approaches to prepare chromones, some of them are displayed in *Scheme 1*. One of the most common pathways is the Claisen condensation of 2-hydroxyaryl alkyl ketone with carboxylic ester in the presence of a strong base (I). In the next step, the dioxophenol intermediate is cyclized by heating in an acidic medium. Other methods involve the Baker-Venkataraman rearrangement of 2-acyloxyacylbenzenes (II) or condensation of 2-hydroxyacetophenones with triethyl orthoformate and a strong acid (III).^{40,41}



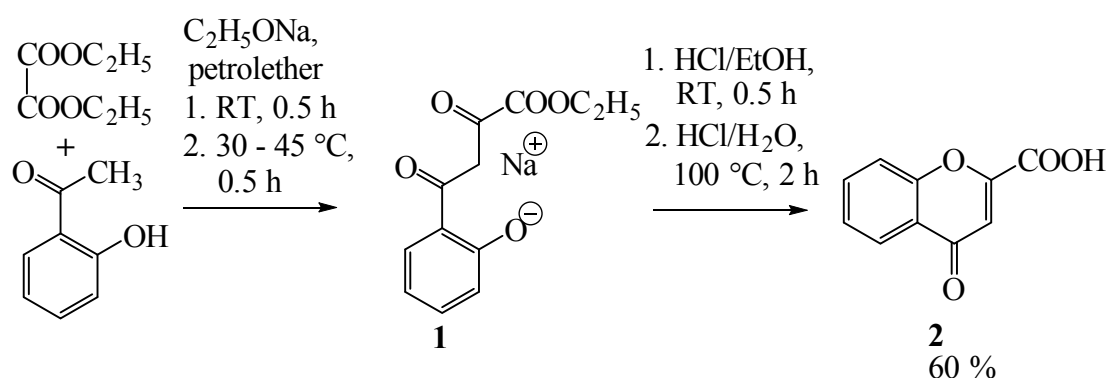
Scheme 1 Synthesis routes for 4H-chromen-4-ones (chromones)^{40,41}

3.1.1 Synthesis of chromone-2-carboxylic acid

The starting compound **2** was prepared by a Claisen condensation following the procedure reported by Nicolas *et al.*⁴² In the presence of a strong base, deprotonation of

Synthesis

2-hydroxyacetophenone yields a nucleophilic enolate anion, which attacks a carbonyl carbon of diethyl oxalate to produce the intermediate sodium 2-(4-ethoxy-3,4-dioxobutanoyl)phenolate (**1**), as depicted in *Scheme 2*. To a suspension of sodium ethoxide in anhydrous petrolether, diethyl oxalate and 2-hydroxyacetophenone were added. The exothermic reaction was cooled to RT using ambient water bath. Finally, petrolether was removed by distillation and the residue was dried *in vacuo*. The ring closure was conducted in a mixture of concentrated HCl in ethanol, the subsequent partial hydrolysis was performed in diluted hydrochloric acid. The pure product was obtained by recrystallization from aqueous methanol in an overall yield of 60 %.



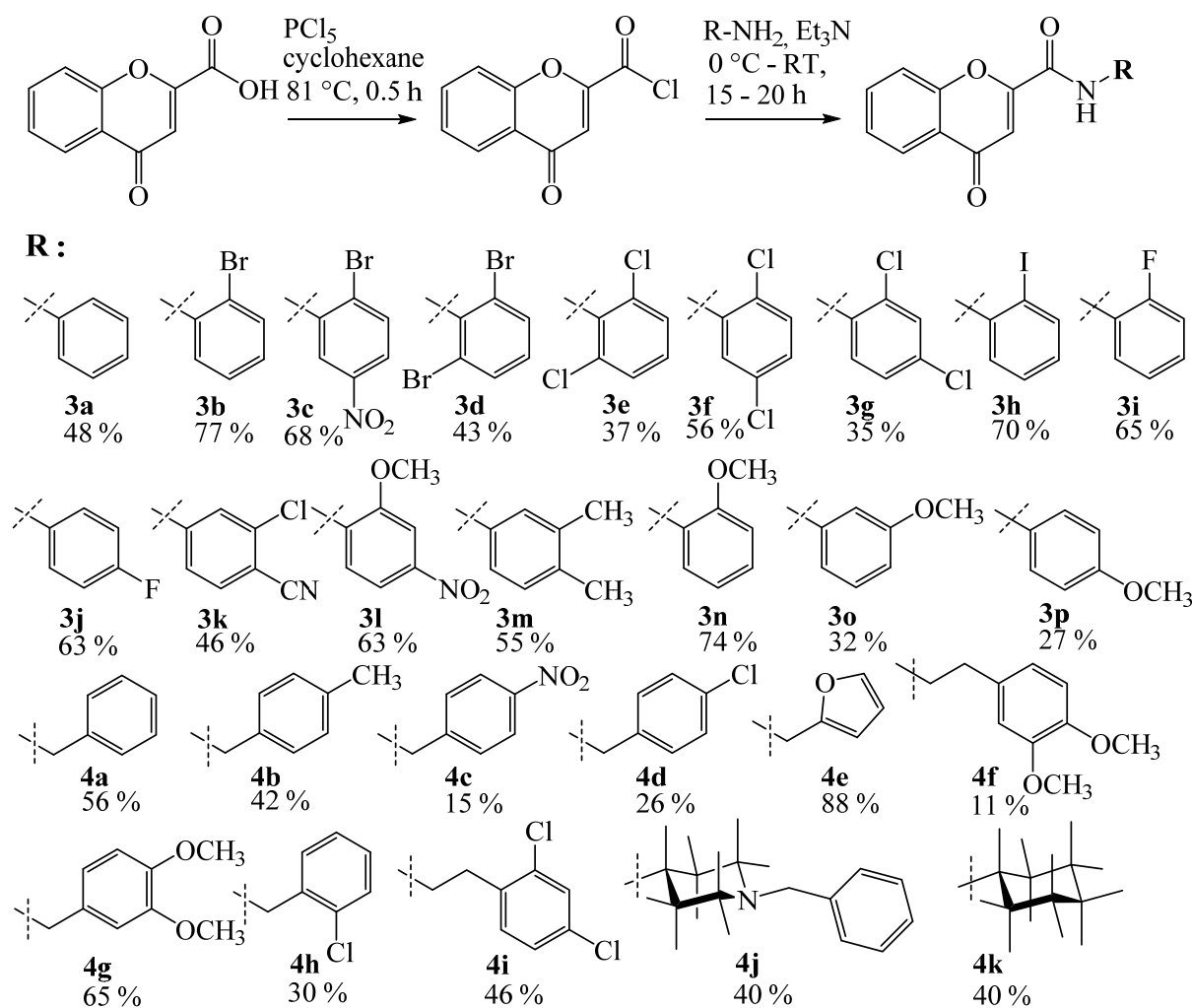
Scheme 2 Synthesis of chromone-2-carboxylic acid **2**

3.1.2 Synthesis of chromone-2-carboxamides

3.1.2.1 Synthesis of **3a-p** and **4a-k**

The amides **3a-p** and **4a-k** were prepared by a classical way in two steps via acyl chloride. Chromone-2-carboxylic acid was treated with 1.1 eq. of phosphorus pentachloride. Within 30 minutes of refluxing in anhydrous cyclohexane, the starting compound dissolved completely while the acyl chloride was formed. In the next step, a corresponding aniline derivative was added. In order to trap the formed HCl, an excess of triethylamine was used. The mixture was stirred overnight at RT. The precipitate was filtered and purified by means of column chromatography or recrystallized. Products were obtained in overall yields of 11 – 88 % (see *Scheme 3*).

Synthesis



Scheme 3 Synthesis of chromone-2-carboxamides **3a-p** and **4a-k**

Side products of the reaction

The synthesis of *N*-(2-aminophenyl)-chromone-2-carboxamide by reaction with 1,2-diaminobenzene was at given conditions not successful. Instead, two other products were obtained: the dimer **5a**, consisting of two chromone molecules connected via amide residue, and the 3,4-dihydroquinoxaline derivative **5b**, formed by Michael reaction between the *ortho*-amino group and the chromone carbon C2 followed by chromone ring opening and formation of a six-membered 3,4-dihydropyrazin-2-one ring (see *Fig. 22*). The synthesis of a *Z*-isomer of compound **5b** has already been described by Markees¹³⁰ and the preference of the *Z*-configuration was confirmed here, too.

Low reaction yields of several amides can be explained by an additional formation of the corresponding imines, formed by an additional reaction of amine with the chromone oxo group at position 4. The imine **6** (*Fig. 22*), obtained from the synthesis of 3-methoxyanilide **3o**, was purified, analysed and tested. According to a TLC experiment, imines were preferably

Synthesis

formed after addition of more than 2 eq. of amine and subsequent stirring over 2 days. The formation of similar side products of ester aminolysis of chromone-2-carboxylic acid esters was already described by Kohlstaedt *et al.*⁴³

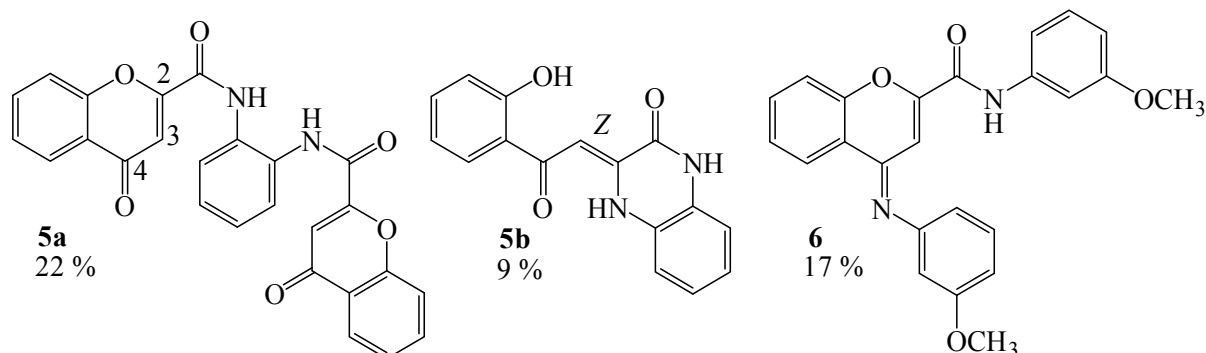
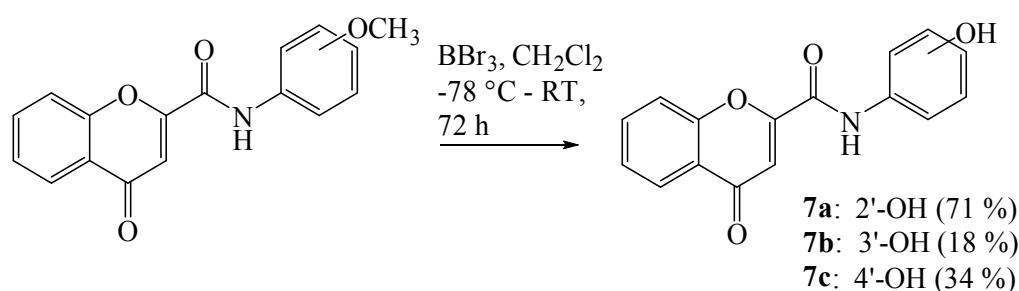


Fig. 22 Side products of the amide synthesis

3.1.2.2 Synthesis of 7a-c

In order to obtain phenolic amides, the methoxyphenylamides **3n-p** were demethylated by the use of boron tribromide in anhydrous dichloromethane at $-78\text{ }^{\circ}\text{C}$, 10 eq. of boron tribromide were added dropwise. After complete cleavage of the methyl group (TLC-control), resulting dibromo(organo)borane was hydrolysed in ice water and the reaction mixture was neutralized with sodium carbonate solution. The precipitate formed was filtered and recrystallized from aqueous methanol to give pure products in 18 – 71% yields (see *Scheme 4*).



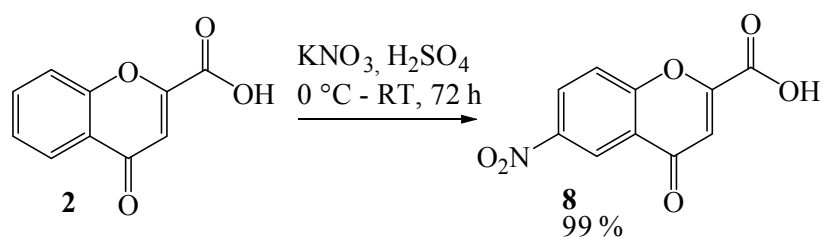
Scheme 4 Synthesis of demethylation products 7a-c

3.1.3 Synthesis of 6-nitrochromone-2-carboxylic acid

Barker and Ellis⁴⁴ reported a direct nitration of the chromone-2-carboxylic acid using a nitric/sulphuric acid mixture. Here, the nitration was conducted under milder conditions by dissolution of compound **2** in concentrated sulphuric acid and subsequent addition of 1.5 eq. of potassium nitrate into the mixture cooled to $0\text{ }^{\circ}\text{C}$. The *in situ* formed nitronium ion was selectively directed to the position 6 of the chromone ring. The reaction was completed after 72 hours, and the mixture was poured on ice. The white precipitate was filtered and

Synthesis

recrystallized from methanol/DMF mixture. The conversion was nearly quantitative (99 %, see *Scheme 5*).



Scheme 5 Nitration of chromone-2-carboxylic acid

3.1.4 Synthesis of 6-nitrochromone-2-carboxamides

3.1.4.1 Synthesis of 9a-j

The amides were prepared by a modified procedure described in *Chap. 3.1.2.1* using the 6-nitrochromone-2-carboxylic acid **8** as a starting compound and dichloromethane as a solvent (see *Scheme 6*). After stirring overnight, the reaction was quenched with water, organic layer separated and the water phase washed with dichloromethane. Organic phases were combined and the solvent removed *in vacuo*. After purification by column chromatography or recrystallization, the amides **9a-j** were obtained in overall yields 23 – 84 %.

Side product of the synthesis of compound 9d

The 2-hydroxy-benzoyl acrylamide derivative **10** was obtained as a yellow-coloured lipophilic side product in the synthesis of **9d**. Similar compounds prepared via nucleophilic attack on the chromone carbon C2 under opening of the γ -pyrone ring were described by Davidson *et al.*¹²³ The *syn*-rotamer configuration of the oxo group at position 4 and the *E*-configuration on the C2-C3 double bond were assumed from the chemical shifts of the broad ¹H signals of the amide- and hydroxyl hydrogens.

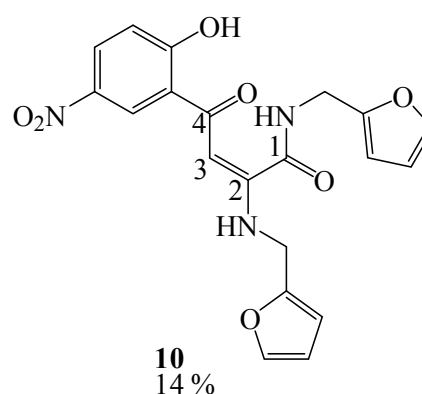
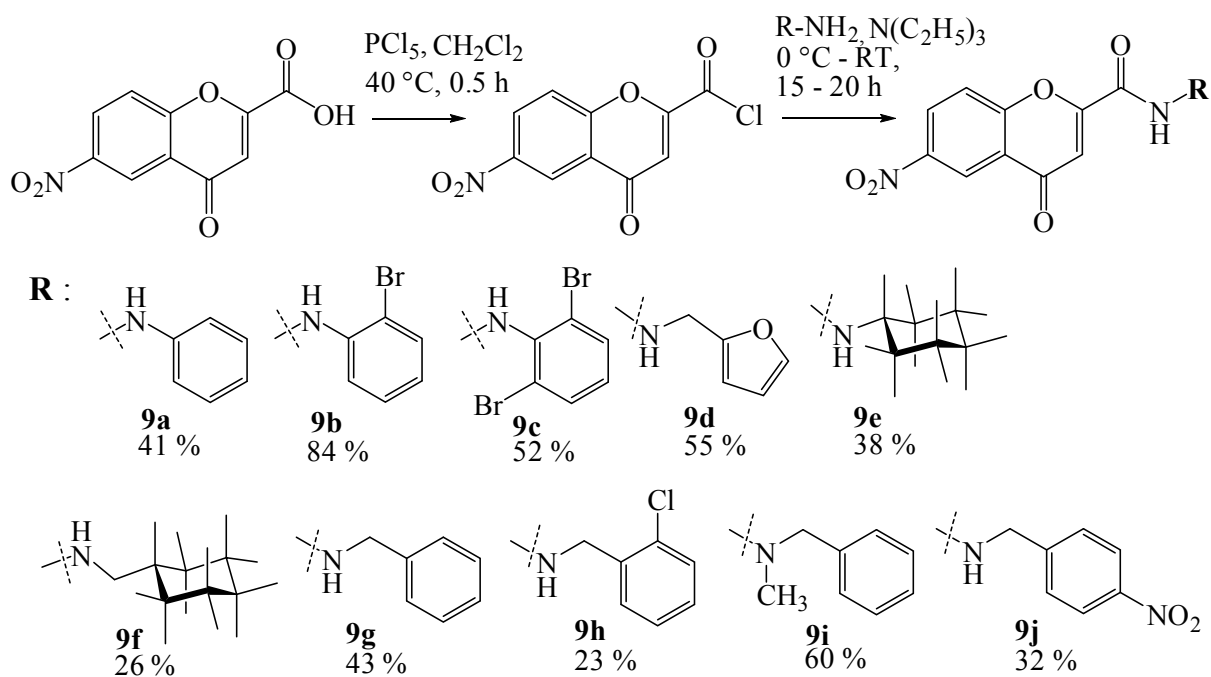


Fig. 23 Structure of compound **10**

Synthesis



Scheme 6 Synthesis of 6-nitrochromone-2-carboxylamides **9a-j**

3.1.5 Synthesis of the succinamic acids

Chromone derivatives with improved water-solubility were prepared by a structural modification reported by Williams *et al.*⁴⁵ and Yap *et al.*⁴⁶ They described a synthesis of flavonols bearing a succinic acid chain. The intermediate 6-acetamidoflavonols were hydrolysed in HCl/ethanol mixture to yield 6-aminoflavonols, isolated as hydrochlorides. These were treated with succinic anhydride in pyridine to give the target succinamic acids. Conversely, Volodymyr *et al.*⁴⁷ reported the introduction of succinic acid moiety into a 6-amino derivative of 3-hydroxychromone by reaction with 1 eq. of succinic anhydride in anhydrous DMF. No additional base was required. Here, the 6-aminochromone intermediates, necessary for the connection to succinic acid, were obtained by reduction of the 6-nitrochromone derivatives **9a-j** (see *Scheme 7*).

3.1.5.1 Synthesis of 6-amino-intermediates **11a-i**

Reduction of the nitro group in position 6 of the chromone ring was achieved in mild conditions using stannous chloride as a reducing agent. Tin(II)chloride dihydrate in a 5-fold excess was added to the mixture of 6-nitrochromone-2-carboxylamide **9a-i** in ethanol and refluxed until the conversion was completed (TLC control). The mixture was stirred overnight at RT. After solvent evaporation, the residue was suspended in water and extracted with ethyl

Synthesis

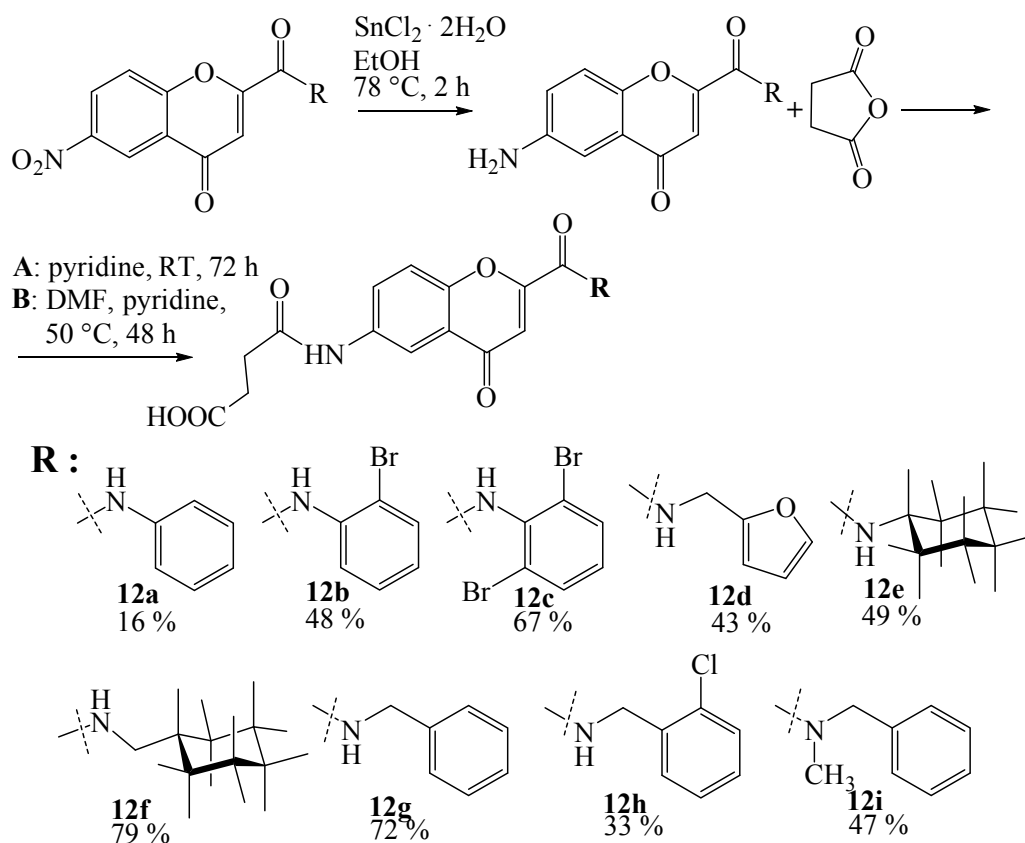
acetate. The products were purified by column chromatography or recrystallized. The resulting solids **11a-i** were used for the next reaction step without further characterization.

3.1.5.2 Synthesis of succinamic acids **12a-i**

Method A: Williams' and Yap's procedure was modified and applied for the synthesis of **12a**.

To a solution of **11a** in anhydrous pyridine, 2 eq. of succinic anhydride were added. The solution was stirred at RT for 72 h, afterwards, cooled to 0 °C and acidified. The precipitate formed was filtered and washed with ice cold water. A yellow solid was obtained after purification by column chromatography in an overall yield 16 %.

Method B: To facilitate the reaction control by TLC, a modified Volodymyr's method was adopted for the synthesis of the above products **12b-i**. Pyridine was added to protect succinic anhydride from hydrolysis. To a solution of **11b-i** in anhydrous DMF, 2 eq. of succinic anhydride and 8 eq. of anhydrous pyridine were added. The mixture was stirred at 50 °C for 48 hours. The crude products were separated after precipitation with diluted HCl solution added dropwise at 0 °C. Purification by column chromatography gave yellow solids in 33 – 79 % overall yields.

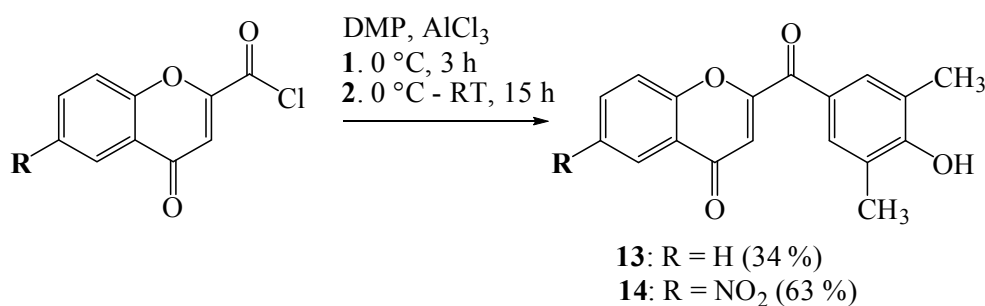


*Scheme 7 Synthesis of succinamic acids **12a-i***

3.1.6 Synthesis of 2-(4-hydroxy-3,5-dimethylbenzoyl)-4*H*-chromene-4-ones **13** and **14**

Diaryl ketones **13** and **14** were prepared via Friedel-Crafts acylation of 2,6-dimethylphenol (DMP) following the procedure reported by Nicolas *et al.*⁴² Chromone-2-carboxylic acid chloride and its 6-nitro analog were used as acylating agents, aluminium chloride as a catalyst. Due to the resonance stabilization of DMP, acylation is directed exclusively to the *para*-position of the aromate.

The synthesis is depicted in *Scheme 8*. First, DMP was dissolved in anhydrous dichloromethane, aluminum chloride was added, and, after 20 min. of stirring at RT, the mixture was cooled to 0 °C and a solution of the corresponding acid chloride in anhydrous dichloromethane was added. The mixture was stirred for 3 h at 0 °C, then overnight at RT. The resulting ketone-aluminium chloride complex was hydrolysed with diluted HCl. The yellow precipitate was separated and purified by recrystallization to obtain the ketones **13** and **14** in 34 and 63 % yields, respectively. A significantly lower yield of compound **13**, comparing to the 95 % reported by Nicolas *et al.*⁴², resulted from a partial loss of product during recrystallization.



Scheme 8 Synthesis of diaryl ketones **13** and **14**

3.1.7 Synthesis of 4-((2-(4-hydroxy-3,5-dimethylbenzoyl)-4-oxo-4*H*-chromen-6-yl)amino)-4-oxobutanoic acid **16**

Succinamic acid **16** (*Fig. 24*) was synthesized following the Method B described in *Chap. 3.1.5.2* from the 6-nitro derivative **14** via its 6-amino-intermediate **15** yielding a yellow solid in an overall yield 34 %.

Synthesis

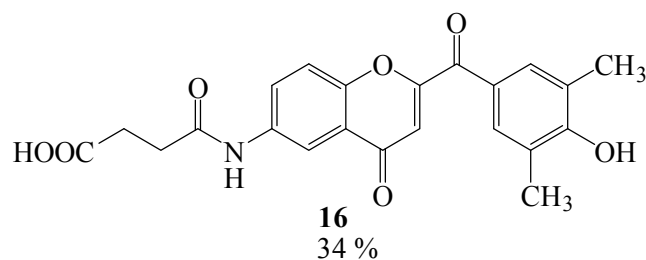
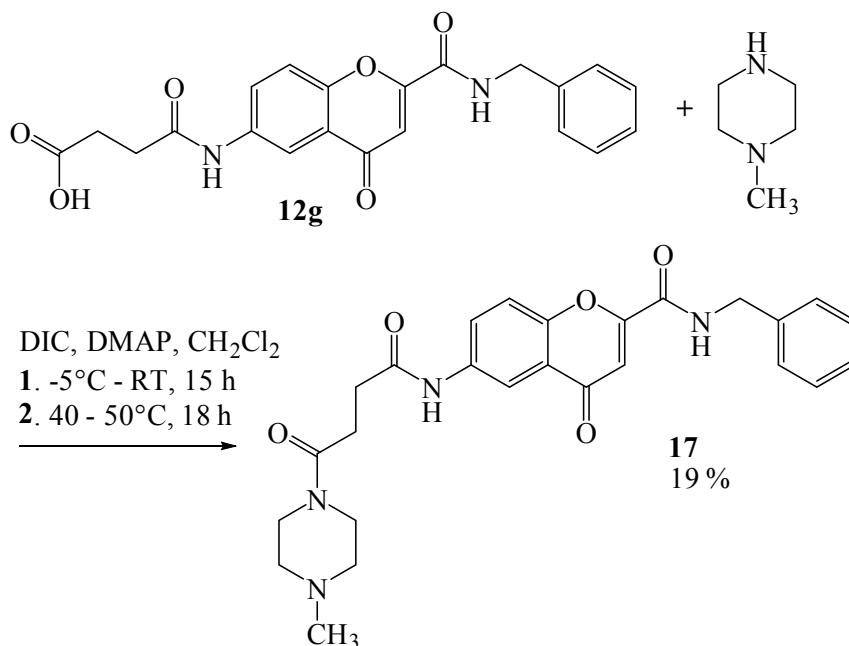


Fig. 24 Structure of compound **16**

3.1.8 Synthesis of *N*-benzyl-6-(4-(4-methylpiperazin-1-yl)-4-oxobutanamido)-4-oxo-4*H*-chromene-2-carboxamide **17**

Condensation of the succinamic acid **12g** with *N*-methylpiperazine was conducted in mild conditions, using *N,N'*-diisopropylcarbodiimide (DIC) as a coupling agent and *N,N'*-dimethylaminopyridine (DMAP) as an acylation catalyst, following the modified procedure reported by Guillaumel *et al.*⁴⁸ for coupling between piperazines and (*E*)-propenoyl derivatives. The formation of amide bond proceeds via unstable *O*-acylisourea intermediate, which reacts with *N*-methylpiperazine to yield the resulting amide (and *N,N'*-diisopropylurea as a by-product).



Scheme 9 Synthesis of compound **17**

The procedure is displayed in **Scheme 9**. Compound **12g**, suspended in anhydrous dichloromethane, was treated with equimolar amounts of DMAP and *N*-methylpiperazine. After cooling to -5 °C, 1.5 eq. of DIC were added. The mixture was then allowed to warm to RT and refluxed for 18 h. Finally, the reaction was quenched with water and the product was

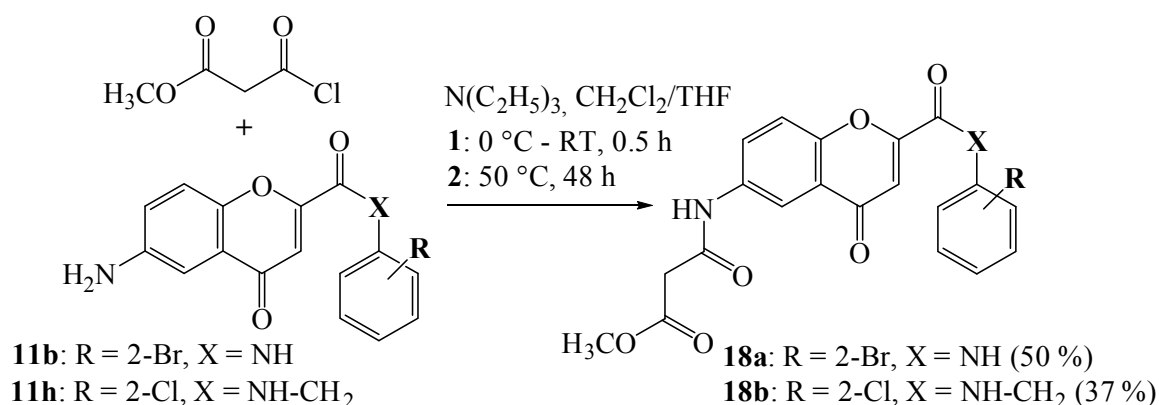
Synthesis

extracted with dichloromethane. Purification by column chromatography and a subsequent recrystallization yielded a white solid in 19 %.

3.1.9 Synthesis of methyl malonyl ester-amides of chromone-2-carboxylic acid **18a** and **18b**

Compounds **18a** and **18b** were prepared following the procedure reported by Lee *et al.*⁴⁹ used for the synthesis of mixed methyl malonyl ester-amides from 4-aminobenzophenone. The aminolysis of methyl malonyl chloride was conducted in a dichloromethane/THF mixture. Triethylamine was used as a non-nucleophilic amine to trap the HCl resulting from the amide formation.

The procedure is depicted in *Scheme 10*. Both starting compounds, the 6-amino-*N*-(2-bromophenyl)-4-oxo-4*H*-chromene-2-carboxamide (**11b**) and the 6-amino-*N*-(2-chlorobenzyl)-4-oxo-4*H*-chromene-2-carboxamide (**11h**), were dissolved in a dichloromethane/THF mixture. The subsequent treatment with 2 eq. of triethylamine and an equimolar amount of methyl malonyl chloride was conducted at 0 °C. The mixture was warmed up to 50 °C and stirred for 48 h. Finally, the reaction was quenched with aqueous sodium hydrogencarbonate solution. The crude products were extracted with dichloromethane. After recrystallization, fine crystalline powders were obtained in 50 and 37% yields, respectively.



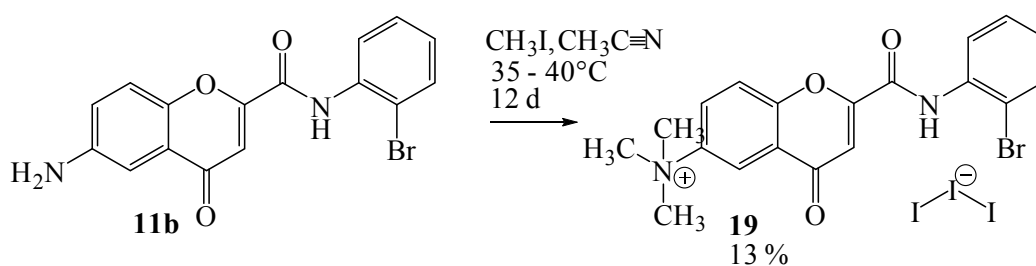
Scheme 10 Synthesis of the mixed ester-amides **18a-b**

3.1.10 Synthesis of 2-((2-bromophenyl)carbonyl)-*N,N,N*-trimethyl-4-oxo-4*H*-chromene-6-aminium triiodone **19**

N-Methylation of the 6-amino-*N*-(2-bromophenyl)-4-oxo-4*H*-chromene-2-carboxamide (**11b**) was performed by a classical way using methyl iodide as a methylation agent. Acetonitrile

Synthesis

was used as a polar aprotic solvent. As the quaternary ammonium salt was the aim of the synthesis, longer reaction time was required. The reaction is displayed in *Scheme 11*. The scarcely soluble 6-amino derivative was suspended in anhydrous acetonitrile and an excess of methyl iodide (20 eq.) was added. The mixture was stirred in a pressure-proved closed vessel protected from light for 12 days at temperature not exceeding 40 °C (oil bath). The conversion was monitored by TLC. Afterwards, the reaction was quenched with ice water. The precipitate was separated and recrystallized to give a brown crystalline solid in a 13% yield.



Scheme 11 Synthesis of the quaternary ammonium salt **19**

3.2 Synthesis of the pyrimidine derivatives

The second model structure obtained from the virtual screening on *KasA* inhibitors³⁸, the pyrimidin-2-one derivative **22a** (*Fig. 25*) was modified in positions 2, 4, 5 and 6 of the pyrimidine ring.

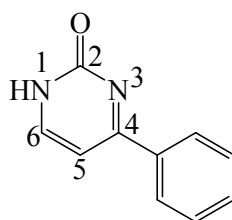


Fig. 25 Structure of compound **22a**

The starting compounds used for the synthesis of the pyrimidine derivatives **21a-e** and **22a-e** were either corresponding enaminones (**20a-b**, *Scheme 12*) or β -diketones (*Scheme 13*). Attempts using an acid-catalyzed condensation of β -diketones directly with urea, following the procedure reported by Evans⁶¹ or its modification for a microwave reactor (1000 W, 165 °C, 10 min, both compounds adsorbed on acidic aluminium oxide), gave very low yields (*e.g.* a 5% yield in the case of **22c**). Therefore, guanidine was used as a N-C-N component for the pyrimidine synthesis. The obtained pyrimidin-2-amines (**21a-e**) were subsequently converted to the corresponding pyrimidin-2-ols (**22a-e**). The synthesis of 1,4-

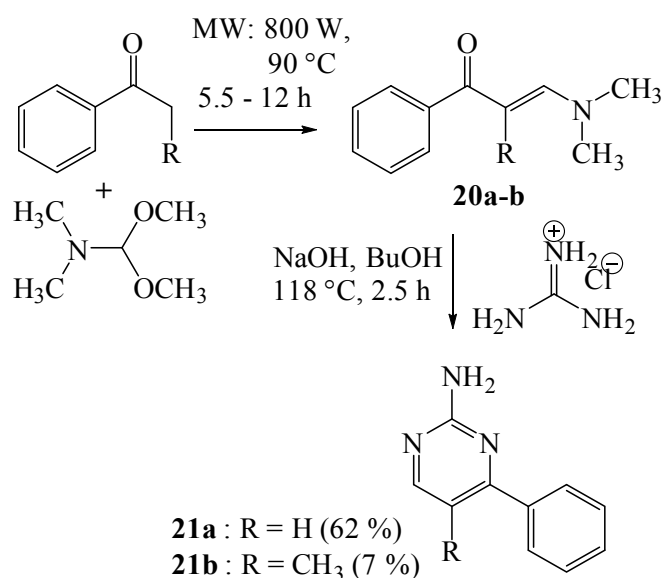
Synthesis

dihydropyrimidine **23** was performed using three reaction components: benzaldehyde, ethyl acetoacetate and urea. Generally, the syntheses required high temperatures and long reaction times, therefore, microwave-assisted synthesis procedures were applied. To enable the heating of nonpolar molecules, a ionic liquid, 1-butyl-3-methylimidazolium chloride, was used as a convenient microwave-absorbing medium. The application of ionic liquids as alternative reaction solvents has been largely implemented in microwave synthesis methods.⁶²

3.2.1 Synthesis of pyrimidin-2-amines **21a-e**

Method A

Both 6-nonsubstituted pyrimidine derivatives **21a** and **21b** were prepared in two steps following a modified procedure reported by Larina *et al.*⁶³ A condensation reaction of arylalkylketone with DMF-dimethyl acetal was performed in microwave reactor. The formed enaminones **20a-b** were subsequently condensed with guanidine while refluxing in butanol for 2.5 h. Finally, the recrystallization of the formed precipitates gave white solids in overall yields 62 and 7 %, respectively.

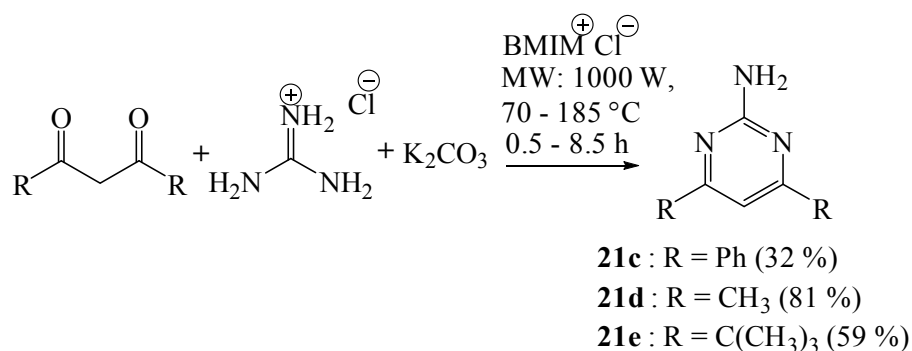


Scheme 12 Synthesis of pyrimidin-2-amines **21a** and **21b**

Method B

The pyrimidin-2-amines **21c-e** were synthesized in one step in a microwave reactor from the corresponding β -diketones and guanidine. An excess of 1-butyl-3-methylimidazolium chloride (BMIM Cl) was added to each mixture. The precipitated products were purified by column chromatography to give white solids in 32 – 81 %.

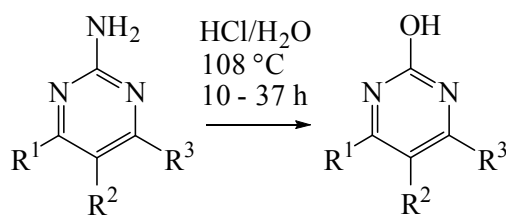
Synthesis



Scheme 13 Synthesis of pyrimidin-2-amines **21 c-e**

3.2.2 Synthesis of pyrimidin-2-ols **22a-e**

A conversion to pyrimidin-2-ols was performed in the next step by acid hydrolysis in boiling 6M HCl following the procedure reported by Teixido *et al.*⁶⁴ (see *Scheme 14*). The products were obtained by recrystallization or column chromatography in 27 – 78% yields.



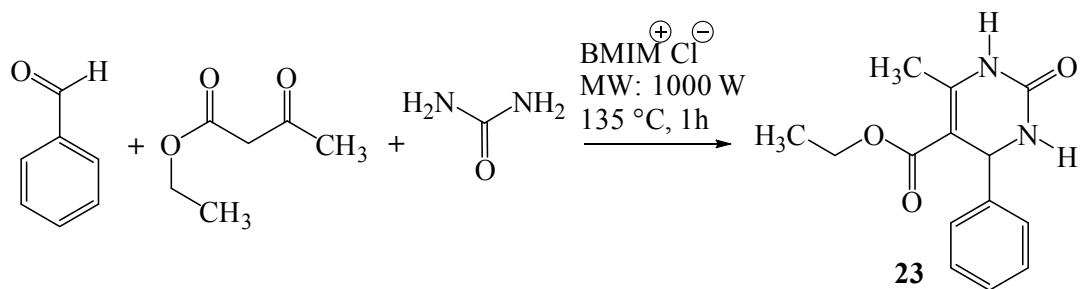
- 22a** : R¹ = H, R² = H, R³ = Ph (78 %)
22b : R¹ = H, R² = CH₃, R³ = Ph (47 %)
22c : R¹ = R³ = Ph, R² = H (27 %)
22d : R¹ = R³ = CH₃, R² = H (40 %)
22e : R¹ = R³ = C(CH₃)₃, R² = H (73 %)

Scheme 14 Synthesis of pyrimidin-2-ones **22a-e**

3.2.3 Synthesis of ethyl 6-methyl-2-oxo-4-phenyl-1,2,3,4-tetrahydropyrimidine-5-carboxylate **23**

The Biginelli synthesis of compound **23** was performed following a modified procedure reported by Joseph *et al.*⁶⁵ (see *Scheme 15*). The mixture of grinded urea mixed with equimolar amount of benzaldehyde and excess amount of ethyl acetoacetate was heated under microwave irradiation using 1-butyl-3-methylimidazolium chloride as a solvent. The product was obtained after recrystallization in a 24% yield.

Synthesis



Scheme 15 Biginelli synthesis of **23**

3.3 NMR Spectroscopy

3.3.1 NMR Spectroscopy of the chromone derivatives

¹H- and ¹³C-signals were assigned using 1D- and 2D-NMR experiments (¹H- and ¹³C-chemical shifts, DEPT, COSY, HMQC and HMBC) performed in deuterated DMSO. The results are summarized in the Experimental section. The assignment of ¹H NMR data is explained on cyclohexylamide **4k** and its corresponding succinamic acid derivative **12e**, exemplarily.

3.3.1.1 ¹H NMR spectrum of the chromone-2-carboxamide **4k**

Although the compound **4k** has already been described by Gaspar *et al.*⁵⁰, the following analysis of its ¹H NMR spectrum (*Fig. 26*) provides more accurate data.

Synthesis

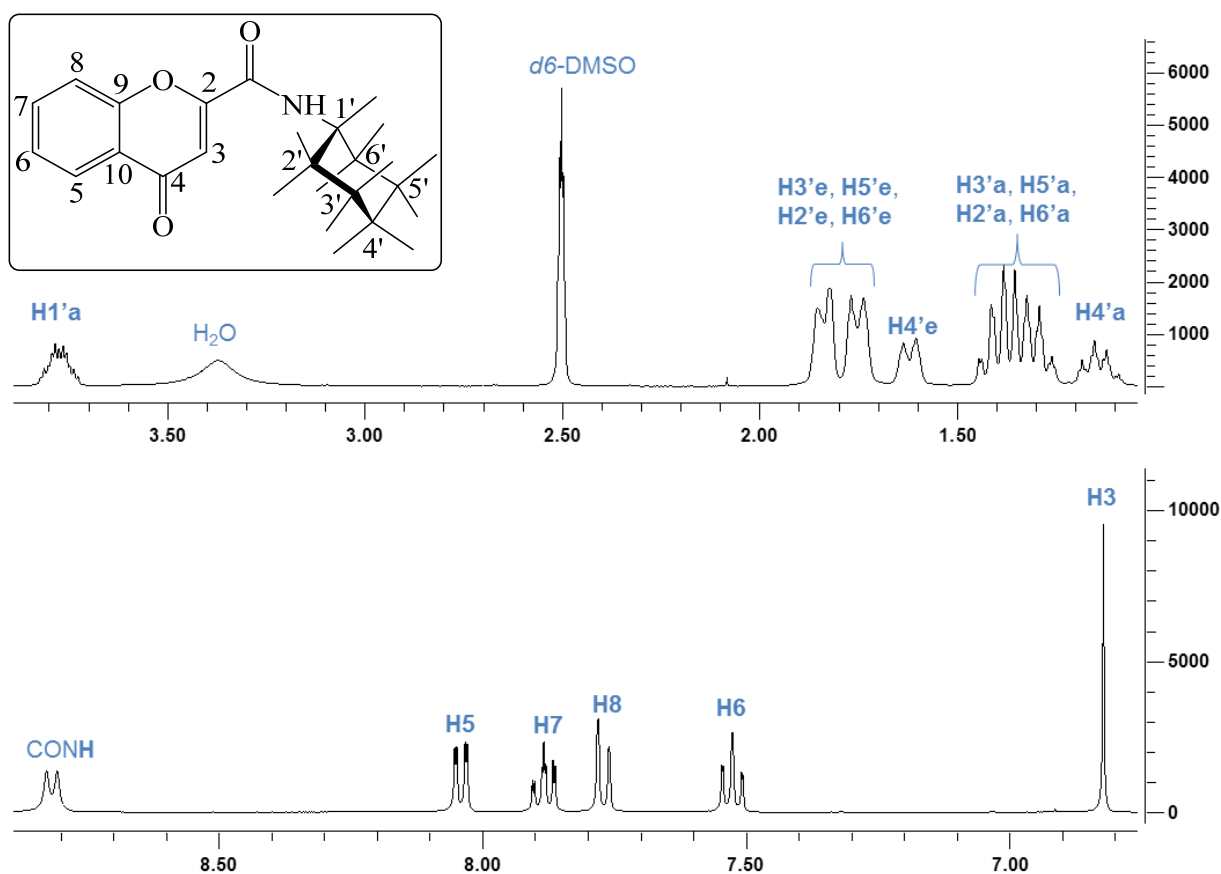


Fig. 26 $^1\text{H-NMR}$ spectrum of **4k** (x axis: chemical shift in ppm, y axis: signal intensity)

The singlet at $\delta = 6.82$ was easily assigned to **H3** of the chromone skeleton. It displayed a long-range correlation with the carbons **C4**, **C10**, **C2** and with the carbonyl carbon of the amide group. The signal of **H5** appears as a double doublet at $\delta = 8.04$ formed by coupling to *ortho*-**H6** and *meta*-**H7** ($^3J = 7.8$, $^4J = 1.6$); **H7** is splitted to a doublet of a double doublet at $\delta = 7.88$ ($^3J_{\text{H7}, \text{H8}} = 8.1$, $^3J_{\text{H7}, \text{H6}} = 7.7$, $^4J_{\text{H7}, \text{H5}} = 1.6$); **H8** appears as a double doublet at $\delta = 7.77$ ($^3J = 8.1$, $^4J = 0.8$) and **H6** is described as a doublet of a double doublet at $\delta = 7.52$ ($^3J_{\text{H6}, \text{H5}} = 7.8$, $^3J_{\text{H6}, \text{H7}} = 7.7$, $^4J_{\text{H6}, \text{H8}} = 0.8$). In the paper published by Gaspar *et al.*⁵⁰, the signals **H6** and **H5** are defined improperly as a double doublet and a doublet, respectively. Finally, the hydrogen attached to the amide nitrogen appears as a doublet at $\delta = 8.82$ splitted by **H1'** ($^3J = 8.0$). Regarding the cyclohexyl ring, an equatorial alignment of cyclohexyl to the amide nitrogen was assumed from steric considerations. Thus, a multiplet at $\delta = 3.78$ was attributed to the axially aligned **H1'**. The typical upfield shift of the axial hydrogens on the cyclohexyl rest, in comparison to the equatorial hydrogens, was confirmed using 2D NMR methods. The multiplets at $\delta = 1.35$ and $\delta = 1.79$, were assigned to the axial and equatorial hydrogens **H2'**, **H6'**, **H3'** and **H5'**, respectively. The remaining multiplets at $\delta = 1.15$ and $\delta = 1.62$ were ascribed to **H4'a** and **H4'e**, respectively.

Synthesis

3.3.1.2 ^1H NMR spectrum of the succinamic acid **12e**

The ^1H NMR spectrum of **12e** is displayed in *Fig. 27*. As the amide part is identical to the one of **4k**, the description is focused on the influence of succinamidyl substituent in position 6 of the chromone ring.

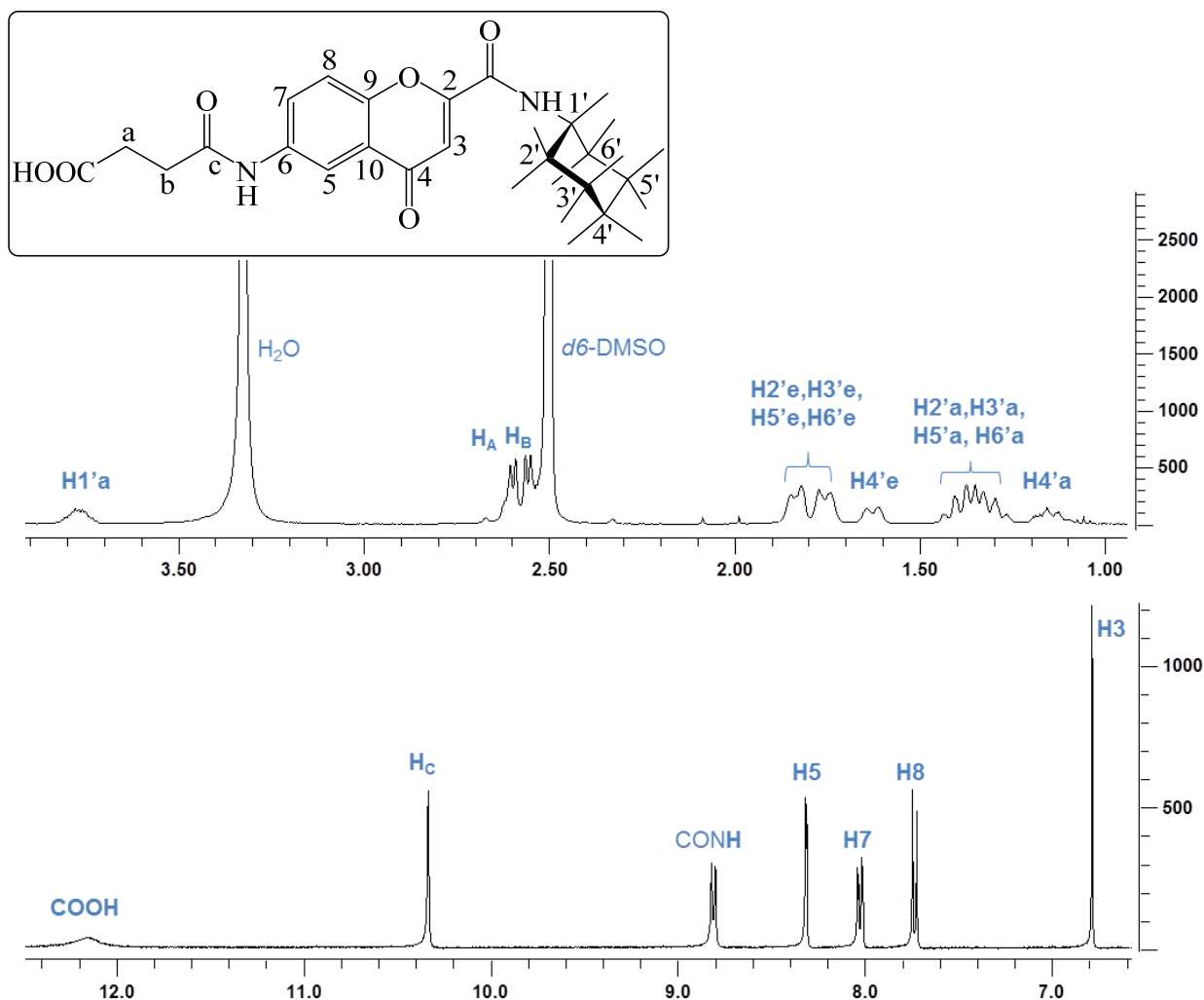


Fig. 27 ^1H -NMR spectrum of **12e** (*x* axis: chemical shift in ppm, *y* axis: signal intensity)

The substitution of hydrogen in position 6 of the chromone ring reduces the multiplicity of the neighbouring signals **H5** and **H7** to a doublet at $\delta = 8.31$ and a double doublet at $\delta = 8.02$, respectively ($^3J = 9.2$, $^4J = 2.7$). The scarcely influenced **H8** appears as a doublet at $\delta = 7.73$ ($^3J = 9.2$). The chemical shift values are influenced by the electron-withdrawing inductive effect of the succinamidyl residue. At most pronounced is the deshielding effect on the *ortho*-hydrogen **H5** (+ 0.27 ppm, compared to **4k**). Regarding the succinic acid chain, both multiplets of the ethylene hydrogens were distinguished by their $^1\text{H} - ^{13}\text{C}$ long-range correlations. The multiplet at $\delta = 2.61$ ppm, assigned to **Ha**, correlated with the amide carbon signal at $\delta = 170.51$ (Cc), whereas the multiplet at $\delta = 2.55$, assigned to **Hb**, displayed a

Synthesis

coupling to the carboxyl carbon at $\delta = 173.73$. The amide hydrogen **Hc** appeared as a singlet at $\delta = 10.33$, displaying long range correlations with the aromatic carbons **C5**, **C7** and the amide carbon **Cc**. Finally, the most downfield shifted signal, a broad singlet at $\delta = 12.15$, was assigned to the carboxyl hydrogen. Obtained ^1H and ^{13}C chemical shifts of the succinic acid moiety are in accordance with the data published by Trujillo-Ferrara *et al.*⁵¹

3.3.1.3 Discussion on the obtained and published NMR data of the synthesized chromone derivatives

3.3.1.3.1 Published ^1H NMR data of the synthesized chromones

^1H NMR data of chromone-2-carboxamides **3a**⁵², **3b**⁵³, **3e**⁵⁴, **3g**⁵⁴, **3n**⁵³, **3o**⁵³, **3p**⁵³, **4a**⁵⁵, **7c**⁵⁶, 6-nitro-chromone-2-carboxamide **9f**⁵⁷ and diarylketone **13**⁴² have already been reported. In case of **3b**, the assignment of the ^1H signals on the benzene ring was reversed comparing to the published results (see *Fig. 28*). For compounds **3a**, **3e** and **3g**, the allocation of reported ^1H signals was not specified. The spectral data for the above carboxamides **3n-p**, **4a** and **7c** as well as for the diarylketone **13** are consistent with the given references. Compound **9f** was described in Japanese.

Assignment of ^1H NMR signals to the benzene hydrogens in compound **3b**

Due to a negative inductive effect of bromine, the most downfield shifted signal, a double doublet at $\delta = 7.78$, attached to the carbon at $\delta = 132.87$, was attributed to the ortho-**H3'** hydrogen. The neighbouring signals were determined using $^1\text{H} - ^1\text{H}$ correlations (*Fig. 28*). The assignment was confirmed by long-range $^1\text{H} - ^{13}\text{C}$ correlations between 1) a carbon signal at $\delta = 135.05$, assigned to **C1'**, and both hydrogens **H5'** and **H3'**, and 2) a carbon signal at $\delta = 120.11$, assigned to **C2'**, coupling to **H4'**, **H6'** and to the hydrogen attached to the amide nitrogen.

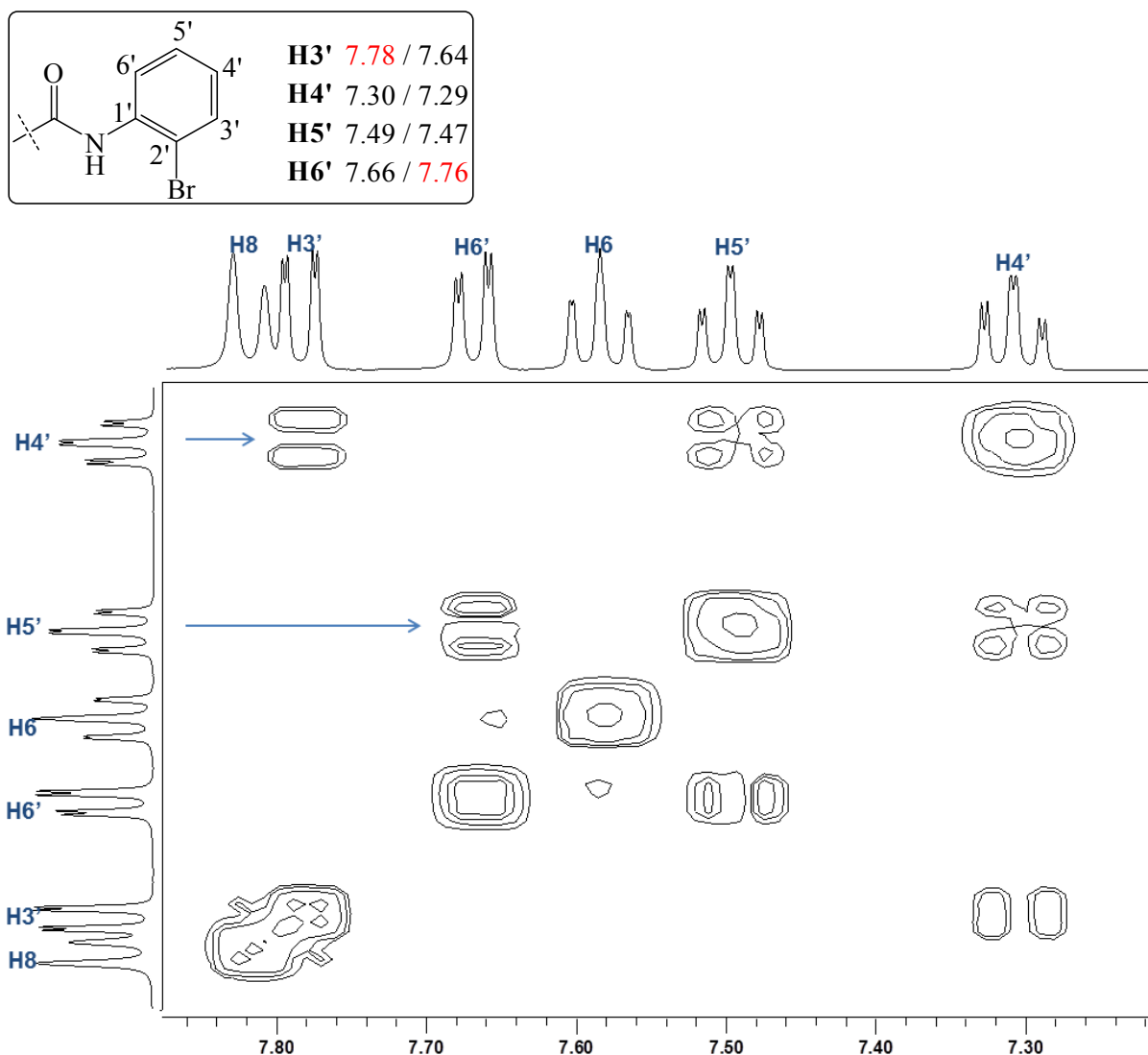


Fig. 28 ^1H NMR signals for the benzene hydrogens of **3b** in δ ppm measured/ published⁵³ (both in DMSO). A section of COSY NMR diagram displaying the correlations between the neighbouring **H3'/H4'** and **H5'/H6'** atoms, respectively.

3.3.1.3.2 Published ^{13}C NMR data of the synthesized chromones

^{13}C NMR spectra for carboxylamides **3b**, **3n**, **3o** and **3p** were reported by Gaspar *et al.*⁵³ Apart from the reversed allocation of the benzene carbons in case of **3b**, due to the reversed assignment of the corresponding ^1H signals, there is a disparity in the assignment of **C2** and **CONH** in all the published compounds. In the article by Gaspar *et al.*⁵³, the carbon signal displaying long range correlations with the amide hydrogen and the hydrogen **H3** was attributed to the quaternary carbon **C2**, whereas the ^{13}C signal coupling only to **H3** was associated with the amide carbon. An opposite assignment was obtained from the data measured here and their comparison among similar compounds. The HMBC diagram of benzylamide **4a** depicted in *Fig. 29* confirms, that the ^{13}C signal coupling to **NH** and **H3**

Synthesis

belongs to the amide carbon, due to its additional long range correlations with the signal of the methylene hydrogens.

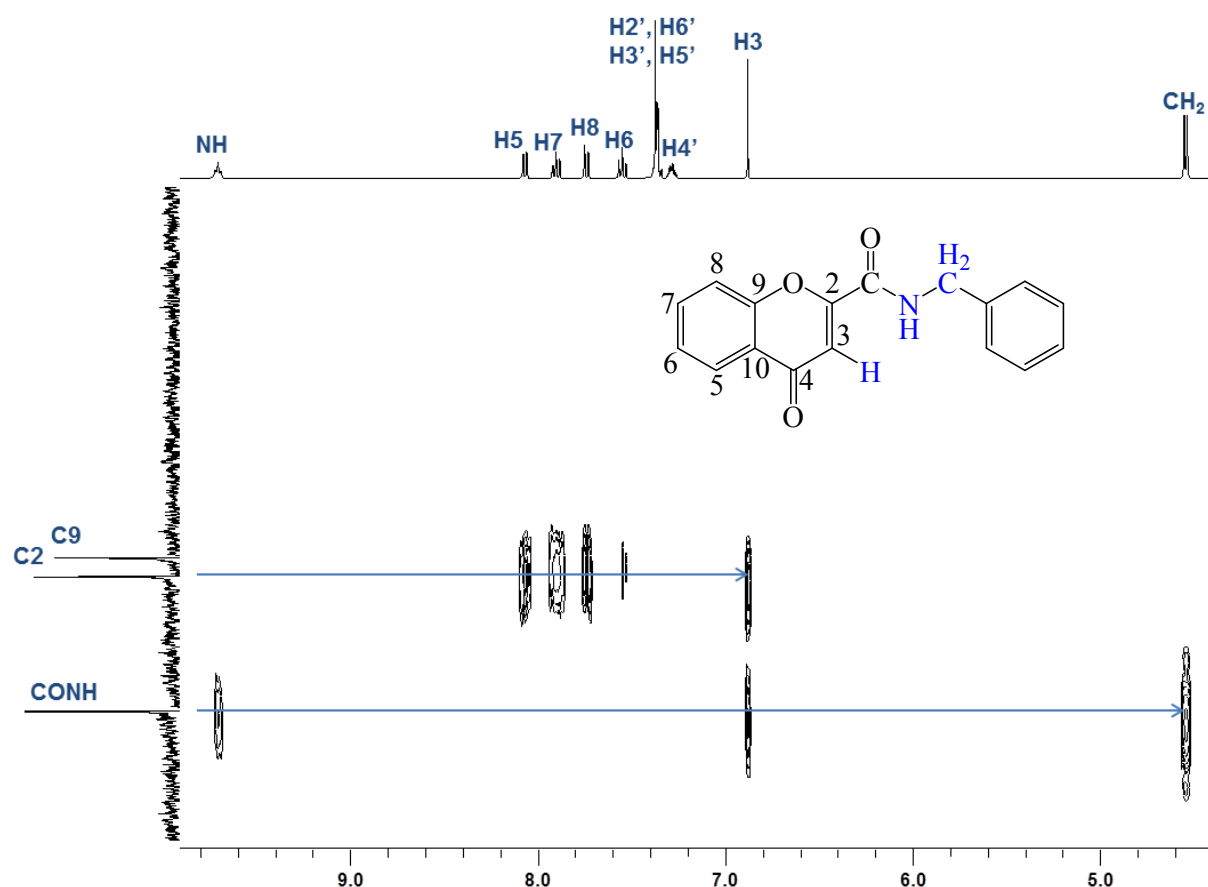


Fig. 29 A section of HMBC NMR diagram of the long-range ^1H - ^{13}C connectivity for **4a** determines the CONH ^{13}C signal as the signal coupling to the amide hydrogen (chemical shift in ppm)

3.3.1.3.3 Rotational isomerism in a series of prepared chromone-2-carboxamides and their 6-substituted derivatives

Due to a pronounced steric hindrance to rotation around both the C2 – CO and CO – N bonds, four conformations of the amide spacer are possible in the chromones synthesized (see **Fig. 30**). *Cis*- and *trans*-rotamers differ in the orientation of the amide carbonyl group, whereas *syn*- and *anti*-rotamers are characterized by a different position of substituents at the amide nitrogen.⁵⁸ Due to a possible formation of an intramolecular hydrogen bond between the amide nitrogen hydrogen and the oxygen in position 1 of the chromone ring, the *trans*-configuration might be energetically more favourable. Accordingly, a characteristic downfield shift (> 9 ppm) of the amide hydrogen, involved in hydrogen bond can be observed for most of the synthesized chromone-2-carboxamides. Finally, the majority of recently reported

Synthesis

crystal structures of *N*-phenyl-chromone-2-carboxamides are nearly planar and assume the *anti/trans*-rotamer configuration as a preferred arrangement in a solid state.^{59,60}

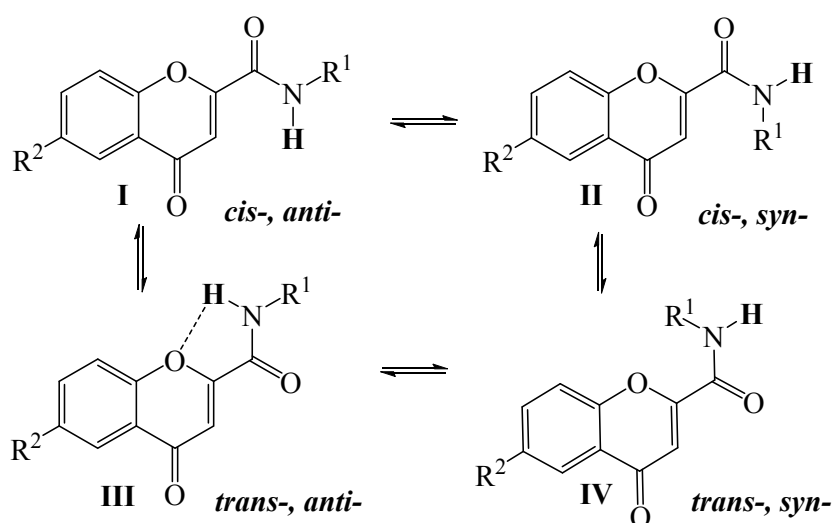


Fig. 30 Four possible conformations of the amide spacer in chromone-2-carboxamides: R^1 = aryl(alkyl)/cyclohexyl(methyl), R^2 = H / NO_2 / $\text{NH-CO-C}_2\text{H}_4\text{-COOH}$. The hydrogen bond between NH and O1 is shown as a dashed line.

A splitting of ^1H and ^{13}C NMR signals was observed in case of compounds **9i** (R^1 = benzyl, R^2 = CH_3 , R^3 = NO_2) and **12i** (R^1 = benzyl, R^2 = CH_3 , R^3 = $\text{NH-CO-C}_2\text{H}_4\text{-COOH}$) only. Both structures contain a tertiary amide moiety. Due to the absence of $\text{N-H}\cdots\text{O}$ hydrogen bond and due to a steric hindrance by the *N*-methyl group, the amide spacer is directed out of the chromone plane and the *cis/trans*-configuration is not possible anymore. The signal splitting is thus attributed to a slow conversion between *syn*- and *anti*-rotamers. A chemical shift difference (expressed as $\Delta\delta$) between the splitted signals measured for compound **9i** is shown in **Fig. 31**. Nearly all hydrogen and carbon atoms are affected. Interestingly, the greatest difference ($\Delta\delta = 0.3$) in ^1H NMR spectrum was detected for **H8**. The highest ^{13}C NMR $\Delta\delta$ values were observed as expected for the both carbon atoms of the amide substituents attached to the amide nitrogen (methylene and methyl, $\Delta\delta = 3.29$ and 2.99 , respectively).

The *syn*-configuration is highly disadvantaged in a series of *N*-phenyl-chromone-2-carboxamides, due to the close proximity of both aromatic rings (see **Fig. 30**, where R^1 = phenyl). In the case of *N*-benzylamides **9i** and **12i**, the ratio of *syn/anti*-configuration is nearly 1:1, when dissolved in DMSO (see Experimental section, **Chap. 7.2.5**, **Chap. 7.2.6**).

Synthesis

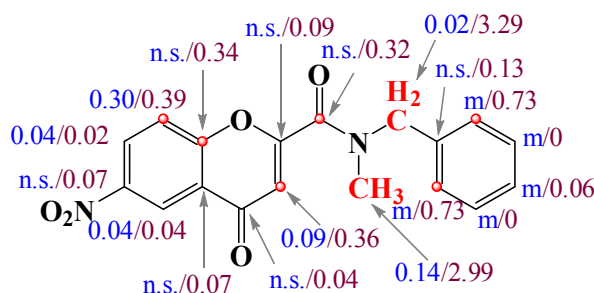


Fig. 31 Signal splitting in compound **9i**: ^1H NMR (blue)/ ^{13}C NMR (purple) $\Delta\delta$ values. The atoms with the highest $\Delta\delta$ values are marked red (n.s. = no signal, m = multiplet)

3.3.2 NMR Spectroscopy of the pyrimidine derivatives

All products synthesized are well known from literature. Though, not all of them have been identified by means of NMR spectroscopy. The ^1H NMR spectra have been reported for all the pyrimidin-2-amine derivatives **21a-e**⁶⁶⁻⁷⁰ and are consistent with the data obtained here. The ^{13}C NMR spectra for **21c** and **21d** are in accordance with the references^{68,71}. The ^1H NMR signals of the pyrimidin-2-ols **22a**, **22c** and **22d** are consistent with the published data⁷²⁻⁷⁴. In the case of compound **22e**, the reported ^1H NMR signals⁷⁵ of the tautomeric pyrimidin-2-one differ from the measured data, which correspond to the pyrimidin-2-ol tautomer (see **Fig. 32** and **Fig. 33**). The reported ^{13}C NMR spectra of **22c** and **22d**^{72,73} are in accordance with the measured values.

3.3.2.1 Lactam-lactim tautomerism of the 2-hydroxy-substituted pyrimidines

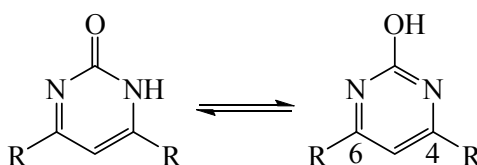


Fig. 32 Lactam-lactim tautomers of 2-hydroxy-substituted pyrimidine derivatives.

The equilibrium between the tautomeric forms of pyrimidin-2-one and pyrimidin-2-ol depends on the state of matter, solvent, and the ring substituents. Crystalline state, polar solvents and substitution by an electron-withdrawing group in position 4 or 6 shift the equilibrium toward the lactam (2-oxo-) form.¹²⁴ As reported by Galvao *et al.*¹²⁵, the lactim tautomer is generally more stable in 2-hydroxy-substituted pyrimidines than in the isomeric pyrimidin-4-ols. By comparison of the NMR spectra obtained here with the published data⁷²⁻⁷⁵, the measured signals were ascribed to the lactim tautomer. Nevertheless, it can be assumed that in the testing conditions (Tris buffer, pH 8.5) the lactam form predominates.

Synthesis

3.3.2.2 ^1H NMR Spectrum of the pyrimidine derivative **22e**

A comparison between obtained and published ^1H NMR signals of compound **22e** is shown in **Fig. 33**. The reported chemical shift at $\delta = 4.90^{75}$ (in CDCl_3) was ascribed to the lactam **NH** hydrogen. The measurement here was conducted in DMSO. Despite the use of more polar solvent, the compound was characterized as the lactim tautomer.

The most upfield-shifted signal at $\delta = 1.23$ belongs to the 18 hydrogens of the both *tert*-butyl groups. Another singlet at $\delta = 6.29$ was assigned to **H5** and finally, the most deshielded broad signal at $\delta = 11.36$ was attributed to the hydroxyl hydrogen in position 2 of the pyrimidine ring.

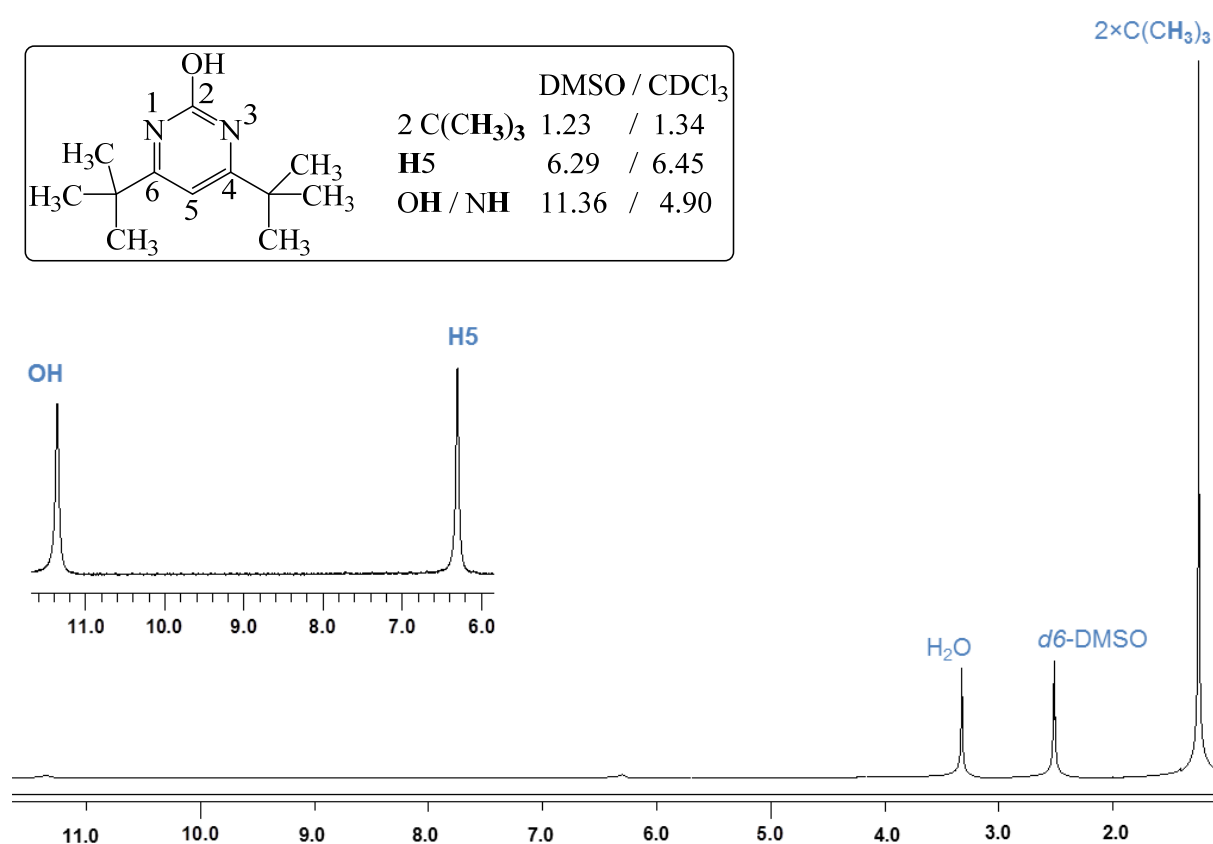


Fig. 33 ^1H NMR spectrum of **22e** and δ ppm of the obtained (DMSO) vs. published (CDCl_3)⁷⁵ signal

4 Biological testing

First, the affinity to KasA was evaluated in a direct binding assay in order to select the most promising inhibitors from each group of structurally similar compounds for further kinetic enzyme assay in order to verify the TLM-like binding mechanism. Additionally, the antimycobacterial properties of all synthesized compounds were evaluated in the whole cells, restraining the enzyme inhibitors to the candidates capable to permeate the mycobacterial membrane. Some products and intermediates were also screened for their antimicrobial properties within the SFB 630. A major problem limiting the biological testing were solubility issues. Experiments on compound solubilization by means of cyclodextrin inclusion are summarized in *Chap. 4.5.3*. Since these attempts were inefficient, derivatives possessing improved aqueous solubility were prepared by chemical modification of the inhibitors preserving the structural features essential for the interaction with KasA.

4.1 KasA direct binding assay

4.1.1 Introduction

The affinity or dissociation constant K_D describes the affinity of an inhibitor to enzyme. The lower the K_D value, the higher the binding affinity. For the binding of TLM to KasA, a slow-onset inhibition mechanism was observed.²⁹ Hence, the binding equilibrium is formed in two steps. The binding rate of each step is characterized by a different affinity constant as described by *Equation 1*. The formation of the initial enzyme-inhibitor (E-I) complex is rapid in comparison to the slow speed formation of the more stable E-I* complex.⁷⁶ A slow-onset binding mechanism is characteristic for tight binding inhibitors. The slow dissociation rate of the E-I* complex is of advantage due to the longer residence time of the inhibitor in the enzyme active site.⁷⁷



The inhibitor binding to KasA was quantified by monitoring of the rapid change in intrinsic tryptophan fluorescence of the enzyme. Therefore, only the initial equilibrium values (K_D) were assessed. The inhibitor is supposed to induce a conformational change in the active site, that is accompanied by a decreased fluorescence emission of the four tryptophan residues

Biological testing

located at each KasA monomer.³⁹ For illustration of the intrinsic enzyme fluorescence, the recorded excitation and emission spectra of KasA in phosphate buffer solution are displayed in *Fig. 34*. The excitation and emission wavelengths used in the binding assay (280 and 337 nm, respectively) were adopted from the procedure reported by Machutta *et al.*²⁹

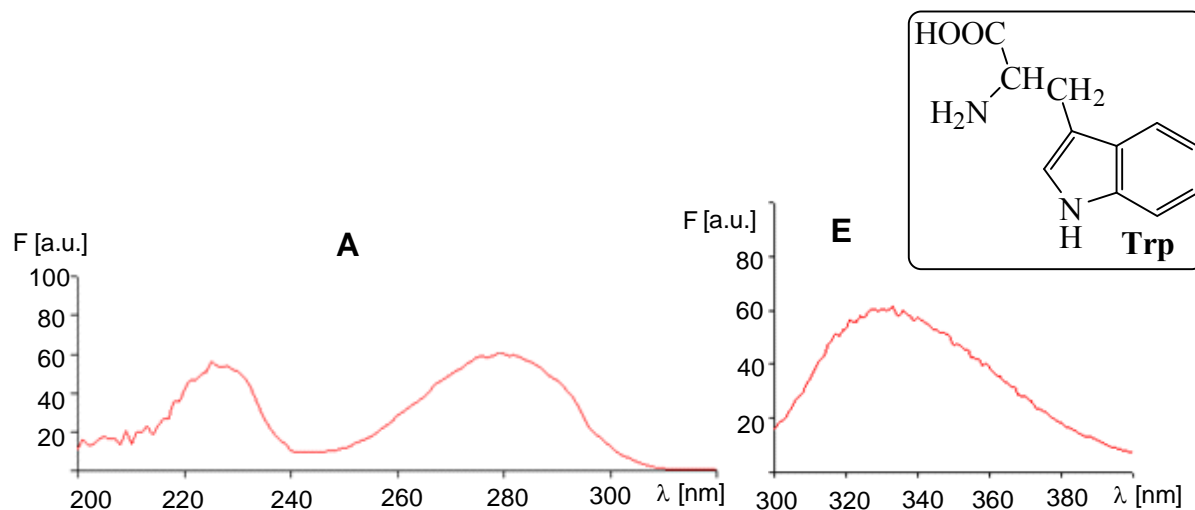


Fig. 34 Recorded absorption (A) and emission (E) fluorescence spectra of wt-KasA originating in enzyme tryptophan residues

A correction of the obtained fluorescence intensities for a time-dependent quenching of the background fluorescence was not necessary, as no significant fluorescence decrease was observed during the time of sample measurement (ca 10 min, see *Fig. 35*).

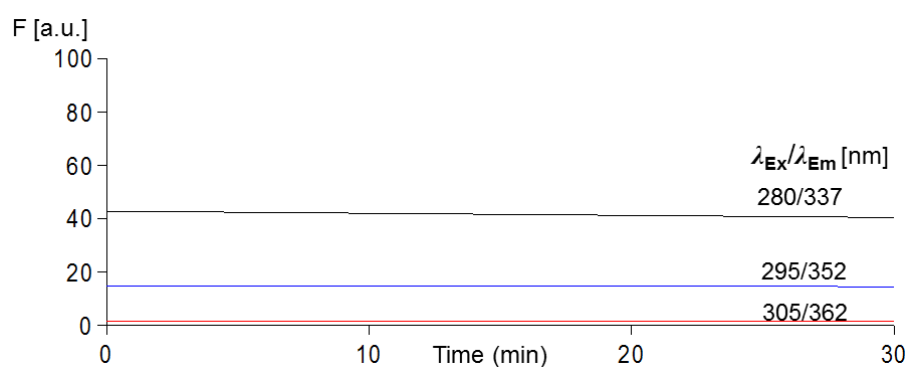


Fig. 35 Intrinsic tryptophan fluorescence of KasA as a function of time

4.1.2 Methods

4.1.2.1 Method A

The first method followed the procedure reported by Topf⁷⁸. An appropriate volume of the enzyme solution (wt-KasA in CHES buffer, see *Chap. 7.5.1*) was pipetted to 0.5 ml of Tris buffer in a cuvette in order to obtain a 0.5 μM enzyme concentration in sample. The intrinsic

Biological testing

tryptophan fluorescence (F_0) was measured. The 5 mM inhibitor solution was titrated into the enzyme/buffer mixture in 10 μM steps from 10 to 40 μM , then in 20 μM steps to reach the concentration of 300 μM . For each step, fluorescence (F) was recorded in triplicate and the values were averaged. TLM-solution was measured in 20 μM steps from 20 to 100 μM , then in 100 μM steps until 1000 μM concentration was reached. Titration curves were corrected for dilution in order to keep the 0.5 μM enzyme concentration and given inhibitor concentrations (I) using linear regression. Fluorescence values expressed as fluorescence change ($FC = F_0 - F$) were fit to a non-linear equation (*Equation 2*) to obtain the dissociation constant K_D and FC_{max} (maximal fluorescence change) values using “Origin“ software.

$$FC = \frac{FC_{\text{max}} \cdot I}{K_D + I} \quad (\text{Equation 2})$$

4.1.2.2 Method B

In order to obtain more reliable data, Method A was modified as follows:

1) Equal concentrations of DMSO stock-solutions and equal titration scheme for samples and reference (TLM) were used. In order to minimize the enzyme denaturation by DMSO, 10 mM stock solutions were prepared. For titration scheme see *Tab. 1*. Due to solubility issues, only lower concentrations were used for some of the compounds (usually < 280 μM).

Tab. 1 Titration scheme for TLM and inhibitors showing the inhibitor concentration steps and the percentage DMSO concentration in each step

c [μM]	0	20	40	60	80	100	120	140	160	180	200
DMSO [%]	0	0.2	0.4	0.6	0.8	1.0	1.19	1.38	1.57	1.77	1.96
c [μM]	220	240	260	280	380	480	580	680			
DMSO [%]	2.15	2.34	2.53	2.72	3.66	4.58	5.48	6.37			

2) Obtained fluorescence data were further corrected for inner-filter effect (IFE) using the equation proposed by Lakowicz⁷⁹ (see *Equation 3*) applicable for the right-angled cell geometry of the fluorimeter. The IFE embraces the attenuation of some of the light before it reaches the midpoint of the cuvette (where the fluorescence is observed) and of the emitted light before it leaves the cell owing to absorption by sample components. Hence, sample absorbance at excitation (A_{Ex}) and emission wavelength (A_{Em}) was recorded for each concentration step. The placement of the cuvette was adjusted in order to reach the lowest possible values for $A_{\text{Ex}} \times d$ and $A_{\text{Em}} \times s$, where d and s stand for the excitation and emission light pathways. The IFE correction is important but turns out erroneous at higher absorbance

Biological testing

values due to non-linearity of the Beer-Lambert's law.⁸⁰ In *Equation 3*, I_{corr} stands for the corrected fluorescence intensity, I_{obs} for the observed one.

$$I_{\text{corr}} = I_{\text{obs}} \cdot 10^{(A_{\text{Ex}} \cdot d + A_{\text{Em}} \cdot s)/2} \quad (\text{Equation 3})$$

3) Dissociation constant K_D was calculated using quadratic Morrison equation (*Equation 4*) which accounts also for the enzyme concentration (E_0) in case of tight inhibitors. Consequently, K_D values were obtained from *Equation 2* with nearly the same results. Both calculations were performed using „R“ software. The template was created by B. Merget following the instructions for Morrison equation in GraFit, vers.7. In *Equation 4*, FC stands for fluorescence change at inhibitor concentration (I) normalized to FC_{max} ($FC_{\text{max}} = 1$). E_0 corresponds to the total enzyme concentration ($E_0 = 0.5 \mu\text{M}$).

$$FC = \frac{K_D + E_0 + I - \sqrt{(K_D + E_0 + I)^2 - 4 \cdot E_0 \cdot I}}{2 \cdot E_0} \quad (\text{Equation 4})$$

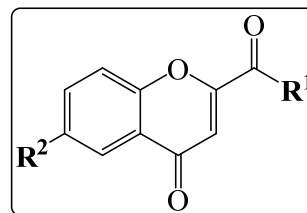
4.1.3 Results

Dissociation constants obtained from the direct binding assay provide information about the affinity of inhibitor to enzyme, yet not about its binding specificity. Hence, they can be compared among structurally very similar compounds only, for which the same binding mode can be assumed. Inhibitors displaying the highest affinity in the given structural group will undergo a kinetic enzyme assay described later in this chapter. Due to the limited enzyme batches and solubility issues, only selected compounds have been tested using the optimized Method B (see K_D^1 values). Reported K_D^2 values were acquired from previous measurements performed in many cases by C. Topf using the Method A^{39,78}. These results were additionally corrected on IFE.

Biological testing

4.1.3.1 Results for the chromone-based compounds

The affinity constants are summarized in *Tab. 2* and *Tab. 3*.



Tab. 2 K_D values for compounds **3a-9d** (n.d. = not determined)

	R^1	R^2	K_D^1	K_D^2
3a	-NH-C ₆ H ₅ *	-H	286.7 ± 5.2	n.d.
3b	-NH-(2-Br)-C ₆ H ₄ *	-H	n.d.	79.7 ± 10.2
3c	-NH-(2-Br,5-NO ₂)-C ₆ H ₃ *	-H	n.d.	n.d.
3d	-NH-(2,6-di-Br)-C ₆ H ₃ *	-H	n.d.	97.8 ± 6.4
3e	-NH-(2,6-di-Cl)-C ₆ H ₃ *	-H	n.d.	128.8 ± 12.3
3f	-NH-(2,5-di-Cl)-C ₆ H ₃ *	-H	n.d.	103.7 ± 20.6
3g	-NH-(2,4-di-Cl)-C ₆ H ₃ *	-H	n.d.	n.d.
3h	-NH-(2-I)-C ₆ H ₄ *	-H	n.d.	118.0 ± 15.0
3i	-NH-(2-F)-C ₆ H ₄	-H	n.d.	92.9 ± 2.2
3j	-NH-(4-F)-C ₆ H ₄ *	-H	n.d.	86.8 ± 5.8
3k	-NH-(3-Cl;4-CN)-C ₆ H ₃ *	-H	n.d.	127.4 ± 17.0
3l	-NH-(2-CH ₃ ;4-NO ₂)-C ₆ H ₃ *	-H	n.d.	n.d.
3m	-NH-(3,4-di-CH ₃)-C ₆ H ₃ *	-H	n.d.	n.d.
3n	-NH-(2-OCH ₃)-C ₆ H ₄ *	-H	165.0 ± 3.9	117.3 ± 22.8
3o	-NH-(3-OCH ₃)-C ₆ H ₄	-H	54.7 ± 2.2	n.d.
3p	-NH-(4-OCH ₃)-C ₆ H ₄	-H	112.4 ± 2.9	n.d.
4a	-NH-CH ₂ -C ₆ H ₅	-H	103.0 ± 0.5	n.d.
4b	-NH-CH ₂ -(4-CH ₃)-C ₆ H ₄ *	-H	n.d.	138.5 ± 13.9
4c	-NH-CH ₂ -(4-NO ₂)-C ₆ H ₄	-H	n.d.	33.9 ± 2.6
4d	-NH-CH ₂ -(4-Cl)-C ₆ H ₄ *	-H	n.d.	122.9 ± 7.1
4e	-NH-CH ₂ -(2-furyl)	-H	163.2 ± 1.5	n.d.
4f	-NH-CH ₂ CH ₂ -(3,4-OCH ₃)-C ₆ H ₃	-H	n.d.	89.5 ± 4.4
4g	-NH-CH ₂ -(3,4-OCH ₃)-C ₆ H ₃	-H	n.d.	177.0 ± 16.8
4h	-NH-CH ₂ -(2-Cl)-C ₆ H ₄ *	-H	n.d.	101.3 ± 6.8
4i	-NH-CH ₂ CH ₂ -(2,4-di-Cl)-C ₆ H ₃ *	-H	n.d.	80.2 ± 11.4
4j	-NH-(1-benzylpiperidin-4-yl)	-H	n.d.	112.0 ± 6.5
4k	-NH-C ₆ H ₁₁	-H	107.9 ± 1.8	n.d.
5a	-NH-C ₆ H ₄ -NH- (dimer) *	-H	n.d.	101.2 ± 13.6
7a	-NH-(2-OH)-C ₆ H ₄	-H	583.4 ± 11.2	n.d.
7b	-NH-(3-OH)-C ₆ H ₅	-H	134.5 ± 2.2	n.d.
7c	-NH-(4-OH)-C ₆ H ₆	-H	283.4 ± 4.2	n.d.
9a	-NH-C ₆ H ₅	-NO ₂	n.d.	n.d.
9b	-NH-(2-Br)-C ₆ H ₄	-NO ₂	677.7 ± 13.1	n.d.
9c	-NH-(2,6-di-Br)-C ₆ H ₃	-NO ₂	n.d.	n.d.
9d	-NH-CH ₂ -(2-furyl)	-NO ₂	96.6 ± 0.7	n.d.

Tab. 3 K_D values for compounds **9e-19** (see the general structure above Tab. 2)

	R^1	R^2	K_D^1	K_D^2
9e	-NH-C ₆ H ₁₁	-NO ₂	72.3 ± 0.7	n.d.
9f	-NH-CH ₂ -C ₆ H ₁₁	-NO ₂	n.d.	n.d.
9g	-NH-CH ₂ -C ₆ H ₅	-NO ₂	40.2 ± 2.4	n.d.
9h	-NH-CH ₂ -(2-Cl)-C ₆ H ₄	-NO ₂	143.2 ± 4.8	n.d.
9i	-NCH ₃ -CH ₂ -C ₆ H ₅	-NO ₂	96.2 ± 1.0	82.5 ± 4.8
9j	-NH-CH ₂ -(4-NO ₂)-C ₆ H ₄	-NO ₂	n.d.	30.6 ± 0.8
12a	-NH-C ₆ H ₅	-NH-CO-CH ₂ CH ₂ -COOH	98.8 ± 1.7	78.4 ± 3.7
12b	-NH-(2-Br)-C ₆ H ₄	-NH-CO-CH ₂ CH ₂ -COOH	75.7 ± 0.8	n.d.
12c	-NH-(2,6-di-Br)-C ₆ H ₃	-NH-CO-CH ₂ CH ₂ -COOH	81.2 ± 0.9	52.4 ± 2.1
12d	-NH-CH ₂ -(2-furyl)	-NH-CO-CH ₂ CH ₂ -COOH	77.3 ± 1.6	100.9 ± 8.1
12e	-NH-C ₆ H ₁₁	-NH-CO-CH ₂ CH ₂ -COOH	74.7 ± 0.9	n.d.
12f	-NH-CH ₂ -C ₆ H ₁₁	-NH-CO-CH ₂ CH ₂ -COOH	95.5 ± 0.9	85.2 ± 2.2
12g	-NH-CH ₂ -C ₆ H ₅	-NH-CO-CH ₂ CH ₂ -COOH	60.6 ± 1.3	n.d.
12h	-NH-CH ₂ -(2-Cl)-C ₆ H ₄	-NH-CO-CH ₂ CH ₂ -COOH	83.0 ± 0.8	50.9 ± 1.1
12i	-NCH ₃ -CH ₂ -C ₆ H ₅	-NH-CO-CH ₂ CH ₂ -COOH	175.4 ± 2.6	104.2 ± 3.2
13	-(3,5-di-CH ₃ ;4-OH)-C ₆ H ₂ *	-H	n.d.	linear fit
14	-(3,5-di-CH ₃ ;4-OH)-C ₆ H ₂	-NO ₂	n.d.	179.7 ± 7.9
16	-(3,5-di-CH ₃ ;4-OH)-C ₆ H ₂	-NH-CO-CH ₂ CH ₂ -COOH	307.5 ± 8.2	n.d.
17	-NH-CH ₂ -C ₆ H ₅	-NH-CO-CH ₂ CH ₂ -CO-(<i>N</i> -methyl-piperazinyl)	100.9 ± 0.8	n.d.
18a	-NH-(2-Br)-C ₆ H ₄	-NH-CO-CH ₂ -CO-OCH ₃	134.7 ± 1.4	n.d.
18b	-NH-CH ₂ -(2-Cl)-C ₆ H ₄	-NH-CO-CH ₂ -CO-OCH ₃	83.9 ± 0.4	57.8 ± 1.6
19	-NH-(2-Br)-C ₆ H ₄	-N ⁺ (CH ₃) ₃ I ₃ ⁻	83.6 ± 0.7	n.d.

Biological testing

4.1.3.2 *Evaluation of the results obtained for the chromone-based compounds*

First, the enzyme affinity to several compounds could not be evaluated, either due to interfering autofluorescence, as in case of compound **6** possessing an imino group at position 4 of the chromone ring (see structure in *Fig. 22*), or due to solubility issues. The affinity constants of poorly soluble compounds (marked with an asterisk) were obtained for their low concentration steps only (mostly up to 120 μM), for which a relevant correction on IFE was possible, *i.e.*, the absorbance curve was linear. Probably due to the low number of data points for the nonlinear fit, these results are often burdened with a high relative standard error ($> 10\%$). Regarding the obtained K_D^1 and K_D^2 values, several inhibitors displayed a good affinity at given assay conditions. K_D values lower than 100 μM are marked bold, K_D values under 50 μM are marked grey. Besides a few exceptions, K_D^2 values, obtained from the more diluted DMSO stock solution, were lower than the corresponding K_D^1 constants (*e.g.* **9i**, **12a**, **12c**, **12h**, see *Tab. 3*), therefore, the affinity results were compared among values resulting from the same titration scheme only. Based on the available data, following **structure-activity relationships** can be derived:

- In the series of chromone-2-carboxanilides, the kind and position of a halogen substituent on the benzene ring appear to have no significant influence on the affinity: **3i** (2-F, 93 μM) \approx **3j** (4-F, 87 μM), **3b** (2-Br, 80 μM) \approx **3d** (2,6-diBr, 98 μM); the affinity constants for *ortho*-substituted halogen derivatives **3b** (2-Br), **3h** (2-I) and **3i** (2-F) range from 80 – 118 μM . Nevertheless, the poor water solubility of the majority of anilides, which restricted the affinity testing to low inhibitor concentration steps, might have seriously affected these data reliability.
- Interesting correlations were obtained in a series of methoxy- and hydroxy-substituted anilides. Generally, the methoxy-substituted compounds showed a higher affinity than the corresponding hydroxy-substituted anilides. The influence of the substituent position on the affinity followed the same tendency in both series: *ortho*- (**3n**, 2-OCH₃, 165 μM) $>$ *para*- (**3p**, 4-OCH₃, 112 μM) $>$ *meta*- (**3o**, 3-OCH₃, 55 μM).
- Replacement of the phenyl motif in the amide part with a more flexible substituent leads to lower affinity values: **3a** (phenyl, 287 μM) $>$ **4a** (benzyl, 103 μM , see *Fig. 36*). Similar trend can be observed, when the amide bridge is further elongated by a methylene unit: **4g** (3,4-dimethoxybenzyl, 177 μM) $>$ **4f** (3,4-dimethoxyphenethyl, 90 μM). Affinity constants of compounds possessing a succinyl rest at position 6 display much lower variability, nevertheless, they follow the same tendency: **12a** (phenyl, 99

Biological testing

μM) > **12g** (benzyl, 61 μM). Conversely, the cyclohexylmethyl-substituted derivative **12f** shows a lower affinity (96 μM) than the corresponding cyclohexyl amide **12e** (75 μM).

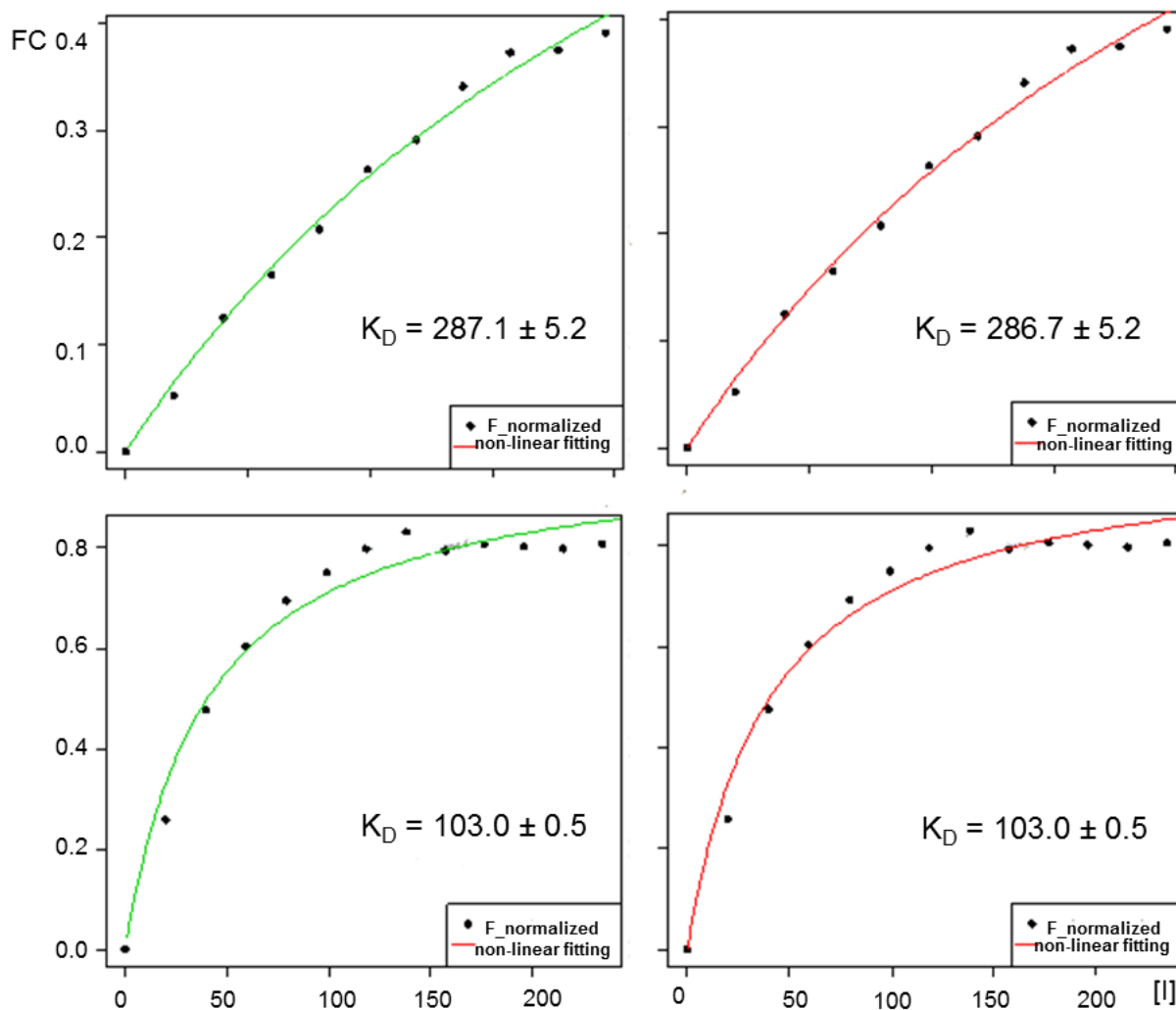


Fig. 36 Saturation curves for **3a** (on the top) and **4a** (below) using **Eq. 2** (on the left) and **Eq. 4** (on the right) showing the fluorescence change (FC, normalized to FC_{max}) as a function of inhibitor concentration (μM)

- Substitution of the amide hydrogen atom with a methyl group yields to a 2-3-fold increase in the affinity constants: **9i** > **9g**, **12i** > **12g**.
- Introduction of a nitro group appears to have a positive effect on the K_D values: benzylamide **4a** (103 μM) > **9g** (6-nitro-, 40 μM), cyclohexylamide **4k** (108 μM) > **9e** (6-nitro-, 72 μM). The best results were achieved for benzylamide **9g** (40 μM) and 4-nitrobenzylamide **9j** (31 μM), both bearing a nitro group in position 6 of the chromone ring. Nevertheless, even the corresponding 4-nitrobenzyl derivative **4c**

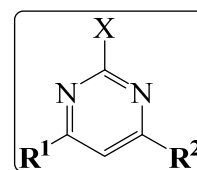
Biological testing

possessing a hydrogen at position 6 of the chromone ring, displayed a very good affinity (34 μM), indicating that the position of a nitro group can be altered.

- Introduction of a succinamidyl moiety in position 6 led to an improvement of affinity, too: benzylamide **4a** (103 μM) > **12g** (61 μM), cyclohexylamide **4k** (108 μM) > **12e** (75 μM). Its replacement by a methylmalonyl group yielded a similar value: 2-chlorobenzylamide **12h** (81 μM) \approx **18b** (84 μM). Its prolongation by the hydrophilic *N*-methylpiperazinyl residue caused nearly a 2-fold increase of the affinity constant: **12g** (61 μM) < **17** (101 μM).
- Titration of the ketone-substituted chromones, in which the amide bridge was replaced by oxo group led either to linear curve indicating a non-specific binding (**13**) or to relatively high affinity constants (**14**: 180 μM , **16**: 308 μM).
- Finally, the obtained affinity constant for the model compound **3b** (80 μM) might be erroneous due to restricted concentration steps, nevertheless, similar affinity values were obtained for its trimethylammonium salt **19** (84 μM) and the 6-succinamidyl derivative **12b** (76 μM).

4.1.3.3 Results for the pyrimidine-based compounds

The obtained affinity constants are summarized in *Tab. 4*.



Tab. 4 Results for compounds **21a-22e**

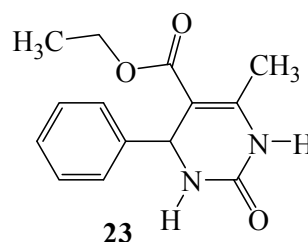
	R ¹	R ²	X	K _D ¹ [μM]	K _D ² [μM]
21a	-C ₆ H ₅	-H	-NH ₂	256.5 \pm 5.4	80.3 \pm 3.7
21b	-C ₆ H ₅	-CH ₃	-NH ₂	Autofluorescence	
21c	-C ₆ H ₅	-C ₆ H ₅	-NH ₂	164.3 \pm 5.6	173.7 \pm 51.1
21d	-CH ₃	-CH ₃	-NH ₂	Autofluorescence	
21e	-C(CH ₃) ₃	-C(CH ₃) ₃	-NH ₂	Autofluorescence	
22a	-C ₆ H ₅	-H	-OH	97.4 \pm 0.7	93.9 \pm 4.0
22b	-C ₆ H ₅	-CH ₃	-OH	Autofluorescence	
22c	-C ₆ H ₅	-C ₆ H ₅	-OH	Autofluorescence	
22d	-CH ₃	-CH ₃	-OH	Autofluorescence	
22e	-C(CH ₃) ₃	-C(CH ₃) ₃	-OH	Autofluorescence	

Dihydropyrimidinone **23** differs structurally from compounds listed in *Tab. 4*, thus its affinity is to be taken in account separately (see *Tab. 5*).

Biological testing

Tab. 5 Affinity constants for compound **23**

	K_D^1 [μ M]	K_D^2 [μ M]
23	105.2 ± 0.8	81.9 ± 1.8



4.1.3.4 Evaluation of the results obtained for the pyrimidine-based compounds

Since the number of results in this group has been very restricted due to some degree of autofluorescence of the most compounds, only few structure-activity relationships can be derived from the remaining data. The great disparity between the K_D^1 and K_D^2 values in compound **21a** can be explained by the use of two different enzyme batches (with a different production date) in both assays. All listed K_D^1 values were obtained using the same enzyme fraction and are thus more reliable. As observed for compounds **22a** and **21a**, replacement of the hydroxyl at position 2 with an amino group has a negative influence on the affinity constants, which is in agreement with the importance of an oxygen atom at this position, which may act as a stronger hydrogen bond acceptor than the amine nitrogen. The increased size of molecule might have a positive effect on the affinity, as can be seen comparing the K_D^1 values of **21a** and **21c**.

4.1.3.4.1 Autofluorescence

All synthesized pyrimidine derivatives were screened on autofluorescence at KasA assay conditions. Only **21a**, **21c** and **22a** did not interfere with the intrinsic enzyme fluorescence. Even a small structural modification led to compound fluorescence in case of **21b**, **21d**, **21e**, **22b**, **22c**, **22d** and **22e** hindering thus the evaluation of the intrinsic fluorescence change. Fluorescence emission by **22c** and **21d** has already been described in literature.^{81,82} Recorded emission spectrum of **22d** is illustrated in *Fig. 37*.

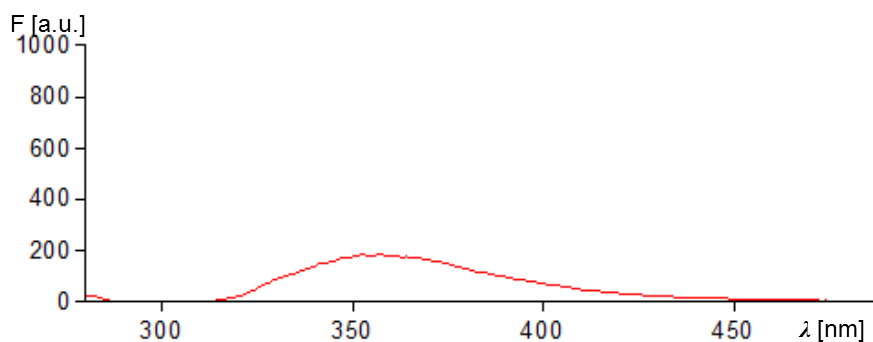


Fig. 37 Emission spectrum of **22d**: maximal fluorescence emission at 357 nm (excitation wavelength: 280 nm)

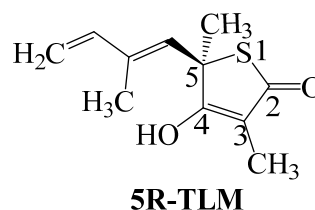
Biological testing

4.1.3.5 Assay for thiolactomycin

As a reference compound, thiolactomycin (TLM) was tested in order to verify the reproducibility of the obtained K_D values. Accordingly with the Method A, 9.5 mM TLM stock solution in DMSO was prepared and titrated into enzyme solution following the given concentration scheme (see *Chap. 4.1.2.1*). Fluorescence change values, corrected for IFE, were fitted in *Equation 2*. Similarly, 10 mM TLM stock solution was prepared following the Method B using the same concentration steps for reference and inhibitors (see *Tab. 1*). Affinity constants were obtained from the Morrison equation. All the resulting K_D values, summarized in *Tab. 6*, were in a relatively narrow range between 115 and 141 μM . Affinity constant published by Machutta *et al.*²⁹ is approximately 2-fold higher ($226 \pm 9 \mu\text{M}$), which might be reasoned by a different way of enzyme purification. In both cases, the enantiomerically pure (5R)-TLM was used. The TLM used here was purchased from Sigma-Aldrich, whereas in the reference mentioned above, TLM was synthesized as described by McFadden *et al.*⁸³

Tab. 6 Obtained affinity constants for TLM

	Method	c(Stock solution) [mM]	K_D [μM]
1	A	9.5	133.2 ± 3.8
2	A	9.5	115.1 ± 3.1
3	A	9.5	116.5 ± 3.2
4	A	9.5	130.7 ± 3.7
5	B	10.0	141.8 ± 1.2
6	B	10.0	122.4 ± 2.3



4.1.4 Discussion and prospects

Several structure-activity relationships could be derived only for the series of chromone derivatives, as outlined in *Chap. 4.1.3.1*. The highest affinity was observed for compounds **4c**, **9g** and **9j** ($K_D = 34 \mu\text{M}$, $40 \mu\text{M}$ and $31 \mu\text{M}$, respectively) possessing a nitro group either in position 6 of the chromone ring (**9g**), or in *para*-position of the benzene ring (**4c**), or both (**9j**).

4.1.4.1 Non-specific fluorescence quenching

Regarding the introduction of nitro group, similar structure-activity relationships have been described for isatine derivatives as reported by Topf³⁹. It arouse suspicion, the fluorescence change was a consequence of a non-specific fluorescence quenching by the nitro group. In order to inquire, which impact would have a titration of a nitro-substituted compound, which is not a suitable ligand for KasA, *para*-nitrophenol was tested. Fluorescence change values were fitted into *Equation 2*. Since this compound displays a significant absorbance at excitation

Biological testing

and emission wavelength, overcorrection of IFE causes a slight baseline fluctuation (see *Fig. 38*). Nevertheless, no significant fluorescence quenching was observed for the tested concentration range and time period (approx. 10 min).

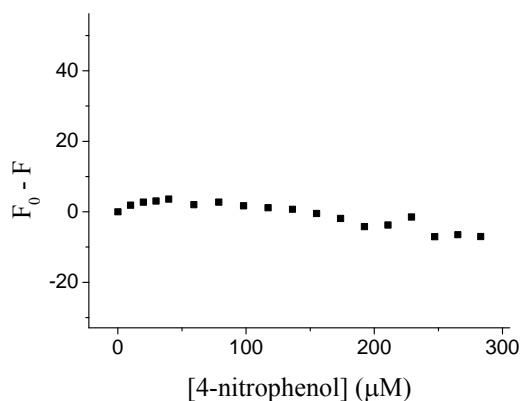


Fig. 38 Titration curve for 4-nitrophenol: fluorescence change as a function of ligand concentration

Additionally, the effect of two typical tryptophane fluorescence quenchers⁷⁹, acrylamide and succinimide, on the titration curve was examined (see *Fig. 39*). In this case, higher concentrations of the quencher were tested (up to 1000 μM). As these compounds are not supposed to bind to the enzyme, linear character of curves was expected, thus, a linear regression was used to depict the tendency of this correlation.

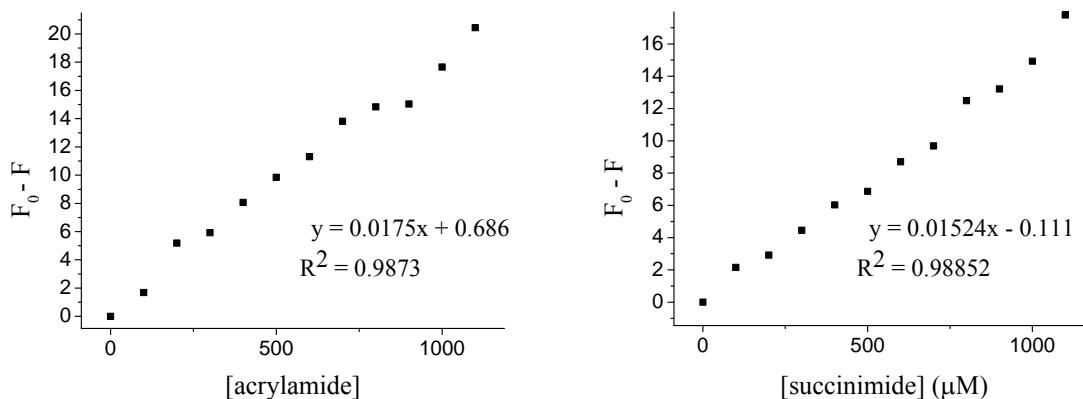


Fig. 39 Titration curves for acrylamide (on the left) and succinimide (on the right) showing the fluorescence change as a function of concentration of the quencher

All presented curves indicate that a non-specific fluorescence quenching has a minor effect on the KasA fluorescence change at given assay conditions. Nevertheless, a saturation curve obtained from the titration of tested inhibitors is still not a proof of specific binding. This binding mode can be confirmed in the kinetic enzyme assay described in the next chapter.

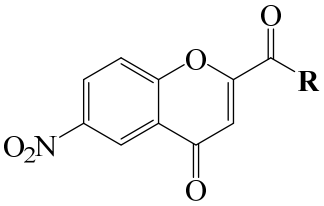
4.1.4.2 Kinetic enzyme assay

The kinetic enzyme assay will be conducted following the procedure published by Machutta *et al.*²⁹ and Schaeffer *et al.*³⁶ Enzyme inhibition (IC₅₀ value) is measured using the same

Biological testing

conditions (pH, buffer) as described for the direct binding study. Conversion of both KsaA substrates, malonyl- and palmitoyl-AcpM, into the β -ketoacyl-AcpM product is evaluated by means of a coupled assay with MabA, the NADPH-dependent FAS-II- β -ketoacyl-ACP reductase, which catalyses the next reaction step (see **Fig. 12**). This method enables to monitor the substrate conversion rate spectrophotometrically as a decrease of NADPH absorbance at 340 nm. The best hits of each structural group resulting from the binding assay will be submitted to further testing. Additionally, the kinetic enzyme assay will be performed with all compounds active in the whole cell assay on *M. tuberculosis*. For some of them, promising affinity data were obtained (see **Tab. 7**). In case of the chromone derivative **9i**, a similar affinity constant (K_D^3) was obtained using the same conditions in the binding assay in a different laboratory*.

Tab. 7 Results overview for compounds active in the whole cell assay (n.d. = not determined), [a] after 21 days of incubation, [b] after 14 days of incubation. A comparison of the affinity data for compound **9i** obtained here (K_D^1) and in the laboratory of Prof. Tonge (K_D^3).



	R	MIC [μ M]	K_D^1 [μ M]	K_D^3 [μ M]
9d	-NH-CH ₂ -(2-furyl)	40 ^a	96.6 \pm 0.7	n.d.
9e	-NH-C ₆ H ₁₁	20 ^a	72.3 \pm 0.7	n.d.
9f	-NH-CH ₂ -C ₆ H ₁₁	40 ^a	n.d.	n.d.
9g	-NH-CH ₂ -C ₆ H ₅	40 ^b	40.2 \pm 2.4	n.d.
9i	-NCH ₃ -CH ₂ -C ₆ H ₅	40 ^b	96.2 \pm 1.0	93.4 \pm 1.7

As reported by Machutta *et al.*²⁹, the affinity constant from the direct binding study ($K_D = 226 \pm 9 \mu\text{M}$) is in a good correlation with the IC_{50} value for TLM ($242 \pm 60 \mu\text{M}$) from the kinetic enzyme assay, proving thus the validity of the direct binding assay for TLM and its derivatives. In case of structurally distinct compounds, these correlations need to be investigated.

4.2 Inhibition activity testing on the whole cells of *M. tuberculosis*

All synthesized compounds were submitted to the whole cell inhibition testing within the SFB 630 using the commercially available BBL MGIT tubes. Obtained inhibitory activity data as well as the MIC values of the active compounds and their toxicity on *J774.1* macrophages are summarized in **Tab. 8**. Experimental results have been confronted with theoretical values describing the probability of compound to permeate the mycobacterial

* Conducted by Dr. K. Kapilashrami, Research group of Prof. Tonge, Stony Brook University, New York

Biological testing

membrane. These values have been calculated by B. Merget[†] using MycPermCheck⁸⁴. In this program, the membrane permeability is evaluated by comprising the results of five “QikProp”¹²⁹ descriptors: *FOSA*, the surface hydrophobicity; *logP*, decadic logarithm of octanol/water partition coefficient; *PISA*, the surface π -interactions; *acctpHB*, the number of H-bond acceptors and *glob*, the generic spherical surface to molecule surface ratio.⁸⁵ The values listed in *Tab. 8* are in range 0 – 1, which stands for 0 – 100 % probability of membrane permeability for the given compound.

4.2.1 Results

Tab. 8 Inhibition activity on the whole cells *M. tuberculosis* (*n.d.* = not determined)

	Formula	M _r [g/mol]	MycPerm- Check Probability	Inhibition activity ⁱ	MIC [μM]			J774.1, IC ₅₀ [μM]
					7 th day	14 th day	21 th day	
3a	C ₁₆ H ₁₁ NO ₃	265.26	0.997	inactive	n.d.	n.d.	n.d.	n.d.
3b	C ₁₆ H ₁₀ BrNO ₃	344.16	0.996	inactive	n.d.	n.d.	n.d.	n.d.
3c	C ₁₆ H ₉ BrN ₂ O ₅	389.16	0.913	inactive	n.d.	n.d.	n.d.	n.d.
3d	C ₁₆ H ₉ Br ₂ NO ₃	423.06	0.998	inactive	n.d.	n.d.	n.d.	n.d.
3e	C ₁₆ H ₉ Cl ₂ NO ₃	334.15	0.997	inactive	n.d.	n.d.	n.d.	n.d.
3f	C ₁₆ H ₉ Cl ₂ NO ₃	334.15	0.996	inactive	n.d.	n.d.	n.d.	n.d.
3g	C ₁₆ H ₉ Cl ₂ NO ₃	334.15	0.996	inactive	n.d.	n.d.	n.d.	n.d.
3h	C ₁₆ H ₁₀ INO ₃	391.16	0.997	inactive	n.d.	n.d.	n.d.	n.d.
3i	C ₁₆ H ₁₀ FNO ₃	283.25	0.996	inactive	n.d.	n.d.	n.d.	n.d.
3j	C ₁₆ H ₁₀ FNO ₃	283.25	0.995	inactive	n.d.	n.d.	n.d.	n.d.
3k	C ₁₇ H ₉ ClN ₂ O ₃	324.72	0.934	inactive	n.d.	n.d.	n.d.	n.d.
3l	C ₁₇ H ₁₂ N ₂ O ₆	340.29	0.414	inactive	n.d.	n.d.	n.d.	n.d.
3m	C ₁₈ H ₁₅ NO ₃	293.32	0.928	inactive	n.d.	n.d.	n.d.	n.d.
3n	C ₁₇ H ₁₃ NO ₄	295.29	0.948	inactive	n.d.	n.d.	n.d.	n.d.
3o	C ₁₇ H ₁₃ NO ₄	295.29	0.940	inactive	n.d.	n.d.	n.d.	n.d.
3p	C ₁₇ H ₁₃ NO ₄	295.29	0.931	inactive	n.d.	n.d.	n.d.	n.d.
4a	C ₁₇ H ₁₃ NO ₃	279.29	0.997	inactive	n.d.	n.d.	n.d.	n.d.
4b	C ₁₈ H ₁₅ NO ₃	293.32	0.978	inactive	n.d.	n.d.	n.d.	n.d.
4c	C ₁₇ H ₁₂ N ₂ O ₅	324.29	0.935	inactive	n.d.	n.d.	n.d.	n.d.
4d	C ₁₇ H ₁₂ ClNO ₃	313.74	0.997	inactive	n.d.	n.d.	n.d.	n.d.
4e	C ₁₅ H ₁₁ NO ₄	269.25	0.953	inactive	n.d.	n.d.	n.d.	n.d.
4f	C ₂₀ H ₁₉ NO ₅	353.37	0.757	inactive	n.d.	n.d.	n.d.	n.d.
4g	C ₁₉ H ₁₇ NO ₅	339.34	0.649	inactive	n.d.	n.d.	n.d.	n.d.
4h	C ₁₇ H ₁₂ ClNO ₃	313.74	0.997	inactive	n.d.	n.d.	n.d.	n.d.
4i	C ₁₈ H ₁₃ Cl ₂ NO ₃	362.21	0.998	inactive	n.d.	n.d.	n.d.	n.d.
4j	C ₂₂ H ₂₂ N ₂ O ₃	362.42	0.964	inactive	n.d.	n.d.	n.d.	n.d.
4k	C ₁₆ H ₁₇ NO ₃	271.31	0.085	inactive	n.d.	n.d.	n.d.	n.d.
5a	C ₂₆ H ₁₆ N ₂ O ₆	452.42	0.999	inactive	n.d.	n.d.	n.d.	n.d.
6	C ₂₄ H ₂₀ N ₂ O ₄	400.43	1.000	inactive	n.d.	n.d.	n.d.	n.d.

[†] Research group Prof. Sotriffer, Institute of Pharmacy and Food Chemistry, Würzburg

Biological testing

	Formula	M _r [g/mol]	MycPerm- Check Probability	Inhibition activity ⁱ	MIC [μM]			J774.1, IC ₅₀ [μM]
					7 th day	14 th day	21 th day	
7a	C ₁₆ H ₁₁ NO ₄	281.26	0.957	inactive	n.d.	n.d.	n.d.	n.d.
7b	C ₁₆ H ₁₁ NO ₄	281.26	0.950	inactive	n.d.	n.d.	n.d.	n.d.
7c	C ₁₆ H ₁₁ NO ₄	281.26	0.948	inactive	n.d.	n.d.	n.d.	n.d.
9a	C ₁₆ H ₁₀ N ₂ O ₅	310.26	0.939	inactive	n.d.	n.d.	n.d.	n.d.
9b	C ₁₆ H ₉ BrN ₂ O ₅	389.16	0.913	inactive	n.d.	n.d.	n.d.	n.d.
9c	C ₁₆ H ₈ Br ₂ N ₂ O ₅	468.05	0.948	inactive	n.d.	n.d.	n.d.	n.d.
9d	C ₁₅ H ₁₀ N ₂ O ₆	314.25	0.525	active	5	20	40	> 100
9e	C ₁₆ H ₁₆ N ₂ O ₅	316.31	0.004	active	n.d.	20	20	> 100
9f	C ₁₇ H ₁₈ N ₂ O ₅	330.34	0.007	active	n.d.	20	40	80.3
9g	C ₁₇ H ₁₂ N ₂ O ₅	324.29	0.934	active	n.d.	40	> 40	> 100
9h	C ₁₇ H ₁₁ ClN ₂ O ₅	358.73	0.932	inactive	n.d.	n.d.	n.d.	n.d.
9i	C ₁₈ H ₁₄ N ₂ O ₅	338.31	0.578	active	5	20	40	> 100
9j	C ₁₇ H ₁₁ N ₃ O ₇	369.29	0.305	inactive	n.d.	n.d.	n.d.	n.d.
12a	C ₂₀ H ₁₆ N ₂ O ₆	380.40	0.310	inactive	n.d.	n.d.	n.d.	n.d.
12b	C ₂₀ H ₁₅ BrN ₂ O ₆	459.25	0.409	inactive	n.d.	n.d.	n.d.	n.d.
12c	C ₂₀ H ₁₄ Br ₂ N ₂ O ₆	538.14	0.385	inactive	n.d.	n.d.	n.d.	n.d.
12d	C ₁₉ H ₁₆ N ₂ O ₇	384.34	0.029	inactive	n.d.	n.d.	n.d.	n.d.
12e	C ₂₀ H ₂₂ N ₂ O ₆	386.40	0.000	inactive	n.d.	n.d.	n.d.	n.d.
12f	C ₂₁ H ₂₄ N ₂ O ₆	400.43	0.000	inactive	n.d.	n.d.	n.d.	n.d.
12g	C ₂₁ H ₁₈ N ₂ O ₆	394.38	0.274	inactive	n.d.	n.d.	n.d.	n.d.
12h	C ₂₁ H ₁₇ ClN ₂ O ₆	428.82	0.292	inactive	n.d.	n.d.	n.d.	n.d.
12i	C ₂₂ H ₂₀ N ₂ O ₆	408.40	0.068	inactive	n.d.	n.d.	n.d.	n.d.
13	C ₁₈ H ₁₄ O ₄	294.30	0.424	inactive	n.d.	n.d.	n.d.	n.d.
14	C ₁₈ H ₁₃ NO ₆	339.30	0.028	inactive	n.d.	n.d.	n.d.	n.d.
16	C ₂₂ H ₁₉ NO ₇	409.39	0.001	inactive	n.d.	n.d.	n.d.	n.d.
17	C ₂₆ H ₂₈ N ₄ O ₅	476.52	0.001	inactive	n.d.	n.d.	n.d.	n.d.
18a	C ₂₀ H ₁₅ BrN ₂ O ₆	459.25	0.677	inactive	n.d.	n.d.	n.d.	n.d.
18b	C ₂₁ H ₁₇ ClN ₂ O ₆	428.82	0.563	inactive	n.d.	n.d.	n.d.	n.d.
19	C ₁₉ H ₁₈ BrI ₃ N ₂ O ₃	782.98	n.d.	inactive	n.d.	n.d.	n.d.	n.d.
21a	C ₁₀ H ₉ N ₃	171.20	0.939	inactive	n.d.	n.d.	n.d.	n.d.
21b	C ₁₁ H ₁₁ N ₃	185.23	0.718	inactive	n.d.	n.d.	n.d.	n.d.
21c	C ₁₆ H ₁₃ N ₃	247.29	1.000	inactive	n.d.	n.d.	n.d.	n.d.
21d	C ₆ H ₉ N ₃	123.16	0.001	inactive	n.d.	n.d.	n.d.	n.d.
21e	C ₁₂ H ₂₁ N ₃	207.32	0.000	inactive	n.d.	n.d.	n.d.	n.d.
22a	C ₁₀ H ₈ N ₂ O	172.18	0.979	inactive	n.d.	n.d.	n.d.	n.d.
22b	C ₁₁ H ₁₀ N ₂ O	186.21	0.883	inactive	n.d.	n.d.	n.d.	n.d.
22c	C ₁₆ H ₁₂ N ₂ O	248.28	1.000	inactive	n.d.	n.d.	n.d.	n.d.
22d	C ₆ H ₈ N ₂ O	124.14	0.000	inactive	n.d.	n.d.	n.d.	n.d.
22e	C ₁₂ H ₂₀ N ₂ O	208.30	0.000	inactive	n.d.	n.d.	n.d.	n.d.
22f	C ₁₈ H ₁₇ N ₃ O	291.35	1.000	inactive	n.d.	n.d.	n.d.	n.d.
23	C ₁₄ H ₁₆ N ₂ O ₃	260.29	0.695	inactive	n.d.	n.d.	n.d.	n.d.

[i] Active compounds displayed in both samples (duplicate) fluorescence intensity lower than 20 F.U. under following conditions: blank sample 20 F.U., reference 7–8 F.U., pos. control 20 F.U., neg. control 7–8 F.U.

Biological testing

4.2.2 Discussion

4.2.2.1 *Derived structure-activity relationships*

All the active compounds possess a nitrogroup in position 6 of the chromone ring (*Fig. 40*). The amide part is substituted by cyclohexylamine, cyclohexylmethylamine or arylmethylamine, providing more flexibility to the molecule in comparison to the planar *N*-arylamides. Tertiary amide **9i** displayed a higher inhibition effect than the corresponding secondary amide **9g**. The highest inhibition activity was observed for substituted *N*-cyclohexylamide **9e** (MIC = 20 μ M, after 21 days of incubation). The insertion of a methylene group between the cyclohexane ring and the amide nitrogen led to increased cytotoxicity as can be seen in case of compound **9f**. All remaining active compounds displayed a low cytotoxicity (IC₅₀ > 100 μ M).

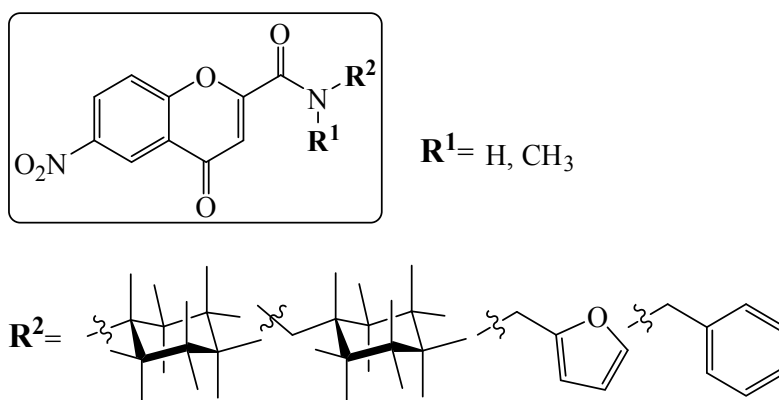


Fig. 40 General structure of compounds active in the whole cell assay

4.2.2.2 *Predicted membrane permeation vs. observed activity*

Among the active compounds, high permeability was predicted only for substituted *N*-benzylamide **9g** (93.4 %). Moderate values were assigned to the both remaining substituted *N*-arylmethylamides **9d** (52.5 %) and **9i** (57.8 %). Very low probability was calculated for the most active compounds **9e** (0.4 %) and **9f** (0.7 %), both containing a cyclohexane ring responsible for the inconvenient constellation of the MycPermCheck⁸⁵ descriptors. The discrepancy between predicted and experimental values could possibly be a consequence of an existing active transport mechanism. Neither transport nor action mode have been examined yet.

4.2.2.3 *Investigation of the observed activity loss in compound 9d*

In case of compound **9d**, a significant time-dependent decrease of inhibition activity was observed during the course of *in vivo* assays. Hence, in order to investigate the possible

Biological testing

compound degradation, stability studies were performed. The active compound content was determined in both, the incubation solution (buffer) and the stock solution (DMSO, see *Chap. 7.3.3*). A sample of the stock solution was injected on a HPLC column and the content of chromone **9d** was determined from the peak area at 254 nm, the wavelength at which the most impurities were detected. The measured peak area corresponded to the concentration of 28.5 µg/ml on the calibration curve, which were only 44.5 % of the expected value. Since the active compound degradation occurred already in the stock solution, the complex incubation solution, which contained highly lipophilic substances (*e.g. M. tuberculosis* metabolites, oleic acid) was not loaded on a HPLC column, but a simple absorbance assay was performed in order to estimate the compound content in the incubation solution. The wavelength of the absorbance maximum of **9d** in a pure incubation buffer was used. After zero adjustment using the pure incubation buffer, the sample absorbance was measured. The obtained 25.4 µM concentration corresponded to 63.4 % of the expected value. Nevertheless, due to the coincident light absorbance by other sample constituents or degradation products, this result might be seriously error burdened.

Regarding the evaluation of degradation products, further stability study was performed and evaluated by ¹H NMR and MS spectroscopy. A sample of the newly synthesized compound **9d** was dissolved in deuterated DMSO. Leaving the solution in a closed vessel at RT for 21 days led to a significant increase of impurity signals, which could not be attributed to none of the starting compounds (see *Fig. 41*). The presence of the 2-hydroxy-benzoyl acrylamide derivative **10**, obtained as a side product of the synthesis, was not confirmed by NMR nor MS spectroscopy. Due to a vast number of interfering background signals in the positive ion mode, only the negative ion spectra were recorded. Beside the mass-to-charge signal for **9d** ($m/z = 313.1$ [$M-H$]), at most abundant was the anion with $m/z = 349.0$. The impurity signals on ¹H NMR spectrum indicate the presence of several degradation products in the sample. Based on the available data, they could not be identified.

Biological testing

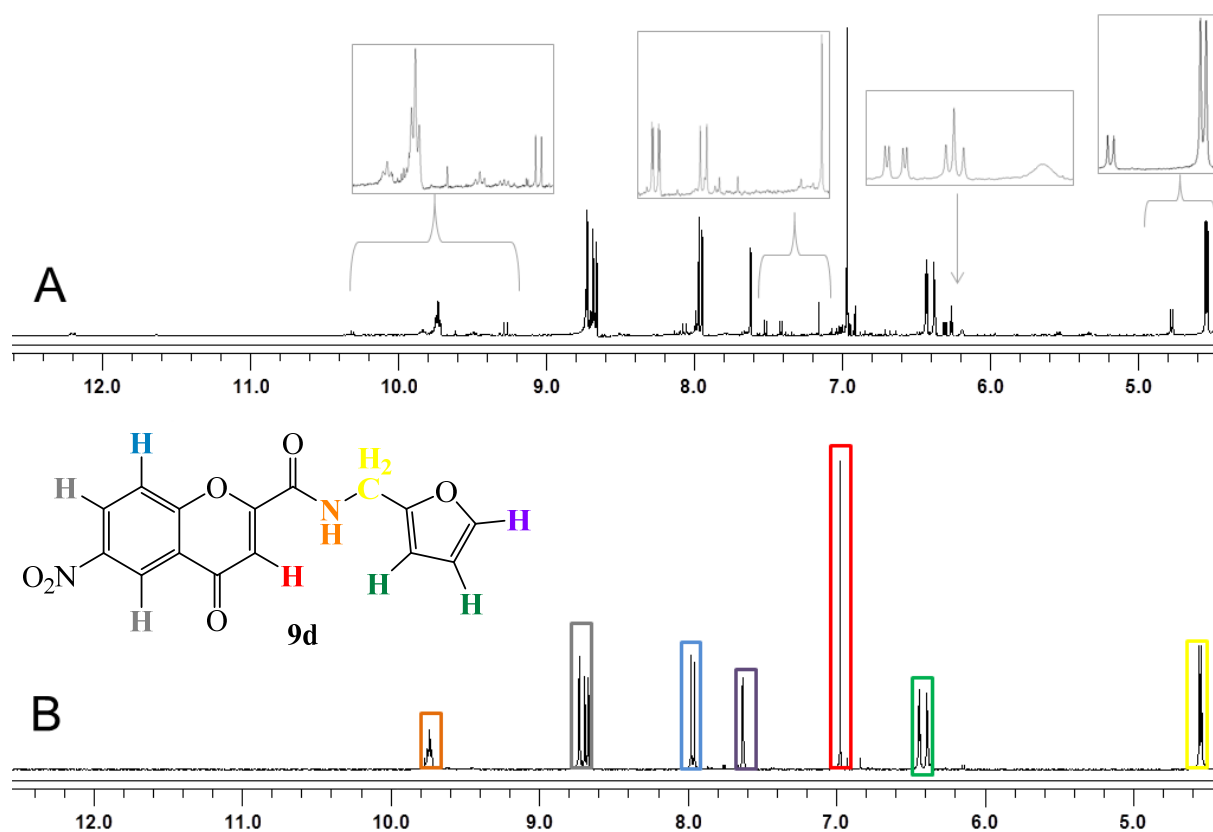


Fig. 41 ^1H NMR Spectrum of the DMSO solution of **9d** measured shortly after preparing (**B**) and 21 days later (**A**)

4.3 Anti-infective screening

Selected compounds were screened within the SFB 630 on their antimicrobial activity using following pathogens: *S. aureus*, *S. epidermidis*, *E. faecalis*, *E. faecium*, *E. coli*, *P. aeruginosa*, *Y. pseudotuberculosis*, *Y. pestis*, *C. albicans* and *L. major*. Cytotoxicity was additionally examined on *J774.1* macrophages. The procedures are described in the SOP protocols on the SFB 630 website.¹¹⁷ The results are summarized in the Experimental section, *Chap. 7.7*. Apart from a week growth-inhibition effect of **4k**, **11e** and **11g** (all three possess a more flexible substituent in the amide part of molecule) on *L. major*, no interesting inhibitory activities were found. Due to solubility issues, deficient activity of the already tested compounds and cost reasons, anti-infective screening was performed only for the first series of compounds synthesized.

4.4 The assay interference potential of chromones

Due to the electron delocalization between the chromone ring oxygen atoms O1 and O4 and the Michael acceptor character, the γ -pyrone ring of chromone is susceptible for nucleophilic reactions directed to the most electron-deficient chromone carbon C2.¹³¹ A high reactivity with nucleophiles such as cystein sulfhydryl groups is typical for “promiscuous inhibitors” (or PAINS – pan-assay interference compounds), and might lead to false positive results in biological assays. The common characteristics of “promiscuous inhibitors” are non-specific and non-competitive inhibition, that is often time-dependent.¹³² The mechanisms of a non-specific inhibition might include: compound aggregation and adsorption on the enzyme surface, irreversible enzyme adduct formation due to the covalent binding on *e.g.* cystein residues, enzyme denaturation, redox cycling, production of reactive oxygen species (ROS), and chelating potential.^{77,135}

On the other hand, there are chromone-based molecules that exhibit a selective and competitive mode of binding, for instance the anti-cancer agent quercetagetin (3,3',4',5,6,7-hydroxyflavone, *Fig. 42*) which interacts non-covalently with the active site amino acids of *pim-1* kinase.¹³³

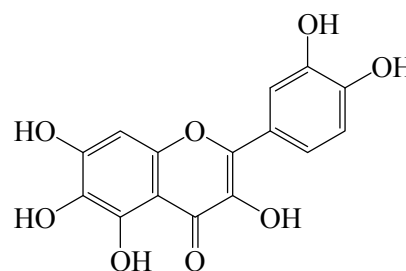


Fig. 42 Structure of quercetagetin

At the conditions used for the synthesis of chromone-2-carboxamides (stirring overnight at pH \approx 9), the nucleophilic attack by the amine nitrogen on the chromone carbon C2, followed by the opening of γ -pyrone ring, was observed in two cases:

- Reaction with 1,2-diaminobenzene yielded the dihydroquinoxalinone derivative **5b**
- Reaction with furfurylamine gave the 2-hydroxy-benzoyl acrylamide derivative **10**

In order to investigate the possible susceptibility of chromone derivatives toward sulfhydryl groups, ¹H NMR and UV spectroscopy experiments using dithiothreitol (DTT), the Kasa assay component, as a sulfhydryl source were performed. During the NMR kinetic measurement (*N*-phenyl-chromone-2-carboxamide **3a**, 54 mM in DMSO), chemical shifts and signal intensities of compound **3a** remained unchanged within 2 hours after addition of 2 eq. of DTT.

Biological testing

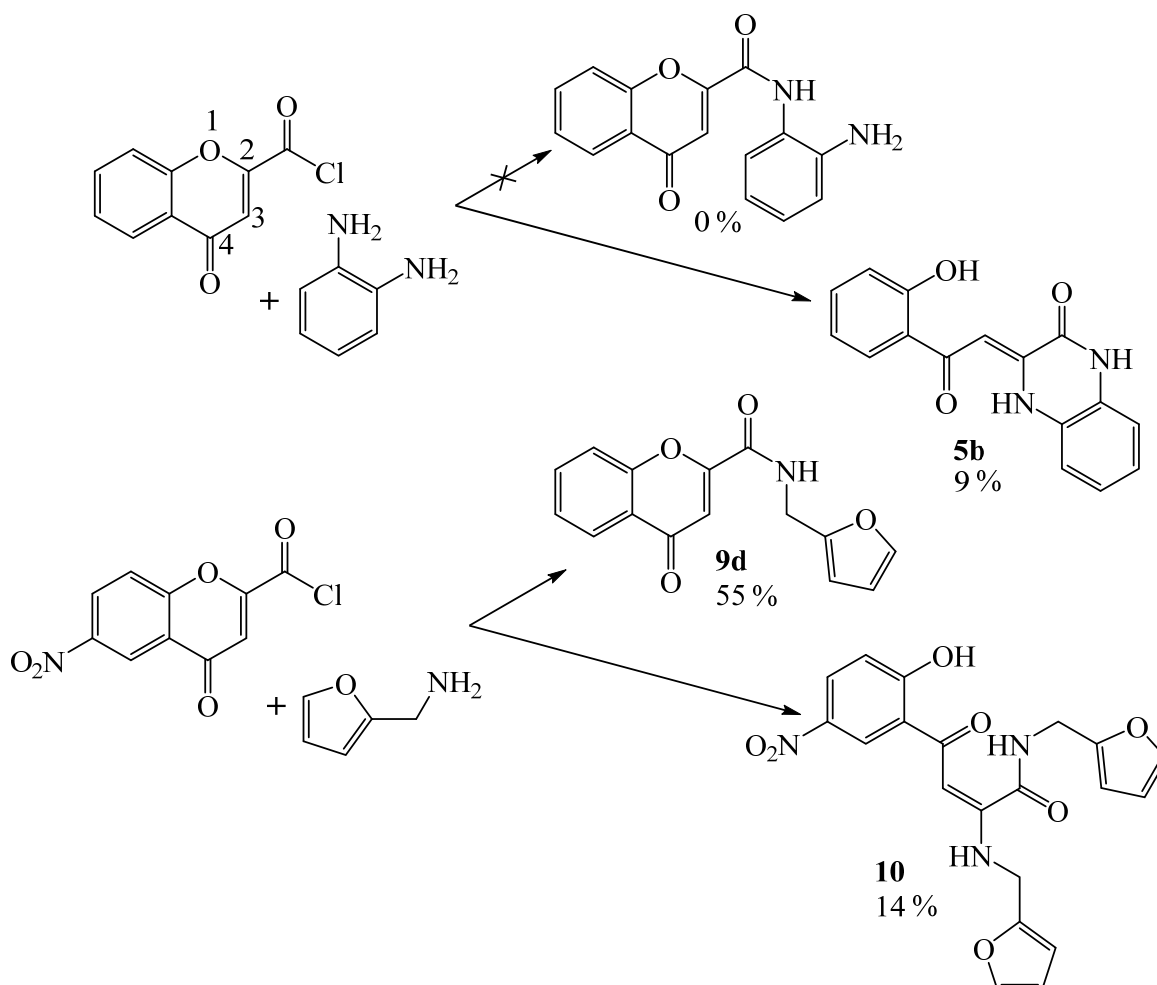


Fig. 43 The formation of the amidation side products **5b** and **10** via Michael reaction

The UV spectroscopy measurement was performed in Tris buffer, pH 8.5 (used for the Kasa assay). The correlation between chromone ring opening and absorbance decrease was based on the observed shift of the absorbance maxima and decrease of the absorbance intensity in compound **10** compared to **9d** (λ_{max} of compound **9d**: 262 and 306 nm; λ_{max} of compound **10**: 237, 378 and 537 nm). In order to avoid a coincident absorbance of the increasing amount of the oxidized form of DTT ($\lambda_{\text{max}} = 283 \text{ nm}$)¹³⁴, sample absorbance was measured at 320 nm.

The chromone derivative **9i** was tested, since it was soluble in the testing buffer (containing 1 % DMSO) and possessed a sufficient absorbance at 100 μM concentration at 320 nm. The absorbance values remained nearly unchanged within 1 hour after addition of 2 eq. of DTT, showing a fluctuation under 1 % (see **Fig. 44**).

Biological testing

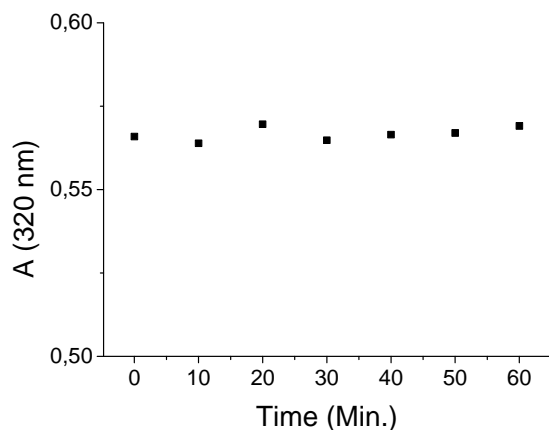


Fig. 44 Absorbance of a buffer solution of **9i** and DTT as a function of time

The results obtained in both environments, DMSO and buffer, indicate, that the susceptibility of the chromone derivatives toward nucleophilic attack by sulfhydryl group and the consequent γ -pyrone ring opening are negligible at the assay conditions. Furthermore, several structure-activity relationships were obtained for the series of chromone derivatives in the KasA binding assay (e.g. the change in affinity due to the replacement of the amide moiety by an oxo group or variation of the position of hydroxyl or methoxy-substituent on the benzene ring in the amide part). Additionally, no apparent cytotoxicity on macrophages, enhanced in case of ROS generation, was detected. Nevertheless, neither competitive binding assay with TLM nor evaluation of affinity toward unrelated model enzymes (e.g. chymotrypsin, β -lactamase) were performed.

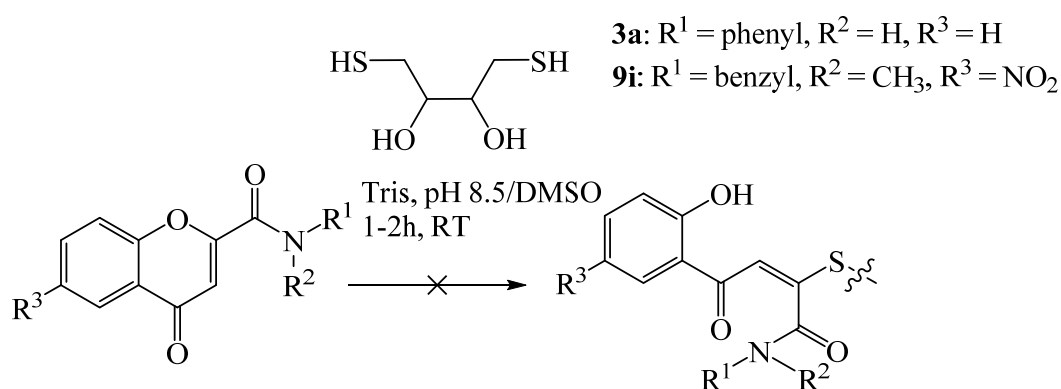


Fig. 45 Testing on the reactivity of chromones **3a** and **9i** toward thiol groups of DTT

4.5 Solubility problems

4.5.1 Introduction

For the majority of the small molecules synthesized here a high probability to permeate the mycobacterial membrane was predicted (see *Tab. 8*). Although the lipophilic character is required to reach intracellular targets, hydrophilic properties are essential for drug delivery and transport through the extracellular fluids. Additionally, most of the biological assays are conducted in hydrophilic buffer environment, precluding the evaluation of activity in lipophilic compounds. The required balance between the lipophilic and hydrophilic properties of a drug candidate is generally expressed as the Lipinski's rule of five¹²⁶ (molecular weight < 500 g/mol, clogP < 5, number of hydrogen bond acceptors < 10 and number of hydrogen bond donors < 5). These requirements for drug-like properties were met also by the chromone-2-carboxanilides **3a-p** derived from the model chromone compound **GS-71 (3b)**. Nevertheless, despite their relatively low partition coefficients (clogP 1.63 – 3.20), molecular weights between 265 – 423 g/mol, the presence of 3 – 6 hydrogen bond acceptors and 1 donor in their molecules, the vast majority of these compounds precipitated at the biological assay conditions (Tris/phosphate buffer, pH 8.5/7.4, approx. 1 – 3 % DMSO) already at concentrations lower than 100 μM.

Since the intrinsic solubility, *i.e.*, the solubility of a non-ionized compound reached after an equilibration period (generally 24 – 72 h), depends on two major factors: compound polarity and crystal forces, it can be estimated from the known melting point (MP) and partition coefficient (clogP) values using the General solubility equation (*Equation 5*).¹²⁷

$$\log S = -0.01 \times (MP - 25) - \text{clog}P + 0.5 \quad (\text{Equation 5})$$

For the virtual screening hit **3b**, logS was calculated from the measured melting point (204 °C) and predicted clogP (2.32, ChemDraw) yielding a value of -3.61. Although this value defines the compound as “very slightly soluble” (according to Ph. Eur.¹²⁸), it corresponds to the solubility of 0.7 mM ($M_r = 344.2$ g/mol), which is sufficient enough to perform biological testing. Unfortunately, the prediction of logS is less accurate than the estimation of logP. The experimental value of intrinsic solubility for the same compound, assessed by the shake flask method proposed by Higuchi and Connors⁹⁴ was approximately 100-fold lower (logS = -5.46) defining the substance as “practically insoluble”.

Biological testing

Since the crystal lattice arrangement is a major factor of intrinsic compound solubility, crystal structures of three chromone derivatives have been inspected. Their characteristics (inter- and intramolecular interactions, planarity) and correlations with the experimentally obtained intrinsic solubility values are described in the next chapter.

4.5.2 Crystal structure and packing of selected chromone derivatives

Crystallographic data, collected by Dr. A. Damme and Dr. K. Radacki, were obtained for *N*-(2-bromophenyl)-chromone-2-carboxamide (**3b**), the quaternary ammonium salt of its 6-amino derivative (**19**), and *N*-methyl-*N*-benzylamide **9i**, possessing a nitro group in position 6 of the chromone ring. Crystal structures of several chromone-2-carboxamides, inclusive compound **3b**, have recently been published by Reis *et al.*⁵⁹ and Gomes *et al.*⁶⁰ and are consistent with the data obtained here. The majority of the reported structures are nearly planar with an *anti/trans*-rotamer configuration as the preferred arrangement in the solid state, enabling the formation of intramolecular hydrogen bonds (see *Fig. 30*). Concerning the already published structures, only the tertiary *N*-methyl-*N*-phenyl-chromone-2-carboxamide showed a *syn*-configuration. The *cis*-rotamer was observed in nonsubstituted *N*-phenyl-4-oxo-4*H*-chromene-2-carboxamide and its *para*-bromo derivative. Conversely, its *ortho*- and *meta*-bromo derivatives showed the more common *trans*-configuration.^{59,60}

4.5.2.1 Intramolecular interactions

Both compounds, **3b** and **19**, possessing an identical substituent in the amide part, represent *anti*-rotamers with *trans*-related oxygen atoms O1 and O21. The carboxamide bridge tends to be planar, due to the electron delocalization and partial double-bond character of the C–N bond. While in compound **3b**, the carboxamide moiety lies nearly in the same plane as the chromone ring (dihedral angle between the rings 1.07°), in compound **19**, the C2–C21 bond is slightly bent out of the chromone plane (dihedral angle between the rings 6.82°), since the bulky trimethylamino substituent hinders the close vertical stacking of the molecules. The planarity of both structures is probably stabilized by intramolecular hydrogen bonds between the chromone oxygen O1 and the amide nitrogen hydrogen and between the same hydrogen and the *ortho*-bromine (see *Fig. 46* and *Tab. 9*). Finally, a weak hydrogen bond between the *ortho*-carbon hydrogen H36 on the benzene ring and the amide oxygen might contribute to the planar character of both compounds. The tertiary amide **9i** shows an *anti*-rotamer

Biological testing

configuration, too. The substitution of amide hydrogen with a methyl group excludes the formation of hydrogen bond with the chromone oxygen O1 and the steric hindrance by the methyl group bends the C2–C21 bond out of the chromone plane (dihedral angle between the rings 12.08°). Selected torsion angles of the carboxamide bridge are summarized in *Tab. 10*.

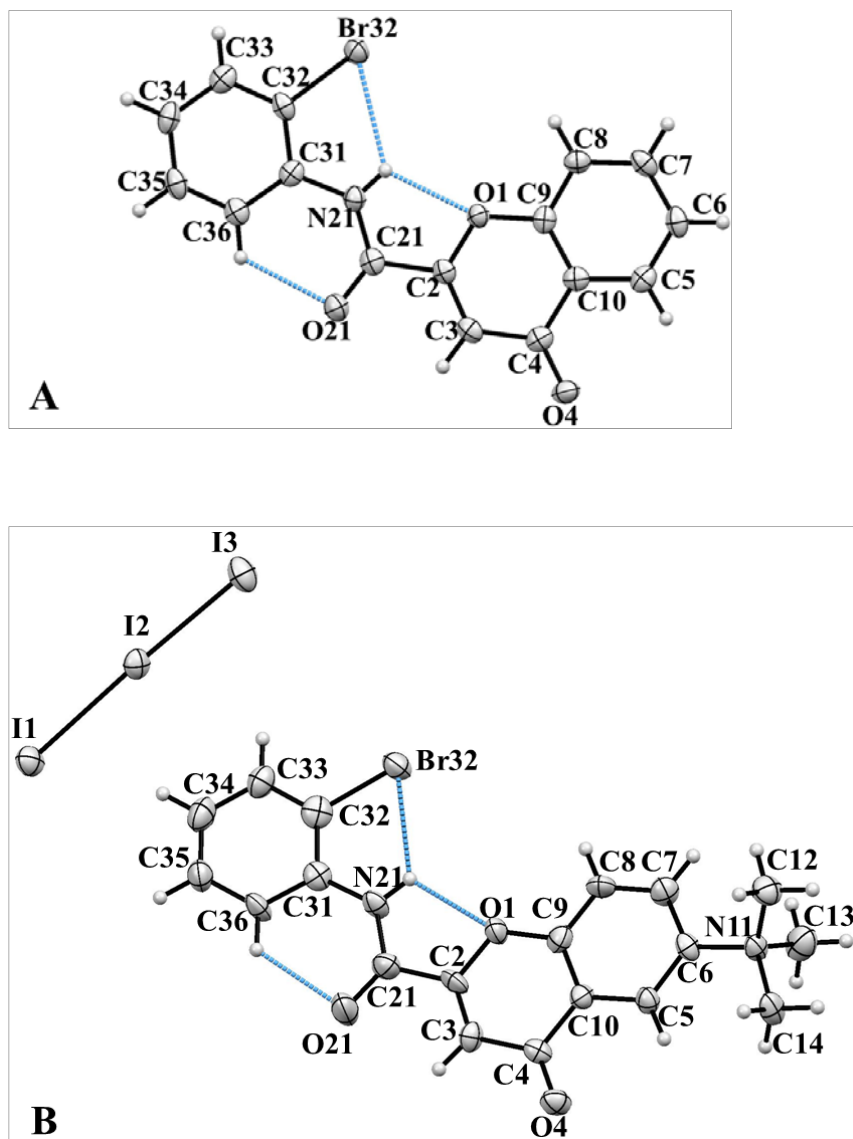


Fig. 46 A view of the molecules of *N*-(2-bromophenyl)-carboxamide **3b** (A) and 6-trimethylammonium triiodide salt of *N*-(2-bromophenyl)-chromone-2-carboxamide **19** (B). Intramolecular hydrogen bonds are shown as blue dashed lines. Hydrogens are designated with the same number as the atoms, to which they belong. Ellipsoids are displaced at 70 % probability level

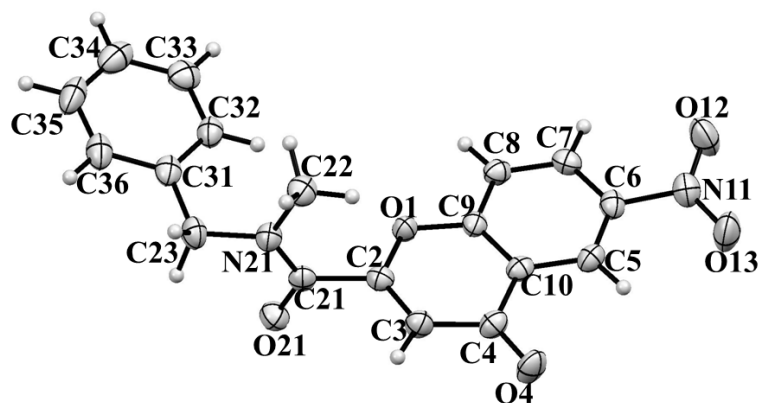


Fig. 47 A view of the molecule of *N*-methyl-*N*-benzyl-6-nitro-chromone-2-carboxamide **9i**. Hydrogens are designated with the same number as the atoms, to which they belong. Ellipsoids are displaced at 70 % probability level

Tab. 9 Selected intramolecular interactions in chromones **3b** and **19**

D-H...A	D-H (Å)	H...A (Å)	D...A (Å)	D-H...A (°)
(3b)				
N21-H21...O1	0.88	2.16	2.603 (3)	111
N21-H21...Br32	0.88	2.54	3.062 (2)	119
C36-H36...O21	0.95	2.26	2.879 (3)	122
(19)				
N21-H21...O1	0.88	2.16	2.613 (1)	111
N21-H21...Br32	0.88	2.56	3.068 (8)	118
C36-H36...O21	0.95	2.23	2.852 (1)	123

Tab. 10 Selected torsions in compounds **3b**, **19** and **9i** (°)

	(3b)	(19)
O1-C2-C21-O21	174.5(2)	173(1)
O1-C2-C21-N21	-4.8(3)	-6(1)
C2-C21-N21-H21	-1(2)	1
C2-C21-N21-C31	-179.2(2)	-179(1)
C21-N21-C31-C32	-176.5(2)	-175(1)
(9i)		
O1-C2-C21-O21	90.9(1)	
O1-C2-C21-N21	-88.5(1)	
C2-C21-N21-C22	0.9(2)	
C2-C21-N21-C23	176.2(1)	
C21-N21-C23-C31	-99.0(1)	
N21-C23-C31-C32	16.7(2)	

Biological testing

4.5.2.2 *Supramolecular structure*

Both chromones **3b** and **19** crystallize in a monoclinic space group (for details see *Tab. 54* in the Experimental section). The molecules form a zig-zag chain along the b-axis linked in both cases via C-H \cdots O hydrogen bonds involving the chromone oxygen O4 (see *Tab. 12*).

The supramolecular structure of compound **3b** is stabilized by the following weak dispersive interactions:

- C-H \cdots O: A pair of parallel molecules is connected by two weak hydrogen bonds between the chromone carbon hydrogens H7 and H8 of a perpendicularly positioned molecule and both O4 atoms of each of the two vertically aligned molecules (see *Fig. 48*).
- C-Br \cdots O: Further structure stabilization is achieved by a halogen bond between the bromine atom Br32 and the chromone oxygen O4 of the perpendicularly situated molecule.
- π - π : The two parallel molecules are relatively tightly stacked with the most proximate contacts between the atoms O21, C21 and C2 of the carboxamide bridge and the chromone carbons C4, C10 and C5, respectively, in an average distance of 3.23 Å. Considering the possible electron delocalization between the chromone carbon C2, carbonyl carbon C21 and the carbonyl oxygen, the close contacts toward the chromone carbons C4, C10 and C5 of the vertically positioned molecule indicate a π - π stacking interaction. The dihedral angle between the two quasi-parallel chromone planes is 6°. The distance between the carbonyl oxygen and the centroid from the vertically situated γ -pyrone ring is 3.42 Å.

In case of compound **19**, a steric hindrance by the voluminous trimethylamino substituent and the triiodide anion increases the dihedral angle between the two zig-zag oriented planes to 132° (calculated from the chromone rings of both molecules) compared to 80° in compound **3b**. The horizontally aligned molecules are stabilized by weak hydrogen bonds between the chromone ring oxygen O4 and the carbon hydrogen H7 (see *Fig. 49*). A possible π - π interaction is formed between the benzene- and γ -pyrone ring with a larger centroid-centroid distance of 3.65 Å. The dihedral angle between the benzene- and γ -pyrone planes of the quasi-parallel molecules is 6°. A close distance between the I2 atom of the triiodide molecule and the benzene hydrogen H34 indicates a halogen-hydrogen bond. Further weak halogen-hydrogen and halogen-halogen interactions may be formed between the triiodide atom I1 and the chromone hydrogen H8 and between the atoms I1 and Br32.

Biological testing

Compound **9i** crystallizes in a triclinic P-1 space group and forms centrosymmetric dimers (see *Fig. 50*). This supramolecular structure is stabilized by weak hydrogen bonds between the chromone carbon hydrogen H8 and the carboxamide oxygen O21 across the centre of symmetry. The chromone oxygen O4 might be involved in a weak hydrogen bond with the benzene carbon hydrogen H35 of the parallel translated molecule. There is a possible π - π stacking across the centre of symmetry between the γ -pyrone- and the benzene ring with a larger centroid-centroid distance of 3.64 Å. The dihedral angle between the quasi-parallel planes is 10°.

4.5.2.3 *Correlations between crystal and solubility data*

Since the crystal lattice significantly affects compound solubility, correlations between the obtained crystal structure and solubility data were derived (see *Tab. 14*). The “practically insoluble” (Ph. Eur.¹²⁸) chromone derivative **3b** constitutes of nearly planar molecules, that are linked into vertically stacked sheets by intermolecular halogen- and C-H \cdots O hydrogen interactions. A nearly 22-fold enhancement of aqueous solubility in compound **19** is mainly due to its ionic character. Additionally, the bulky trimethyl amino substituent and the triiodide anion affect both the molecular planarity and the tight vertical stacking. The tertiary amide **9i** possesses a 6-fold higher solubility compared to compound **3b**. Despite the reduced accessibility of the amide nitrogen for solvent molecules, the solubility is enhanced due to the steric hindrance by the *N*-methyl substituent, which disrupts the molecular planarity and leads to greater distances between the vertically stacked molecules. The decrease in crystal lattice energy is reflected in the reduction of melting point from 204 °C in **3b** to 132 °C in case of **9i**.

Biological testing

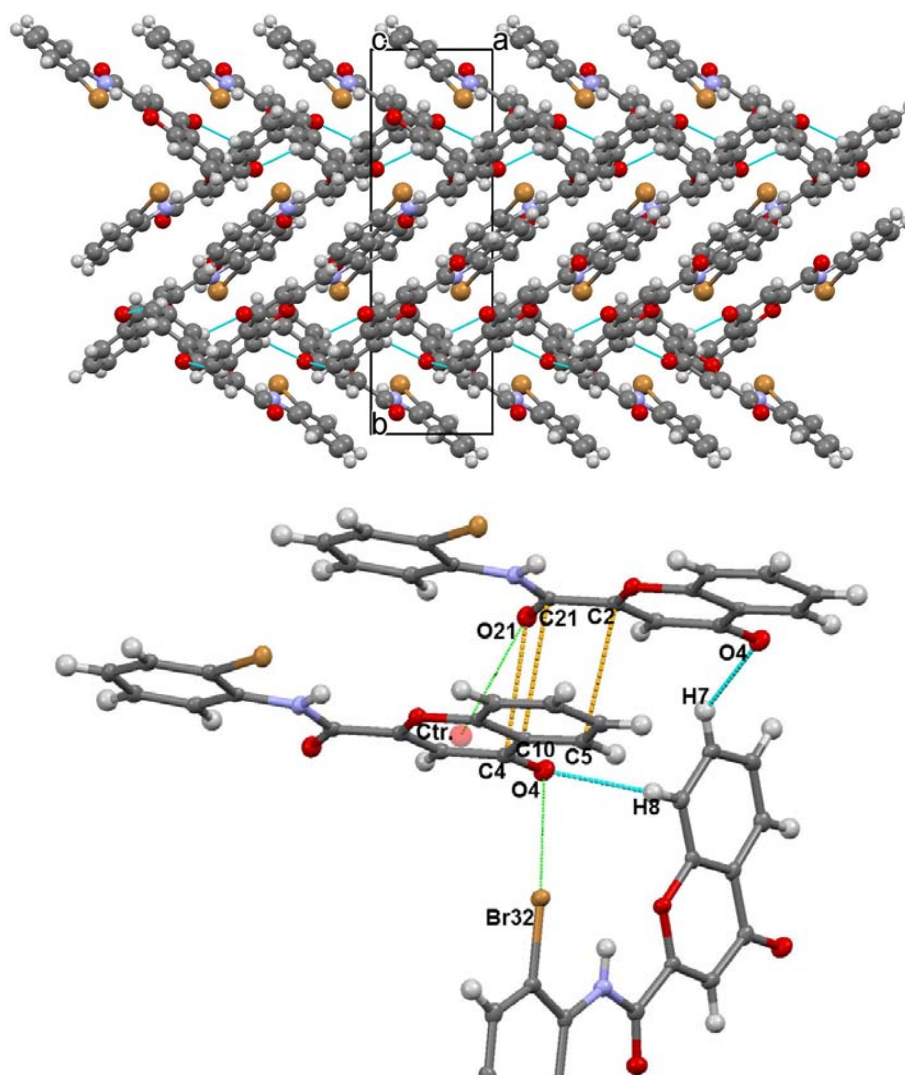


Fig. 48 *On the top:* Molecular packing of **3b** viewed down the *c* axis. Monoclinic $P2_1/n$ system: $a = 5.5 \text{ \AA}$, $b = 17.3 \text{ \AA}$, $c = 13.9 \text{ \AA}$; $\beta = 92.1^\circ$. *At the bottom:* The weak $C-H \cdots O$ hydrogen bonds to the chromone O4 atom from the hydrogens H7 and H8 of the two vertically stacked molecules are marked blue. The close contacts between the atoms C2, C21, O21 and C5, C10 and C4 are marked yellow. The distances between the bromine atom and the chromone oxygen O4 and between the centroid (Ctr.) of the γ -pyrone ring toward the carbonyl oxygen O21 (π - π interaction) are marked by green dotted lines.

Tab. 11 Selected intermolecular interactions in chromone **3b**. Symmetry codes: (i) $1/2+x, 1/2-y, -1/2+z$, (ii) $-1/2+x, 1/2-y, -1/2+z$, (iii) $-1+x, y, z$

D-H\cdotsA	D-H (Å)	H\cdotsA (Å)	D\cdotsA (Å)	D-H\cdotsA ($^\circ$)
C7-H7 \cdots O4 ⁱ	0.95	2.51	3.25 (3)	134
C8-H8 \cdots O4 ⁱⁱ	0.95	2.50	3.33 (3)	146
D-X\cdotsA	D-X (Å)	X\cdotsA (Å)	D\cdotsA (Å)	D-X\cdotsA ($^\circ$)
C32-Br32 \cdots O4 ⁱⁱ	1.90 (3)	3.53 (2)	5.14 (3)	140
π-π	(Å)			
C2-C5 ⁱⁱⁱ	3.30 (4)			
C21-C10 ⁱⁱⁱ	3.26 (4)			
O21-C4 ⁱⁱⁱ	3.13 (3)			
O21-Ctr. ⁱⁱⁱ	3.42			

Biological testing

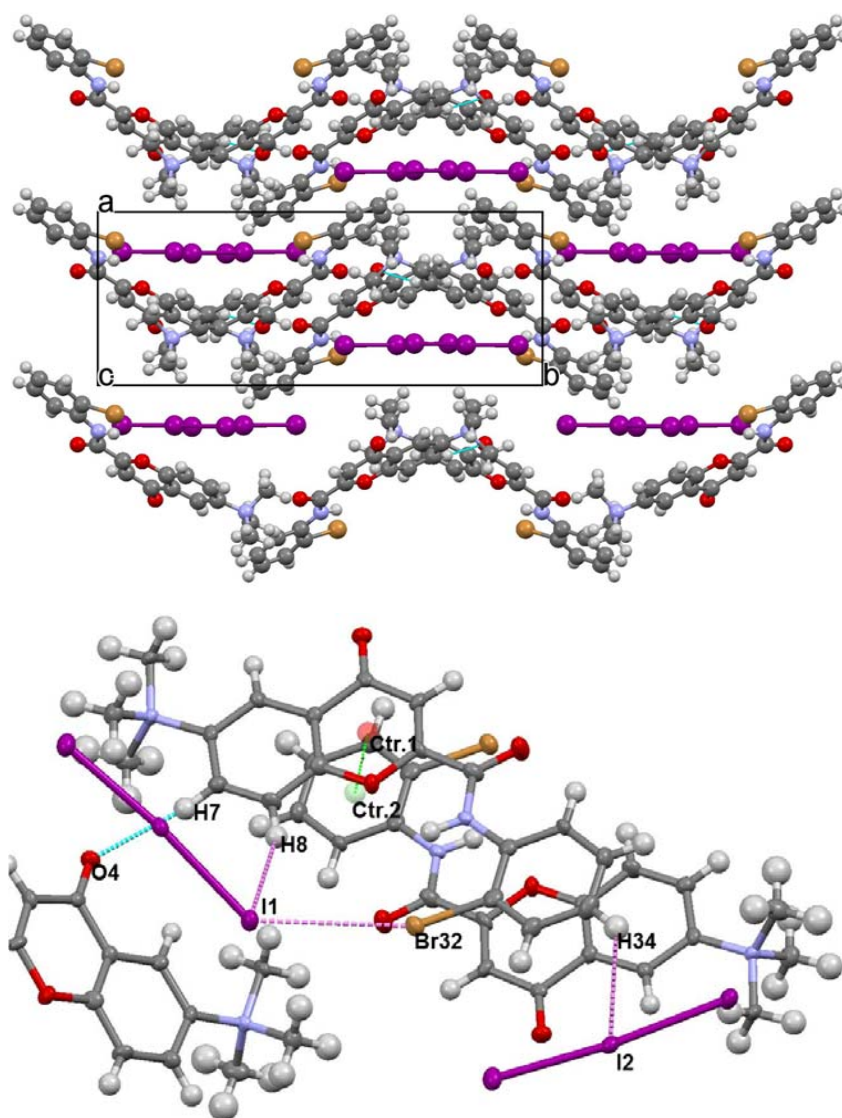


Fig. 49 *On the top:* Molecular packing of **19** viewed down the c axis. Monoclinic $P2_1/c$ system: $a = 8.4 \text{ \AA}$, $b = 21.4 \text{ \AA}$, $c = 13.0 \text{ \AA}$; $\beta = 90.8^\circ$. *At the bottom:* The weak $C-H\cdots O$ hydrogen bond between the chromone oxygen $O4$ and the hydrogen $H7$ of the horizontally aligned molecule (along the b axis) is marked blue. Close contacts indicating halogen-hydrogen and halogen-halogen interactions are marked violet. The distance between the centroids of the γ -pyrone- (Ctr.1) and benzene ring (Ctr.2) of the vertically stacked molecules are marked by a green dotted line.

Tab. 12 Selected intermolecular interactions in chromone **19**. Symmetry codes: (i) $x, 3/2-y, 1/2+z$, (ii) x, y, z , (iii) $-x, -1/2+y, 3/2-z$, (iv) $1-x, 2-y, 1-z$

D-H \cdots A	D-H (\AA)	H \cdots A (\AA)	D \cdots A (\AA)	D-H \cdots A ($^\circ$)
C7-H7 \cdots O4 ⁱ	0.95	2.48	3.41 (1)	165
C34-H34 \cdots I2 ⁱⁱ	0.95	3.08	3.78 (1)	132
C8-H8 \cdots I1 ⁱⁱⁱ	0.95	3.10	3.97 (1)	153
D-X \cdots A	D-X (\AA)	X \cdots A (\AA)	D \cdots A (\AA)	D-X \cdots A ($^\circ$)
C32-Br32 \cdots I1 ⁱⁱⁱ	1.91 (1)	3.81 (1)	5.63 (1)	158
π - π	(\AA)			
Ctr.1-Ctr.2 ^{iv}	3.65			

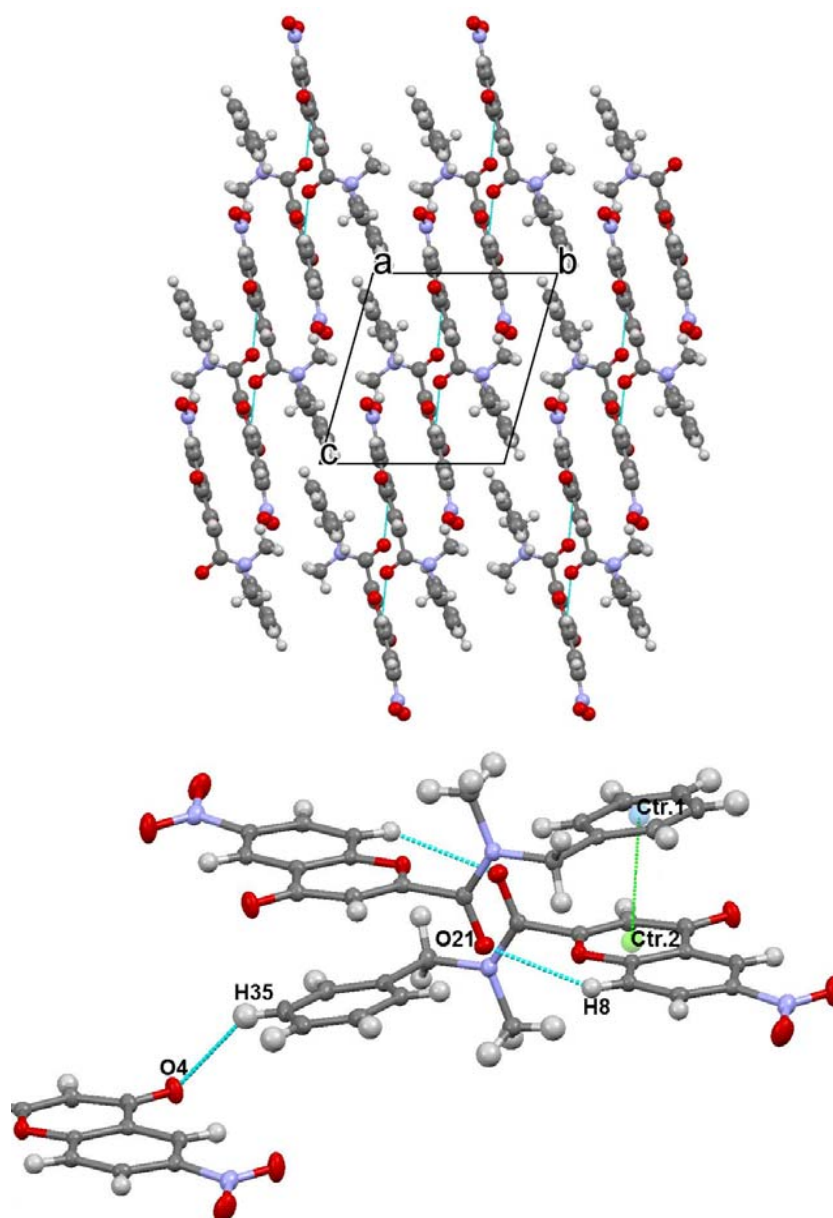


Fig. 50 *On the top:* Molecular packing of **9i** viewed down the *a* axis. Triclinic *P*-1 system: $a = 8.0 \text{ \AA}$, $b = 9.7 \text{ \AA}$, $c = 10.6 \text{ \AA}$; $\alpha = 105.1^\circ$, $\beta = 101.4^\circ$, $\gamma = 91.0^\circ$. *At the bottom:* The weak C-H \cdots O hydrogen bonds between the amide O21 atom and the hydrogen H8 of the centrosymmetrically situated molecules and between the chromone oxygen O4 and the benzene hydrogen H35 of the parallel translated molecules are marked blue. The distance between the centroids of the vertically stacked benzene and γ -pyrone plane is marked by a green dotted line.

Tab. 13 Selected intermolecular interactions in chromone **9i**. Symmetry codes: (i) $1-x, 1-y, 1-z$, (ii) $-1+x, -1+y, -1+z$, (iii) $1-x, 1-y, 1-z$

D-H \cdots A	D-H (Å)	H \cdots A (Å)	D \cdots A (Å)	D-H \cdots A ($^\circ$)
C8-H8 \cdots O21 ⁱ	0.95	2.64	3.43 (2)	141
C35-H35 \cdots O4 ⁱⁱ	0.95	2.69	3.49 (2)	142
π-π				
Ctr.1-Ctr.2 ⁱⁱⁱ	3.64			

Biological testing

Tab. 14 Correlation between assessed solubility and crystal/polarity data of compounds **3b**, **19** and **9i**.
[*] between the chromone and benzene plane in the molecule

	dihedral angle [°]*	π - π stacking [Å]	clogP	m.p. [°C]	Solubility [μ M]	logS
3b	1.07	3.42	2.32	204	10	-5.46
19	6.82	3.64	-1.92	215	217	-3.77
9i	12.08	3.65	1.96	132	61	-4.69

Compound solubilities were assessed in the KasA buffer (Tris, pH 8.5) by the shake flask method⁹⁴ using excess amounts (5 – 10 mg) of the tested compound suspended in buffer and equilibrated for 48 hours. After filtration through 0.45 μ m membrane filter, absorbance of each sample was measured at 342 nm. The resulting saturation concentration was calculated by linear regression from a calibration curve for each sample. Since no DMSO as a co-solvent was added, the obtained solubility values were substantially lower than the concentration steps, at which precipitation or deviation from the Beer-Lambert law occurred during the course of biological testing.

4.5.3 Solubilization assays

To prevent compound precipitation in aqueous environment, solubility enhancement can be achieved by diverse methods. Several references describe a solubilization of chromone-based compounds by the use of cyclodextrins.⁸⁶⁻⁸⁸ Furthermore, a variety of other solubilization techniques and their combinations are available, *e.g.* the use of co-solvents, lipid-based systems, amorphous dispersions or the formation of co-crystals, salts and prodrugs.⁸⁹

4.5.3.1.1 Cyclodextrins as solubilizing agents

Cyclodextrins are cyclic (α -1,4)-linked oligosaccharides, which consist of glucose units arranged in a form of truncated cone (see *Fig. 51*). The exterior surface is hydrophilic, while the cavity interior is nonpolar. A lipophilic ligand molecule of appropriate size can thus be enclosed in the cavity. Although cyclodextrins are mainly employed as aqueous solubility enhancers, they can also improve compound stability, bioavailability and prevent undesirable drug properties, *e.g.* taste, smell or irritation potential.⁹⁰ Cyclodextrins are degradation products of starch. The most common native cyclodextrins, α -, β - and γ -cyclodextrin (CD) contain six, seven, and eight glucopyranose units, respectively. α -Cyclodextrin binds appropriate aliphatic ligands, whereas the cavity size of β - and γ -CD is suitable for aromatic compounds. The water solubility of native CDs is limited (*e.g.* 18.5 g/l for β -CD at 25 °C) due to the strong intramolecular hydrogen bonds between the secondary hydroxyl groups, which

Biological testing

makes them less accessible for hydration. Solubilizing agents of significant industrial relevance are the CD derivatives prepared by etherification of the free hydroxyl groups.⁹¹ Finally, their applicability as solubilizers in enzyme assay was described for various β -CD derivatives.^{92,93}

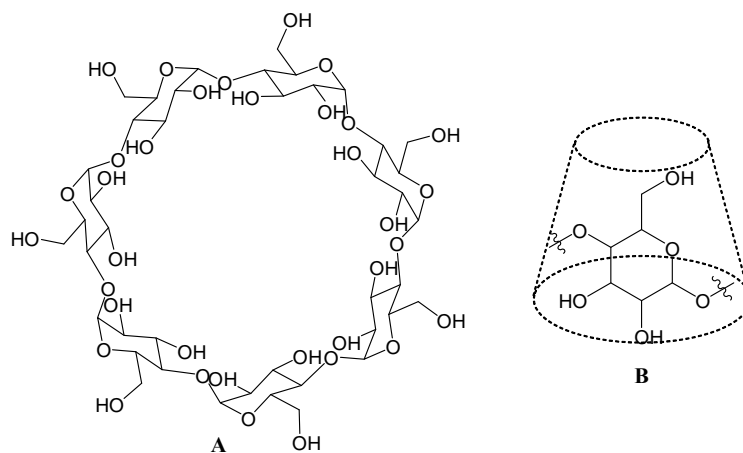


Fig. 51 Structure of β -cyclodextrin (A) and the arrangement of glucopyranose unit in the cycle, where the secondary hydroxyl groups are directed to the wider edge of the cone, while the primary hydroxyl groups shape the narrow edge (B)

4.5.3.2 Methods and results

4.5.3.2.1 Screening on suitable solubilizing agents among cyclodextrins

Since the problem of compound precipitation appeared first during the anti-infective screening, the aim of the initial cyclodextrin assay was to find suitable solubilizing agents improving the aqueous solubility of tested compounds at the conditions of antimicrobial testing (phosphate buffer, pH 7.4). Based on the cavity size (central cavity diameter 6 – 6.5 Å)⁹⁰ and available references for chromone-based compounds⁸⁶⁻⁸⁸, mainly the β -cyclodextrins were used (native β -cyclodextrin, heptakis-(2,6-di-*O*-methyl)- β -cyclodextrin (DIMEB), (2-hydroxypropyl)- β -cyclodextrin (HP- β -CD), triacetyl- β -cyclodextrin (TA- β -CD), β -cyclodextrin sulfate, native γ -cyclodextrin). At first, solubility of the ligand-cyclodextrin mixture was examined in buffer after an equilibration period (see *Method A*); afterwards, cyclodextrin was added to DMSO, in order to adopt the same procedure steps (DMSO stock solution, dilution in buffer, see *Method B*), as applied during the biological testing.

Method A: Stock solution containing 1 – 8 eq. of cyclodextrin (CD) in 10 mM potassium phosphate buffer, pH 7.4, was pipetted to 6 μ mol of **3b** in an eppendorf cap or a centrifuge tube. Pure buffer was added to reach equal concentration of **3b** in each series. Samples were shaken at 800 rpm (Thermomixer) at 30 °C for 24 hours.

Biological testing

Method B: Stock solution containing 1 – 8 eq. of CD in DMSO was pipetted to 6 μmol of **3b**. An appropriate volume of DMSO was added to reach equal concentration of **3b** in each series. After stirring (Vortex), stock solution was diluted with buffer in a 1:100 ratio and stirred for about 1 minute.

Evaluation and results

Solubility of all samples was inspected visually after centrifugation comparing the sediment layer of a CD/compound mixture to a reference of the pure substance. The absence of sediment was observed in samples with 2 eq. of DIMEB prepared from DMSO stock solution, which after dilution with buffer yielded a final 200 μM solution of **3b**. Method B using a DMSO stock solution containing 2 eq. of DIMEB was further applied on compounds **3a-4k**. The absence of sediment was observed for **3a, 3b, 3i, 3n, 4e, 4j** and **4k**.

4.5.3.2.2 Experiments on the complexation of **3b** with cyclodextrins by UV spectroscopy

4.5.3.2.2.1 Phase solubility study

Phase solubility techniques described by Higuchi and Connors⁹⁴ are widely used to investigate the effect of cyclodextrin on the solubility of tested compound. Following their method, excess amounts of **3b** (2 – 3 mg) were suspended in 1 ml of phosphate buffer solutions containing increasing amounts (0 – 3 eq.) of cyclodextrin (HP- β -CD, DIMEB). Blank solutions were prepared for each cyclodextrin concentration. All samples and blanks were equilibrated protected from light for 96 h by shaking at 25 °C. The supernatants were filtered through a 0.45 μm membrane filter. Subsequently, the absorbance of samples was measured in a cuvette at 305 nm after the zero adjustment with an appropriate blank solution. To transform absorbance data into corresponding concentrations, calibration line was formed using 1.0 mM DMSO stock solution of **3b** diluted in phosphate buffer. All samples were measured in duplicate. Increased absorbance values correlating with enhanced concentration of **3b** were observed after addition of both cyclodextrins (*Fig. 52*). Intrinsic concentration (without cyclodextrin) was 7 μM . Addition of 3 eq. of HP- β -CD increased the concentration to 56 μM (8-fold) and 3 eq. of DIMEB to 100 μM (14-fold). Higher CD concentrations would be necessary to verify the ascending tendency of the curve. The calibration curve in buffer/DMSO was linear till approximately 140 μM .

Biological testing

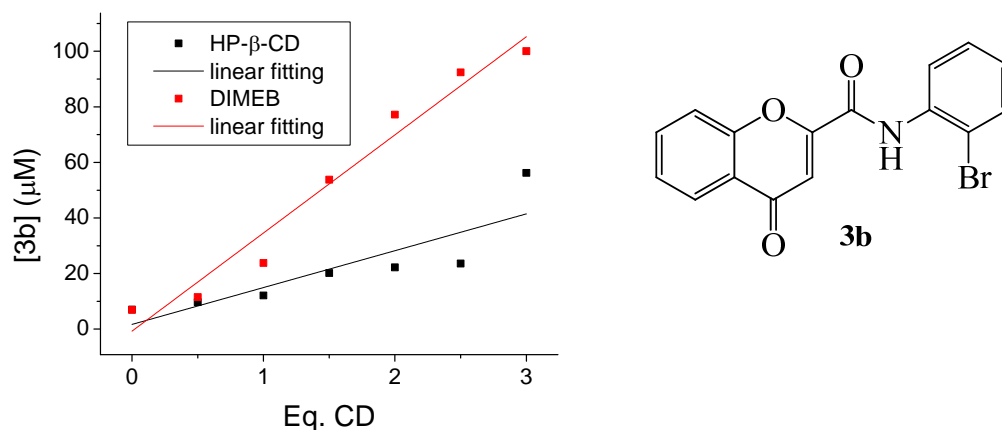


Fig. 52 Phase solubility diagram displaying the solubility of **3b** as a function of molar equivalents of the cyclodextrin (HP- β -CD, DIMEB) added

4.5.3.2.2.2 Method of continuous variation – Job Plot

Job Plot method enables the determination of complex stoichiometry. In this case, the curve in **Fig. 53** displays the absorbance change between the free and complexed state as a function of increasing ligand mole fraction in the ligand-cyclodextrin mixture. Alternatively, a change in chemical shift or fluorescence values can be obtained to assess complex stoichiometry. If possible, water should be used as a preferred solvent, since organic solvents might reduce the complexation efficiency through competitive binding or by decreased dielectric constant.⁹⁰ Nevertheless, absorbance measurements are only applicable for systems which conform the Beer-Lambert law, *i.e.*, the relation between measured absorbance and concentration is linear. When these conditions were met in aqueous solutions, sample absorbance was too small to be evaluated. Hence, 50% aqueous methanol was used as a solvent to prepare 0.05 mM stock solutions of **3b** and DIMEB. The samples 0 – 10 (see **Chap. 7.4.2.2**) with the increasing ligand mole fraction, as well as standards for the calibration line, were equilibrated for 24 h by shaking at RT in sealed centrifuge tubes. All samples were prepared in duplicate and the absorbances were measured at 305 nm promptly after removing the seal.

Biological testing

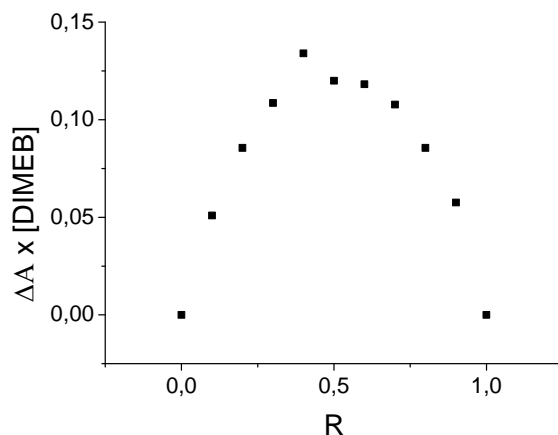


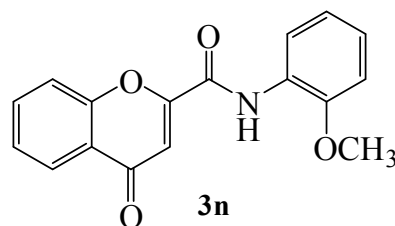
Fig. 53 Job plot for **3b** in a complex with DIMEB; x axis shows the varied molar ratio $R = [3b]/([DIMEB]+[3b])$, $[DIMEB]+[3b] = 1$; y axis shows the measured absorbance values (A_i) transformed into ΔA ($\Delta A = A_0 - A_i$, A_0 = absorbance of sample 0, A_i = absorbance of samples 1 – 10) and multiplied by molar equivalents of **3b** in samples 0 – 10

The absorbance values were plotted as reported by Negi and Singh⁹⁵. Maximum in absorbance difference at $R = 0.5$ is distinctive for 1:1 complex.⁹⁶ Complexes of 1:1 stoichiometry between chromone-based molecules and β -cyclodextrin have already been described in literature.^{86,88}

4.5.3.2.3 Cyclodextrin in the KasA binding assay

Based on the results of the first solubilization experiment, Method B was adapted to the KasA assay conditions.

Compound **3n** was dissolved in a 10 mM cyclodextrin (DIMEB) solution in DMSO to obtain a 5 mM concentration of **3n**. This stock solution was titrated into the enzyme/buffer mixture.



A decrease in the intrinsic tryptophan fluorescence was recorded immediately after addition of each concentration step as performed in case of other samples. Similarly as in the corresponding sample without DIMEB, the solution became turbid at 100 μM , but while in the sample without DIMEB the precipitate was visible at the 140 μM step, the sample with DIMEB remained turbid but lacking visible particles till the concentration of 300 μM . After correction of the obtained fluorescence data on the inner filter effect, the affinity constant was calculated from the nonlinear *Equation 2* using Origin software. The resulting curve (*Fig. 54*)

Biological testing

resembles a saturation curve at first till the concentration of 80 μM . Afterwards, the curve declines and raises again from the concentration step of 200 μM . This might be reasoned by an overcorrection on IFE at concentrations beyond the Beer-Lambert law, nevertheless, such a steep decline and repeated increase of saturation curve after reaching the maximum did not occur in any other sample tested. Other possible reasons could be enzyme denaturation, a prolonged lag phase due to the complexation or several different binding modes. The low affinity value calculated from the first part of the curve (K_D [$3n + \text{DIMEB}$]: $32.1 \pm 8.2 \mu\text{M}$, K_D [$3n$]: $117.3 \pm 22.8 \mu\text{M}$) does not conform the assumption, the rate of inhibitor binding to enzyme would decrease due to the competition between enzyme and cyclodextrin, since this behaviour would cause contrarily an increased affinity constant. Similarly, neither the affinity increase due to a higher DMSO content in the sample (titration of 5 mM stock solution) can be explained by a competitive non-specific binding of DMSO, since this competition would yield a higher affinity constant, too (a decreased affinity).

Kinetic experiments using different cyclodextrin concentrations would be needed in order to investigate the binding mode. Due to the limited enzyme batches, further measurements were not performed.

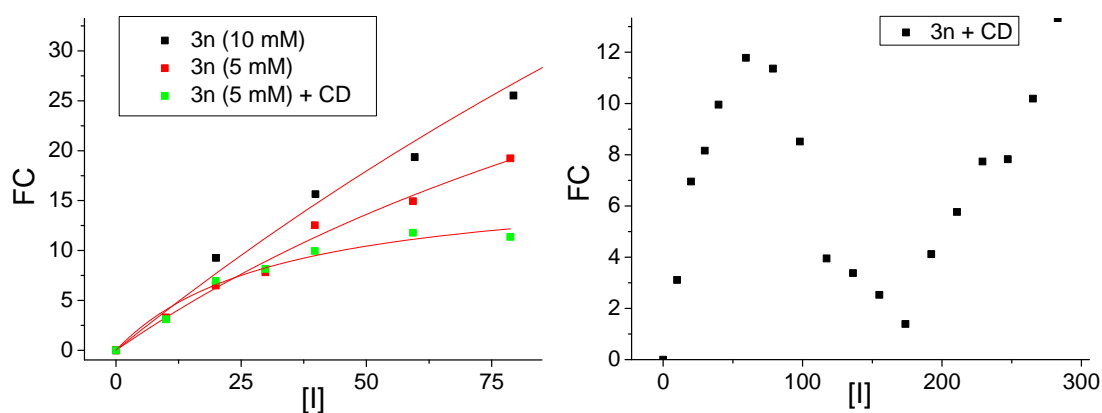


Fig. 54 Fluorescence change as a function of inhibitor concentration. **On the left:** titration curves using the 5 mM and 10 mM DMSO stock solutions of compound **3n** and of the 5 mM solution with cyclodextrin added, all of them till the 80 μM concentration of **3n**. **On the right:** titration curve of the 5 mM DMSO-cyclodextrin stock solution of **3n** till the concentration of 300 μM .

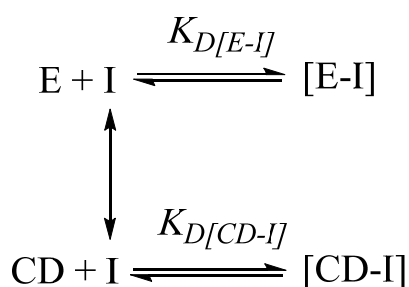
4.5.3.3 Discussion and prospects

The first solubilization assay yielded 7 compounds that appeared soluble in the conditions of anti-infective screening: 4-oxo-*N*-phenyl-4*H*-chromene-2-carboxamide **3a**, its *ortho*-substituted derivatives **3b** (2-bromo), **3i** (2-fluoro), **3n** (2-methoxy), as well as the *N*-furylmethyl, *N*-benzylpiperidinyl and *N*-cyclohexyl derivatives **4e**, **4j** and **4k**, respectively.

Biological testing

They were submitted to biological testing delivered in a 40 mM DIMEB-DMSO stock solution. Nevertheless, the results were not reproducible, as the first four compounds precipitated at 100 μ M concentration step during biological testing, and thus, their antimicrobial activity could not be evaluated. Although the final concentration of DMSO in the sample did not exceed 1 %, the complexation efficiency might be significantly decreased due to the initial dissolution of cyclodextrin in DMSO.

Regarding the phase solubility study in a phosphate buffer used for KasA assay, the dissolved fraction of **3b** increased with rising amounts of HP- β -CD and DIMEB added to the mixture. The reported Job plot for **3b** and DIMEB indicates the formation of 1:1 complex stoichiometry. Results obtained from a previous Job plot performed by NMR analysis (lyophilized from deuterated water and dissolved in MeOD/D₂O mixture) were not considered, due to the precipitate formation in some of the samples. The results derived from the fluorescence enzyme assay using compound **3n** dissolved in DIMEB/DMSO stock solution are not reliable due to the limited solubility. Further experiments would be necessary to identify the cyclodextrin complex and to prepare a stock solution in buffer that could replace the DMSO stock solution used in the KasA binding assay. The influence of cyclodextrin complexation on affinity constant must be considered, as the fraction of free inhibitor is decreased and the rate of this process is characterized by equilibrium constants for inclusion formation.⁹²



Scheme 16 Equilibria between the free and bound inhibitor fractions for a 1:1 cyclodextrin complex. The rate of binding to enzyme is characterized by an overall dissociation constant $K_{D[\text{E-I}]}$, whereas the rate of binding to cyclodextrin is characterized by an overall dissociation constant $K_{D[\text{CD-I}]}$.

4.6 Docking of compound **9i** into the KasA binding pocket

For the model chromone compound **GS-71** (**3b**), no reliable KasA binding data were obtained due to its poor solubility in testing buffer. Therefore, to enable a comparison between the *in silico* and the *in vitro* assessed affinity, the chromone derivative **9i** was docked into the KasA binding site. The docking was performed in the research group of Prof. Sottriffer in cooperation with his postgraduate student M. Kuhn. The protein and ligand setup and the subsequent docking were conducted using the same settings as reported by Topf³⁹. Only the use of a new program version (GOLD, v. 5.2) and a higher number of GA runs differed from the published procedure. Simultaneously, TLM was redocked into KasA binding site and the docking of **GS-71** was repeated using the parameters as for compound **9i**. The procedure is described in the Experimental section, *Chap. 7.8*.

4.6.1 Introduction

Docking is a process that enables the prediction of the most advantageous ligand orientation with respect to its possible inter- and intramolecular interactions in the enzyme active site. Conversely, the ligand pose known from a solved crystal structure of the ligand-enzyme complex can be virtually restored in a process called redocking. A root-mean-square-distance (RMSD) between the experimental and the predicted ligand pose is used to verify the docking parameters. This value might usually not exceed 2 Å. Besides generating the preferred ligand pose, a docking program can also estimate ligand affinity by means of “scoring functions“, which enable the evaluation of the docking results according to their descending affinity.¹¹⁹ The docking program GOLD¹²⁰ (Genetic Optimization for Ligand Docking), used by Topf³⁹ for compound **GS-71**, applies a genetic algorithm to reveal the possible ligand and active site conformations. Genetic algorithm (GA) is a computational technique imitating the natural selection in a process of evolution. The possible orientations of each rotatable bond in a given structure are compared to the hereditary potential bound on chromosomes, whereas the resulting docking poses represent the various phenotypes of the second generation formed by exchange of the parent genetic information, involving their mutation and cross-over. At the end of this iterative process, only the best solutions, *i.e.*, the docking poses with the highest fitness, are selected and ranked using scoring functions.¹²⁰ The force-field-based scoring function GOLDScore¹²⁰, implemented in GOLD, summarizes the scores of inter- and intramolecular hydrogen bonds and van der Waals interactions, including the intramolecular strain.¹¹⁹ The latter scoring function applied here, SFC_290m¹²¹, is an empirical function

Biological testing

derived from the analysis of known affinity data for a large collection of complex crystal structures. This scoring function evaluates a plenty of descriptors, for instance the number of rotatable bonds, contact surface area, ring-ring interactions, using a multiple linear regression, which yields the pKi value that can be directly compared to the experimental affinity data obtained from a kinetic enzyme assay.¹²¹

4.6.2 Docking results

4.6.2.1 Redocking of TLM

All the obtained solutions possessed similar scoring results, ranging from 51.11 to 52.84 (GOLDscore) and 5.00 to 5.36 (SFCscore: SFC_290m), respectively. The docking pose with the highest sum of the both scoring values (*Fig. 55*) displayed a high similarity to the crystal structure with RMSD value of 0.98.

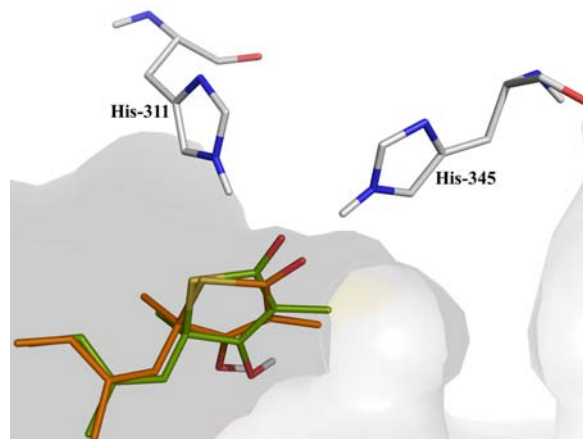


Fig. 55 Overlap of redocked (orange) and native (green backbone) TLM structures. Nonpolar hydrogens have been omitted.

4.6.2.2 Repeated docking of GS-71

The solutions obtained for GS-71 possessed generally higher values for both scoring functions, and thus, a higher affinity than TLM. GOLDscore results were found in a wider range from 52.69 to 60.35, whereas SFCscore values were between 6.10 and 6.98. Three main solution clusters with descending GOLDscore results can be recognized:

- The solution resembling at most the docking pose published by Topf³⁹ belonged to the lowest ranked cluster. Its orientation in the binding site is displayed in *Fig. 56* as Pose 1. The oxo group of the chromone ring (O4) is directed toward His-311 and His-345, the benzene ring of the chromone moiety is oriented toward the large hydrophobic pocket, whereas the amide part shows no overlap with the TLM

Biological testing

structure. The amide bridge is situated nearly on the same plane as the chromone ring, the benzene ring is inclined to the chromone plane by dihedral angle 33.39° (calculated in Mercury, v. 2.4). The *trans* position between the amide carbonyl and the chromone ether oxygen (O1) enables the formation of an intramolecular hydrogen bond between the amide nitrogen and the chromone oxygen O1 (D-A: 2.7 Å, H-A: 2.1 Å).

- Slightly higher GOLDScore- and SFCscore values were received for Pose 2 (see *Fig. 56*). Similarly as in the previous pose, the chromone oxygen O4 is directed toward the both active site histidines. Nevertheless, the rest of the molecule is horizontally inverted, and thus the amide part is located inside the large hydrophobic pocket. The amide bridge is bent out of the chromone plane.
- Finally, the docking pose representing the best ranked cluster is shown in *Fig. 56* as Pose 3. Conversely to the both previously described poses, there is no hydrogen bond between the oxo group of the chromone ring and the both histidines. The chromone moiety is situated in the large hydrophobic pocket, whereas the amide oxygen is oriented toward His-311.

4.6.2.3 Docking of compound **9i**

The predicted affinity values for the newly synthesized chromone compound were generally higher than those of **GS-71**. The lowest GOLDScore result was 55.02, the highest value reached 62.04, whereas the SFCscore results ranged from 6.60 to 7.40. Despite the wide value range in case of both scoring functions, the docking poses for nearly all solutions resembled the orientation in Pose 3 of **GS-71**. Due to the enhanced compound flexibility, the amide oxygen is situated in a higher proximity of the both active site histidines, where it might serve as a dual hydrogen bond acceptor. Unlike the previously described poses of **GS-71**, where the substituents on the amide C-N bond are in the *anti*-rotamer-configuration, **9i** shows a *syn*-orientation of both rings, probably due to the steric hindrance of the active site amino acids. A representative docking pose with the shortest distance between the amide oxygen and the proximate hydrogens of both histidines is shown in *Fig. 56*.

Biological testing

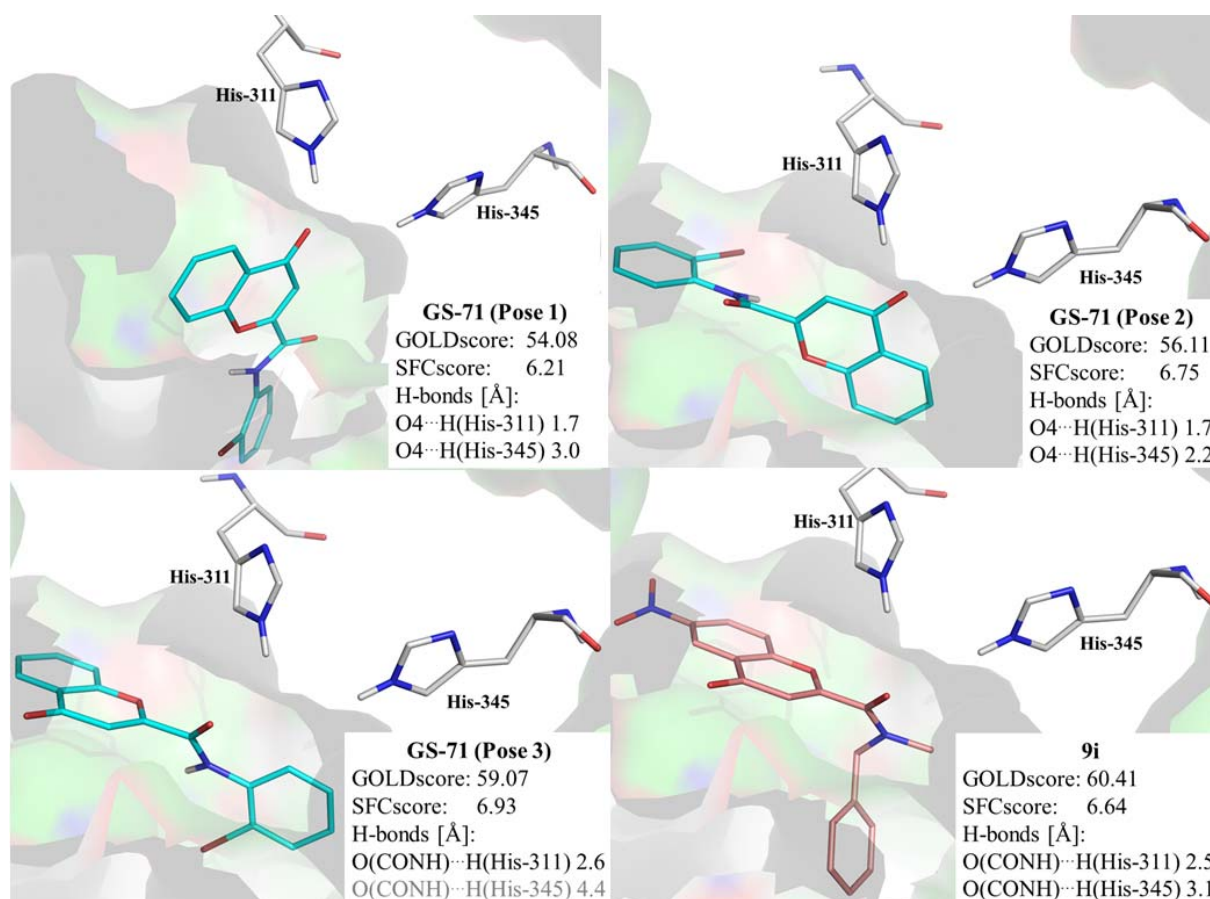


Fig. 56 The resulting docking poses of **GS-71** (turquoise) and **9i** (coral) with the highest sum of GOLD- and SFCscore values and with the closest contact between the polar hydrogens of the active site histidines and the corresponding hydrogen bond acceptor

4.6.3 Discussion

The docking parameters were successfully verified as can be seen from the low RMSD value for TLM in redocking (0.98). Regarding the repeated docking of **GS-71**, a similar docking pose (Pose 1) was obtained as published by Topf³⁹. Beside this pose, further two preferred ligand orientations were generated (Pose 2 and 3). For both of them, a higher affinity was predicted. Due to the lacking dual hydrogen bond acceptor in Pose 3 replacing the thiolactone oxygen in the interaction with the two active site histidines, this orientation might not be included in the selection of docking hits. Considering the remaining poses, their GOLD- and SFC-score results are not significantly different from each other, and thus their ranking results might be strongly dependent on the program version used. The scoring results obtained for TLM and **GS-71** using GOLD, v. 5.2 were higher in comparison to those generated in GOLD, v. 4.0 (see *Tab. 15*), maintaining though the same tendency. Furthermore, the planar character of the amide bridge and the possible intramolecular hydrogen bond formation might favour Pose 1 as an energetically more stable option than Pose 2, considering the absence of any

Biological testing

accessible hydrogen bond acceptor among the amino acids in the closest proximity of the amide nitrogen. Regarding the newly synthesized chromone **9i**, the preferred orientation is in agreement with the best ranked pose for **GS-71** and appears to be the pose, that optimally suits the enzyme cavity. In case of **9i**, the amide oxygen is situated in a closer proximity of the active site histidines, where it can replace the thiolactone oxygen of TLM as a dual hydrogen bond acceptor.

Tab. 15 Predicted (pK_i) and experimental (pK_D) affinity values obtained from two different GOLD versions and assessed in the binding assay (n.d. = not determined)

	TLM	GS-71	9i
pK_i predicted (GOLD, v. 5.2)	5.27	6.21	6.64
pK_i predicted (GOLD, v. 4.0)³⁹	4.84	5.85	n.d.
pK_D / K_D [μM] experimental	3.84 / 142	n.d.	4.02 / 96

As displayed in *Tab. 15*, the *in silico* obtained pK_i values for TLM and **9i** are higher than the corresponding *in vitro* results, nevertheless, the tendency remains similar, *i.e.*, the affinity results for compound **9i** surpass those obtained for TLM. Due to the distinct binding poses obtained for both chromone compounds, **GS-71** and **9i**, the affinity values assessed meanwhile in the binding assay for chromone-2-carboxylic acid anilides and for the corresponding benzylamides, respectively, might be evaluated separately, unless their binding mode is elucidated by an x-ray analysis of the ligand-enzyme complex or their affinity is confirmed in a kinetic enzyme assay.

5 Summary

With 9.6 million new cases and 1.2 million deaths in 2014, tuberculosis (TB) is alongside with AIDS the most deadly infection.⁸ Foremost, the increased prevalence of resistant strains of *M. tuberculosis* among the TB-infected population represents a serious threat. Hence, in the last decades, novel drug targets have been investigated worldwide. So far a relatively unexplored target is the cell wall enzyme β -ketoacyl-ACP-synthase “KasA”, which plays a crucial role in maintaining the membrane impermeability and hence the cell ability to resist to the immune response and drug therapy. KasA is a key enzyme in the fatty acid synthase “FAS-II” elongation cycle, responsible for the extension of the growing acyl chain within the biosynthesis of precursors for the most hydrophobic constituents of the cell wall – mycolic acids. Design of the novel KasA inhibitors, performed in the research group of Prof. Sotriffer by C. Topf and B. Schaefer, was based on the recently published crystal structure of KasA³⁵ in complex with its known inhibitor thiolactomycin (TLM). Considering the essential ligand-enzyme interactions, a pharmacophore model was built and applied in the virtual screening of a modified ZINC database. Selected hits with the best *in silico* affinity data have been reported by Topf³⁹ and Schaefer³⁸.

In this work, two of the obtained hits were synthesized and their structure was systematically varied. First, a virtual screening hit, chromone-2-carboxamide derivative **GS-71 (3b, Fig. 57)**, was modified in the amide part. Since the most of the products (**3a-p, 4a-k**) possessed a very low solubility in the aqueous buffer medium used in biological assays, polar groups (nitro, succinamidyl and trimethyl-amino substituent in position 6 of the chromone ring – compounds **9a-j, 12a-i, 19**, or hydroxyl group on the benzene ring in the amide part – compounds **7a-c**) have been inserted to the molecule. Further variations yielded diaryl ketones (**13, 14**), diaryl ketone bearing a succinamidyl substituent (**16**), carboxamide bearing a methylpiperazinyl-4-oxobutanamido group (**17**) and methyl-malonyl ester amides (**18a-b**). Basically, the essential structural features necessary for the ligand-enzyme interactions have been maintained. The latter virtual screening hit, a pyrimidinone derivative **VS-8**³⁸ (**22a, Fig. 58**) was synthesized and the structure was modified by substitution in positions 2, 4, 5 and 6 of the pyrimidine ring (compounds **21a-e, 22a-e, 23**). Due to autofluorescence, detected in most of the products, this model structure was not further varied.

Summary

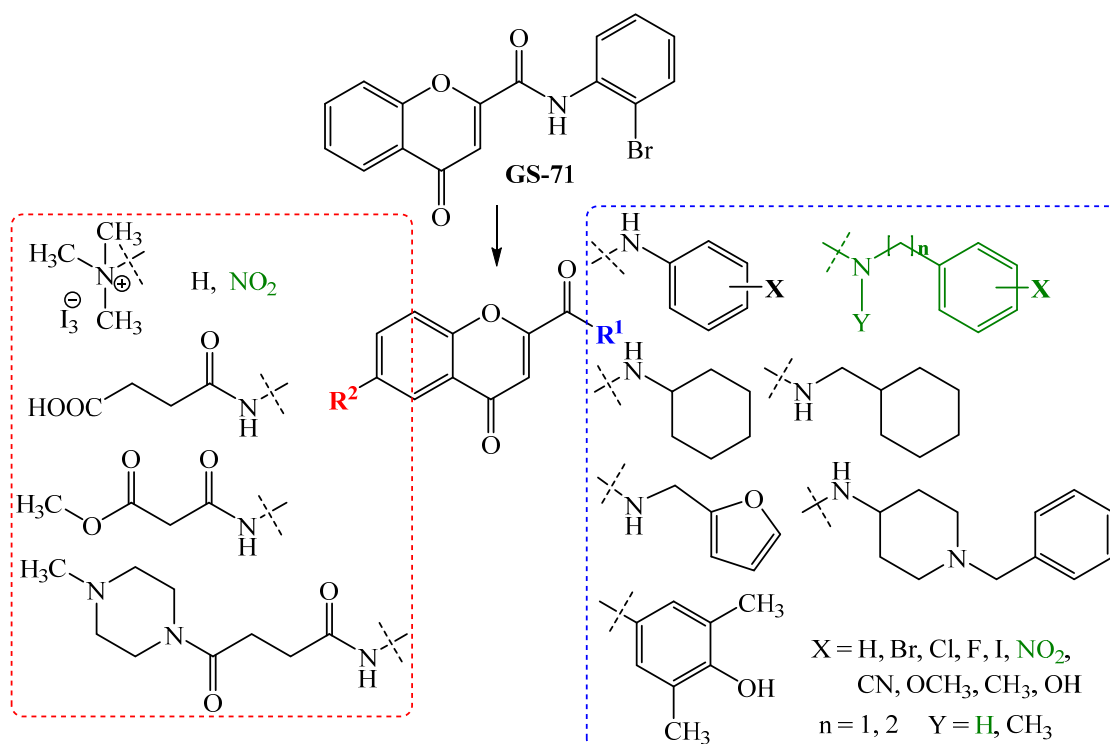


Fig. 57 General structure of products derived from model compound **GS-71** (substituents of the most active compounds with $K_D < 50\mu\text{M}$ are marked green)

Simultaneously, experiments on solubilization of the first chromone-2-carboxamides with cyclodextrins, cyclic oligosaccharides known to form water-soluble inclusion complexes, were performed. Although the assessed solubility of the chromone **3b**/DIMEB (1:3) mixture exceeded 14-fold the intrinsic one, the achieved 100 μM solubility was still not sufficient to be used as a stock solution in the binding assay. The experiments with cyclodextrin in combination with DMSO were ineffective. Owing to high material costs necessary for the appropriate cyclodextrin amounts, the aim focused on structural modification of the hydrophobic products.

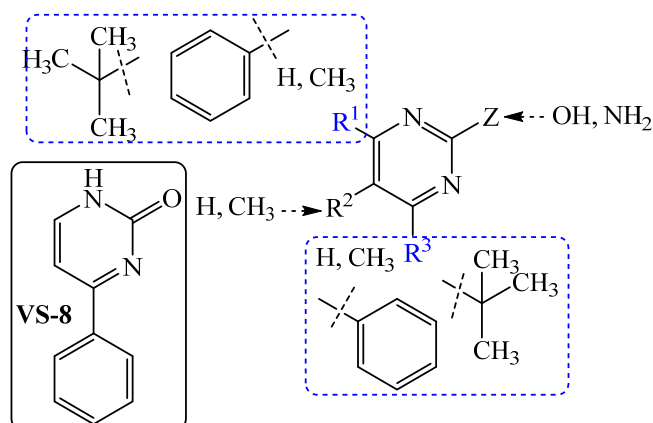


Fig. 58 General structure of products derived from **VS-8**

Summary

Precise structural data have been obtained from the solved crystal structures of three chromone derivatives: the screening hit **3b** (**GS-71**), its trimethylammonium salt **18** and 6-nitro-substituted *N*-benzyl-*N*-methyl-chromone-2-carboxamide **9i**. The first two compounds are nearly planar with an *anti*-/*trans*-rotamer configuration. In the latter structure, the carboxamide bridge is bent out of the chromone plane, showing an *anti*-rotamer, too. Considering the relatively low partition coefficient of compound **3b** (cLogP = 2.32), the compound planarity and correlating tight molecular packing might be the factors significantly affecting its poor solubility.

Regarding the biological results of the chromone-based compounds, similar structure-activity correlations could be drawn from the binding assay and the whole cell activity testing on *M. tuberculosis*. In both cases, the introduction of a nitro group to position 6 of the chromone ring and the presence of a flexible substituent in the amide part showed a positive effect. In the binding study, the nitro group at position 4 on the *N*-benzyl residue was of advantage, too. The highest enzyme affinity was observed for *N*-(4-nitrobenzyl)-chromone-2-carboxamide **4c** ($K_D = 34 \mu\text{M}$), 6-nitro substituted *N*-benzyl-chromone-2-carboxamide **9g** ($K_D = 40 \mu\text{M}$) and 6-nitro-substituted *N*-(4-nitrobenzyl)-chromone-2-carboxamide **9j** ($K_D = 31 \mu\text{M}$), which could not be attributed to the fluorescence quenching potential of the nitro group. The assay interference potential of chromones, due to a covalent binding on the enzyme sulfhydryl groups, was found to be negligible at the assay conditions. Moderate *in vivo* activity was detected for 6-nitro-substituted *N*-benzyl-chromone-2-carboxamide **9g** and its *N*-benzyl-*N*-methyl-, *N*-furylmethyl-, *N*-cyclohexyl- and *N*-cyclohexylmethyl derivatives **9i**, **9d**, **9e**, **9f**, for which MIC values 20 – 40 μM were assessed (see *Tab. 16*). Cytotoxicity was increased in the *N*-cyclohexylmethyl derivative only. None of the pyrimidine-based compounds showed activity *in vivo*. The affinity of the model structure, **VS-8** (**22a**), surpassed with $K_D = 97 \mu\text{M}$ the assessed affinity of TLM ($K_D = 142 \mu\text{M}$).

Since for the model chromone compound **GS-71** no reliable KasA binding data could be obtained, a newly synthesized chromone derivative **9i** was docked into the KasA binding site, in order to derive correlation between the *in silico* and *in vitro* assessed affinity. For the 6-nitro-derivative **9i** a moderate *in vivo* activity on *M. tuberculosis* was obtained. The *in silico* predicted pK_i values for TLM and **9i** were higher than the corresponding *in vitro* results, maintaining though a similar tendency, *i.e.*, the both affinity values for compound **9i** (pK_i predicted = 6.64, pK_D experimental = 4.02) surpassed those obtained for TLM

Summary

(pK_i predicted = 5.27, pK_D experimental = 3.84). Nevertheless, the experimental pK_D values are considered preliminary results.

Tab. 16 Compounds active in the whole cell assay (see general structure in **Fig. 57**) [a] 21th day of incubation, [b] 14th day of incubation

	R ¹	R ²	MIC [μ M]	K _D [μ M]
9d	-NO ₂	-NH-CH ₂ -(2-furyl)	40 ^a	97
9e	-NO ₂	-NH-C ₆ H ₁₁	20 ^a	72
9f	-NO ₂	-NH-CH ₂ -C ₆ H ₁₁	40 ^a	n.d.
9g	-NO ₂	-NH-CH ₂ -C ₆ H ₅	40 ^b	40
9i	-NO ₂	-NCH ₃ -CH ₂ -C ₆ H ₅	40 ^a	96

The binding assay method has been improved in order to acquire more accurate data. Owing to the method development, limited enzyme batches and solubility issues, only selected compounds could be evaluated. The best hits, together with the compounds active on the whole cells of *M. tuberculosis*, will be submitted to the kinetic enzyme assay, in order to confirm the TLM-like binding mechanism. Regarding the *in vivo* testing results, no correlations could be drawn between the predicted membrane permeability values and the experimental data, as for the most active compounds **9e** and **9f**, a very low permeability was anticipated (0.4 and 0.7 %, respectively). Further biological tests would be required to investigate the action- or transport mode.

6 Zusammenfassung

Mit 9.6 Millionen Neuerkrankungen und 1.2 Millionen Todesfällen im Jahr 2014 ist Tuberkulose (TB) neben AIDS die häufigste Todesursache unter Infektionskrankheiten.⁸ Insbesondere die zunehmende Verbreitung resistenter Stämme von *M. tuberculosis* stellt eine ernste Gefahr dar. In den letzten Jahrzehnten wurde daher weltweit nach neuen möglichen Wirkstoff-Zielen gesucht. Bisher noch relativ unerforschtes Ziel ist das Zellwand-Enzym β -Ketoacyl-ACP-Synthase "KasA", das eine entscheidende Rolle bei der Aufrechterhaltung der Membran-Dichtigkeit spielt, und somit den Zellen ermöglicht, gegen den Immunabwehr und Arzneimitteltherapie Resistenz zu zeigen. KasA ist ein Schlüsselenzym in der Fettsäure-Synthase-(FAS-II)-Elongationsrunde, die für die Erweiterung der wachsenden Acylkette während der Biosynthese der Vorstufen der hydrophobesten Zellwand-Bestandteilen – der Mykolsäuren, verantwortlich ist. Das Design der neuen KasA-Hemmer, das im Arbeitskreis von Prof. Sotriffer von C. Topf und B. Schäfer durchgeführt wurde, basiert auf der kürzlich veröffentlichten Kristallstruktur von KasA im Komplex mit seinem bekannten Inhibitor Thiolactomycin (TLM)³⁵. In Anbetracht der essentiellen Ligand-Enzym-Wechselwirkungen wurde ein Pharmakophor-Modell erstellt und im virtuellen Screening einer modifizierten ZINC-Datenbank angewendet. Die ausgewählten "Hits" mit den besten *In-silico*-Affinitätsdaten wurden in den Doktorarbeiten von Topf³⁹ und Schaefer³⁸ veröffentlicht.

In Rahmen dieser Arbeit wurden zwei der erhaltenen "Hits" synthetisiert und ihre Struktur systematisch variiert. Erste Modellstruktur, das Chromon-2-Carboxamid-Derivat **GS-71**³⁹ (**3b**, *Fig. 59*) wurde zunächst in dem Amid-Rest modifiziert. Da die meisten Produkte (**3a-p**, **4a-k**) eine sehr geringe Löslichkeit im wässrigen Puffermedium aufwiesen, wurden polare Gruppen in das Molekül eingefügt (Nitro, Succinamidyl- und Trimethyl-Amino-Substituenten in der 6 Stellung des Chromon-Rings - Verbindungen **9a-j**, **12a-i**, **19**, oder eine Hydroxyl-Gruppe am Benzolring im Amid-Teil - Verbindungen **7a-c**). Weitere Variationen ergaben Diarylketone (**13**, **14**), ein Diarylketon mit der Succinamidyl Kette (**16**), ein Carboxamid mit dem Methylpiperazinyl-4-oxobutanamido-Substituenten (**17**) und Methyl-Malonyl-Ester-Amide (**18a-b**). Grundsätzlich wurden alle Strukturmerkmale notwendig für die Ligand-Enzym-Wechselwirkungen beibehalten. Die letztere Modellstruktur aus dem virtuellen Screening, das Pyrimidinon Derivat **VS-8**³⁸ (**22a**, *Fig. 60*) wurde synthetisiert, und die Struktur wurde durch Substitution in den Positionen 2, 4, 5 und 6 des Pyrimidin-Rings modifiziert

Summary

(Verbindungen **21a-e**, **22a-e**, **23**). Wegen Eigenfluoreszenz, detektiert in den meisten Produkten, wurde diese Modellstruktur nicht weiter variiert.

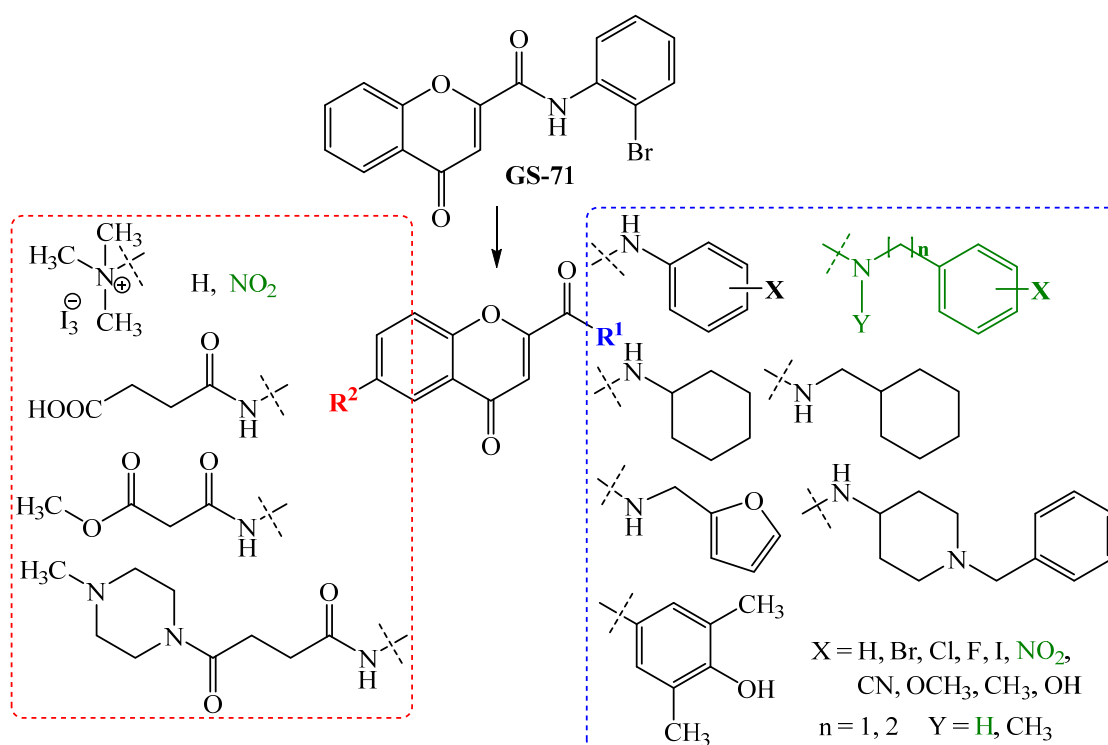


Fig. 59 Allgemeinstruktur der Derivaten abgeleitet von **GS-71** (Substituenten der am meisten aktiven Verbindungen mit $K_D < 50\mu\text{M}$ sind grün markiert)

Gleichzeitig wurden Experimente zur Solubilisierung der ersten Chromon-2-Carbonsäureamide mit Cyclodextrinen, cyclischen Oligosacchariden, die bekanntlich wasserlösliche Einschlusskomplexe bilden, durchgeführt. Obwohl die gemessene Löslichkeit des **3b**/DIMEB (1:3)-Gemisches die intrinsische Löslichkeit um das 14-fache überschritt, war die erzielte Löslichkeit von 100 μM noch nicht ausreichend, um diese Lösung als Stammlösung im Assay zu verwenden. Die Experimente mit Cyclodextrin in Kombination mit DMSO waren unproduktiv. Aufgrund der hohen Materialkosten für die benötigten Cyclodextrinmengen wurden die Löslichkeit-Tests an dieser Stelle abgebrochen und eine strukturelle Modifizierung der hydrophoben Produkte stand in Vordergrund des Interesses.

Summary

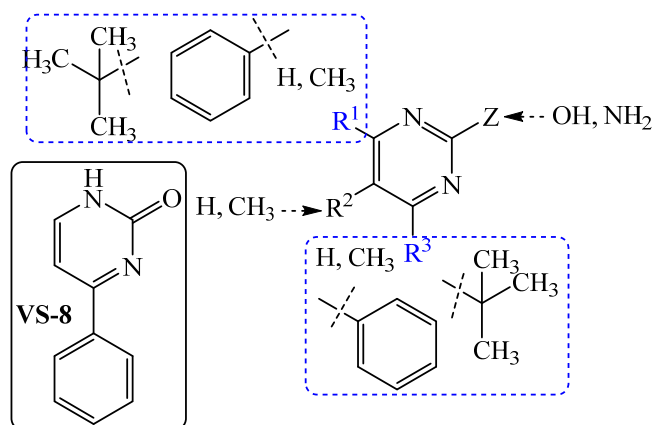


Fig. 60 Allgemeinstruktur der Derivaten abgeleitet von VS-8

Genauere Strukturdaten wurden aus den aufgeklärten Kristallstrukturen von drei Chromon-Derivaten, der Modellstruktur **3b** (GS-71), seiner Trimethylammoniumsalz **18** und dem 6-Nitro-substituierten *N*-Benzyl-*N*-methyl-Chromon-2-Carboxamid **9i**, erhalten. Die ersten beiden Verbindungen sind mit einer *anti*-/*trans*-Rotamer Konfiguration fast planar. Die Carbonsäureamid-Brücke der letzteren Struktur, die ebenso ein *anti*-Rotamer darstellt, wird aus der Chromon Ebene gebogen. Angesichts des relativ geringen Verteilungskoeffizienten der Verbindung **3b** ($\text{clogP} = 2.32$), die Ebenheit des Moleküls und das damit verbundene enge Molekülpackung könnten die wesentlich schlechtere Löslichkeit begründen.

In Bezug auf die biologischen Ergebnisse der Chromon-basierten Verbindungen, ähnliche Struktur-Aktivitäts-Beziehungen können aus dem Bindungs-Assay, sowie aus dem Ganzzellaktivitätstests auf *M. tuberculosis* gezogen werden. In beiden Fällen zeigte die Einführung einer Nitrogruppe in die Position 6 des Chromon-Rings und das Vorhandensein eines flexiblen Substituenten im Amidrest einen positiven Effekt. In dem Bindungs-Assay war die Nitrogruppe in Position 4 des *N*-Benzyl-Rests ebenso vorteilhaft. Die höchste Enzymaffinität wurde im Falle des *N*-(4-Nitrobenzyl)-Chromon-2-Carboxamid **4c** ($K_D = 34 \mu\text{M}$), des substituierten 6-nitro-*N*-Benzyl-Chromon-2-Carboxamid **9g** ($K_D = 40 \mu\text{M}$) und des 6-Nitro-substituierten *N*-(4-Nitrobenzyl)-Chromon-2-Carboxamid **9j** ($K_D = 31 \mu\text{M}$), beobachtet, allerdings konnte sie nicht dem Fluoreszenzlöschungspotenzial der Nitrogruppe zugeschrieben werden. Das Assay-Störpotential der Chromonverbindungen aufgrund einer kovalenten Bindung an die Sulfhydryl-Gruppen des Enzyms zeigte sich in den Assay-Bedingungen als vernachlässigbar. Moderate *in vivo*-Aktivitäten wurden für den 6-nitro substituierten *N*-Benzyl-Chromon-2-Carboxamid **9g** und dessen *N*-Benzyl-*N*-Methyl- (**9i**), *N*-Furfurylmethyl- (**9d**), *N*-Cyclohexyl- (**9e**) und *N*-Cyclohexylmethyl- (**9f**) Derivate, für denen die MIC-Werte zwischen 20 und 40 μM erhalten wurden (siehe Tab. 17). Die Zytotoxizität wurde erhöht nur im Falle des *N*-Cyclohexylmethyl Derivates. Keine der

Summary

Pyrimidin-basierten Verbindungen wies eine Aktivität *in vivo* auf. Die KasA-Affinität der Modellstruktur **VS-8 (22a)** übertraf mit $K_D = 97 \mu\text{M}$ die gemessene Affinität von TLM ($K_D = 142 \mu\text{M}$).

Da für die Modell Chromon-Verbindung **GS-71** keine zuverlässigen KasA Bindungsdaten erhalten werden konnten, ein neu-synthetisierte Chromon-Derivat **9i** wurde in die KasA Bindungsstelle gedockt, um die Korrelation zwischen den *In-silico*- und *In-vitro*-Affinitätswerten abzuleiten. Für den 6-Nitroderivat **9i** wurde eine mäßige Aktivität *in vivo* auf *M. tuberculosis* bestimmt. Die *in silico*-vorhergesagten pKi-Werte für TLM und **9i** waren allgemein höher als die entsprechenden experimentellen Ergebnisse. Sie bewiesen allerdings eine ähnliche Tendenz, d.h. die beiden Affinitätswerte für die Verbindung **9i** (pKi vorhergesagt = 6.64, pK_D experimentell = 4.02) übertrafen die Werte von TLM (pKi vorhergesagt = 5.27, pK_D experimentell = 3.84). Dennoch sind die experimentellen Affinitätsdaten nur als vorläufige Resultate zu betrachten, solange die Bindungsweise mittels des kinetischen Enzymassays verifiziert wird.

Tab. 17 Verbindungen aktiv im Ganzzell-Assay (siehe allgemeine Struktur in **Fig. 59**) [a] 21. Tag der Inkubation, [b] 14. Tag der Inkubation

	R¹	R²	MIC [μM]	K_D [μM]
9d	-NO ₂	-NH-CH ₂ -(2-furyl)	40 ^a	97
9e	-NO ₂	-NH-C ₆ H ₁₁	20 ^a	72
9f	-NO ₂	-NH-CH ₂ -C ₆ H ₁₁	40 ^a	n.d.
9g	-NO ₂	-NH-CH ₂ -C ₆ H ₅	40 ^b	40
9i	-NO ₂	-NCH ₃ -CH ₂ -C ₆ H ₅	40 ^a	96

Die Assay-Methode wurde verbessert, um zuverlässigere Daten zu erhalten. Aufgrund der Verfahrensentwicklung, den limitierten Enzymchargen und Löslichkeitsprobleme konnten nur ausgewählte Verbindungen bewertet werden. Die besten "Hits", zusammen mit den Verbindungen, die auf den ganzen Zellen von *M. tuberculosis* aktiv waren, werden dem kinetischen Enzymtest vorgelegt. In Bezug auf die *In-vivo*-Testergebnisse, es konnten keine Korrelationen zwischen den vorhergesagten Membranpermeabilität-Werten und den experimentellen Daten gezogen werden, da bei den wirksamsten Verbindungen **9e** und **9f** nur eine sehr geringe Permeabilität erwartet wurde (zu 0.4 und 0.7 %). Weitere biologische Tests wären erforderlich, um das Wirkungsmechanismus oder die Transportweise zu untersuchen.

7 Experimental section

7.1 General Methods

7.1.1 Measuring devices

Melting points were determined on a MPD350.BM 3.5 Sanyo Gallenkamp BV melting point apparatus (Leicestershire, UK) and were not corrected.

¹H- und ¹³C-NMR spectra were recorded on a Bruker Avance 400 spectrometer (400.132 MHz) at 300 K, (Bruker BioSpin MRI GmbH, Ettlingen, Germany). Chemical shifts δ were referenced against the solvent signal (¹H-NMR/¹³C-NMR: δ (DMSO-*d*6) = 2.50/39.52 ppm. Signal multiplicities are abbreviated as follows: s = singlet, d = doublet, dd = doublet of doublet, t = triplet, q = quartet, dt = doublet of triplets, ddd = doublet of doublet of doublet, td = triplet of doublets, m = multiplet, b = broad signal. The NMR spectra were analysed using Topspin, vers. 3.0.

IR spectra were recorded on a diamond ATR crystal using a Jasco FT-IR-6100 Spectrophotometer (Jasco, Gross-Umstadt, Germany).

UV-Vis-absorbance spectra were recorded on an UVmini-1240 Spectrophotometer (Shimadzu, Duisburg, Germany).

ESI-MS spectra of selected compounds were recorded on LC/MSD Trap G2445D (Agilent, Waldbronn, Germany).

Fluorescence spectra were recorded on a Varian Cary Eclipse Fluorescence spectrophotometer (Agilent, Böblingen, Germany). Fluorescence data were recorded using Cary Eclipse Software Package.

X-ray crystal data were collected on a Bruker X8APEX diffractometer (Ettlingen, Germany) with a CCD area detector and multi-layer mirror monochromated MoK α radiation. The structures were solved applying direct methods, refined with the Shelx software package (Sheldrick, 2008)¹¹³ and expanded using Fourier techniques. Bond lengths, angles and torsions were calculated using Mercury software, vers. 2.4.

Microwave-assisted reactions were performed in a MLS-rotapREP microwave system, (Milestone, Leutkirch, Germany). An ionic liquid, 1-butyl-3-methyl-imidazolium chloride (BMIM Cl) was used as a solvent to enhance the absorbance of the microwave radiation.

Experimental section

Stirring and shaking devices used for solubilization experiments included: Thermomixer comfort (Eppendorf, Hamburg, Germany), Vortex Genie 2 (Scientific Industries, Inc., Bohemia, New York, USA), OS-500 Shaker (VWR International, Darmstadt, Germany).

7.1.2 Chromatography

Thin layer chromatography was performed on TLC silica gel sheets SIL G-25 UV254, (Macherey Nagel, Düren, Germany). Fluorescence quenching was monitored after UV irradiation at 254 nm. Amines and carboxylic acids were also detected using Ehrlich's and bromocresol green reagents.

Column chromatography was conducted using the wet method of column loading with a dispersion of Silica gel 60 (Merck, Darmstadt, Germany) in a given mobile phase.

HPLC measurements were performed on an Agilent HPLC-System, Series 1100 und 1200 (Waldbronn, Germany) using a diode array detector (DAD) and the following HPLC columns:

- Inertsil ODS-2 (5 μm , 150 \times 4.6 mm, MZ-Analysetechnik, Mainz, Germany) for *LogP and peak purity determination*
- Hypersil Gold (5 μm , 150 \times 4.6 mm, Thermo Fisher Scientific Inc.) for *Content determination of compound 9d*

7.1.3 Chemicals

Chemicals and solvents were purchased from Sigma-Aldrich (Schnelldorf, Germany), Acros Organics (Geel, Belgium), Fisher Scientific (Schwerte, Germany), Merck (Darmstadt, Germany), Alfa-Aesar (Karlsruhe, Germany) and VWR International (Darmstadt, Germany).

Anhydrous organic solvents used in water-sensitive reactions were prepared by refluxing in the presence of phosphorus pentoxide (acetonitrile), calcium chloride (chloroform, dichloromethane), magnesium (ethanol, methanol), sodium (cyclohexane, petrolether) and by subsequent distillation. Anhydrous solvents were kept under argon and stored over molecular sieves (0.3 or 0.4 nm). Only HPLC- (methanol, acetonitrile) or molecular biology grade (DMSO) solvents were used for analytical and biological purposes. The percentage of solvent mixtures is reported in volume percent (v/v). **Water** used in synthesis was demineralized. For analytical and biological experiments, water was purified by Milli-Q-System, Merck Millipore GmbH (Schwalbach am Taunus, Germany).

Experimental section

7.1.4 Software

Molecular weights (M_r), exact masses (M) and partition coefficients ($\log P/\text{clog} P$) were calculated in ChemDrawUltra, vers. 12. Dissociation constants were calculated using OriginPro, vers. 8.6.0, and „R“, vers. 2.15.1. Protein and ligand structure was viewed in PyMOL, vers. 1.3.

7.2 Synthesis

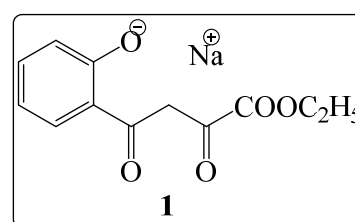
7.2.1 Synthesis of 4-oxo-4H-chromene-2-carboxylic acid **2**

Starting compound **2** was prepared in two steps following mainly the procedure reported by Nicolas *et al.*⁴²

Sodium 2-(4-ethoxy-3,4-dioxobutanoyl)phenolate (**1**)

2.4 g (104.3 mmol) of sodium were added gradually into 40 ml of anhydrous ethanol. The mixture was refluxed until complete reaction of the metal. The excessive solvent was removed by distillation first under normal pressure, than *in vacuo*. The fresh sodium ethoxide was suspended in 50 ml of anhydrous petrolether. Subsequently, a mixture of diethyl oxalate (5 ml; 36.8 mmol) and 2-hydroxyacetophenone (4 ml, 33.2 mmol) in 30 ml of anhydrous petrolether was added dropwise over a period of 30 min. while the mixture was cooled to RT. Finally, petrolether was removed by distillation, the residue was dried *in vacuo* and stored overnight over phosphorus pentoxide. The intermediate **1** was used for the next step without further purification.

Formula:	$C_{12}H_{11}NaO_5$
M_r [g/mol]:	258.2
Appearance:	orange solid
Yield:	6.76 g (79 %)
M.p. [Lit.]:	204 – 207 °C [210 – 212] ⁹⁷

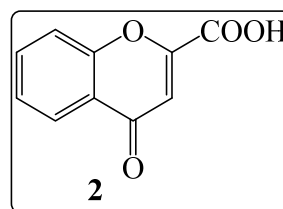


4-Oxo-4H-chromene-2-carboxylic acid (**2**)

A ring closure and a partial hydrolysis of **1** occurred by adding a mixture of conc. HCl in ethanol (1:1, 10 ml), stirring for 30 min at RT and subsequent reflux with 20 ml of 10% HCl for 2 hours. Ethanol was removed by distillation and the residue was cooled on ice bath. The precipitate was separated by filtration, washed carefully with ice cold water and dried over phosphorus pentoxide. The crude product was purified by recrystallization from a methanol/water mixture (2:1). Obtained analytical data are consistent with literature^{42,98}.

Experimental section

Formula:	C ₁₀ H ₆ O ₄
M _r [g/mol]:	190.2
Appearance:	white solid
Yield [Lit.]:	3.77 g (79 %) [89 %] ⁴²
M.p. [Lit.]:	258 – 259 °C [254 – 256] ⁴²
Reaction control:	CHCl ₃ /EtOH 20:1, R _f = 0.38

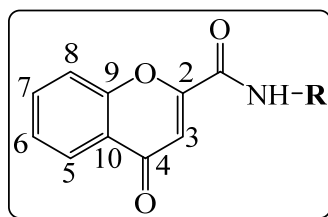


7.2.2 Synthesis of 4-oxo-4H-chromene-2-carboxamides 3a–p and 4a–k

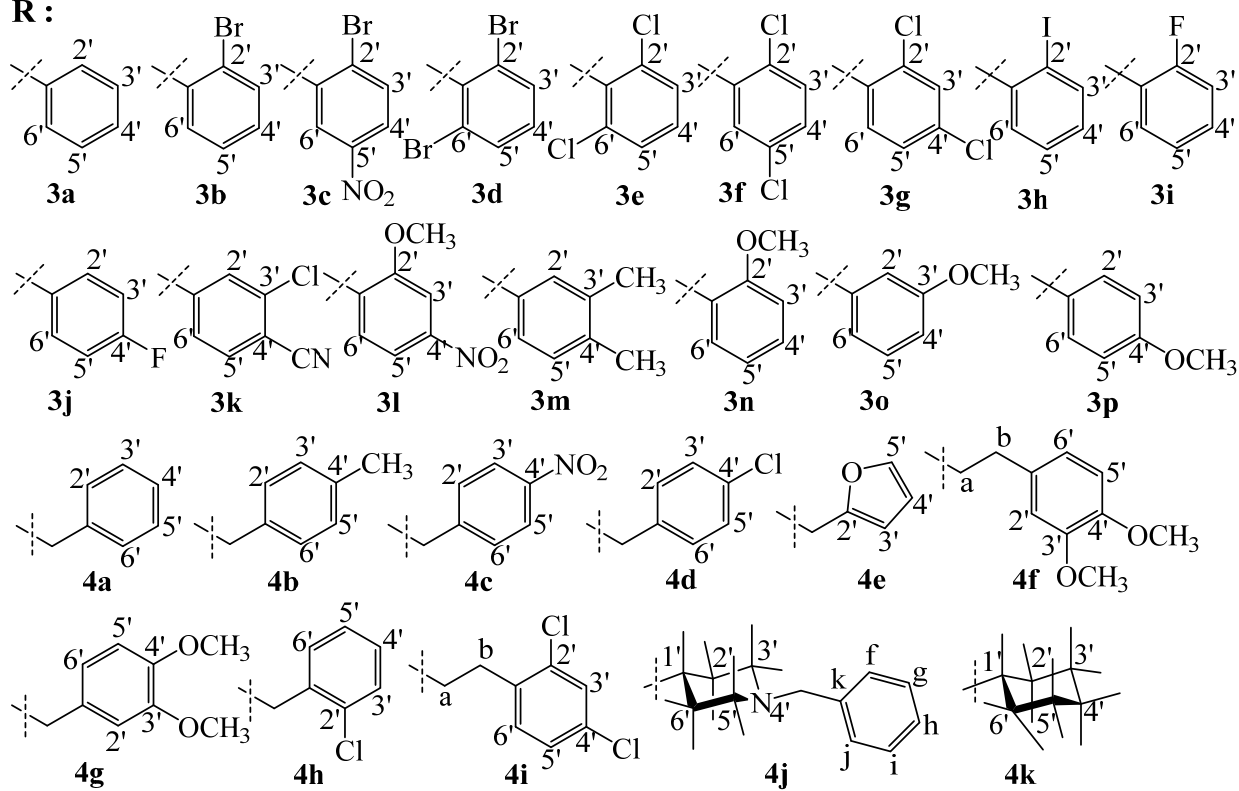
7.2.2.1 General procedure

To a suspension of **2** in 15 - 20 ml of anhydrous cyclohexane, 1.1 eq. of phosphorus pentachloride were added. The mixture was refluxed for 30 min. under argon, while the *in situ*-formed chloride completely dissolved. After cooling to 0 °C, 3.6 eq of triethylamine were added dropwise. Then, 1.8 eq. of the corresponding amine were added (see *Tab. 18*). The mixture was stirred overnight at RT. After cooling to 0 °C, the precipitate formed was filtered, washed with water and dried over phosphorus pentoxide. Reaction products depicted in *Scheme 17* were obtained as solids after purification by column chromatography („C“) or recrystallization („R“, see *Tab. 19*).

Experimental section



R :



Scheme 17 *Products 3a-p and 4a-k*

Tab. 18 Reaction details for the synthesis of 3a-p and 4a-k

	Name	Compound 2	PCl ₅	Amine	Et ₃ N	Yield [Lit.]
3a	4-oxo- <i>N</i> -phenyl-4 <i>H</i> -chromene-2-carboxamide ^{99,100}	0.29 g (1.5 mmol)	0.34 g (1.7 mmol)	aniline, 0.25 ml (2.7 mmol)	0.82 ml (5.4 mmol)	0.19 g (48 %) [86 %] ⁹⁹
3b	<i>N</i> -(2-bromophenyl)-4-oxo-4 <i>H</i> -chromene-2-carboxamide ⁵³	1.00 g (5.3 mmol)	1.2 g (5.8 mmol)	2-bromoaniline, 1.08 ml (9.5 mmol)	2.92 ml (19.0 mmol)	1.40 g (77 %) [45 %] ⁵³
3c	<i>N</i> -(2-bromo-5-nitrophenyl)-4-oxo-4 <i>H</i> -chromene-2-carboxamide	0.41 g (2.2 mmol)	0.50 g (2.4 mmol)	2-bromo-5-nitroaniline, 0.84 g (3.9 mmol)	1.18 ml (7.8 mmol)	0.57 g (68 %)
3d	<i>N</i> -(2,6-dibromophenyl)-4-oxo-4 <i>H</i> -chromene-2-carboxamide	0.41 g (2.2 mmol)	0.50 g (2.4 mmol)	2,6-dibromoaniline, 0.98 g (3.9 mmol)	1.18 ml (7.8 mmol)	0.39 g (43 %)
3e	<i>N</i> -(2,6-dichlorophenyl)-4-oxo-4 <i>H</i> -chromene-2-carboxamide ⁵⁴	0.55 g (2.9 mmol)	0.66 g (3.2 mmol)	2,6-dichloroaniline, 0.85 g (5.2 mmol)	1.60 ml (10.4 mmol)	0.36 g (37 %) [59 %] ⁵⁴
3f	<i>N</i> -(2,5-dichlorophenyl)-4-oxo-4 <i>H</i> -chromene-2-carboxamide	0.30 g (1.6 mmol)	0.37 g (1.8 mmol)	2,5-dichloroaniline, 0.47 g (2.9 mmol)	0.88 ml (5.8 mmol)	0.30 g (56 %)
3g	<i>N</i> -(2,4-dichlorophenyl)-4-oxo-4 <i>H</i> -chromene-2-carboxamide ⁵⁴	0.55 g (2.9 mmol)	0.66 g (3.2 mmol)	2,4-dichloroaniline, 0.85 g (5.2 mmol)	1.60 ml (10.4 mmol)	0.34 g (35 %) [59 %] ⁵⁴
3h	<i>N</i> -(2-iodophenyl)-4-oxo-4 <i>H</i> -chromene-2-carboxamide ¹⁰¹	0.30 g (1.6 mmol)	0.36 g (1.8 mmol)	2-iodoaniline, 0.63 g (2.9 mmol)	0.88 ml (5.8 mmol)	0.44 g (70 %)
3i	<i>N</i> -(2-fluorophenyl)-4-oxo-4 <i>H</i> -chromene-2-carboxamide	0.50 g (2.6 mmol)	0.60 g (2.9 mmol)	2-fluoroaniline, 0.45 ml (4.7 mmol)	1.42 ml (9.4 mmol)	0.48 g (65 %)
3j	<i>N</i> -(4-fluorophenyl)-4-oxo-4 <i>H</i> -chromene-2-carboxamide	0.50 g (2.6 mmol)	0.60 g (2.9 mmol)	4-fluoroaniline, 0.45 ml (4.7 mmol)	1.42 ml (9.4 mmol)	0.46 g (63 %)
3k	<i>N</i> -(3-chloro-4-cyanophenyl)-4-oxo-4 <i>H</i> -chromene-2-carboxamide	0.19 g (1.0 mmol)	0.23 g (1.1 mmol)	3-chloro-4-cyanoaniline, 0.27 g (1.8 mmol)	0.54 ml (3.6 mmol)	0.15 g (46 %)
3l	<i>N</i> -(2-methoxy-4-nitrophenyl)-4-oxo-4 <i>H</i> -chromene-2-carboxamide	0.30 g (1.6 mmol)	0.36 g (1.8 mmol)	2-methoxy-4-nitrophenylaniline, 0.48 g (2.9 mmol)	0.88 ml (5.8 mmol)	0.34 g (63 %)
3m	<i>N</i> -(3,4-dimethylphenyl)-4-oxo-4 <i>H</i> -chromene-2-carboxamid	0.50 g (2.6 mmol)	0.60 g (2.9 mmol)	3,4-dimethylaniline, 0.57 g (4.7 mmol)	1.42 ml (9.4 mmol)	0.42 g (55 %)
3n	<i>N</i> -(2-methoxyphenyl)-4-oxo-4 <i>H</i> -chromene-2-carboxamide ⁵³	0.31 g (1.6 mmol)	0.37 g (1.8 mmol)	2-methoxyaniline, 0.33 ml (2.9 mmol)	0.88 ml (5.8 mmol)	0.35 g (74 %) [90 %] ⁵³
3o	<i>N</i> -(3-methoxyphenyl)-4-oxo-4 <i>H</i> -chromene-2-carboxamide ⁵³	0.36 g (1.9 mmol)	0.43 g (2.1 mmol)	3-methoxyaniline, 0.38 ml (3.4 mmol)	1.04 ml (6.8 mmol)	0.18 g (32 %) [65 %] ⁵³

	Name	Compound 2	PCl ₅	Amine	Et ₃ N	Yield [Lit.]
3p	<i>N</i> -(4-methoxyphenyl)-4-oxo-4 <i>H</i> -chromene-2-carboxamide ⁵³	0.49 g (2.6 mmol)	0.59 g (2.8 mmol)	4-methoxyaniline, 0.58 g (4.7 mmol)	1.42 ml (9.4 mmol)	0.21 g (27 %) [85 %] ⁵³
4a	<i>N</i> -benzyl-4-oxo-4 <i>H</i> -chromene-2-carboxamide ⁵⁵	0.41 g (2.1 mmol)	0.49 g (2.3 mmol)	benzylamine, 0.41 ml (3.8 mmol)	1.06 ml (7.6 mmol)	0.33 g (56 %)
4b	<i>N</i> -(4-methylbenzyl)-4-oxo-4 <i>H</i> -chromene-2-carboxamide	0.33 g (1.7 mmol)	0.39 g (1.9 mmol)	4-methylbenzylamine, 0.39 ml (3.1 mmol)	0.94 ml (6.2 mmol)	0.21 g (42 %)
4c	<i>N</i> -(4-nitrobenzyl)-4-oxo-4 <i>H</i> -chromene-2-carboxamide	0.27 g (1.4 mmol)	0.32 g (1.5 mmol)	(4-nitrophenyl)methanamine hydrochloride, 0.47 g (2.5 mmol)	0.71 ml (5.0 mmol)	0,07 g (15 %)
4d	<i>N</i> -(4-chlorobenzyl)-4-oxo-4 <i>H</i> -chromene-2-carboxamide	0.29 g (1.5 mmol)	0.35 g (1.7 mmol)	4-chlorobenzylamine, 0.33 ml (2.7 mmol)	0.82 ml (5.4 mmol)	0.12 g (26 %)
4e	<i>N</i> -(furan-2-ylmethyl)-4-oxo-4 <i>H</i> -chromene-2-carboxamide ⁴³	0.36 g (1.9 mmol)	0.43 g (2.1 mmol)	2-furylmethylamine, 0.31 ml (3.4 mmol)	1.04 ml (6.8 mmol)	0.45 g (88 %)
4f	<i>N</i> -(3,4-dimethoxyphenethyl)-4-oxo-4 <i>H</i> -chromene-2-carboxamide	0.30 g (1.6 mmol)	0.36 g (1.8 mmol)	3,4-methoxyphenethylamine, 0.47 ml (2.8 mmol)	0.86 ml (5.6 mmol)	0.06 g (11 %)
4g	<i>N</i> -(3,4-dimethoxybenzyl)-4-oxo-4 <i>H</i> -chromene-2-carboxamide	0.30 g (1.6 mmol)	0.36 g (1.8 mmol)	3,4-methoxybenzylamine, 0.42 ml (2.8 mmol)	0.86 ml (5.6 mmol)	0.35 g (65 %)
4h	<i>N</i> -(2-chlorobenzyl)-4-oxo-4 <i>H</i> -chromene-2-carboxamide	0.30 g (1.6 mmol)	0.36 g (1.8 mmol)	2-chlorobenzylamine, 0.35 ml (2.9 mmol)	0.88 ml (5.8 mmol)	0.15 g (30 %)
4i	<i>N</i> -(2,4-dichlorophenethyl)-4-oxo-4 <i>H</i> -chromene-2-carboxamide	0.29 g (1.5 mmol)	0.34 g (1.7 mmol)	2,4-dichlorophenethylamine, 0.41 ml (2.7 mmol)	0.82 ml (5.4 mmol)	0.25 g (46 %)
4j	<i>N</i> -(1-benzylpiperidin-4-yl)-4-oxo-4 <i>H</i> -chromene-2-carboxamide	0.30 g (1.6 mmol)	0.36 g (1.8 mmol)	4-amino-1-benzylpiperidine, 0.59 ml (2.9 mmol)	0.88 ml (5.8 mmol)	0.23 g (40 %)
4k	<i>N</i> -cyclohexyl-4-oxo-4 <i>H</i> -chromene-2-carboxamide ⁵⁰	0.45 g (2.4 mmol)	0.54 g (2.6 mmol)	cyclohexylamine, 0.49 ml (4.3 mmol)	1.32 ml (8.6 mmol)	0.26 g (40 %) [60 %] ⁵⁰

Experimental section

Tab. 19 Purification and characterization of **3a-p** and **4a-k**

	M_r [g/mol]	Formula	Colour	Purification (Reaction control)	m.p. [Lit.]	CLogP
3a	265.3	C ₁₆ H ₁₁ NO ₃	white	C, PE/EE (1:1), R _f = 0.71	231 – 233 °C [225 – 226] ⁹⁹	2.25
3b	344.2	C ₁₆ H ₁₀ BrNO ₃	white	C, PE/EE (1:1), R _f = 0.81	202 – 204 °C	2.32
3c	389.2	C ₁₆ H ₉ BrN ₂ O ₅	white	R , MeOH (TLC, PE/EE (1:1), R _f = 0.69)	298 – 300 °C	2.33
3d	423.1	C ₁₆ H ₉ Br ₂ NO ₃	white	C, CHCl ₃ /MeOH (20:1), R _f = 0.61	282 – 283 °C	2.34
3e	334.2	C ₁₆ H ₉ Cl ₂ NO ₃	white	C, cyclohex./EE (3:1), R _f = 0.64	277 – 278 °C [134 – 136] ⁵⁴	2.10
3f	334.2	C ₁₆ H ₉ Cl ₂ NO ₃	white	C, cyclohex./EE (3:1), R _f = 0.78	229 – 231 °C	2.95
3g	334.2	C ₁₆ H ₉ Cl ₂ NO ₃	yellow	C, cyclohex./EE (3:1), R _f = 0.72	225 – 226 °C [156 – 160] ⁵⁴	2.95
3h	391.2	C ₁₆ H ₁₀ INO ₃	white	C, PE/EE (1:1), R _f = 0.79	208 – 210 °C [197 – 198] ¹⁰¹	2.40
3i	283.3	C ₁₆ H ₁₀ FNO ₃	white	C, CHCl ₃ /MeOH (20:1), R _f = 0.58	210 – 212 °C	1.88
3j	283.3	C ₁₆ H ₁₀ FNO ₃	white	R , MeOH, (TLC, PE/EE (1:1), R _f = 0.65)	227 – 229 °C	2.48
3k	324.7	C ₁₇ H ₉ ClN ₂ O ₃	white	R , MeOH, (TLC, PE/EE (1:1), R _f = 0.46)	330 – 332 °C	2.66
3l	340.3	C ₁₇ H ₁₂ N ₂ O ₆	yellow	R , MeOH, (TLC, PE/EE (1:1), R _f = 0.60)	277 – 279 °C	1.75
3m	293.3	C ₁₈ H ₁₅ NO ₃	yellow	C, PE/EE (1:1), R _f = 0.75	224 – 225 °C	3.20
3n	295.3	C ₁₇ H ₁₃ NO ₄	white	C, PE/EE (1:1), R _f = 0.67	186 – 190 °C	1.63
3o	295.3	C ₁₇ H ₁₃ NO ₄	white	C, PE/EE (1:1), R _f = 0.61	202 – 204 °C	2.22
3p	295.3	C ₁₇ H ₁₃ NO ₄	yellow	C, PE/EE (1:1), R _f = 0.60	221 – 223 °C	2.22
4a	279.3	C ₁₇ H ₁₃ NO ₃	white	R , MeOH, (TLC, PE/EE (1:1), R _f = 0.52)	183 – 185 °C [181 – 183] ⁵⁵	2.43
4b	293.3	C ₁₈ H ₁₅ NO ₃	white	R , EE/MeOH, 1:3, (TLC, PE/EE (1:1), R _f = 0.57)	190 – 191 °C	2.93
4c	324.3	C ₁₇ H ₁₂ N ₂ O ₅	beige	C, PE/EE (1:1), R _f = 0.45	234 °C (decomp.)	2.17
4d	313.7	C ₁₇ H ₁₂ ClNO ₃	white	C, PE/EE (1:1), R _f = 0.44	202 – 204 °C	3.14
4e	269.3	C ₁₅ H ₁₁ NO ₄	white	C, PE/EE (1:1), R _f = 0.63	184 – 185 °C [183 – 184] ⁴³	1.61
4f	353.4	C ₂₀ H ₁₉ NO ₅	yellow	R , EtOH, (TLC, PE/EE (1:1), R _f = 0.38)	171 – 173 °C	2.22

Experimental section

	M_r [g/mol]	Formula	Colour	Purification (Reaction control)	m.p. [Lit]	CLogP
4g	339.3	C ₁₉ H ₁₇ NO ₅	yellow	R , EtOH, (TLC, PE/EE (1:1), R _f = 0.35)	147 – 149 °C	2.09
4h	313.7	C ₁₇ H ₁₂ ClNO ₃	white	C , PE/EE (1:1), R _f = 0.65	218 – 220 °C	3.14
4i	362.2	C ₁₈ H ₁₃ Cl ₂ NO ₃	white	R , MeOH, (TLC, PE/EE (1:1), R _f = 0.59)	226 – 228 °C	3.98
4j	362.4	C ₂₂ H ₂₂ N ₂ O ₃	white	C , CHCl ₃ /MeOH (5:1), R _f = 0.35	189 – 190 °C	2.31
4k	271.3	C ₁₆ H ₁₇ NO ₃	white	R , MeOH, (TLC, PE/EE (1:1), R _f = 0.71)	182 – 183 °C [183 – 184] ⁵⁰	2.49

Tab. 20 IR data for **3a-p** and **4a-k**

3a	3358, 3054, 1683, 1642, 1598, 1542, 1496, 1098, 749
3b	3375, 3097, 1697, 1655, 1605, 1583, 1526, 1380, 1128, 753
3c	3369, 3086, 1701, 1660, 1609, 1575, 1531, 1337, 1123, 870, 761
3d	3201, 3081, 1696, 1644, 1608, 1497, 1391, 1124, 898, 768
3e	3196, 3086, 1697, 1645, 1608, 1497, 1390, 1125, 781
3f	3384, 3102, 1704, 1654, 1586, 1527, 1214, 1126, 888, 818
3g	3386, 1698, 1654, 1606, 1519, 1377, 1128, 876, 830, 759
3h	3339, 3097, 1686, 1658, 1603, 1524, 1121, 878, 758, 747
3i	3214, 3097, 1689, 1646, 1608, 1519, 1394, 1128, 753
3j	3333, 3074, 1693, 1631, 1614, 1556, 1388, 1138, 845, 760
3k	3312, 3097, 2227, 1700, 1623, 1592, 1382, 1139, 846, 762
3l	3390, 3088, 3011, 1703, 1655, 1588, 1545, 1340, 1124, 882, 807, 765
3m	3330, 3074, 1685, 1632, 1610, 1545, 1378, 1136, 877, 813, 752
3n	3407, 2939, 1687, 1654, 1627, 1600, 1464, 1383, 1127, 748
3o	3344, 3097, 2939, 1694, 1647, 1614, 1599, 1465, 1387, 1124, 761
3p	3303, 2925, 1641, 1596, 1542, 1462, 1386, 1035, 754
4a	3298, 3069, 3029, 1680, 1639, 1605, 1460, 1386, 1132, 759, 691
4b	3300, 3023, 2921, 1681, 1644, 1522, 1460, 1386, 1114, 757
4c	3278, 3023, 1682, 1642, 1606, 1514, 1459, 1390, 1346, 1111, 852, 757
4d	3292, 3084, 1682, 1643, 1606, 1523, 1385, 1013, 1091, 755
4e	3229, 3043, 1678, 1643, 1606, 1467, 1393, 1144, 1012, 752
4f	3300, 2928, 2829, 1684, 1641, 1622, 1459, 1257, 1025, 867, 757
4g	3305, 2931, 2835, 1650, 1588, 1498, 1260, 1139, 1021, 865, 744
4h	3260, 3062, 1682, 1644, 1605, 1460, 1388, 1038, 751
4i	3272, 3090, 2956, 1685, 1643, 1608, 1462, 1384, 1145, 759
4j	3363, 3066, 2949, 2798, 1670, 1642, 1612, 1392, 957, 755
4k	3317, 3061, 2928, 2852, 1645, 1611, 1463, 1392, 1146, 755

None of the above listed IR data are described in literature.

Tab. 21 ¹H NMR data for 3a-p and 4a-k

	H3	H6	H8	H7	H5	CONH	Residual ¹ H signals
3a	6.98 (s)	7.55 – 7.59 (ddd; 7.8, 7.7, 0.8)	7.84 – 7.86 (dd; 8.2, 0.8)	7.91 – 7.95 (ddd; 8.2, 7.7, 1.6)	8.07 – 8.10 (dd; 7.8, 1.6)	10.73 (s)	7.18 – 7.23 (m, 1H, H4'); 7.41 – 7.45 (m, 2H, H3' , H5'); 7.79 – 7.81 (m, 2H, H2' , H6')
3b	6.97 (s)	7.56 – 7.60 (ddd; 7.8, 7.7, 0.8)	7.80 – 7.82 (dd; 8.2, 0.8)	7.91 – 7.95 (ddd; 8.2, 7.7, 1.6)	8.09 – 8.10 (dd; 7.8, 1.6)	10.67 (s)	7.28 – 7.32 (td, 1H, H4' , 7.9, 1.5); 7.47 – 7.51 (td, 1H, H5' , 7.9, 1.5); 7.65 – 7.67 (dd, 1H, H6' , 7.9, 1.5); 7.77 – 7.79 (dd, 1H, H3' , 7.9, 1.5)
3c	7.01 (s)	7.57 - 7.60 (ddd; 7.8, 7.7, 0.8)	7.81 - 7.83 (dd; 8.2, 0.8)	7.93 – 7.97 (ddd; 8.2, 7.7, 1.6)	8.08 – 8.13 (m)	10.87 (s)	8.08 – 8.13 (m, 3H, H5 , H3' , H4'); 8.57 (d, 1H, H6' , 1.3)
3d	6.97 (s)	7.57 – 7.61 (ddd; 7.8, 7.7, 0.8)	7.80 – 7.84 (m)	7.92 – 7.96 (ddd; 8.0, 7.7, 1.6)	8.09 – 8.11 (dd; 7.8, 1.6)	11.12 (s)	7.29 – 7.33 (m, 1H, H4'); 7.80 – 7.84 (m, 3H, H8 , H3' , H5')
3e	6.98 (s)	7.56 – 7.60 (ddd; 7.8, 7.7, 0.7)	7.79 – 7.81 (dd; 8.1, 0.7)	7.92 – 7.96 (ddd; 8.1, 7.7, 1.6)	8.08 – 8.11 (dd; 7.8, 1.6)	11.07 (s)	7.45 – 7.49 (m, 1H, H4'); 7.65 – 7.67 (d, 2H, H3' , H5' , 7.9)
3f	6.97 (s)	7.56 – 7.60 (ddd; 7.8, 7.7, 0.8)	7.80 – 7.83 (m)	7.91 – 7.95 (ddd; 7.9, 7.7, 1.6)	8.08 – 8.10 (dd; 7.8, 1.6)	10.74 (s)	7.45 – 7.47 (dd, 1H, H4' , 8.8, 2.6); 7.65 – 7.68 (d, 1H, H3' , 8.8); 7.80 – 7.83 (m, 2H, H8 , H6')
3g	6.97 (s)	7.53 – 7.60 (m)	7.80 – 7.82 (m)	7.91 – 7.95 (ddd; 8.0, 7.8, 1.6)	8.08 – 8.10 (dd; 7.8, 1.6)	10.74 (s)	7.53 – 7.60 (m, 2H, H6 , H5'); 7.68 – 7.70 (d, 1H, H6' , 8.6); 7.80 – 7.82 (m, 2H, H8 , H3')
3h	6.98 (s)	7.57 – 7.60 (m)	7.80 – 7.82 (dd; 8.1, 0.8)	7.92 – 7.96 (ddd; 8.1, 7.7, 1.6)	8.09 – 8.11 (dd; 7.8, 1.6)	10.66 (s)	7.11 – 7.15 (td, 1H, H4' , 7.6, 1.4); 7.48 – 7.52 (td, 1H, H5' , 7.6, 1.4); 7.57 – 7.60 (m, 2H, H6' , H6); 7.97 – 8.00 (dd, 1H, H3' , 7.6, 1.4)
3i	6.96 (s)	7.55 – 7.59 (ddd; 7.8, 7.7, 0.8)	7.80 – 7.82 (dd; 8.1, 0.8)	7.91 – 7.95 (ddd; 8.1, 7.7, 1.5)	8.08 – 8.10 (dd; 7.8, 1.5)	10.74 (s)	7.26 – 7.31 (m, 1H, H5'); 7.35 – 7.38 (m, 2H, H3' , H4'); 7.61 – 7.65 (t, 1H, H6' , 7.8)
3j	6.97 (s)	7.54 – 7.58 (ddd; 7.8, 7.7, 0.8)	7.79 – 7.84 (m)	7.90 – 7.92 (ddd; 7.9, 7.7, 1.5)	8.07 – 8.09 (dd; 7.8, 1.5)	10.79 (s)	7.24 – 7.29 (m, 2H, H3' , H5'); 7.79 – 7.84 (m, 3H, H8 , H2' , H6')
3k	7.02 (s)	7.56 – 7.60 (ddd; 7.8, 7.7, 0.8)	7.82 – 7.84 (dd; 8.2, 0.8)	7.93 – 7.99 (m)	8.08 – 8.10 (dd; 7.8, 1.5)	11.17 (s)	7.93 – 7.99 (m, 2H, H7 , H6'); 8.02 – 8.05 (m, 1H, H5'); 8.23 – 8.24 (d, 1H, H2' , 1.9)
3l	6.98 (s)	7.56 – 7.60 (ddd; 7.8, 7.7, 0.8)	7.85 – 7.87 (dd; 8.2, 0.8)	7.92 – 7.96 (m)	8.08 – 8.11 (dd; 7.8, 1.5)	10.18 (s)	4.08 (s, 3H, OCH₃); 7.92 – 7.96 (m, 2H, H7 , H3'); 7.98 – 8.01 (dd, 1H, H5' , 8.7, 2.6); 8.28 – 8.30 (d, 1H, H6' , 8.7)
3m	6.95 (s)	7.52 – 7.58 (m)	7.84 – 7.86 (dd; 8.2, 0.8)	7.91 – 7.95 (ddd; 8.2, 7.7, 1.6)	8.07 – 8.09 (dd; 7.8, 1.6)	10.60 (s)	2.22 (s, 3H, 3'-CH₃); 2.25 (s, 3H, 4'-CH₃); 7.16 – 7.18 (d, 1H, H5' , 7.9); 7.52 – 7.58 (m, 3H, H6' , H2' , H6)
3n	6.94 (s)	7.55 – 7.59 (ddd; 7.8, 7.7, 0.8)	7.83 – 7.85 (m)	7.90 – 7.95 (ddd; 7.9, 7.7, 1.5)	8.08 – 8.10 (dd; 7.8, 1.5)	10.03 (s)	3.90 (s, 3H, OCH₃); 7.00 – 7.04 (td, 1H, H5' , 7.8, 1.5); 7.15 – 7.18 (m, 1H, H3'); 7.24 – 7.29 (td, 1H, H4' , 7.8, 1.5); 7.83 – 7.85 (m, 2H, H8 , H6')
3o	6.98 (s)	7.55 – 7.59 (ddd; 7.8, 7.7, 0.8)	7.84 – 7.86 (dd; 8.2, 0.8)	7.91 – 7.95 (ddd; 8.2, 7.7, 1.6)	8.07 – 8.10 (dd; 7.8, 1.6)	10.69 (s)	6.78 – 6.80 (d, 1H, H4' , 7.9); 7.31 – 7.35 (m, 1H, H5'); 7.40 – 7.42 (d, 1H, H6' , 7.9); 7.47 – 7.48 (m, 1H, H2')

	H3	H6	H8	H7	H5	CONH	Residual ¹ H signals
3p	6.96 (s)	7.54 – 7.58 (ddd; 7.8, 7.7, 0.8)	7.83 – 7.85 (dd; 8.1, 0.8)	7.91 – 7.95 (ddd; 8.1, 7.7, 1.6)	8.07 – 8.09 (dd; 7.8, 1.6)	10.65 (s)	3.77 (s, 3H, OCH ₃); 6.97 – 7.01 (dt, 2H, H3', H5', 9.1, 2.2); 7.69 – 7.73 (dt, 2H, H2', H6', 9.1, 3.3)
4a	6.87 (s)	7.52 – 7.56 (ddd; 7.8, 7.8, 0.8)	7.72 – 7.74 (dd; 7.9, 0.8)	7.87 – 7.91 (ddd; 7.9, 7.8, 1.6)	8.05 – 8.07 (dd; 7.8, 1.6)	9.68 – 9.71 (t; 6.0)	4.52 – 4.54 (d, 2H, CH ₂ , 6.0); 7.25 – 7.30 (m, 1H, H4'); 7.35 – 7.36 (m, 4H, H2', H6', H3', H5')
4b	6.86 (s)	7.52 – 7.56 (ddd; 7.8, 7.7, 0.8)	7.72 – 7.74 (dd; 8.1, 0.8)	7.87 – 7.91 (ddd; 8.1, 7.7, 1.6)	8.04 – 8.07 (dd; 7.8, 1.6)	9.63 – 9.66 (t; 6.0)	2.28 (s, 3H, CH ₃), 4.47 – 4.48 (d, 2H, CH ₂ , 6.0); 7.14 – 7.16 (d, 2H, H3', H5', 7.9); 7.23 – 7.25 (d, 2H, H2', H6', 7.9)
4c	6.88 (s)	7.53 – 7.57 (ddd; 7.8, 7.8, 0.8)	7.72 – 7.74 (dd; 7.9, 0.8)	7.88 – 7.93 (ddd; 7.9, 7.8, 1.6)	8.05 – 8.08 (dd; 7.8, 1.6)	9.82 – 9.85 (t; 6.1)	4.65 – 4.66 (d, 2H, CH ₂ , 6.1); 7.62 – 7.64 (m, 2H, H2', H6', 8.8); 8.20 – 8.24 (dt, 2H, H3', H5', 8.8, 1.9)
4d	6.86 (s)	7.52 – 7.56 (ddd; 7.8, 7.7, 0.8)	7.71 – 7.73 (dd; 8.2, 0.8)	7.87 – 7.92 (ddd; 8.2, 7.7, 1.5)	8.05 – 8.07 (dd; 7.8, 1.5)	9.67 – 9.73 (t; 6.1)	4.50 – 4.52 (d, 2H, CH ₂ , 6.1); 7.37 – 7.42 (m, 4H, H2', H3', H5', H6')
4e	6.85 (s)	7.51 – 7.55 (ddd; 7.8, 7.7, 0.8)	7.72 – 7.74 (dd; 8.1, 0.8)	7.87 – 7.91 (ddd; 8.1, 7.7, 1.6)	8.04 – 8.06 (dd; 7.8, 1.6)	9.62 – 9.65 (t; 5.9)	4.51 – 4.52 (d, 2H, CH ₂ , 5.9); 6.35 – 6.36 (dd, 1H, H3', 3.2, 0.7); 6.41 – 6.43 (dd, 1H, H4', 3.2, 1.8); 7.60 – 7.61 (dd, 1H, H5', 1.8, 0.7)
4f	6.82 (s)	7.52 – 7.56 (ddd; 7.8, 7.7, 0.8)	7.71 – 7.73 (dd; 7.9, 0.8)	7.87 – 7.92 (ddd; 7.9, 7.7, 1.5)	8.04 – 8.06 (dd; 7.8, 1.5)	9.18 – 9.21 (t; 6.4)	2.80 – 2.84 (t, 2H, Hb, 6.4); 3.49 – 3.54 (q, 2H, Ha, 6.4); 3.71 (s, 3H, C4'-OCH ₃); 3.73 (s, 3H, C3'-OCH ₃); 6.75 – 6.78 (dd, 1H, H6', 8.2, 1.9); 6.85 – 6.86 (d, 1H, H2', 1.9); 6.86 – 6.88 (d, 1H, H5', 8.2)
4g	6.86 (s)	7.52 – 7.56 (ddd; 7.8, 7.7, 0.8)	7.72 – 7.74 (dd; 7.9, 0.8)	7.87 – 7.91 (ddd; 7.9, 7.7, 1.6)	8.04 – 8.07 (dd; 7.8, 1.6)	9.58 – 9.61 (t; 6.0)	3.73 – 3.75 (d, 6H, 2x OCH ₃); 4.44 – 4.46 (d, 2H, CH ₂ , 6.0); 6.87 – 6.93 (m, 2H, H5', H6'); 6.97 – 6.98 (d, 1H, H2', 1.7)
4h	6.88 (s)	7.53 – 7.57 (ddd; 7.8, 7.7, 0.8)	7.74 – 7.76 (dd; 7.9, 0.8)	7.88 – 7.93 (ddd; 7.9, 7.7, 1.5)	8.06 – 8.08 (dd; 7.8, 1.5)	9.67 – 9.70 (t; 5.8)	4.59 – 4.61 (d, 2H, CH ₂ , 5.8); 7.32 – 7.35 (m, 2H, H4', H5'); 7.42 – 7.44 (m, 1H, H6'); 7.47 – 7.49 (m, 1H, H3')
4i	6.80 (s)	7.52 – 7.56 (ddd; 7.7, 7.6, 0.8)	7.70 – 7.72 (dd; 8.1, 0.8)	7.88 – 7.92 (ddd; 8.1, 7.6, 1.5)	8.04 – 8.07 (dd; 7.7, 1.5)	9.24 – 9.27 (t; 6.4)	2.98 – 3.02 (t, 2H, Hb, 6.4); 3.52 – 3.57 (q, 2H, Ha, 6.4); 7.36 – 7.41 (m, 2H, H5', H6'); 7.59 – 7.60 (d, 1H, H3', 1.5)
4j	6.82 (s)	7.52 – 7.55 (ddd; 7.7, 7.7, 0.8)	7.76 – 7.78 (dd; 7.9, 0.8)	7.87 – 7.92 (ddd; 7.9, 7.7, 1.5)	8.04 – 8.06 (dd; 7.7, 1.5)	8.87 – 8.89 (d; 7.7)	1.65 – 1.72 (m, 2H, H2'a, H6'a); 1.78 – 1.81 (m, 2H, H2'e, H6'e); 2.01 – 2.08 (m, 2H, H3'a, H5'a); 2.83 – 2.86 (m, 2H, H3'e, H5'e); 3.48 (s, 2H, CH ₂); 3.75 – 3.84 (m, 1H, H1'a); 7.24 – 7.27 (m, 1H, Hh); 7.30 – 7.35 (m, 4H, Hf, Hg, Hi, Hj)
4k	6.82 (s)	7.50 – 7.54 (ddd; 7.8, 7.7, 0.8)	7.76 – 7.78 (dd; 8.1, 0.8)	7.86 – 7.90 (ddd; 8.1, 7.7, 1.6)	8.03 – 8.05 (dd; 7.8, 1.6)	8.81 – 8.83 (d; 8.0)	1.12 – 1.18 (m, 1H, H4'a); 1.25 – 1.44 (m, 4H, H2'a, H3'a, H5'a, H6'a); 1.60 – 1.63 (m, 1H, H4'e); 1.73 – 1.85 (m, 4H, H3'e, H5'e, H2'e, H6'e); 3.73 – 3.82 (m, 1H, H1'a)

¹H NMR spectra for **3a**⁵², **3b**⁵³, **3e**⁵⁴, **3g**⁵⁴, **3n**⁵³, **3o**⁵³, **3p**⁵³, **4a**⁵⁵ and **4k**⁵⁰ have already been published. For details see *Chap. 3.3.1.3*.

Tab. 22 ¹³C NMR data for 3a-p and 4a-k

	C3	C8	C10	C5	C6	C7	C9	C2	CONH	C4	Residual ¹³ C signals
3a	111.06	119.01	123.68	124.92	126.11	135.03	155.15	155.69	157.71	177.28	121.10 (C2 [′] , C6 [′]); 124.94 (C4 [′]); 128.81 (C3 [′] , C5 [′]); 137.50 (C1 [′])
3b	111.21	118.90	123.67	125.00	126.21	135.17	155.07	155.15	158.00	177.20	120.11 (C2 [′]), 128.27 (C6 [′]), 128.40 (C5 [′]), 128.70 (C4 [′]), 132.87 (C3 [′]), 135.05 (C1 [′])
3c	111.50	118.88	123.70	125.05	126.30	135.27	154.81	155.05	158.40	177.16	122.10 (C6 [′]); 122.68 (C4 [′]); 127.31 (C2 [′]); 134.19 (C3 [′]); 136.48 (C1 [′]); 147.04 (C5 [′])
3d	111.43	118.91	123.69	125.04	126.31	135.29	154.70	155.13	157.89	177.10	124.18 (C2 [′] , C6 [′]); 131.09 (C4 [′]); 132.44 (C3 [′] , C5 [′]); 134.36 (C1 [′])
3e	111.47	118.89	123.71	125.03	126.27	135.25	154.52	155.12	158.07	177.11	128.75 (C3 [′] , C5 [′]); 130.21 (C4 [′]); 131.61 (C1 [′]); 133.79 (C2 [′] , C6 [′])
3f	111.40	118.90	123.68	125.01	126.25	135.22	154.81	155.04	158.19	177.15	127.48 (C6 [′]); 127.98 (C2 [′]); 128.06 (C4 [′]); 131.11 (C3 [′]); 131.69 (C5 [′]); 134.88 (C1 [′])
3g	111.33	118.90	123.68	124.99	126.22	135.18	154.89	155.06	158.17	177.17	127.94 (C5 [′]); 129.27 (C3 [′]); 129.33 (C6 [′]); 130.52 (C2 [′]); 131.76 (C4 [′]); 132.78 (C1 [′])
3h	111.17	118.86	123.66	125.01	126.22	135.18	155.08	155.28	157.93	177.20	97.86 (C2 [′]); 127.73 (C6 [′]); 128.90 (C4 [′]); 129.06 (C5 [′]); 138.30 (C3 [′]); 139.06 (C1 [′])
3i	111.24	118.93	123.69	124.95	126.14	135.11	154.62	155.12	158.11	177.22	115.95 – 116.14 (d, C3 [′] , ² J _{C,F} 19.7); 124.00 – 124.12 (d, C1 [′] , ² J _{C,F} 12.2); 124.53 – 124.57 (d, C5 [′] , ⁴ J _{C,F} 3.6); 127.33 (C6 [′]); 128.08 – 128.16 (d, C4 [′] , ³ J _{C,F} 7.7); 157.09 (C2 [′])
3j	111.09	118.97	123.68	124.94	126.13	135.07	155.13	155.58	157.70	177.27	115.38 – 115.60 (d, C3 [′] , C5 [′] , ² J _{C,F} 22.4); 123.07 – 123.15 (d, C2 [′] , C6 [′] , ³ J _{C,F} 8.0); 133.84 – 133.87 (d, C1 [′] , ⁴ J _{C,F} 2.6); 157.79 – 160.20 (d, C4 [′] , ¹ J _{C,F} 241.7)
3k	111.66	118.94	123.71	125.00	126.29	135.24	154.74	155.07	158.63	177.18	107.15 (C4 [′]); 119.50 (C6 [′]); 120.95 (C2 [′]); 135.29 (C5 [′]); 135.86 (C3 [′]); 143.03 (C1 [′])
3l	111.38	118.99	123.68	125.00	126.29	135.18	154.85	154.96	157.90	177.16	56.87 (OCH ₃); 106.45 (C3 [′]); 116.66 (C5 [′]); 121.86 (C6 [′]); 132.01 (C1 [′]); 144.59 (C4 [′]); 150.28 (C2 [′])
3m	110.90	119.00	123.67	124.90	126.08	135.00	155.14	155.78	157.39	177.29	18.88 (3 [′] -CH ₃); 19.58 (4 [′] -CH ₃); 118.54 (C6 [′]); 122.16 (C2 [′]); 129.65 (C5 [′]); 132.90 (C1 [′]); 135.18 (C4 [′]); 136.50 (C3 [′])
3n	110.95	118.95	123.65	124.96	126.15	135.06	155.02	155.42	157.36	177.24	55.88 (OCH ₃); 111.60 (C3 [′]); 120.42 (C5 [′]); 123.84 (C6 [′]); 125.26 (C1 [′]); 126.75 (C4 [′]); 151.31 (C2 [′])

	C3	C8	C10	C5	C6	C7	C9	C2	CONH	C4	Residual ¹³ C signals
3o	111.07	119.02	123.68	124.92	126.12	135.03	155.13	155.62	157.71	177.28	106.74 (C2 [']); 110.47 (C4 [']); 113.22 (C6 [']); 129.63 (C5 [']); 138.69 (C1 [']); 159.46 (C3 ['])
3p	110.88	118.99	123.67	124.92	126.09	135.01	155.15	155.86	157.29	177.30	55.24 (OCH ₃); 113.95 (C3 ['] , C5 [']); 122.69 (C2 ['] , C6 [']); 130.47 (C1 [']); 156.41 (C4 ['])
4a	110.61	118.78	123.64	124.92	126.00	134.98	155.10	155.59	159.12	177.30	127.05 (C4 [']); 127.45 (C2 ['] , C6 [']); 128.37 (C3 ['] , C5 [']); 138.49 (C1 ['])
4b	110.58	118.78	123.64	124.92	126.00	134.97	155.09	155.63	159.02	177.30	20.66 (CH ₃); 42.43 (CH ₂); 127.46 (C2 ['] , C6 [']); 128.89 (C3 ['] , C5 [']); 135.46 (C1 [']); 136.15 (C4 ['])
4c	110.72	118.74	123.66	124.96	126.06	135.05	155.08	155.33	159.43	177.27	42.27 (CH ₂); 123.54 (C3 ['] , C5 [']); 128.45 (C2 ['] , C6 [']); 146.46 (C1 [']); 146.61 (C4 ['])
4d	110.64	118.75	123.64	124.93	126.02	135.00	155.08	155.48	159.20	177.28	42.03 (CH ₂); 128.31 (C3 ['] , C5 [']); 129.34 (C2 ['] , C6 [']); 131.63 (C4 [']); 137.54 (C1 ['])
4e	110.66	118.79	123.64	124.90	126.01	134.98	155.07	155.39	158.99	177.27	35.97 (CH ₂), 107.59 (C3 [']), 110.54 (C4 [']), 142.33 (C5 [']), 151.19 (C2 ['])
4f	110.37	118.71	123.61	124.93	126.01	135.00	155.06	155.70	158.88	177.28	34.28 (Cb); 41.03 (Ca); 55.35 – 55.50 (d, 2×OCH ₃); 111.96 (C5 [']); 112.52 (C2 [']); 120.46 (C6 [']); 131.47 (C1 [']); 147.33 (C4 [']); 148.65 (C3 ['])
4g	110.57	118.79	123.64	124.91	126.00	134.96	155.10	155.69	158.98	177.31	42.49 (CH ₂); 55.49 – 55.57 (d, 2×OCH ₃); 111.74 – 111.80 (C2 ['] , C5 [']); 118.79 (C8); 119.76 (C6 [']); 130.88 (C1 [']); 148.01 (C4 [']); 148.66 (C3 ['])
4h	110.69	118.82	123.67	124.93	126.05	135.24	155.12	155.40	159.37	177.30	40.56 (CH ₂); 127.27 (C5 [']); 128.88 (C4 [']); 128.92 (C6 [']); 129.19 (C3 [']); 131.99 (C2 [']); 135.02 (C1 ['])
4i	110.41	118.74	123.61	124.93	126.04	135.03	155.06	155.56	159.06	177.27	31.98 (Cb); 38.85 (Ca); 127.43 (C5 [']); 128.69 (C3 [']); 131.87 (C4 [']); 132.42 (C6 [']); 134.11 (C2 [']); 135.66 (C1 ['])
4j	110.50	118.89	123.61	124.88	125.98	134.91	155.10	155.74	158.29	177.29	31.14 (C2 ['] , C6 [']); 47.32 (C1 [']); 52.09 (C3 ['] , C5 [']); 61.99 (CH ₂); 126.84 (Ch); 128.15 (Cg, Ci); 128.66 (Cf, Cj); 138.61 (Ck)
4k	110.46	118.89	123.61	124.85	125.93	134.85	155.09	155.88	158.03	177.28	24.83 (C3 ['] , C5 [']); 25.11 (C4 [']); 32.01 (C2 ['] , C6 [']); 48.76 (C1 ['])

¹³C NMR spectra for **3b**, **3n**, **3o** and **3p** have already been published by Gaspar *et al.*⁵³ For details see *Chap. 3.3.1.3.2*.

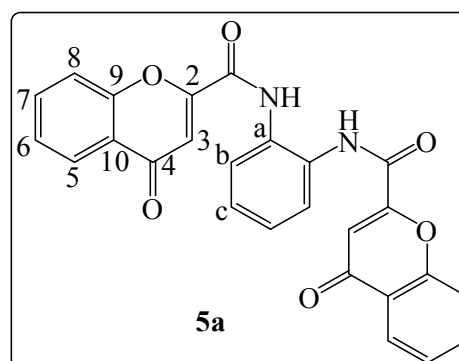
Experimental section

7.2.2.1.1 Side-products of the synthesis of 4-oxo-4H-chromene-2-carboxylic acid amides **3a-p** and **4a-k**

The dimer **5a** and the dihydroquinoxaline derivative **5b** were obtained from the reaction with 1,2-diaminobenzene using 0.30 g (1.6 mmol) of compound **2**, 0.37 g (1.8 mmol) of phosphoryl pentachloride, 0.31 g (2.9 mmol) of 1,2-diaminobenzene and 0.88 ml (5.8 mmol) of triethylamine.

N,N'-(1,2-Phenylene)bis(4-oxo-4H-chromene-2-carboxamide) (**5a**)

Formula:	C ₂₆ H ₁₆ N ₂ O ₆
M _r [g/mol]:	452.4
Appearance:	beige solid
Yield:	0.08 g (22 %)
M.p.:	306 – 309 °C
CLogP:	2.15
R _f (PE/EE, 1:1)	0.36



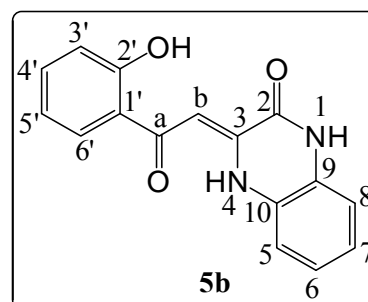
¹H NMR: 7.02 (s, 2H, **H3**); 7.40 – 7.43 (m, 2H, **Hb**); 7.51 – 7.55 (m, 2H, **H6**); 7.70 – 7.72 (m, 2H, **H8**); 7.74 – 7.77 (m, 2H, **Hc**); 7.81 – 7.86 (ddd, 2H, **H7**, 7.8, 7.8, 1.6); 8.05 – 8.07 (dd, 2H, **H5**, 7.8, 1.6); 10.63 (s, 2H, CONH);

¹³C NMR: 111.08 (C3), 118.72 (C8), 123.62 (C10), 124.95 (C5), 126.05 (Cc), 126.13 (C6), 126.54 (Cb), 129.99 (Ca), 135.04 (C7), 155.04 (C9), 155.40 (C2), 158.14 (CONH), 177.28 (C4)

IR: 3277, 3067, 1701, 1666, 1605, 1463, 1382, 1123, 744

(Z)-3-(2-(2-Hydroxyphenyl)-2-oxoethylidene)-3,4-dihydroquinoxalin-2(1H)-one (**5b**)

Formula:	C ₁₆ H ₁₂ N ₂ O ₃
M _r [g/mol]:	280.3
Appearance:	yellow solid
Yield:	0.04 g (9 %)
M.p.:	313 – 316 °C [315 – 317] ¹³⁰
CLogP:	3.28
R _f (PE/EE, 1:1)	0.71



¹H NMR: 6.90 (s, 1H, **Hb**); 6.92 – 6.96 (m, 2H, **H3'**, **H5'**); 7.14 – 7.17 (m, 3H, **H5**, **H6**, **H8**); 7.43 – 7.48 (ddd, 1H, **H4'**, 7.7, 8.1, 1.4); 7.60 – 7.62 (m, 1H, **H7**); 7.87 – 7.89 (dd, 1H, **H6'**, 8.1, 1.4); 12.11 (s, 1H, **H4**); 12.87 (s, 1H, OH); 13.12 (s, 1H, **H1**);

¹³C NMR: 89.03 (Cb); 115.37 (C7); 116.89 (C6); 117.83 (C3'); 119.11 (C5'); 120.77 (C1'); 123.68 (C5); 123.84 (C10); 124.42 (C8); 126.74 (C9); 128.66 (C6'); 134.70 (C4'); 145.79 (C3); 155.46 (C2); 161.08 (C2'); 191.54 (Ca)

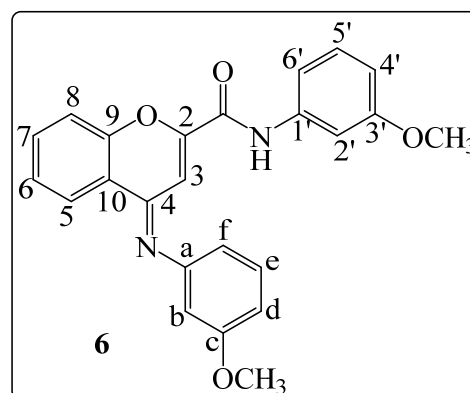
IR spectrum is in accordance with the published data¹³⁰.

Experimental section

(E)-N-(3-Methoxyphenyl)-4-((3-methoxyphenyl)imino)-4H-chromene-2-carboxamide (6)

The imine **6** was obtained from the synthesis of amide **3o**. The formation of similar side-products of ester aminolysis of the chromone-2-carboxylic acid esters has already been reported by Kohlstaedt *et al.*⁴³

Formula:	C ₂₄ H ₂₀ N ₂ O ₄
M _r [g/mol]:	400.4
Appearance:	yellow solid
Yield:	0.13 g (17 %)
M.p.:	181 – 183 °C
ClogP:	3.20
R _f (PE/EE, 1:1)	0.81



¹H NMR: 3.75 (s, 3H, 3'-OCH₃); 3.76 (d, 3H, c-OCH₃); 6.46 – 6.47 (m, 2H, H_b, H_f); 6.70 – 6.72 (dd, 1H, H_d, 8.0, 1.3); 6.74 – 6.76 (dd, 1H, H_{4'}, 8.1, 1.7); 6.82 (s, 1H, H₃); 7.26 – 7.36 (m, 3H, H_e, H_{6'}, H_{5'}); 7.43 – 7.44 (m, 1H, H_{2'}); 7.46 – 7.50 (m, 1H, H₆); 7.68 – 7.70 (dd, 1H, H₈, 8.0, 0.8); 7.75 – 7.79 (ddd, 1H, H₇, 8.0, 7.7, 1.3); 8.24 – 8.26 (dd, 1H, H₅, 7.9, 1.3); 10.49 (s, 1H, CONH);

¹³C NMR: 55.06 (3'-OCH₃); 55.09 (c-OCH₃); 102.66 (C₃); 105.92 (C_b); 106.80 (C_{2'}); 109.16 (C_d); 110.40 (C_{4'}); 112.37 (C_f); 113.28 (C_{6'}); 118.44 (C₈); 121.90 (C₁₀); 124.44 (C₅); 125.91 (C₆); 129.53 (C_{5'}); 130.18 (C_e); 132.93 (C₇); 138.68 (C_{1'}); 150.56 (C_a); 150.67 (C₉); 152.02 (C₂); 152.65 (CONH); 158.00 (C₄); 159.41 (C_{3'}); 160.26 (C_c)

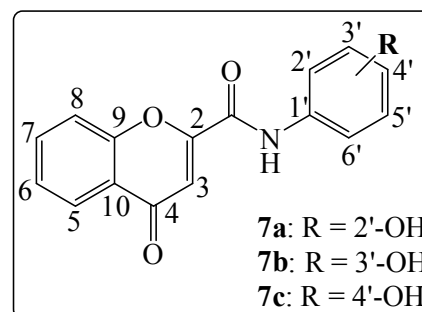
IR: 3347, 1685, 1638, 1607, 1587, 1542, 1461, 1213, 1147, 1029, 790, 768

7.2.3 Synthesis of 4-oxo-4H-chromene-2-carboxylic acid amides 7a-c

7.2.3.1 General procedure

A 40 mM solution of *N*-methoxyphenyl-4-oxo-4H-chromene-2-carboxamide **3n-p** in anhydrous dichloromethane under argon atmosphere (for reaction details see *Tab. 23*) was cooled to -78 °C (dry ice/acetone). Boron tribromide (10 eq.) was added dropwise.

The mixture was allowed to warm up to RT and stirred for 3 days. Then, it was poured on ice and neutralized with a sodium carbonate solution. The precipitate formed was filtered and recrystallized from a methanol/water mixture (5:1) to yield a yellow solid.



Tab. 23 Reaction details for 7a-c

	Name	Starting amide	BBr ₃	Reaction control	Yield [Lit.]
7a	<i>N</i> -(2-hydroxyphenyl)-4-oxo-4 <i>H</i> -chromene-2-carboxamide	3n ; 0.13 g (0.4 mmol)	0.41 ml (4.2 mmol)	PE/EE (1:1) R _f = 0.29	0.08 (71 %)
7b	<i>N</i> -(3-hydroxyphenyl)-4-oxo-4 <i>H</i> -chromene-2-carboxamide	3o ; 0.12 g (0.4 mmol)	0.40 ml (4.2 mmol)	PE/EE (1:1) R _f = 0.26	0.02 (18 %)
7c	<i>N</i> -(4-hydroxyphenyl)-4-oxo-4 <i>H</i> -chromene-2-carboxamide ⁵⁶	3p ; 0.09 g (0.3 mmol)	0.28 ml (2.9 mmol)	PE/EE (1:1) R _f = 0.22	0.04 (34 %) [51 %] ⁵⁶

Tab. 24 Analytical data for 7a-c

	Formula	M _r [g/mol]	m.p. [Lit]	CLogP	IR
7a	C ₁₆ H ₁₁ NO ₄	281.3	278 – 280 °C	1.81	33911, 1686, 1636, 1529, 1457, 1388, 1132, 750
7b	C ₁₆ H ₁₁ NO ₄	281.3	258 – 260 °C	1.58	3285, 1674, 1620, 1561, 1451, 1393, 1080, 864, 778
7c	C ₁₆ H ₁₁ NO ₄	281.3	281 – 282 °C, [277 – 281] ⁵⁶	1.58	3263, 1633, 1541, 1466, 1392, 1246, 823, 756

Tab. 25 ¹H NMR data for 7a-c (The ¹H NMR spectrum of 7c is consistent with literature⁵⁶)

	H3	H6	H8	H7	H5	CONH	Residual ¹ H signals
7a	6.94 (s)	7.55 – 7.59 (ddd; 7.8, 7.7, 1.6)	7.79 – 7.81 (dd; 8.2, 0.7)	7.90 – 7.94 (ddd; 8.2, 7.7, 1.6)	8.08 – 8.10 (dd; 7.8, 1.6)	10.03 (s)	6.85 – 6.89 (td, 1H, H5', 7.9, 1.4); 6.96 – 6.98 (dd, 1H, H3', 7.9, 1.4); 7.08 – 7.12 (td, 1H, H4', 7.9, 1.4); 7.76 – 7.78 (dd, 1H, H6', 7.9, 1.4); 9.96 (s, 1H, OH)
7b	6.96 (s)	7.55 – 7.59 (ddd; 7.8, 7.7, 1.6)	7.84 – 7.86 (dd; 8.2, 0.7)	7.91 – 7.95 (ddd; 8.2, 7.7, 1.6)	8.07 – 8.09 (dd; 7.8, 1.6)	10.59 (s)	6.59 – 6.62 (dt, 1H, H6', 6.5, 2.6); ; 7.17 – 7.22 (m, 2H, H4', H5'); 7.35 – 7.36 (m, 1H, H2'); 9.55 (s, 1H, OH)

Tab. 26 ¹³C NMR data for 7a-c

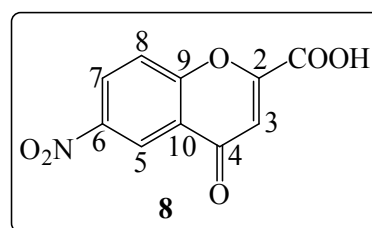
	C3	C8	C10	C5	C6	C7	C9	C2	CONH	C4	Residual ¹³ C signals
7a	110.86	118.88	123.65	124.99	126.15	135.10	155.02	155.60	157.34	177.28	115.64 (C3'); 119.10 (C5'); 123.94 (C6'); 124.25 (C1'); 126.59 (C4'); 149.49 (C2')
7b	111.00	119.05	123.68	124.90	126.10	135.01	155.15	155.78	157.61	177.29	108.09 (C2'); 111.71 (C4'); 112.05 (C6'); 129.47 (C5'); 138.52 (C1'); 157.57 (C3')
7c	110.78	118.99	123.67	124.92	126.07	134.99	155.15	155.98	157.12	177.31	115.19 (C3', C5'); 122.92 (C2', C6'); 128.94 (C1'); 154.68 (C4')

Experimental section

7.2.4 Synthesis of 6-nitro-4-oxo-4H-chromene-2-carboxylic acid **8**

1.30 g (6.8 mmol) of **2** were diluted in 20 ml conc. sulphuric acid. After cooling to 0 °C, 1.0 g (10.3 mmol, 1.5 eq) of potassium nitrate was added and the mixture was stirred for 72 h at RT. Then, the solution was poured on ice and stirred for 30 min. The precipitate was filtered and washed with water. The crude product was purified by recrystallization (MeOH/DMF, 10:1) to yield a white solid. The synthesis of **8** reported by Barker and Ellis⁴⁴ was conducted in a nitric/sulphuric acid mixture. No spectral data have been reported.

Formula: C₁₀H₅NO₆
M_r [g/mol]: 235.2
Yield [Lit]: 1.59 g (99 %)
[65 %]⁴⁴
M.p. [Lit]: 272 – 274 °C
[268]⁴⁴
Reaction control: EE/MeOH+HCOOH
(3:1+0.1), R_f= 0.42



¹H NMR: 7.02 (s, 1H, **H3**); 7.99 – 8.01 (d, 1H, **H8**, 9.2); 8.59 – 8.62 (dd, 1H, **H7**, 9.2, 2.9); 8.71 – 8.72 (d, 1H, **H5**, 2.9);

¹³C NMR: 113.73 (**C3**); 120.91 (**C5**); 121.21 (**C8**); 123.72 (**C10**); 129.15 (**C7**); 144.64 (**C6**); 153.89 (**C9**); 158.45 (**C2**); 160.94 (**CONH**); 176.84 (**C4**)

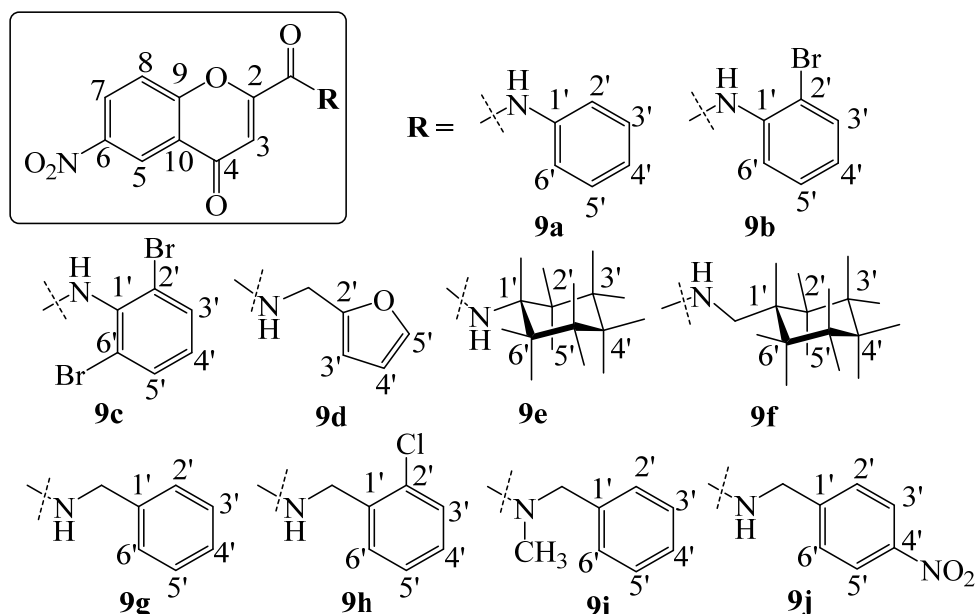
IR: 3092, 1735, 1642, 1604, 1524, 1456, 1338, 1190, 843, 777, 711

7.2.5 Synthesis of 6-nitro-4-oxo-4H-chromene-2-carboxamides **9a-j**

7.2.5.1 General procedure

To a suspension of **8** in 15 - 20 ml of anhydrous dichloromethane, 1.1 eq. of phosphorus pentachloride were added. The mixture was refluxed for 30 min. under argon to form the acyl chloride. After cooling to 0 °C, 3.6 eq of triethylamine were added dropwise. Then, 1.8 eq. of the corresponding amine were added (see *Tab. 27*). The mixture was stirred overnight at RT. Then, 50 ml of water were added, the layers separated and the water phase was washed twice with 50 ml dichloromethane. Organic layers were combined, dried over sodium sulphate, filtered and evaporated. Purification yielded a solid product (see *Tab. 28*).

Experimental section

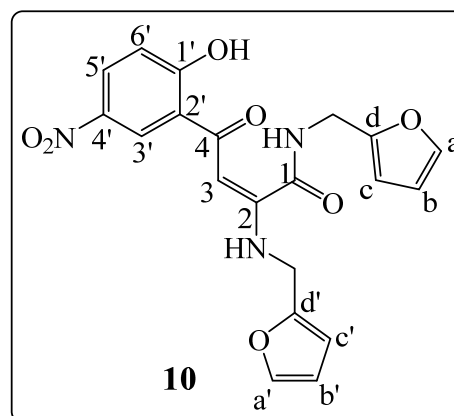


Scheme 18 Products 9a-j

Side product of the synthesis of 9d:

(*E*)-*N*-(Furan-2-ylmethyl)-2-((furan-2-ylmethyl)amino)-4-(2-hydroxy-5-nitrophenyl)-4-oxobut-2-enamide (**10**)

Formula:	C ₂₀ H ₁₇ N ₃ O ₇
M _r [g/mol]:	411.4
Appearance:	yellow solid
Yield:	0.13 g (14 %)
M.p.:	207 - 209 °C
CLogP:	3.39
R _f (PE/EE, 1:1)	0.84



¹H NMR: 4.42 – 4.44 (d, 2H, CH₂Cd, 5.3); 4.61 – 4.62 (d, 2H, CH₂Cd', 5.4); 6.11 (s, 1H, H₃); 6.26 – 6.33 (m, 2H, H_c, H_{c'}); 6.41 – 6.43 (m, 2H, H_b, H_{b'}); 7.06 – 7.08 (d, 1H, H_{6'}, 9.2); 7.57 – 7.66 (m, 2H, H_a, H_{a'}); 8.23 – 8.26 (dd, 1H, H_{5'}, 9.2, 2.2); 8.63 – 8.64 (d, 1H, H_{3'}, 2.2); 9.39 – 9.42 (t, 1H, NH, 5.4); 10.59 – 10.61 (b, 1H, CONH); 13.69 (b, 1H, OH);
¹³C NMR: 35.67 (CH₂Cd); 40.74 (CH₂Cd'); 90.45 (C₃); 107.34 – 108.24 (C_c; C_{c'}); 110.53 – 110.64 (C_b; C_{b'}); 118.72 (C_{6'}); 120.96 (C_{2'}); 124.91 (C_{3'}); 128.76 (C_{5'}); 139.25 (C_{4'}); 142.35 – 142.99 (C_a; C_{a'}); 150.51 (C_{d'}); 151.11 (Cd); 160.10 (C₂); 162.52 (CONH); 165.62 (C_{1'}); 188.68 (C₄)
 IR: 3261, 1656, 1592, 1565, 1335, 1274, 1119, 744
 ESI-MS: m/z = 410.1 [M-H]⁻

Tab. 27 Reaction details for 9a-j

	Name	Compound 8	PCl ₅	Amine	Et ₃ N	Yield
9a	6-nitro-4-oxo- <i>N</i> -phenyl-4 <i>H</i> -chromene-2-carboxamide	0.51 g (2.2 mmol)	0.50 g (2.6 mmol)	aniline, 0.36 ml (3.9 mmol)	1.09 ml (7.8 mmol)	0.28 g (41 %)
9b	<i>N</i> -(2-bromophenyl)-6-nitro-4-oxo-4 <i>H</i> -chromene-2-carboxamide	0.54 g (2.3 mmol)	0.53 g (2.5 mmol)	2-bromoaniline 0.47 ml (4.1 mmol)	1.15 ml (8.3 mmol)	0.75 g (84 %)
9c	<i>N</i> -(2,6-dibromophenyl)-6-nitro-4-oxo-4 <i>H</i> -chromene-2-carboxamide	0.30 g (1.3 mmol)	0.29 g (1.4 mmol)	2,6-dibromoaniline, 0.59 g (2.3 mmol)	0.64 ml (4.6 mmol)	0.22 g (52 %)
9d	<i>N</i> -(furan-2-ylmethyl)-6-nitro-4-oxo-4 <i>H</i> -chromene-2-carboxamide	0.53 g (2.3 mmol)	0.52 g (2.5 mmol)	furfurylamine, 0.37 ml (4.1 mmol)	1.13 ml (8.1 mmol)	0.38 g (55 %)
9e	<i>N</i> -cyclohexyl-6-nitro-4-oxo-4 <i>H</i> -chromene-2-carboxamide	0.78 g (3.3 mmol)	0.76 g (3.6 mmol)	cyclohexylamine, 0.68 ml (6.0 mmol)	1.67 ml (12.0 mmol)	0.40 g (38 %)
9f	<i>N</i> -(cyclohexylmethyl)-6-nitro-4-oxo-4 <i>H</i> -chromene-2-carboxamide ⁵⁷	0.48 g (2.0 mmol)	0.47 g (2.2 mmol)	cyclohexylmethanamine, 0.47 ml (3.7 mmol)	1.03 ml (7.4 mmol)	0.17 g (26 %)
9g	<i>N</i> -benzyl-6-nitro-4-oxo-4 <i>H</i> -chromene-2-carboxamide	0.58 g (2.5 mmol)	0.57 g (2.8 mmol)	benzylamine, 0.49 ml (4.4 mmol)	1.24 ml (8.9 mmol)	0.35 g (43 %)
9h	<i>N</i> -(2-chlorobenzyl)-6-nitro-4-oxo-4 <i>H</i> -chromene-2-carboxamide	0.62 g (2.6 mmol)	0.60 g (2.9 mmol)	(2-chlorophenyl)methanamin, 0.57 ml (4.7 mmol)	1.32 ml (9.5 mmol)	0.21 g (23 %)
9i	<i>N</i> -benzyl- <i>N</i> -methyl-6-nitro-4-oxo-4 <i>H</i> -chromene-2-carboxamide	0.39 g (1.7 mmol)	0.38 g (1.8 mmol)	<i>N</i> -methylbenzylamine, 0.38 ml (3.0 mmol)	0.83 ml (6.0 mmol)	0.34 g (60 %)
9j	6-nitro- <i>N</i> -(4-nitrobenzyl)-4-oxo-4 <i>H</i> -chromene-2-carboxamide	0.30 g (1.3 mmol)	0.29 g (1.4 mmol)	(4-nitrophenyl)methanamine hydrochloride, 0.43 g (2.3 mmol)	0.64 ml (4.6 mmol)	0.21 g (32 %)

Compound 9f has already been described, the patent⁵⁷ is available in Japanese.

Tab. 28 Analytical data for 9a-j

	M_r [g/mol]	Formula	Colour	Purification (Reaction control)	M.p.	CLogP	IR
9a	310.3	C ₁₆ H ₁₀ N ₂ O ₅	white	C , PE/EE (1:1), R _f = 0.72	269 – 270 °C	2.11	3335, 3087, 1695, 1624, 1599, 1524, 1338, 1096, 762, 740, 694
9b	389.2	C ₁₆ H ₉ BrN ₂ O ₅	white	R , MeOH (TLC: PE/EE 1:1), R _f = 0.79)	259 – 262 °C	2.12	3373, 3097, 3068, 1699, 1662, 1621, 1593, 1581, 1525, 1340, 1125, 770, 743
9c	468.1	C ₁₆ H ₈ Br ₂ N ₂ O ₅	white	C , PE/EE (1:1), R _f = 0.64	173 – 175 °C	2.12	3305, 3084, 1663, 1620, 1583, 1515, 1342, 1126, 786, 726
9d	314.3	C ₁₅ H ₁₀ N ₂ O ₆	white	C , PE/EE (1:1), R _f = 0.58	157 – 159 °C	1.46	3300, 3104, 1684, 1648, 1619, 1521, 1337, 1130, 767, 743
9e	316.3	C ₁₆ H ₁₆ N ₂ O ₅	white	R , EtOH (TLC: PE/EE (1:1), R _f = 0.64)	210 – 211 °C	2.35	3310, 2936, 2856, 1654, 1617, 1530, 1341, 1127, 848
9f	330.3	C ₁₇ H ₁₈ N ₂ O ₅	white	C , PE/EE (1:1), R _f = 0.49	187 – 188 °C	2.97	3317, 2922, 2852, 1686, 1654, 1619, 1530, 1337, 1131, 876, 744
9g	324.3	C ₁₇ H ₁₂ N ₂ O ₅	white	R , MeOH (TLC: PE/EE (1:1), R _f = 0.52)	189 – 191 °C	2.29	3313, 1678, 1647, 1621, 1538, 1379, 1342, 1129, 742, 704
9h	358.7	C ₁₇ H ₁₁ ClN ₂ O ₅	white	C , PE:EE (1:1), R _f = 0.55	206 – 209 °C	3.00	3291, 3083, 1663, 1633, 1620, 1551, 1527, 1336, 1287, 1120, 743
9i	338.3	C ₁₈ H ₁₄ N ₂ O ₅	white	C , PE:EE (1:1), R _f = 0.46	130 – 132 °C	1.96	3060, 1649, 1615, 1577, 1526, 1338, 1118, 878, 726
9j	369.3	C ₁₇ H ₁₁ N ₃ O ₇	red	C , CH ₂ Cl ₂ /EE (10:1), R _f = 0.78	228 – 231 °C	2.03	3302, 3090, 1683, 1657, 1618, 1511, 1336, 833

Tab. 29 ¹H NMR data for 9a-j

	H3	H8	H7	H5	CONH	Residual ¹ H signals
9a	7.08 (s)	8.06 – 8.09 (d; 9.1)	8.69 – 8.72 (dd; 9.1, 2.9)	8.73 – 8.74 (d; 2.4)	10.78 (s)	7.20 – 7.24 (m, 1H, H4 ^c); 7.41 – 7.46 (m, 2H, H3 ^c , H5 ^c); 7.78 – 7.80 (m, 2H, H2 ^c , H6 ^c)
9b	7.08 (s)	8.03 – 8.05 (d; 9.2)	8.68 – 8.71 (dd; 9.2, 2.9)	8.74 – 8.75 (d; 2.9)	10.79 (s)	7.30 – 7.34 (td, 1H, H4 ^c , 7.9, 1.5); 7.48 – 7.52 (td, 1H, H5 ^c , 7.9, 1.5); 7.61 – 7.64 (dd, 1H, H6 ^c , 7.9, 1.5); 7.78 – 7.80 (dd, 1H, H3 ^c , 7.9, 1.5)
9c	7.10 (s)	8.02 – 8.04 (d; 9.2)	8.68 – 8.71 (dd; 9.2, 2.9)	8.75 – 8.76 (d; 2.9)	11.21 (s)	7.30 – 7.34 (t, 1H, H4 ^c , 8.1); 7.83 – 7.85 (d, 2H, H3 ^c , H5 ^c , 8.1)
9d	6.95 (s)	7.93 – 7.95 (d; 9.2)	8.64 – 8.67 (dd; 9.2, 2.9)	8.70 – 8.71 (d; 2.9)	9.70 – 9.73 (t; 5.8)	4.52 – 4.54 (d, 2H, CH ₂ , 5.8); 6.37 – 6.38 (dd, 1H, H3 ^c , 3.2, 0.7); 6.42 – 6.43 (dd, 1H, H4 ^c , 3.2, 1.8); 7.61 – 7.62 (dd, 1H, H5 ^c , 1.8, 0.7)
9e	6.91 (s)	7.99 – 8.01 (d; 9.1)	8.65 – 8.68 (dd; 9.1, 2.7)	8.69 – 8.70 (d; 2.7)	8.89 – 8.91 (d; 8.0)	1.10 – 1.19 (m, 1H, H4 ^a); 1.27 – 1.44 (m, 4H, H2 ^a , H3 ^a , H5 ^a , H6 ^a); 1.62 – 1.65 (m, 1H, H4 ^e); 1.75 – 1.86 (m, 4H, H3 ^e , H5 ^e , H2 ^e , H6 ^e); 3.74 – 3.82 (m, 1H, H1 ^a)
9f	6.91 (s)	7.95 – 7.98 (d; 9.2)	8.65 – 8.68 (dd; 9.2, 2.9)	8.70 – 8.71 (d; 2.9)	9.16 – 9.18 (t; 5.9)	0.91 – 0.99 (m, 2H, H2 ^a , H6 ^a); 1.10 – 1.24 (m, 3H, H4 ^a , H3 ^a , H5 ^a); 1.56 – 1.63 (m, 2H, H1 ^a , H4 ^e); 1.68 – 1.74 (m, 4H, H2 ^e , H6 ^e , H3 ^e , H5 ^e); 3.15 – 3.18 (t, 2H, CH ₂ , 5.9)
9g	6.97 (s)	7.94 – 7.96 (d; 9.2)	8.65 – 8.68 (dd; 2.9, 9.2)	8.71 – 8.72 (d; 2.9)	9.77 – 9.80 (t; 5.9)	4.53 – 4.55 (d, 2H, CH ₂ , 5.9); 7.26 – 7.31 (m, 1H, H4 ^c); 7.33 – 7.37 (m, 4H, H2 ^c , H3 ^c , H5 ^c , H6 ^c)
9h	6.98 (s)	7.95 – 7.97 (d; 9.2)	8.65 – 8.68 (dd; 9.2, 2.9)	8.72 – 8.73 (d; 2.9)	9.75 – 9.78 (t; 5.9)	4.60 – 4.62 (d, 2H, CH ₂ , 5.9); 7.31 – 7.37 (m, 2H, H3 ^c , H5 ^c); 7.43 – 7.49 (m, 2H, H4 ^c , H6 ^c)
9i [*]	6.74 (s)	7.68 – 7.71 (d; 9.2)	8.55 – 8.58 (dd; 9.2, 2.9)	8.68 – 8.69 (d; 2.9)	CONCH ₃	2.93 (s, 3H, CH ₃); 4.70 (s, 2H, CH ₂); 7.30 – 7.43 (m, 10H, H2 ^c , H3 ^c , H4 ^c , H5 ^c , H6 ^c)
	6.83 (s)	7.99 – 8.01 (d; 9.2)	8.59 – 8.62 (dd; 9.2, 2.9)	8.72 – 8.73 (d; 2.9)	CONCH ₃	3.07 (s, 3H, CH ₃); 4.68 (s, 2H, CH ₂); 7.30 – 7.43 (m, 10H, H2 ^c , H3 ^c , H4 ^c , H5 ^c , H6 ^c)
9j	6.97 (s)	7.93 – 7.96 (d; 9.2)	8.66 – 8.69 (dd; 9.2, 2.9)	8.71 – 8.72 (d; 2.9)	9.90 - 9.93 (t; 6.1)	4.66 – 4.68 (d, 2H, CH ₂ , 6.1); 7.63 – 7.65 (m, 2H, H2 ^c , H6 ^c); 8.20 – 8.24 (dt, 2H, H3 ^c , H5 ^c , 8.8, 2.4)

Tab. 30 ^{13}C NMR data for **9a-j**

	C3	C5	C8	C10	C7	C6	C9	CONH	C2	C4	Residual ^{13}C signals
9a	111.36	120.91	121.29	123.66	129.20	144.69	158.10	157.08	156.11	176.45	121.10 (C2', C6'); 125.09 (C4'); 128.86 (C3', C5'); 137.35 (C1')
9b	111.58	121.01	121.21	123.73	129.31	144.77	158.08	157.53	155.61	176.41	120.28 (C2'); 128.45 (C6'); 128.54 (C5'); 128.94 (C4'); 132.95 (C3'); 134.87 (C1'); 144.77 (C6)
9c	111.82	121.03	121.19	123.82	129.37	144.78	155.05	157.36	158.13	176.32	124.08 (C2', C6'); 131.18 (C4'); 132.49 (C3', C5'); 134.16 (C1')
9d	110.98	120.88	121.07	123.67	129.13	144.61	158.08	158.43	155.84	176.46	35.99 (CH ₂); 107.71 (C3'), 110.54 (C4'); 142.40 (C5'), 151.02 (C2')
9e	110.78	120.85	121.20	123.62	129.05	144.58	158.11	157.45	156.27	176.46	24.81 (C3', C5'); 25.10 (C4'); 32.01 (C2', C6'); 48.87 (C1')
9f	110.69	120.88	121.13	123.62	129.09	144.59	158.10	158.42	156.22	176.50	25.35 (C3', C5'); 25.95 (C4'); 30.42 (C2', C6'); 37.34 (C1'); 45.46 (CH ₂)
9g	110.94	120.92	121.08	123.67	129.16	144.63	158.12	158.59	156.06	176.51	42.73 (CH ₂); 127.12 (C4'); 127.48 (C2', C6'); 128.40 (C3', C5'); 138.34 (C1')
9h	111.01	120.93	121.12	123.68	127.27	144.65	158.12	158.83	155.87	176.50	40.64 (CH ₂); 128.96 – 129.03 (d, 2C, C3', C5'); 129.18 – 129.23 (d, 2C, C4', C6'); 132.06 (C2'); 135.10 (C1')
9i*	110.83	120.80	120.64	123.80	128.77	144.65	158.84	161.52	158.46	175.82	32.90 (CH ₃), 53.51 (CH ₂); 127.15 (C2', C6'); 127.53 (C4'); 128.69 (C3', C5'); 136.24 (C1')
	111.19	120.84	121.03	123.87	128.79	144.58	158.50	161.20	158.37	175.86	35.89 (CH ₃); 50.22 (CH ₂); 127.59 (C4'); 127.88 (C2', C6'); 128.69 (C3', C5'); 136.11 (C1')
9j	111.03	120.94	121.04	123.67	129.23	144.65	158.08	158.91	155.82	176.47	42.30 (CH ₂); 123.55 (C3', C5'); 128.48 (C2', C6'); 146.30 (C1'); 146.65 (C4')

[*] 2 rotamers with regard to the amide C-N bond: *syn/anti* (see Fig. 30)

Experimental section

7.2.6 Synthesis of 4-oxo-4*H*-chromen-6-yl-aminobutanoic acids

12a-i

7.2.6.1 Synthesis of 6-amino-4-oxo-4*H*-chromene-2-carboxamide intermediates 11a-i

6-Nitro-4-oxo-4*H*-chromene-2-carboxamide **9a-i** were dissolved or suspended in 15 ml ethanol, and 5 eq. of tin(II)chloride dihydrate were added. The mixture was refluxed for 2 hours, then stirred overnight at RT. Ethanol was removed and the residue was suspended in 30 ml water. The mixture was extracted with 30 ml of ethyl acetate four times. Collected organic fractions were dried over sodium sulphate and evaporated. Solid intermediates **11a-i** (*Tab. 31*) obtained after purification by column chromatography, „C“, (EE/MeOH/NH₃, 95:5:1) or recrystallization, „R“, (ACN/MeOH, 5:1) were used in the next reaction step without further characterization.

Tab. 31 Reaction details and purification of the intermediates **11a-i**

	Name	M _r [g/mol]
11a	6-amino-4-oxo- <i>N</i> -phenyl-4 <i>H</i> -chromene-2-carboxamide	280.3
11b	6-amino- <i>N</i> -(2-bromophenyl)-4-oxo-4 <i>H</i> -chromene-2-carboxamide	359.2
11c	6-amino- <i>N</i> -(2,6-dibromophenyl)-4-oxo-4 <i>H</i> -chromene-2-carboxamide	468.1
11d	6-amino- <i>N</i> -(furan-2-ylmethyl)-4-oxo-4 <i>H</i> -chromene-2-carboxamide	284.3
11e	6-amino- <i>N</i> -cyclohexyl-4-oxo-4 <i>H</i> -chromene-2-carboxamide	286.3
11f	6-amino- <i>N</i> -(cyclohexylmethyl)-4-oxo-4 <i>H</i> -chromene-2-carboxamide	300.4
11g	6-amino- <i>N</i> -benzyl-4-oxo-4 <i>H</i> -chromene-2-carboxamide	294.3
11h	6-amino- <i>N</i> -(2-chlorobenzyl)-4-oxo-4 <i>H</i> -chromene-2-carboxamide	328.8
11i	6-amino- <i>N</i> -benzyl- <i>N</i> -methyl-4-oxo-4 <i>H</i> -chromene-2-carboxamide	308.3

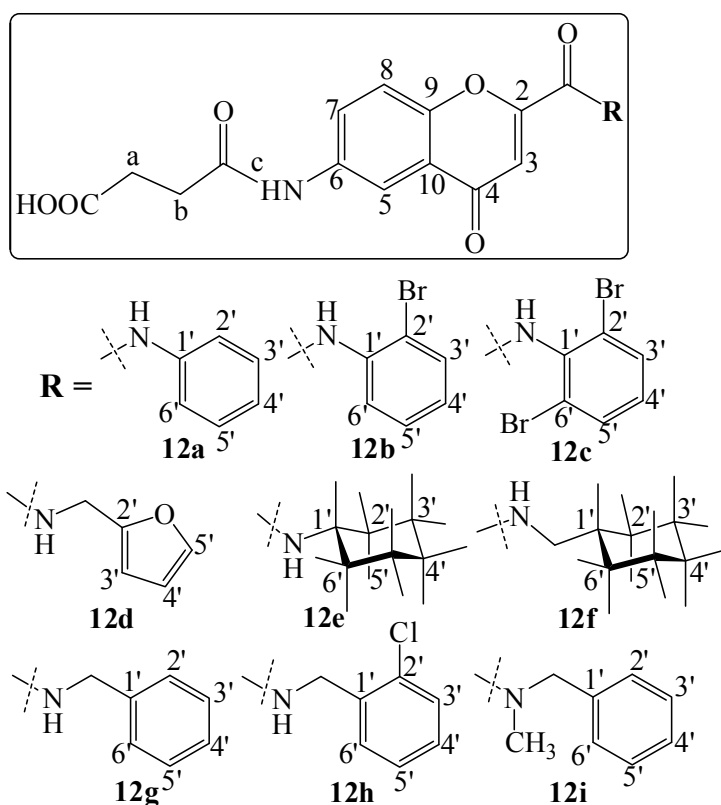
	Starting compound	SnCl ₂ ·2H ₂ O	Yield	Colour	Purification (Reaction control)
11a	9a ; 0.28 g (1.0 mmol)	1.10 g (5.0 mmol)	0.19 g (49 %)	yellow	C, R _f = 0.75
11b	9b ; 0.54 g (1.4 mmol)	1.57 g (7.0 mmol)	0.34 g (69 %)	red	R (TLC: CHCl ₃ /MeOH/NH ₃ (15:1:0.1), R _f = 0.27)
11c	9c ; 0.17 (0.4 mmol)	0.41g (1.8 mmol)	0.12 g (73 %)	yellow	C, R _f = 0.79
11d	9d ; 0.35 g (1.1 mmol)	1.25 g (5.5 mmol)	0.29 (92 %)	orange	C, R _f = 0.70
11e	9e ; 0.38 g (1.2 mmol)	1.38 g (6.0 mmol)	0.22 g (64 %)	orange	C, R _f = 0.65
11f	9f ; 0.17 g (0.5 mmol)	0.58 g (2.6 mmol)	0.15 g (99 %)	yellow	C, R _f = 0.63
11g	9g ; 0.20 g (0.6 mmol)	0.70 g (3.0 mmol)	0.17 g (96 %)	orange	R (TLC: EE/MeOH/NH ₃ (95:5:1), R _f = 0.69)
11h	9h ; 0.21 g (0.6 mmol)	0.67 g (3.0 mmol)	0.17 g (88 %)	yellow	C, R _f = 0.73
11i	9i ; 0.29 g (0.9 mmol)	1.00 g (4.4 mmol)	0.18 g (69 %)	orange	C, R _f = 0.61

Experimental section

7.2.6.2 Synthesis of 4-oxo-4H-chromen-6-yl-aminobutanoic acids 12a-i

Method A (for 12a): followed a modified procedures reported by Williams *et al.*⁴⁵ and Yap *et al.*⁴⁶ To a 0.2 M solution of **11a** in 3.0 ml (37.2 mmol) of anhydrous pyridine, 0.12 g (1.2 mmol, 2 eq.) of succinic anhydride were added. The solution was stirred at RT for 72 h. After being cooled to 0 °C, conc. hydrochloric acid solution was added to adjust pH to 5 – 6. The precipitate formed was filtered and washed with ice cold water. Purification by column chromatography, „C“, (EE/MeOH/FA = 10:1:0.1) yielded a yellow solid.

Method B (for 12b-i): followed a modified procedure reported by Volodymyr *et al.*⁴⁷ The corresponding 6-amino-4-oxo-4H-chromene-2-carboxamide **11a-i** (0.6 mmol) was dissolved in 2.0 ml anhydrous DMF. Subsequently, 0.12 g (1.2 mmol, 2 eq.) of succinic anhydride and 0.39 ml (4.8 mmol, 8 eq.) of anhydrous pyridine were added. The mixture was stirred at 50 °C for 48 hours. After cooling to 0 °C, a 0.2 M hydrochloric acid solution was used to adjust pH to 5 – 6. Purification (see Method A) yielded a yellow solid (see *Tab. 32*).



Scheme 19 Products 12a-i

Tab. 32 Reaction details for 12a-i

	Name	Yield	M _r [g/mol]	Formula	R _f	M.p.	CLogP
12a	4-oxo-4-((4-oxo-2-(phenylcarbamoyl)-4 <i>H</i> -chromen-6-yl)amino)butanoic acid	0.08 g (34 %)	380.4	C ₂₀ H ₁₆ N ₂ O ₆	0.50	256 – 260 °C	1.23
12b	4-((2-((2-bromophenyl)carbamoyl)-4-oxo-4 <i>H</i> -chromen-6-yl)amino)-4-oxobutanoic acid	0.19 g (70 %)	459.3	C ₂₀ H ₁₅ BrN ₂ O ₆	0.55	265 – 268 °C	1.31
12c	4-((2-((2,6-dibromophenyl)carbamoyl)-4-oxo-4 <i>H</i> -chromen-6-yl)amino)-4-oxobutanoic acid	0.29 g (91 %)	538.1	C ₂₀ H ₁₄ Br ₂ N ₂ O ₆	0.54	236 – 239 °C	1.32
12d	4-((2-((furan-2-ylmethyl)carbamoyl)-4-oxo-4 <i>H</i> -chromen-6-yl)amino)-4-oxobutanoic acid	0.11 g (47 %)	384.3	C ₁₉ H ₁₆ N ₂ O ₇	0.52	221 °C (decomp.)	0.59
12e	4-((2-(cyclohexylcarbamoyl)-4-oxo-4 <i>H</i> -chromen-6-yl)amino)-4-oxobutanoic acid	0.18 g (77 %)	386.4	C ₂₀ H ₂₂ N ₂ O ₆	0.50	283 – 286 °C	1.47
12f	4-((2-((cyclohexylmethyl)carbamoyl)-4-oxo-4 <i>H</i> -chromen-6-yl)amino)-4-oxobutanoic acid	0.19 g (80 %)	400.4	C ₂₁ H ₂₄ N ₂ O ₆	0.50	266 – 269 °C	2.09
12g	4-((2-(benzylcarbamoyl)-4-oxo-4 <i>H</i> -chromen-6-yl)amino)-4-oxobutanoic acid	0.18 g (75 %)	394.4	C ₂₁ H ₁₈ N ₂ O ₆	0.53	266 – 269 °C	1.41
12h	4-((2-((2-chlorobenzyl)carbamoyl)-4-oxo-4 <i>H</i> -chromen-6-yl)amino)-4-oxobutanoic acid	0.10 g (37 %)	428.8	C ₂₁ H ₁₇ ClN ₂ O ₆	0.54	269 – 273 °C	2.12
12i	4-((2-(benzyl(methyl)carbamoyl)-4-oxo-4 <i>H</i> -chromen-6-yl)amino)-4-oxobutanoic acid	0.17 g (68 %)	408.4	C ₂₂ H ₂₀ N ₂ O ₆	0.50	185 – 188 °C	1.35

Tab. 33 IR data for 12a-i

12a	3356, 3298, 3088, 1739, 1697, 1666, 1614, 1483, 1151, 748
12b	3371, 3315, 3064, 1689, 1639, 1610, 1487, 1020, 755
12c	3489, 3240, 3094, 1697, 1641, 1607, 1486, 1175, 770
12d	3304, 3249, 3082, 1732, 1691, 1628, 1487, 1202, 847, 752
12e	3371, 3304, 3084, 1738, 1699, 1635, 1487, 1154, 830
12f	3372, 3308, 3082, 1737, 1698, 1634, 1483, 1198, 1156, 828
12g	3384, 3307, 3084, 1733, 1698, 1633, 1486, 1201, 1157, 833
12h	3362, 3304, 3083, 1733, 1697, 1634, 1485, 1198, 1154, 823
12i	3326, 3066, 2923, 1716, 1686, 1640, 1487, 1232, 1176, 871, 704

Tab. 34 ¹H NMR data for 12a-i

	H3	H8	H7	H5	Hc	CONH	OH	Residual ¹ H signals
12a	6.94 (s)	7.78 – 7.82 (m)	8.03 – 8.06 (dd; 9.1, 2.6)	8.36 – 8.37 (d; 2.6)	10.37 (s)	10.73 (s)	12.18 (b)	2.54 – 2.57 (m, 2H, Hb); 2.60 – 2.63 (m, 2H, Ha); 7.18 – 7.22 (m, 1H, H4'); 7.40 – 7.44 (m, 2H, H3' , H5'); 7.78 – 7.82 (m, 3H, H8 , H2' , H6')
12b	6.93 (s)	7.76 – 7.78 (m)	8.03 – 8.06 (dd; 9.1, 2.7)	8.37 – 8.38 (d; 2.7)	10.37 (s)	10.64 (s)	12.15 (b)	2.54 – 2.57 (m, 2H, Hb); 2.61 – 2.64 (m, 2H, Ha); 7.27 – 7.32 (td, 1H, H4' , 7.8, 1.5); 7.46 – 7.51 (td, 1H, H5' , 7.8, 1.5); 7.64 – 7.67 (dd, 1H, H6' , 7.8, 1.5); 7.76 – 7.78 (m, 2H, H8 , H3')
12c	6.94 (s)	7.76 – 7.78 (d; 9.1)	8.04 – 8.07 (dd; 9.1, 2.7)	8.38 – 8.39 (d; 2.7)	10.38 (s)	11.10 (s)	12.16 (b)	2.54 – 2.58 (m, 2H, Hb); 2.61 – 2.64 (m, 2H, Ha); 7.28 – 7.32 (t, 1H, H4' , 8.1); 7.81 – 7.83 (m, 2H, H3' , H5')
12d	6.81 (s)	7.67 – 7.70 (d; 8.9)	8.01 – 8.04 (m)	8.36 (m)	10.61 (s)	9.66 – 9.68 (t; 5.3)	—	*2.58 – 2.59 (m, 2H, Ha); 4.49 – 4.50 (d, 2H, CH₂ , 5.3); 6.35 – 6.41 (m, 2H, H3' , H4'); 7.60 (m, 1H, H5') [*] Hb covered by DMSO signal
12e	6.78 (s)	7.72 – 7.74 (d; 9.2)	8.00 – 8.03 (dd; 9.2, 2.7)	8.30 – 8.31 (d; 2.7)	10.33 (s)	8.80 – 8.82 (d; 8.1)	12.15 (b)	2.53 – 2.56 (m, 2H, Hb); 2.59 – 2.62 (m, 2H, Ha); 1.09 – 1.19 (m, 1H, H4'a); 1.26 – 1.43 (m, 4H, H2'a , H3'a , H5'a , H6'a); 1.61 – 1.64 (m, 1H, H4'e); 1.74 – 1.84 (m, 4H, H3'e , H5'e , H2'e , H6'e); 3.72 – 3.80 (m, 1H, H1'a)
12f	6.78 (s)	7.69 – 7.71 (d; 9.1)	8.00 – 8.03 (dd; 9.1, 2.7)	8.31 – 8.32 (d; 2.7)	10.33 (s)	9.04 – 9.07 (t; 6.3)	12.16 (b)	2.53 – 2.56 (m, 2H, Hb); 2.59 – 2.62 (m, 2H, Ha); 0.88 – 0.97 (m, 2H, H2'a , H6'a); 1.09 – 1.24 (m, 3H, H4'a , H3'a , H5'a); 1.52 – 1.62 (m, 2H, H1'a , H4'e); 1.67 – 1.72 (m, 4H, H2'e , H6'e , H3'e , H5'e); 3.13 – 3.16 (t, 2H, CH₂ , 6.3)
12g	6.83 (s)	7.67 – 7.70 (d; 9.1)	8.00 – 8.03 (dd; 9.1, 2.7)	8.33 – 8.34 (dd; 2.7)	10.34 (s)	9.66 – 9.69 (t; 6.1)	12.14 (b)	2.53 – 2.56 (m, 2H, Hb); 2.59 – 2.63 (m, 2H, Ha); 4.51 – 4.53 (d, 2H, CH₂ , 6.1); 7.25 – 7.30 (m, 1H, H4'); 7.34 – 7.36 (m, 4H, H2' , H3' , H5' , H6')
12h	6.84 (s)	7.69 – 7.71 (d; 9.1)	8.01 – 8.04 (dd; 9.1, 2.7)	8.34 – 8.35 (d; 2.7)	10.35 (s)	9.65 – 9.68 (t; 5.9)	12.15 (b)	2.53 – 2.57 (m, 2H, Hb); 2.60 – 2.63 (m, 2H, Ha); 4.58 – 4.60 (d, 2H, CH₂ , 5.9); 7.30 – 7.37 (m, 2H, H5' , H4'); 7.41 – 7.45 (m, 1H, H6'); 7.46 – 7.49 (m, 1H, H3')
12i*	6.53 (s)	7.28 – 7.42 (m)	7.88 – 7.91 (dd; 9.1, 2.6)	8.32 – 8.33 (d; 2.6)	10.30 (s)	CONCH ₃	12.14 (b)	2.54 – 2.56 (m, 4H, Hb); 2.57 – 2.60 (m, 4H, Ha); 2.93 (s, 3H, CH₃); 4.65 (s, 2H, CH₂); 7.28 – 7.42 (m, 11H, H2' , H3' , H4' , H5' , H6' , H8)
	6.60 (s)	7.68 – 7.71 (d; 9.1)	7.94 – 7.97 (dd; 9.1, 2.6)	8.36 – 8.37 (d; 2.6)	10.33 (s)	CONCH ₃		2.54 – 2.56 (m, 4H, Hb); 2.57 – 2.60 (m, 4H, Ha); 3.02 (s, 3H, CH₃); 4.67 (s, 2H, CH₂); 7.28 – 7.42 (m, 11H, H2' , H3' , H4' , H5' , H6')

Tab. 35 ¹³C-NMR data for 12a-i

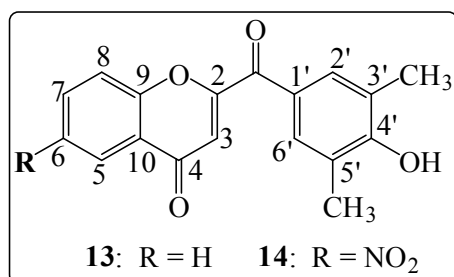
	Cb	Ca	C3	C5	C8	C10	C7	C6	C9	C2	CONH	Cc	COOH	C4	Residual ¹³ C signals
12a	28.73	31.08	110.43	112.9	119.6	123.94	126.3	137.22	150.87	155.51	157.8	170.57	173.74	177.14	121.08 (C2', C6'); 124.93 (C4'); 128.83 (C3', C5'); 137.54 (C1')
12b	28.69	31.06	110.56	112.92	119.48	123.92	126.39	137.29	150.77	154.9	158.05	170.55	173.72	177.04	120.10 (C2'); 128.25 (C6'); 128.40 (C5'); 128.69 (C4'); 132.86 (C3'); 135.04 (C1')
12c	28.7	31.08	110.77	112.92	119.52	123.96	126.47	137.36	150.84	154.5	157.97	170.59	173.74	176.96	124.21 (C2', C6'); 131.09 (C4'); 132.43 (C3', C5'); 134.40 (C1')
12d	29.50	31.56	110.03	112.86	119.33	123.87	126.32	137.29	150.79	155.20	159.10	170.91	174.32	177.18	35.98 (CH ₂); 107.56 (C3'); 110.56 (C4'); 142.32 (C5'); 151.26 (C2')
12e	28.71	31.05	109.85	112.9	119.46	123.86	126.15	137.08	150.83	155.71	158.13	170.51	173.73	177.16	24.84 (C3', C5'); 25.13 (C4'); 32.02 (C2', C6'); 48.75 (C1')
12f	28.71	31.06	109.76	112.91	119.39	123.85	126.18	137.09	150.82	155.62	159.07	170.51	173.73	177.18	25.36 (C3', C5'); 25.98 (C4'); 30.44 (C2', C6'); 37.34 (C1'); 45.39 (CH ₂)
12g	28.69	31.05	109.97	112.91	119.34	123.88	126.23	137.12	150.81	155.39	159.18	170.50	173.71	177.14	42.65 (CH ₂); 127.04 (C4'); 127.43 (C2', C6'); 128.37 (C3', C5'); 138.51 (C1')
12h	28.7	31.06	110.07	112.92	119.40	123.91	126.27	137.16	150.84	155.21	159.45	170.53	173.74	177.16	40.57 (CH ₂); 127.28 (C5'); 128.88 (C4'); 128.92 (C6'); 129.20 (C3'); 131.99 (C2'); 135.27 (C1')
12i*	28.68	31.03	109.88 110.18	112.97	118.86 119.20	123.90	125.92	137.06 137.12	150.97 151.12	162.15 161.81	158.15 157.89	170.48	173.71	176.42 176.48	32.98 (CH ₃); 53.58 (CH ₂); 127.08 (C2', C6'); 127.50 (C4'); 128.69 (C3', C5'); 136.30 (C1') 35.89 (CH ₃); 50.17 (CH ₂); 127.56 (C4') 127.84 (C2', C6'); 128.69 (C3', C5'); 136.24 (C1')

[*] 2 rotamers with regard to the amide C-N bond: *syn/anti* (see Fig. 30)

Experimental section

7.2.7 Synthesis of 2-(4-hydroxy-3,5-dimethylbenzoyl)-4*H*-chromen-4-ones **13** and **14**

A Friedel-Crafts acylation was performed following the procedure reported by Nicolas *et al.*⁴² To a solution of 2,6-dimethylphenol (0.46 g, 3.8 mmol, 1.5 eq) in 5 ml of anhydrous dichloromethane, aluminium chloride (0.86 g, 6.5 mmol, 2.6 eq) was added under argon. After 20 min. of stirring at RT, the mixture was cooled to 0 °C and 5 ml of a solution containing 2.5 mmol (1.0 eq) of acid chloride (see *Tab. 36*) in anhydrous dichloromethane was added dropwise. The mixture was stirred for 3 h at 0 °C, then at RT overnight. Solvent was removed by distillation *in vacuo* and the residue was cooled on an ice bath and precipitated using 10 ml of a 10% HCl solution. The crude product was filtered, washed with water and recrystallized from an acetone/ethanol mixture (2:1) to yield a yellow solid.



Tab. 36 Reaction details for **13** and **14**

	Name	Acid chloride	Yield [Lit.]
13	2-(4-hydroxy-3,5-dimethylbenzoyl)-4 <i>H</i> -chromen-4-one ⁴²	4-oxo-4 <i>H</i> -chromene-2-carbonyl chloride; 0.52 g (2.5 mmol)	0.25 g (34 %) [95 %] ⁴²
14	2-(4-hydroxy-3,5-dimethylbenzoyl)-6-nitro-4 <i>H</i> -chromen-4-one	6-nitro-4-oxo-4 <i>H</i> -chromene-2-carbonyl chloride; 0.63 g (2.5 mmol)	0.53 g (63 %)

Tab. 37 Analytical data for **13** and **14**, [*] (PE/EE, 1:1)

	M _r [g/mol]	Formula	R _f [*]	m.p. [Lit.]	CLogP	IR
13	294.3	C ₁₈ H ₁₄ O ₄	0.77	218 – 221 °C [215] ⁴²	3.33	3167, 2974, 1660, 1631, 1583, 1189, 931, 755
14	339.3	C ₁₈ H ₁₃ NO ₆	0.66	275 – 277 °C	3.11	3295, 3097, 1638, 1621, 1585, 1530, 1339, 1175, 930, 746

Experimental section

Tab. 38 ^1H NMR data for **13** and **14**

	H3	H8	H7	H5	R
14	6.81 (s)	7.97 – 7.99 (d; 9.2)	8.60 – 8.63 (dd; 9.2, 2.9)	8.75 – 8.76 (d; 2.9)	2.24 (s, 6H, 2×CH ₃); 7.71 (s, 2H, H2', H6'); 9.66 (b, 1H, OH)

Tab. 39 ^{13}C NMR data for **13** and **14**

	C3	C8	C10	C5	C6	C7	C9	C2	C4	R
13	112.81	118.84	123.93	124.93	126.02	135.01	155.45	159.13	177.10	16.50 (2×CH ₃); 124.57 (C3', C5'); 125.33 (C1'); 131.26 (C2', C6'); 159.86 (C4'); 185.82 (CO)
14	113.01	121.20	123.96	120.86	144.64	128.98	158.53	159.63	176.35	16.48 (2×CH ₃); 124.65 (C3', C5'); 125.07 (C1'); 131.38 (C2', C6'); 160.12 (C4'); 185.23 (CO)

^1H NMR spectrum of compound **13** is consistent with the published data⁴².

7.2.8 Synthesis of 4-((2-(4-hydroxy-3,5-dimethylbenzoyl)-4-oxo-4H-chromen-6-yl)amino)-4-oxobutanoic acid **16**

7.2.8.1 Synthesis of 6-amino-2-(4-hydroxy-3,5-dimethylbenzoyl)-4H-chromen-4-one intermediate **15**

Compound **14** (0.17 g, 0.5 mmol) was dissolved in 15 ml ethanol and 5 equivalents of tin(II)chloride dihydrate (0.56 g, 2.5 mmol) were added. The mixture was refluxed for 2 h, then stirred overnight at RT. Ethanol was removed and the residue suspended in 30 ml water. The mixture was extracted with 30 ml of ethyl acetate four times. Collected organic fractions were dried over sodium sulphate, filtered and evaporated. Purification by column chromatography (PE/EE/MeOH/NH₃, 5:5:1:0.1, R_f = 0.56) yielded an orange solid; yield 0.13 g (84 %), m.p. 264 °C. The intermediate **15** was used in the next reaction step without further characterization.

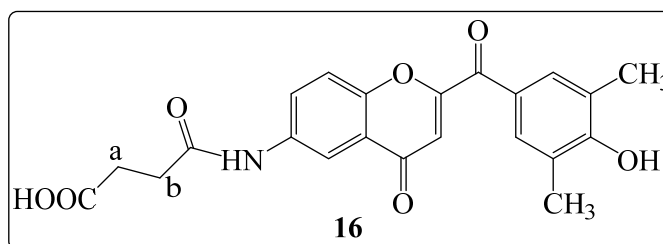
7.2.8.2 Synthesis of 4-((2-(4-hydroxy-3,5-dimethylbenzoyl)-4-oxo-4H-chromen-6-yl)amino)-4-oxobutanoic acid **16**

Compound **15** (0.13 g, 0.4 mmol) was dissolved in 2.0 ml of anhydrous DMF under argon. Subsequently, 0.08 g (0.8 mmol, 2 eq.) of succinic anhydride and 0.27 ml (3.4 mmol, 8 eq.) of anhydrous pyridine were added. The mixture was stirred at 50 °C for 48 h. After being cooled

Experimental section

to 0 °C, a 0.2M HCl solution was added dropwise to adjust pH 5 – 6. Purification (EE/MeOH/HCOOH, 95:5:1, R_f = 0.73) yielded a yellow solid.

Formula: $C_{22}H_{19}NO_7$
M_r: 409.4
Yield: 0.07 g (41 %)
M.p.: 282 – 284 °C
CLogP: 2.26

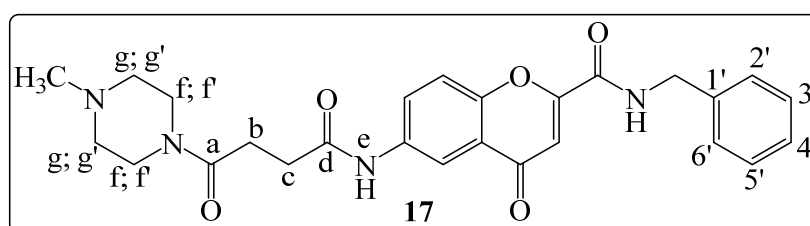


¹H NMR: 2.24 (s, 6H, 2×CH₃); 2.54 – 2.57 (m, 2H, **H**_b); 2.60 – 2.64 (m, 2H, **H**_a); 6.63 (s, 1H, **H**₃); 7.67 (s, 2H, **H**₂['], **H**₆[']); 7.69 – 7.71 (d, 1H, **H**₈, 9.1); 7.96 – 7.99 (dd, 1H, **H**₇, 9.1, 2.7); 8.40 – 8.41 (d, 1H, **H**₅, 2.7); 9.60 (b, 1H, **O****H**); 10.35 (s, 1H, **N****H**); 12.15 (b, 1H, **COOH**); ¹³C NMR: 16.51 (2×CH₃); 28.69 (C_b); 31.06 (C_a); 112.28 (C₃); 112.89 (C₅); 119.45 (C₈); 124.16 (C₁₀); 124.57 (C₃['], C₅[']); 125.40 (C₁[']); 126.27 (C₇); 131.24 (C₂['], C₆[']); 137.17 (C₆); 151.20 (C₉); 158.86 (C₂); 159.81 (C₄[']); 170.51 (CONH); 173.73 (COOH); 176.97 (C₄); 185.89 (CO)

IR: 3483, 3305, 3104, 2918, 1753, 1708, 1631, 1488, 1195, 829

7.2.9 Synthesis of *N*-benzyl-6-(4-(4-methylpiperazin-1-yl)-4-oxobutanamido)-4-oxo-4*H*-chromene-2-carboxamide **17**

Following a modified procedure reported by Guillaumel *et al.*⁴⁸ for (*E*)-propenoyl derivatives, the succinamic acid **12g** (0.10 g, 0.3 mmol) was suspended in 30 ml anhydrous dichloromethane under argon. Then, 0.03 g (0.3 mmol, 1 eq.) of *N,N*-dimethylaminopyridine and 0.03 ml (0.3 mmol, 1 eq.) of *N*-methylpiperazine were added. After cooling to -5 °C, 0.06 ml (0.4 mmol, 1.5 eq.) of *N,N'*-diisopropylcarbodiimide were added dropwise. The mixture was warmed to RT and refluxed for 18 h. Water was added and the product was extracted with dichloromethane (3×30 ml). Organic phases were collected, dried over sodium sulphate and filtered. After solvent evaporation *in vacuo*, the residue was purified by column chromatography (CHCl₃/MeOH/NH₃, 5:1:0.01, R_f = 0.54) and recrystallized from ethanol to yield a white solid.



Experimental section

Formula: C₂₆H₂₈N₄O₅
M_r [g/mol]: 476.5

Yield: 0.02 g (19 %)
M.p.: 228 – 230 °C
CLogP: 2.01

¹H NMR: 2.18 (s, 6H, 2×CH₃); 2.24 (m, 4H, 4×Hg); 2.32 (m, 4H, 4×Hg'); 2.57 – 2.61 (m, 2H, Hc); 2.63 – 2.67 (m, 2H, Hb); 3.42 – 3.47 (m, 8H, 4×Hf, 4×Hf'); 4.51 – 4.53 (d, 4H, 2×CH₂, 6.1); 6.82 (s, 2H, 2×CH₃); 7.24 – 7.30 (m, 2H, 2×H4'); 7.34 – 7.36 (m, 8H, 2×(H2', H6', H3', H5')); 7.67 – 7.69 (d, 2H, 2×H8, 9.1); 7.99 – 8.02 (dd, 2H, 2×H7, 9.1, 2.7); 8.34 – 8.35 (d, 2H, 2×H5, 2.7); 9.65 – 9.68 (t, 2H, 2×CONH, 6.1); 10.32 (s, 2H, 2×He);

¹³C NMR: 27.40 (2×Cb); 31.36 (2×Cc); 41.02 (Cg); 42.65 (2×CH₂); 44.54 (Cg'); 45.62 (2×CH₃); 54.29 (Cf); 54.69 (Cf'); 109.96 (2×C3); 112.83 (2×C5); 119.29 (2×C8); 123.86 (2×C10); 126.20 (2×C7); 127.03 (2×C4'); 127.42 (2×(C2', C6')); 128.37 (2×(C3', C5')); 137.25 (2×C6); 138.51 (2×C1'); 150.75 (2×C9); 155.38 (2×C2); 159.19 (2×CONH); 169.60 (2×Ca); 171.03 (2×Cd); 177.16 (2×C4)

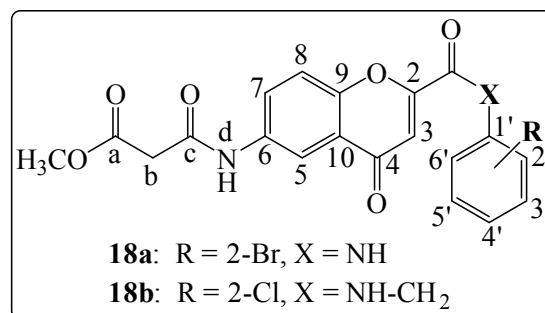
(a mixture of 2 conformers with regard to the piperazine ring, 1:1)

IR: 3309, 2935, 2790, 1686, 1630, 1287, 1001, 727, 695

7.2.10 Synthesis of methyl 3-((-4-oxo-4H-chromen-6-yl)amino)-3-oxopropanoates **18a** and **18b**

Synthesis followed the procedure reported by Lee *et al.*⁴⁹ for 4-aminobenzophenone. Into a 0.37 M solution of 6-amino-4-oxo-4H-chromene-2-carboxamide intermediate (see *Tab. 40*) dissolved in a mixture of anhydrous THF/CH₂Cl₂ (1:3), 2 eq. of triethylamine were added under argon. After being cooled to 0 °C, 1 eq. of methyl malonyl chloride (MMCl) was added dropwise and the mixture was stirred at 50 °C for 48 h. The reaction was quenched with 50 ml of a 0.1 M aqueous sodium hydrogencarbonate solution.

The organic phase was separated and the aqueous layer was washed twice with 30 ml of dichloromethane. Organic layers were combined, washed with 30 ml water, dried over sodium sulphate and evaporated *in vacuo*. Recrystallization from an ethyl acetate/methanol mixture (5:1) yielded a solid product.



Tab. 40 Reaction details for 18a-b

	Name	Starting compound	Et ₃ N	MMCl	Yield
18a	Methyl 3-((2-((2-bromophenyl)carbamoyl)-4-oxo-4H-chromen-6-yl)amino)-3-oxopropanoate	11b; 0.40 g (1.1 mmol)	0.30 ml (2.2 mmol)	0.12 ml (1.1 mmol)	0.25 g (50 %)
18b	Methyl 3-((2-((2-chlorobenzyl)carbamoyl)-4-oxo-4H-chromen-6-yl)amino)-3-oxopropanoate	11h; 0.15 g (0.5 mmol)	0.11 ml (0.9 mmol)	0.05 ml (0.5 mmol)	0.08 g (37 %)

Tab. 41 Analytical data for 18a-b

	M _r [g/mol]	Formula	Colour	R _f CHCl ₃ /MeOH (5:1)	m.p.	CLogP
18a	459.3	C ₂₀ H ₁₅ BrN ₂ O ₆	white	0.88	337 °C (decomp.)	1.43
18b	428.8	C ₂₁ H ₁₇ ClN ₂ O ₆	yellow	0.82	202 – 205 °C	2.25

IR: 18a 3365, 3324, 3076, 2950, 1732, 1699, 1644, 1534, 1212, 1145, 832, 746
 18b 3323, 3277, 3111, 3065, 2948, 1736, 1686, 1665, 1639, 1544, 1157, 850, 741

Tab. 42 ¹H-NMR data for 18a-b

	H3	H8	H7	H5	CONH	Residual ¹ H signals
18a	6.94 (s)	7.76 – 7.81 (m)	8.01 – 8.04 (dd; 9.1, 2.7)	8.36 – 8.37 (d; 2.7)	10.66 (s)	3.54 (s, 2H, Hb); 3.68 (s, 3H, CH ₃); 7.28 – 7.32 (td, 1H, H4', 7.9, 1.4); 7.47 – 7.51 (td, 1H, H5', 7.9, 1.4); 7.64 – 7.66 (dd, 1H, H6', 7.9, 1.4); 7.76 – 7.81 (m, 2H, H3', H8); 8.36 – 8.37 (d, 1H, H5, 2.7) 10.61 (s, 1H, Hd)
18b	6.85 (s)	7.72 – 7.74 (d; 9.1)	7.99 – 8.02 (dd; 9.1, 2.7)	8.32 – 8.33 (d; 2.7)	9.66 – 9.69 (t; 5.9)	3.53 (s, 2H, Hb); 3.67 (s, 3H, CH ₃); 4.58 – 4.60 (d, 2H, CH ₂ , 5.9); 7.30 – 7.37 (m, 2H, H4', H5'); 7.41 – 7.44 (m, 1H, H6'); 7.47 – 7.49 (m, 1H, H3'); 10.58 (s, 1H, Hd)

Tab. 43 ¹³C-NMR data for 18a-b

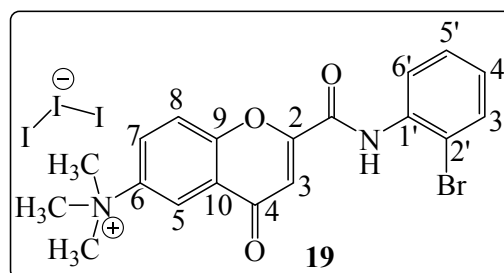
	C3	C5	C8	C10	C7	C6	C9	C2	CONH	C4	Residual ¹³ C signals
18a	110.64	113.29	119.69	123.94	126.50	136.76	151.11	154.97	158.03	176.99	43.48 (Cb); 52.04 (CH ₃); 120.14 (C2'); 128.31 (C6'); 128.40 (C5'); 128.72 (C4'); 132.87 (C3'); 135.03 (C1'); 164.43 (Cc); 167.91 (Ca)
18b	110.13	113.28	119.60	123.92	126.38	136.62	151.17	155.27	159.41	177.10	40.57 (CH ₂); 43.48 (Cb); 52.04 (CH ₃); 127.28 (C5'); 128.88 (C4'); 128.92 (C6'); 129.20 (C3'); 131.99 (C2'); 135.25 (C1'); 164.41 (Cc); 167.92 (Ca)

Experimental section

7.2.11 Synthesis of 2-((2-bromophenyl)carbamoyl)-*N,N,N*-trimethyl-4-oxo-4*H*-chromen-6-aminium triiodone **19**

Compound **11b** (0.37 g, 1.0 mmol) was suspended in 15 ml anhydrous acetonitrile. While stirred under argon, 1.27 ml of methyl iodide (20.0 mmol, 20 eq.) were added dropwise in two portions (1. and 5. day of stirring). After 12 days of stirring (TLC control) in a pressure-proofed closed vessel protected from light at 35 – 40 °C, the mixture was poured on ice. The precipitate formed was filtered and recrystallized from ethanol to yield bright dark brown crystals.

Formula: C₁₉H₁₈BrI₃N₂O₃
M_r [g/mol]: 783.0
Yield: 0.10 g (13 %)
M.p.: 213 – 215 °C

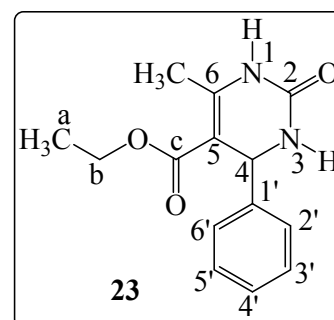


¹H NMR: 3.72 (s, 9H, 3×CH₃); 7.09 (s, 1H, **H3**); 7.30 – 7.34 (td, 1H, **H4'**, 7.9, 1.5); 7.48 – 7.52 (td, 1H, **H5'**, 7.9, 1.5); 7.63 – 7.65 (dd, 1H, **H6'**, 7.9, 1.5); 7.78 – 7.80 (dd, 1H, **H3'**, 7.9, 1.5); 8.05 – 8.08 (d, 1H, **H8**, 8.5); 8.53 – 8.56 (m, 2H, **H7**, **H5**); 10.73 (s, 1H, CONH);
¹³C NMR: 56.62 (3×CH₃); 111.40 (**C3**); 117.66 (**C5**); 120.14 (**C2'**); 121.28 (**C8**); 123.71 (**C10**); 127.60 (**C7**); 128.38 (**C6'**); 128.47 (**C5'**); 128.90 (**C4'**); 132.94 (**C3'**); 134.83 (**C1'**); 144.34 (**C6**); 154.75 (**C9**); 155.63 (**C2**); 157.66 (CONH); 176.47 (**C4**)
IR: 3358, 3052, 1695, 1656, 1524, 1486, 1155, 869, 761

7.2.12 Synthesis of ethyl 6-methyl-2-oxo-4-phenyl-1,2,3,4-tetrahydropyrimidine-5-carboxylate **23**

Synthesis was performed following a modified procedure reported by Joseph *et al.*⁶⁵ The mixture of 1.18 g (19.6 mmol) of grinded urea, 2.0 ml (19.6 mmol, 1 eq.) of benzaldehyde and 3.7 ml (29.4 mmol, 1.5 eq.) of ethyl aceto-acetate was heated in a microwave on 135°C for 1 h (5 min. temperating on 135 °C, 1000 W). A ionic liquid BMIM Cl (4.32 g, 24.7 mmol) was used as a solvent. After cooling to RT, the crude product was precipitated with 30 ml water. Recrystallization from ethyl acetate yielded a white solid.

Formula: C₁₄H₁₆N₂O₃
M_r [g/mol]: 260.3
Yield [Lit]: 1.20 g (24 %) [98 %]⁶⁵
M.p. [Lit]: 203 – 205 °C [202]⁶⁵
CLogP 2.92



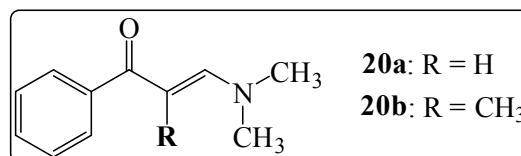
Experimental section

^{13}C NMR: 14.06 (Ca); 17.76 (CH_3); 53.95 (C4); 59.16 (Cb); 99.25 (C5); 126.22 (C2', C6'); 127.23 (C4'); 128.36 (C3', C5'); 144.85 (C1'); 148.32 (C6); 152.10 (C2); 165.31 (Cc)

The obtained IR and ^1H NMR spectral data of compound **23** are consistent with literature⁶⁵.

7.2.13 Synthesis of pyrimidin-2-amines 21a-e

Method A: Following the modified procedure reported by Larina *et al.*⁶³, 37.6 mmol of the corresponding ketone (see *Tab. 44*) and 5 ml (37.6 mmol, 1 eq.) of DMF-dimethyl acetal were mixed and heated to 90 °C in a microwave (5 min. temperating to 90°C, 800 W). After being cooled to RT, 30 ml of pentane were added. The crude product was precipitated by means of ultrasound, then filtered and dried over phosphorus pentoxide. Recrystallization from ethyl acetate yielded a corresponding enaminone (**20a**, **20b**).



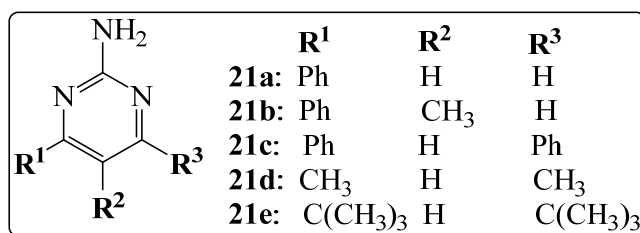
Tab. 44 Reaction details for **20a-b**

	Name	Ketone	Reaction time (h)	Yield [Lit]	M_r [g/mol]	Colour
20a	3-(dimethylamino)-1-phenylprop-2-en-1-one ⁶³	acetophenone; 4.4 ml (37.6 mmol)	5.5	5.06 g (77 %) [91 %] ⁶³	175.2	yellow
20b	3-(dimethylamino)-2-methyl-1-phenylprop-2-en-1-one ¹⁰³	propiophenone; 5.0 ml (37.6 mmol)	12.0	1.30 g (18 %) [98 %] ¹⁰³	189.3	white

In the next step, 1 eq. of the enaminone intermediate was suspended in 30 – 50 ml of butanol. Subsequently, 1 eq. of guanidine hydrochloride (GH) and 1 eq. of sodium hydroxide were added. The mixture was refluxed for 2.5 h. After cooling, the precipitate formed was separated by filtration and dried *in vacuo*. Purification yielded a white solid product (see *Tab. 45*).

Method B: 1 eq. of the corresponding β -diketone (see *Tab. 45*), 1 eq. of guanidine hydrochloride (GH) and 1 eq. of potassium carbonate were mixed with approx. 5 eq. of BMIM Cl. The mixture was heated in microwave (1000 W, 10 min. temperating on the final temperature). The product was purified by column chromatography to yield a white solid.

Experimental section



Scheme 20 *Products 21a-e*

Tab. 45 Reaction details for *21a-e*

	Name	Method	Starting compounds	Yield
21a	4-phenylpyrimidin-2-amine ^{66,104}	A	19a 4.76 g (27 mmol), GH 2.58 g (27 mmol), NaOH 1.08 g (27 mmol)	3.70 g (80 %) [49 %] ⁶⁶
21b	5-methyl-4-phenylpyrimidin-2-amine ^{67,105}	A	19b 0.53 g (2.8 mmol), GH 0.27 g (2.8 mmol), NaOH 0.11 g (2.8 mmol)	0.19 g (37 %) [73 %] ¹⁰⁵
21c	4,6-diphenylpyrimidin-2-amine ^{68,106,107}	B (185 °C, 35 min.)	1,3-diphenylpropane-1,3-dione 1.02 g (4.5 mmol), GH 0.43 g (4.5 mmol), K ₂ CO ₃ 0.63 g (4.5 mmol)	0.35 g (32 %) [39 %] ¹⁰⁷
21d	4,6-dimethylpyrimidin-2-amine ^{69,71,108}	B (110 °C, 3.5 h)	pentane-2,4-dione 5.00 ml (47.4 mmol), GH 4.53 g (47.4 mmol), K ₂ CO ₃ 6.55 g (47.4 mmol)	4.75 g (81 %) [85.2 %] ⁶⁹
21e	4,6-di-tert-butylpyrimidin-2-amine ⁷⁰	B (70 °C, 8.5 h)	2,2,6,6-tetramethylheptane-3,5-dione 1 ml (4.9 mmol), GH 0.47 g (4.9 mmol), K ₂ CO ₃ 0.67 g (4.9 mmol)	0.60 g (59 %) [6 %] ⁷⁰

Tab. 46 Analytical data for *21a-e*

	M _r [g/mol]	Formula	Purification (Reaction control, R _f)	m.p. [Lit]	CLogP
21a	171.2	C ₁₀ H ₉ N ₃	R: H ₂ O/MeOH, 3:1 (TLC, PE/EE, 1:1, R _f = 0.20)	166 – 168 °C [165 - 167] ¹⁰⁴	1.77
21b	185.2	C ₁₁ H ₁₁ N ₃	R: H ₂ O/MeOH, 3:1 (TLC, PE/EE, 1:1, R _f = 0.18)	183 – 185 °C [181 - 182.5] ¹⁰⁵	1.97
21c	247.3	C ₁₆ H ₁₃ N ₃	C: PE/EE/MeOH/NH ₃ , 3:1:0.1:0.01 (R _f = 0.47)	133 – 136 °C [133 - 136] ¹⁰⁶	3.87
21d	123.2	C ₆ H ₉ N ₃	C: EE/MeOH/NH ₃ , 8:1:0.04 (R _f = 0.48)	157 – 159 °C [156 - 158] ¹⁰⁸	0.67
21e	207.3	C ₁₂ H ₂₁ N ₃	C: PE/EE/MeOH/NH ₃ , 6:1:0.1:0.01 (R _f = 0.65)	119 – 121 °C [127] ⁷⁰	3.33

Tab. 47 IR data for *21a-e*

21a	3304, 3148, 1654, 1551, 1472, 1218, 764, 700
21b	3293, 3160, 1628, 1541, 1472, 1201, 770, 708
21d	3408, 3305, 3182, 1620, 1595, 1566, 1463, 1241, 792

Experimental section

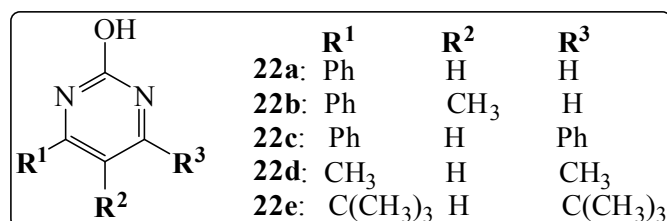
Tab. 48 ^{13}C NMR data for **21a-e**

	C5	C6	C4	C2	Residual ^{13}C signals
21a	105.79	159.01	163.57	163.79	126.66 (C2', C6'); 128.66 (C3', C5'); 130.43 (C4'); 137.00 (C1')
21b	115.27	159.82	162.32	164.72	15.65 (CH ₃); 128.00 (C2', C6'); 128.48 (C3', C5'); 128.69 (C4'); 138.61 (C1')
21e	99.95	177.73	177.73	162.80	29.26 (2×C(CH ₃) ₃); 36.90 (2×C(CH ₃) ₃)

^1H NMR spectra of **21a-e** are consistent with the references⁶⁶⁻⁷⁰. For **21c** and **21d**, ^{13}C NMR spectra have been reported in literature^{68,71} and are in accordance with the obtained data. IR data are known for **21c**⁶⁸ and **21e**⁷⁰ and correspond with the measured spectra.

7.2.14 Synthesis of pyrimidine-2-ols **22a-e**

The partial hydrolysis of **21a-e** was performed following the procedure reported by Teixido⁶⁴ using 3 – 20 ml of a 6 M HCl solution (see Tab. 49). The mixture was refluxed until complete conversion. After cooling to 0 °C, the mixture was diluted with water and neutralized with a 10% NaOH solution (to adjust pH 7 – 8). The precipitate was filtered and washed with water. Purification yielded a white solid (see Tab. 50).



Scheme 21 Products **22a-e**

Tab. 49 Reaction details for **22a-e**

	Name	Starting compounds	Reflux	Yield*
22a	4-phenylpyrimidin-2-ol ¹⁰⁹	20a , 3.34 g (19.5 mmol); 6 M HCl, 20,0 ml (120 mmol)	36 h	2.60 g (78 %) [45 %] ¹⁰⁹
22b	5-methyl-4-phenylpyrimidin-2-ol ¹¹⁰	20b , 0.10 g (0.5 mmol); 6 M HCl, 3 ml (18.0 mmol)	36 h	0.05 g (47 %) [100 %] ¹¹⁰
22c	4,6-diphenylpyrimidin-2-ol ^{73,111}	20c , 0.11 g (0.4 mmol); 6 M HCl, 3 ml (18.0 mmol)	10 h	0.03 g (27 %) [95 %] ⁷³
22d	4,6-dimethylpyrimidin-2-ol ^{74,112}	20d , 2.49 g (20.2 mmol), 6 M HCl, 20 ml (120 mmol)	10 h	1.00 g (40 %) [65 %] ⁷⁴
22e	4,6-di-tert-butylpyrimidin-2-ol ⁷⁵	20e , 0.51 g (2.5 mmol), 6 M HCl, 5 ml (30.0 mmol)	37 h	0.38 g (73 %) [68 %] ⁷⁵

[*] All the referenced reaction yields were obtained from different synthesis procedures.

Experimental section

Tab. 50 Analytical data for **22a-f**

	M_r [g/mol]	Formula	Purification (Reaction control)	m.p. [Lit]	CLogP
22a	172.2	C ₁₀ H ₈ N ₂ O	R: MeOH, H ₂ O (TLC: CH ₂ Cl ₂ /MeOH, 5:1, R _f = 0.47)	245 – 248 °C [240 - 241] ¹⁰⁹	2.41
22b	186.2	C ₁₁ H ₁₀ N ₂ O	R: MeOH, H ₂ O (TLC: CH ₂ Cl ₂ /MeOH, 5:1, R _f = 0.44)	171 – 173 °C	2.61
22c	248.3	C ₁₆ H ₁₂ N ₂ O	C: CH ₂ Cl ₂ /MeOH (5:1), R _f = 0.84	234 – 237 °C [233 - 240] ¹¹¹	4.50
22d	124.1	C ₆ H ₈ N ₂ O	C: CH ₂ Cl ₂ /MeOH (5:1), R _f = 0.32	198 – 202 °C [194 - 196] ¹¹²	1.31
22e	208.3	C ₁₂ H ₂₀ N ₂ O	C: CH ₂ Cl ₂ /EE/MeOH (5:5:1), R _f = 0.62	264 – 266 °C [223 - 224] ⁷⁵	3.96

Tab. 51 IR data for **22a-e**

22a	3007, 1669, 1594, 1416, 1247, 803, 768, 703
22b	2768, 1661, 1615, 1404, 1208, 904, 772, 707
22e	3116, 2966, 1639, 1606, 1441, 1257, 1132, 937, 636

The IR data for **22c** and **22d** are in accordance with the references^{73,74}.

Tab. 52 ¹H NMR data for **22b-e**

	OH	H5	H6	Residual ¹ H signals
22b	11.84 (b)	–	8.05 (s)	2.01 (s, 3H, CH ₃); 7.48 – 7.51 (m, 3H, H ₃ ', H ₄ ', H ₅ '); 7.53 – 7.57 (m, 2H, H ₂ ', H ₆ ')
22e	11.36 (b)	6.29 (s)	–	1.23 (s, 18H, 2×C(CH ₃) ₃)

Tab. 53 ¹³C NMR data for **22a-e**

	C5	C6	C4	C2	Residual ¹³ C signals
22a	100.34	148.23	156.74	170.42	127.53 (C ₂ ', C ₆ '); 128.81 (C ₃ ', C ₅ '); 131.73 (C ₄ '); 135.99 (C ₁ ')
22b	110.73	152.83	157.25	168.55	15.05 (CH ₃); 128.20 (C ₂ ', C ₆ '); 128.32 (C ₃ ', C ₅ '); 129.61 (C ₄ '); 136.80 (C ₁ ')
22e	95.63	158.38	158.38	175.64	28.33 (2×C(CH ₃) ₃); 35.68 (2×C(CH ₃) ₃)

The ¹H NMR data for **22a**, **22c** and **22d** and ¹³C NMR data for **22c** and **22d** are consistent with the references⁷²⁻⁷⁴. A difference in the obtained and published ¹H NMR signals for compound **22e**⁷⁵ are discussed in *Chap. 3.3.2.2*.

7.3 Additional analytical experiments

7.3.1 Crystal analysis

Crystallographic data of the three chromone-based compounds were collected by Dr. A. Damme and Dr. K. Radacki in the research group of Prof. Braunschweig* on a Bruker X8APEX diffractometer with a CCD area detector and multi-layer mirror monochromated MoK α radiation, and deposited within the Cambridge Crystallographic Data Center¹¹⁴, designated as AD203 (**3b**), AD064 (**19**) and KR839 (**9i**), respectively. The structures were solved applying direct methods, refined with the Shelx software package¹¹³ and expanded using Fourier techniques. Bond lengths, angles and torsions were calculated using Mercury. All non-hydrogen atoms were refined anisotropically. Hydrogen atoms were included in structure factors calculations. All hydrogens were placed at idealized geometric positions using the riding-hydrogen model with C-H distances 0.98 Å for methyl ($U_{\text{iso}} = 1.5 U_{\text{eq}}$), 0.88 Å for N-H and 1.00 and 0.95 Å for tert. aliphatic and aromatic C-H, respectively ($U_{\text{iso}} = 1.2 U_{\text{eq}}$). Measurement details are summarized in *Tab. 54* and the structures are described in *Chap. 4.5.2*.

Tab. 54 X-ray measurement details

	3b (AD203)	19 (AD064)	9i (KR839)
<i>Formula</i>	C ₁₆ H ₁₀ BrNO ₃	C ₁₉ H ₁₈ BrI ₃ N ₂ O ₃	C ₁₈ H ₁₄ N ₂ O ₅
<i>M_r (g/mol)</i>	344.16	782.96	338.31
<i>Solvent for recrystallization</i>	toluene, methanol	ethanol	methanol
<i>Radiation, λ (Å)</i>	MoK α , 0.71073		
<i>Temperature (K)</i>	100(2)		
<i>Crystal appearance</i>	colourless needle	red block	colourless plate
<i>Size (mm)</i>	0.436×0.107×0.085	0.200×0.158×0.120	0.050×0.120×0.260
<i>System; Space group</i>	monoclinic; P2 ₁ /n	monoclinic; P2 ₁ /c	triclinic; P-1
<i>Z</i>	4	4	2
<i>Unit cell lengths (Å)</i>	a = 5.4671(3); b = 17.3027(8) c = 13.9042(7)	a = 8.3714(4); b = 21.4156(9); c = 12.9840(6)	a = 7.977(2); b = 9.654(3); c = 10.562(3)
<i>Unit cell angles (°)</i>	$\alpha = \gamma = 90$; $\beta = 92.053(2)$	$\alpha = \gamma = 90$; $\beta = 90.779(2)$	$\alpha = 105.105(15)$; $\beta = 101.410(12)$; $\gamma = 90.990(13)$
<i>Volume (Å³)</i>	1314.43(12)	2327.54(18)	767.7(4)
<i>Calc. Density (mg/m³)</i>	1.739	2.234	1.463
<i>Absorption coefficient (mm⁻¹)</i>	3.137	5.767	0.109
<i>F(000)</i>	688	1456	352

*Institute of Inorganic Chemistry, University of Würzburg

Experimental section

	3b (AD203)	19 (AD064)	9i (KR839)
<i>Theta range for collection</i>	1.88 to 26.76°	1.83 to 26.10°	2.562 to 26.371°
<i>Reflections collected, Independent reflections</i>	11499, 2785	36359, 4612	22137, 3116
<i>Minimum/maximum transmission</i>	0.5220/0.7454	0.5632/0.7453	0.6989/0.7457
<i>Refinement method</i>	Full-matrix least-squares on F2		
<i>Data / parameters / restraints</i>	2785 / 194 / 1	4612 / 253 / 0	3116 / 228 / 0
<i>Goodness-of-fit on F²</i>	1.029	1.151	1.079
<i>Final R indices [I > 2σ(I)]</i>	R1 = 0.0316, wR2 = 0.0753	R1 = 0.0645, wR2 = 0.1630	R1 = 0.0371, wR2 = 0.0955
<i>R indices (all data)</i>	R1 = 0.0455, wR2 = 0.0809	R1 = 0.0722, wR2 = 0.1664	R1 = 0.0422, wR2 = 0.0994
<i>Maximum/minimum residual electron density (e·Å⁻³)</i>	0.679 / -0.412	4.665 / -1.141	0.266 / -0.254

7.3.2 LogP and peak purity determination

In a series of four chromone derivatives (see *Fig. 6I*), the predicted partition coefficients (*logP* and *clogP*) were compared to the experimental *logP* values derived from capacity factors (*k'*) determined by means of a HPLC experiment from retention times (*t_R*) of the analysed compounds. The measurement was performed by Dr. G. Hiltensperger[†] following the method reported by Muth¹¹⁵. The capacity factors were calculated using *Equation 6*, where *t₀* is the time needed for the mobile phase to pass through the column.

$$k' = (t_R - t_0)t_0 \quad (\text{Equation 6})$$

LogP values of the samples were obtained from their calculated *logk'* values by linear regression using a calibration line of references with known *logP* coefficients¹¹⁶.

Peak purity was determined from the peak area in a subsequent measurement allowing a better separation. A correlation to chemical purity is approximate only, due to the unknown spectral character of impurities.

HPLC conditions

Eluent: 10 mM potassium phosphate-buffer, pH 7.4 (A)
MeOH + 0.028 % dimethylhexylamine (B)
Flow-rate: 1.5 ml/min. (*logP*); 1.0 ml/min. (peak purity)
Temp.; λ: 30 °C; 254 nm
Method 1: isocratic, A/B, 30 : 70 (*logP*)

[†] Research group Prof. Holzgrabe, Institute of Pharmacy and Food Chemistry, University of Würzburg

Experimental section

Method 2: gradient B: 30 – 80 % in 25 min., from 80 – 30 % in 3 min., 30 % in 2 min. (peak purity)

References: 4 mg/ml solutions of 2-phenylethanol, benzene, *N,N*-dimethylaniline, chlorobenzene, toluene, ethylbenzene, biphenyl and anthracene in DMSO

Samples: **4k, 9e, 11e, 12e** (4 mg/ml in DMSO, measured in duplicate)

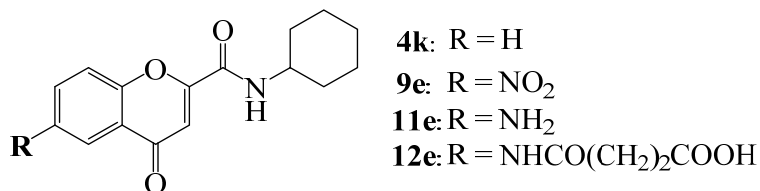


Fig. 61 General structure of the analysed chromone compounds

Tab. 55 Experimental $\log P$ ($\log P_{Exp}$) and predicted $\log P$ and $clog P$ values ($\log P_{Calc}/clog P_{Calc}$) of compounds **4k**, **9e**, **11e** and **12e** and the both difference/relative difference values between $\log P_{Exp}$ and $\log P_{Calc}$ ($D1/RD1$) and between $\log P_{Exp}$ and $clog P_{Calc}$ ($D2/RD2$). The assessed peak purity of the measured compounds is shown in percent. [*] extrapolated value (beyond the standards used)

	M_r (g/mol)	$\log P_{Exp}$	$\log P_{Calc}$	$D1/RD1$ [%]	$clog P_{Calc}$	$D2/RD2$ [%]	Peak purity
4k	271.30	2.39	1.41	0.98/41	2.49	0.10/4	> 99.9
9e	316.31	2.54	2.25	0.29/11	2.35	0.19/8	98.1
11e	286.33	1.92	0.61	1.31/68	1.47	0.45/23	> 99.9
12e	386.40	-0.19*	-0.02	0.17/89	1.47	1.66/876	98.0

Results

The experimental $\log P$ values of compounds **4k**, **9e** and **11e** assessed by means of HPLC show a better correlation to the predicted fragment-based partition coefficients ($clog P_{Calc}$ values, relative difference 4 – 23 %) than to the estimated atomic-based partition coefficients ($\log P_{Calc}$ values, relative difference 11 – 68 %). The extrapolated experimental $\log P$ value for succinamic acid **12e** has been neglected due to the ionizable character of the compound at given conditions.

Experimental section

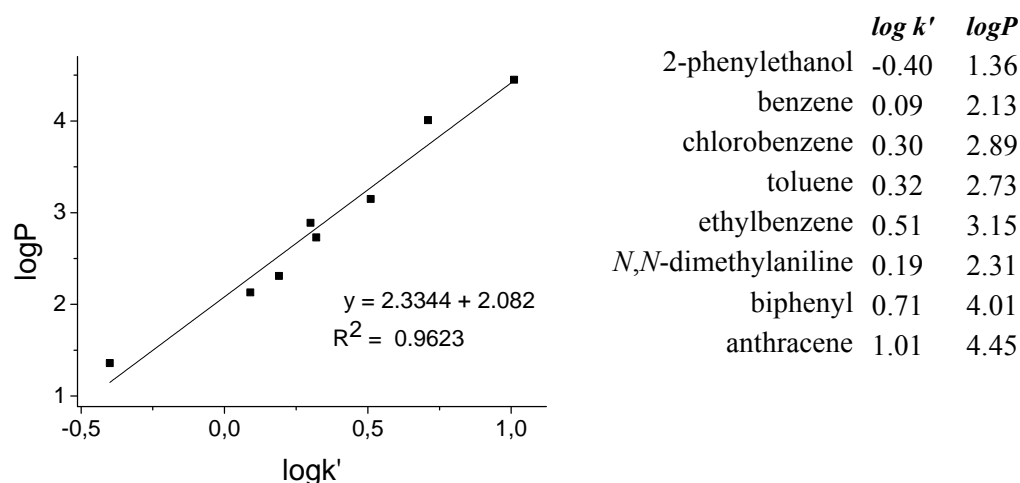


Fig. 62 Calibration line of the references showing the calculated $\log k'$ values and the published partition coefficients¹¹⁶

7.3.3 Content determination of compound 9d

20 mM DMSO stock solution and 40 μ M incubation solution of **9d** (the stock solution diluted in a Middlebrook 7H9 Broth base with OADC enrichment – oleic acid, albumin, dextrose, catalase; incubated 21 days at 37 °C), both used for the whole cell activity testing against *M. tuberculosis* in SFB 630, were examined on the active compound content. The stock solution was analysed by a HPLC method conducted by J. Wiest*. The compound content in the incubation solution was assessed by means of UV absorbance measurement at 320 nm using a blank buffer solution (DMSO + testing buffer, incubated for 21 days at 37 °C) as a reference. All samples had been stored at -20 °C before being analysed.

Consequently, a stability study was conducted using a newly synthesized batch of **9d**, 10 mg of which were dissolved in deuterated DMSO. ¹H NMR Spectrum was recorded immediately and compared to the spectrum obtained after 21 days. After solvent evaporation, the residue was dissolved in acetonitrile and ESI-MS spectrum was recorded. The results are discussed in *Chap. 4.2.2.3*.

7.3.3.1 Content determination in the stock solution by HPLC method

HPLC conditions

Eluent: millipore water (A), acetonitrile (B)
Flow-rate, temp., λ : 1.0 ml / min., 25 °C, 254 nm
Method: Gradient B: 0 – 80 % in 30 min, 80 % in 30. – 32. min, 80 – 10 % in 32. – 35. min, 10 % in 35. – 40. min
Calibration curve: reference **9d** solutions in acetonitrile,

*Research group Prof. Holzgrabe, Institute of Pharmacy and Food Chemistry, University of Würzburg

Experimental section

Sample: 0.24, 0.12, 0.06, 0.03 and 0.015 mg/ml
20 mM DMSO stock solution of **9d** ($M_r = 314.25$ g/mol)

After stirring, 100 μ l of the stock solution were dried *in vacuo* (0.6 mbar) at RT for 5 hours, then dissolved in 1 ml acetonitrile. The sample measurement was repeated 6 times. Retention time of the analyte was 17 min.

Results

In the stock solution of **9d**, a content of 44.5 % was determined (see *Tab. 56*).

Tab. 56 Expected and obtained values

	Concentration [mg/ml]	Content [%]
<i>Expected</i>	0.0640	100
<i>Measured</i>	0.0285	44.53

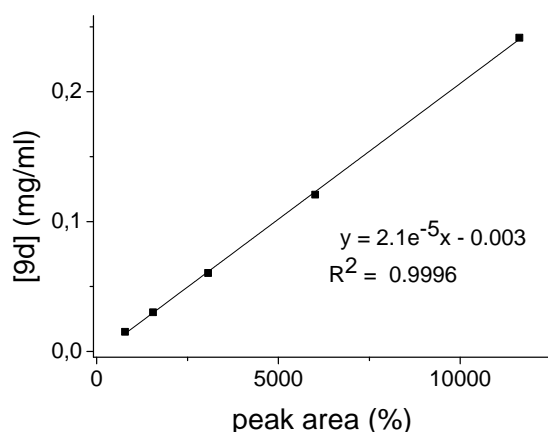
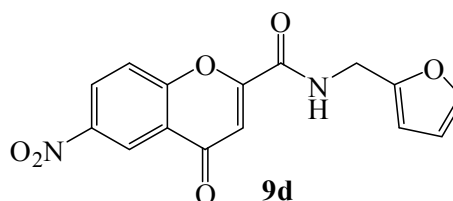


Fig. 63 Calibration line of **9d** showing the peak area for each concentration step

7.3.3.2 Content determination of **9d** by means of UV absorbance assay

Measurement conditions

Cuvette: quartz fluorescence cuvette 28-F/Q/10 (Starna, Pfungstadt, Germany)
Light path length: 1 cm
Blank: 500 μ l of the testing blank solution
Calibration curve: blank + 1 – 8 μ l of 5mM DMSO solution of **9d**
Temp., λ : RT, 320 nm (near λ_{max} , stable absorbance values)
Sample: 500 μ l of 40 μ M incubation solution

Experimental section

Results

Concentration was determined from the measured absorbance value by linear regression in accordance with the Beer-Lambert law. Calibration curve of the reference concentration steps is shown in *Fig. 64*. The content of 63.4 % (see *Tab. 57*) was assessed by linear regression comparing the 40 μM concentration of the calibration line to the value derived from sample measurement.

Tab. 57 Content determination of **9d**

A	c [μM]	Content [%]
0.2691	40.0	100%
0.1776	25.4	63.4%

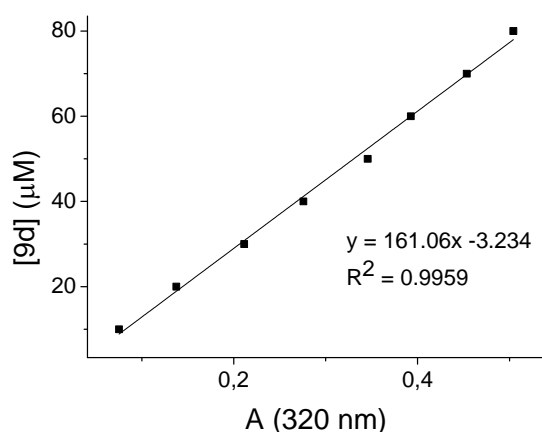


Fig. 64 Calibration curve for **9d** at 320 nm

7.4 Solubilization assays

7.4.1 Screening on suitable solubilizing agents among cyclodextrins

The solubility of the **3b**/CD mixtures prepared according to *Tab. 58* was assessed visually after equilibrating/shaking the samples and the subsequent centrifugation. Following cyclodextrins were tested: native β -cyclodextrin; heptakis(2,6-di-*O*-methyl)- β -cyclodextrin (DIMEB), (2-hydroxypropyl)- β -cyclodextrin (HP- β -CD), triacetyl- β -cyclodextrin (TA- β -CD), β -cyclodextrin sulfate, native γ -cyclodextrin. The methods and results are described in *Chap. 4.5.3.2.1*.

Experimental section

Tab. 58 Solubility testing for **3b** using various stock solutions of cyclodextrins

CD	Stock solution [mM]	Pipetted Stock sol. [μ l]	Added solvent [μ l]	3b	Method	Precipitate
native β-CD , $M_r = 1334.98$ g/mol	12.8	468.7 (1 eq.)	3280.9	2.04 mg (6.0 μ mol)	A	yes
		937.4 (2 eq.)	2812.2			
		1874.8 (4 eq.)	1874.8			
		3749.6 (8 eq.)	0			
	27.8	215.5 (1 eq.)	1508.5			
		431.0 (2 eq.)	1293			
		862.0 (4 eq.)	862			
		1724.0 (8 eq.)	0			
DIMEB , $M_r = 1331.40$ g/mol	250	24.2 (1 eq.)	169.4	2.04 mg (6.0 μ mol)	A	no
		48.4 (2 eq.)	145.2			
		96.8 (4 eq.)	96.8			
		193.6 (8 eq.)	0			
	40.1	149.7 (1 eq.)	149.7			
		299.4 (2 eq.)	0			
HP-β-CD , $M_r = 1396$ g/mol	40.1	149.7 (1 eq.)	449.1	B	yes	
		299.4 (2 eq.)	299.4			
		598.8 (4 eq.)	0			
TA-β-CD , $M_r = 2017.75$ g/mol	20	300 (1 eq.)	300	B	yes	
		600 (2 eq.)	0			
β-CD-sulphate , $M_r = 2053$ g/mol	20	300 (1 eq.)	300	B	yes	
		600 (2 eq.)	0			
γ-CD , $M_r = 1297.12$ g/mol	20	300 (1 eq.)	300	B	yes	
		600 (2 eq.)	0			

7.4.2 Experiments on complexation by means of UV spectroscopy

7.4.2.1 Assay conditions

Cuvette: quartz fluorescence cuvette 28-F/Q/10 (Starna, Pfungstadt, Germany)
 Light path length: 1 cm
 Temp., λ : 25 °C or RT, 305 nm (λ_{\max})
 Cyclodextrin: DIMEB, HP- β -CD

7.4.2.2 Samples used for the method of continuous variation – Job Plot

Sample 0: stock solution of **3b**
Samples 1-9: 9 dilutions of **3b** and DIMEB from the stock solutions in 1:9, 2:8, 3:7, 4:6, 5:5, 6:4, 7:3, 8:2 and 9:1 ratios
Sample 10: stock solution of DIMEB
Calibration line: dilutions of **3b**, in the same ratio as above, with pure solvent (instead of DIMEB-stock solution)

Experimental section

Blank samples: dilutions of DIMEB in the same ratio as above, with pure solvent instead of stock solution of **3b** (for zero adjustment)
Y axis: measured absorbance values A_i transformed into ΔA ($\Delta A = A_0 - A_i$, A_0 = absorbance of sample 0, A_i = absorbance of samples 1 – 10) and multiplied by molar equivalents of **3b** in samples 0 – 10
X axis: $R = [3b]/([DIMEB]+[3b])$, where $[DIMEB]+[3b] = 1$

7.5 KasA binding assay

7.5.1 Assay conditions

Wild type KasA, obtained from *M. smegmatis*, was expressed and purified in the research group of Prof. Kisker* by C. Topf and J. Schiebel as published by Luckner *et al.*³⁵ After previous storage at -80 °C, the enzyme solution was thawed and kept on ice prior to the measurement. For each day of measurement, new enzyme fraction was used. The decrease in the intrinsic tryptophan fluorescence of KasA upon inhibitor binding was recorded using a Varian Cary Eclipse fluorimeter. The measurements were conducted at RT in a quartz fluorescence cuvette 28-F/Q/10 (Starna, Pfungstadt, Germany) with the parameters 1×0.2 cm. The excitation and emission wavelengths were 280 nm (λ_{Ex}) and 337 nm (λ_{Em}), respectively. Slit widths of 5 nm were used. Fluorescence data were acquired using Cary Eclipse Software Package. Dissociation constants (K_D) were calculated by OriginPro and „R“.

7.5.2 Sample details

Enzyme solution: 71.1 μ M wild-type KasA in 9.5 mM CHES, 500 mM NaCl
Buffer: 50 mM Tris, pH 8.5, 150 mM NaCl, 1 mM dithiothreitol (DTT)
Sample stock solutions: 5 (method A) and 10 mM (method B) inhibitor solutions in DMSO
Reference: 9.5 (method A) and 10 mM (method B) TLM in DMSO

7.6 Whole cell inhibition activity testing

7.6.1 Assay conditions and method

The growth inhibition of *M. tuberculosis* was investigated in the research group of Dr. Ölschläger† by S. Sologub in accordance with the SOP M-Z1-013-01¹¹⁷ within the SFB 630. The commercially available BBL MGIT tubes (Becton and Dickinson, Heidelberg, Germany) were used. The MGIT tube enriched with 500 μ l of MGIT OADC buffer and 9 μ l

* Rudolf Virchow Center, University of Würzburg

† Institute for Molecular Infection Biology (IMIB), University of Würzburg

Experimental section

of 20 mM DMSO stock solution of tested compound was inoculated with 20 µl of *M. tuberculosis* H3/A (IGC Genomics, Berlin) glycerol culture. All samples were prepared in duplicate. The reappearance of fluorescence emission, originating in the fluorescence indicator embedded in the MGIT tube, was measured at 365 nm using a *BACTEC* MicroMGIT Fluorescence Reader (Becton and Dickinson, Heidelberg, Germany) after 7, 14 and 21 days of incubation at 37 °C as a result of oxygen consumption due to the increased mycobacterial growth. Compound activity was considered under following conditions: the detected fluorescence intensity for both samples (duplicate) was lower than 20 F.U., for blank sample 20 F.U., for references 7 - 8 F.U., for positive control 20 F.U. and for negative control 7 – 8 F.U. In case of compound activity, the minimal inhibitory concentration on *M. tuberculosis* and the half maximal inhibitory concentration on *J774.1* macrophages was determined. For results and discussion see *Chap. 4.2*.

7.6.2 Sample details

<i>Buffer:</i>	Middlebrook 7H9 Broth base with OADC enrichment (oleic acid, albumin, dextrose)
<i>References:</i>	<i>BACTEC</i> S.I.R.E. Drug Kit (streptomycin, isoniazid, rifampin, ethambutol)
<i>Blank:</i>	9 µl of DMSO instead of DMSO stock solution of tested compound
<i>Positive control:</i>	5 ml of 0.4% Na ₂ SO ₃ solution, fluorescence measured after 1 hour at RT
<i>Negative control:</i>	unopened, uninoculated MGIT tube

7.7 Anti-infective screening

The antimicrobial screening of selected compounds was executed by the research team of Dr. Bruhn[‡] on the following pathogens and strains: *Staphylococcus aureus* NCTC 8325, *Staphylococcus epidermidis* RP62A, *Enterococcus faecalis* JH212, *Enterococcus faecium* 6413, *Escherichia coli* 536, *Pseudomonas aeruginosa* (environmental isolate), *Yersinia pseudotuberculosis* 252 01A, *Yersinia pestis* KUMA, *Candida albicans* 5314 (ATCC 90028) and *Leishmania major* MHOM/IL/81/FE/BNI. Compound cytotoxicity was additionally examined on *J774.1* macrophages. For procedure descriptions see the SOP protocols on the SFB 630 web site¹¹⁷. The obtained values of minimal inhibitory concentration (MIC), percentage of growth inhibition (*L. major*), the inhibition of *S. epidermidis* RP62A biofilm

[‡] Institute for Molecular Infection Biology, University of Würzburg

Experimental section

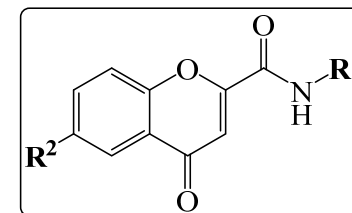
formation and the half maximal inhibitory concentration (IC_{50}) on *J774.1* macrophages are summarized in *Tab. 59*. The results are discussed in *Chap. 4.3*.

7.8 Docking

The docking of chromone-2-carboxamide **9i** was performed in the research group of Prof. Sotriffer in cooperation with his postgraduate student M. Kuhn adopting the settings reported by Topf³⁹. The new program version of the docking program GOLD was used (Gold Suite v. 5.2.2, visualized in Hermes, v. 1.6.2). The redocking of TLM and the repeated docking of **GS-71** were conducted using the same procedure and parameters as for compound **9i**.

Procedure description

The structure of KasA in complex with TLM was downloaded from PDB (<http://www.rcsb.org>, **2wge**, Luckner *et al.*³⁵). Prior to docking, the structure was prepared, *i.e.*, protonated, energy minimized (MMFF94¹¹⁸), unnecessary atoms were removed, using MOE (v. 2015.11). Analogically to KasA, ligand structures (TLM, **GS-71**, **9i**) were loaded in MOE and prepared for docking. In GOLD, the KasA binding site was defined as a sphere ($r = 12 \text{ \AA}$) with the sulphur atom of TLM in the mid-point. For each ligand, the number of GA runs was set on 50 and the redocking of TLM was referred to the TLM crystal structure in **2wge**. The scoring function GOLDscore was applied. Regarding the ligand flexibility, amide bonds were allowed to flip and internal hydrogen bonds were taken in consideration. Following GA parameters were set: population size 100, selection pressure 1.1, No. of operations 150 000, No. of islands 5, niche size 2, migrate 10, mutate 95, crossover 95. Subsequently, the docking results were ranked using the SFC_290m scoring function. The final docking poses were viewed in PyMOL, v. 1.7.4.3.



Tab. 59 Antimicrobial activity of selected compounds (see the general structure above)

	4e	4j	4k	9d	11a	11e	11g	12a	12b
R ¹	furan-2-ylmethyl	(1-benzyl)-piperidin-4-yl	cyclohexyl	furan-2-ylmethyl	phenyl	cyclohexyl	benzyl	phenyl	2-Br-phenyl
R ²	H	H	H	NO ₂	NH ₂	NH ₂	NH ₂	NHCO(CH ₂) ₂ COOH	
<i>S. aureus</i> , MIC [μ M]	> 40	> 40	> 40	> 40	> 40	> 40	> 40	> 40	> 40
<i>S. epidermidis</i> , MIC [μ M]	> 40	> 40	> 40	> 40	> 40	> 40	> 40	> 40	> 40
biofilm inhibition	0	0	0	0	0	0	0	0	0
<i>E. faecalis</i> , MIC [μ M]	> 40	> 40	> 40	> 40	> 40	> 40	> 40	> 40	> 40
<i>E. faecium</i> , MIC [μ M]	> 40	> 40	> 40	> 40	> 40	> 40	> 40	> 40	> 40
<i>E. coli</i> , MIC [μ M]	> 40	> 40	> 40	> 40	> 40	> 40	> 40	> 40	> 40
<i>P. aeruginosa</i> , MIC [μ M]	> 40	> 40	> 40	> 40	> 40	> 40	> 40	> 40	> 40
<i>Y. pseudotuberculosis</i> , MIC [μ M]	> 40	> 40	> 40	> 40	> 40	> 40	> 40	> 40	> 40
<i>Y. pestis</i> , MIC, [μ M]	> 40	> 40	> 40	> 40	> 40	> 40	> 40	> 40	> 40
<i>C. albicans</i> , MIC [μ M]	> 40	> 40	> 40	> 40	> 40	> 40	> 40	> 40	> 40
<i>L. major</i> , IC ₅₀ [μ M]	> 100	> 100	> 100	> 100	> 100	> 100	> 100	> 100	> 100
<i>L. major</i> , growth inhibition [%]	0	0	20	0	0	26.7	28	0	0
<i>J774.1</i> , IC ₅₀ [μ M]	> 100	> 100	> 100	> 100	> 100	44.4	> 100	> 100	> 100

8 Appendix

8.1 Poster presentations related to the thesis

Kesetovic, D.¹, Topf, C.¹, Holzgrabe, U.¹: Low molecular chromone-based compounds as potential drugs against *Mycobacterium tuberculosis*, Annual Meeting of the German Pharmaceutical Society (2010), Braunschweig

Topf, C.¹, Kesetovic, D.¹, Schiebel, J.², Kisker, C.², Sotriffer, C. A.¹, Holzgrabe, U.¹: Design, synthesis and testing of novel small-molecule inhibitors of KasA for treatment of tuberculosis, Joint Meeting of the Austrian and German Pharmaceutical Societies (2011), Innsbruck

¹ Institute of Pharmacy and Food Chemistry, University of Würzburg

² Rudolf Virchow Center, University of Würzburg

Appendix

8.2 List of abbreviations

A	absorbance	<i>E. faecalis</i>	<i>Enterococcus faecalis</i>
ACP/AcpM	(mycobacterial) acyl carrier protein	<i>E. faecium</i>	<i>Enterococcus faecium</i>
AG	arabinogalactan	Emb/E	ethambutol
AIDS	acquired immune deficiency syndrome	eq.	equivalent
Ala	alanine	Eq.	equation
ART	antiretroviral therapy	Eto	ethionamide
A.U.	arbitrary unit	F.U.	fluorescence unit
BCG	Bacillus Calmette–Guérin	FA	formic acid
BMIM Cl	1-butyl-3-methylimidazolium chloride	FabB	β -ketoacyl-ACP-synthase I from <i>E. coli</i>
c	molar concentration	FabF	β -ketoacyl-ACP-synthase II from <i>E. coli</i>
<i>C. albicans</i>	<i>Candida albicans</i>	FAS	fatty acid synthase
CCD	charge-coupled device	Gly	glycine
CD	cyclodextrin	h	hour
CDCl ₃	deuterated chloroform	HadAB	β -hydroxyacyl-ACP dehydratase
CoA	coenzyme A	His	histidine
COSY	correlated spectroscopy	HIV	human immunodeficiency virus
CYP3A4	cytochrome P450 3A4	HMBC	heteronuclear multiple bond correlation
Cys	cystein	HMQC	heteronuclear multiple quantum coherence
Dcs	<i>D</i> -cycloserine	HPLC	high-performance liquid chromatography
DEPT	distortionless enhancement by polarization transfer	HP- β -CD	(2-hydroxypropyl)- β -cyclodextrin
DIMEB	heptakis(2,6-di- <i>O</i> -methyl)- β -cyclodextrin	CHES	N-Cyclohexyl-2-aminoethanesulfonic acid
DMF	<i>N,N</i> -dimethylformamide	I	inhibitor
DMSO	dimethyl sulfoxide	IC ₅₀	half maximal inhibitory concentration
DNA	deoxyribonucleic acid	IFE	inner filter effect
DOTS	directly observed treatment, short course	Inh/H	isoniazid
DST	drug-susceptibility testing	InhA	NADH-dependent trans-2-enoyl-ACP-reductase
E	enzyme		
<i>E. coli</i>	<i>Escherichia coli</i>		
EE	ethyl acetate		

Appendix

IR	infrared (spectroscopy)	Phe	phenylalanine
<i>J</i>	coupling constant	pKi	here: negative decadic
KasA	β -ketoacyl-ACP-synthase		logarithm of dissociation constant
KatG	catalase-peroxidase	Pks13	polyketide synthase
K_D	dissociation constant	Ppm	parts per million
<i>L. major</i>	<i>Leishmania major</i>	Pro	proline
logP	decadic logarithm of partition coefficient	Pto	prothionamide
<i>M. tuberculosis</i>	<i>Mycobacterium tuberculosis</i>	Pza/Z	pyrazinamide
MabA	NADPH-dependent β -ketoacyl-ACP-reductase	Rf	retention factor
MDR-TB	multidrug-resistant tuberculosis	Rfb	rifabutin
MGIT	mycobacterial growth indicator tube	Rif/R	rifampicin (rifampin)
MIC	minimal inhibitory concentration	RNA	ribonucleic acid
M_r	relative molecular weight	Rpt/P	rifapentine
mRNA	messenger RNA	rRNA	ribosomal RNA
MRSA	methicillin-resistant <i>Staphylococcus aureus</i>	RT	room temperature
MTB	<i>M. tuberculosis</i>	<i>S. aureus</i>	<i>Staphylococcus aureus</i>
NADH	nicotinamide adenine dinucleotide, reduced form	<i>S. epidermidis</i>	<i>Staphylococcus epidermidis</i>
NADPH	nicotinamide adenine dinucleotide phosphate, reduced form	SFB 630	Sonderforschungs-bereich 630 (Collaborative Research Center 630)
NMR	nuclear magnetic resonance (spectroscopy)	SOP	standard operating procedure
<i>P. aeruginosa</i>	<i>Pseudomonas aeruginosa</i>	Stm/S	streptomycine
PE	petrolether	$t_{1/2}$	half-life
PG	peptidoglycan (murein)	TB	tuberculosis
pH	negative decadic logarithm of $[H^+]$	TDR-TB	totally drug-resistant TB
		TEA	triethylamine
		Thz	thioacetazone
		TLC	thin layer chromatography
		TLM	thiolactomycin
		Trd	terizidone
		tRNA	transfer RNA
		UV-Vis	ultraviolet-visible (spectroscopy)
		VRE	vancomycin-resistant <i>Enterococcus</i>

Appendix

WHO	World Health Organization	<i>Y. pestis</i>	<i>Yersinia pestis</i>
wtKasA	wild-type KasA	<i>Y. pseudotuberculosis</i>	<i>Yersinia pseudotuberculosis</i>
XDR-TB	extensively drug-resistant TB		

Bibliography

9 Bibliography

- ¹ Koch, R., *Berliner Klinischen Wochenschrift* (1882), **15** (10): 221 – 230
- ² Cole, S. T., Brosch, R., Parkhill, J., Garnier, T., Churcher, C., Harris, D., Gordon, S. V., Eiglmeier, K., Gas, S., Barry, C. E., Tekaiia, F., Badcock, K., Basham, D., Brown, D., Chillingworth, T., Connor, R., Davies, R., Devlin, K., Feltwell, T., Gentles, S., Hamlin, N., Holroyd, S., Hornsby, T., Jagels, K., Krogh, A., McLean, J., Moule, S., Murphy, L., Oliver, K., Osborne, J., Quail, M. A., Rajandream, M.-A., Rogers, J., Rutter, S., Seeger, K., Skelton, J., Squares, R., Squares, S., Sulston, J. E., Taylor, K., Whitehead, S., Barrell, B. G., *Nature* (1998), **393**: 537 – 544
- ³ Wessner, D. R., Dupont, C., Charles, T. C., *Microbiology* (2013), John Wiley & Sons, ISBN 978-0471694342
- ⁴ Hett, E. C., Rubin, E. J., *Microbiology and Molecular Biology Reviews* (2008), **72** (1): 126 – 156
- ⁵ Koul, A., Arnoult, E., Lounis, N., Guillemont, J., Andries, K., *Nature* (2011), **469**: 483 - 489
- ⁶ <http://www.who.int/mediacentre/factsheets/fs104/en/> - Stand: 1.3.2015
- ⁷ Chatterjee, D., Pramanik, A. K., *Pathophysiology* (2015), **22**: 72 – 83
- ⁸ WHO Global tuberculosis report 2015:
http://www.who.int/tb/publications/global_report/en/ - Stand: 30.11.2015
- ⁹ <http://www.who.int/tb/dots/whatisdots/en/index4.html> - Stand: 1.3.2015
- ¹⁰ Treatment of tuberculosis, WHO guidelines, 4.ed., (2010):
http://whqlibdoc.who.int/publications/2010/9789241547833_eng.pdf?ua=1
Stand: 1.3.2015
- ¹¹ Steingart K., Schiller, I., Horne, D. J., Pai, M., Boehme, C., Dendukuri, N., *Cochrane Database Syst Rev* (2014), DOI: 10.1002/14651858.CD009593.pub3
- ¹² http://whqlibdoc.who.int/publications/2011/9789241500708_eng.pdf?ua=1
- ¹³ Miesel, L., Rozwarski, D. A., Sacchettini, J. C, Jacobs, W. R., *Novartis Found Symp* (1998), **217**: 209 – 221
- ¹⁴ Steinhilber, D., Schubert-Zsilavec, M., Roth, H. J., *Medizinische Chemie* (2010), 2. ed., Deutscher Apotheker Verlag, ISBN 978-3-7692-5002-2
- ¹⁵ Zhang, Y., Wade, M., M., Scorpio, A., Zhang, H., Sun, Z., *J Antimicrob Chemother* (2003), **52**: 790 – 795

Bibliography

- ¹⁶ Zumla, A., Nahid, P., Cole, S. T., *Nature Reviews Drug Discovery* (2013), **12**: 388 - 404
- ¹⁷ Akbergenov, R., Shcherbakov, D., Matt, T., Duscha, S., Meyer, M., Wilson, D. N., Böttger, E., C., *Antimicrob Agents Chemother* (2011), **55** (10): 4712 – 4717
- ¹⁸ Portero, J.-L., Rubio, M., *Expert Opin Ther Patents* (2007), **17** (6): 617 – 637
- ¹⁹ Wang, F., Langley, R., Gulten, G., Dover, L. G., Besra, G. S., Jacobs, W. R., Sacchettini, J. C., *J Exp Med* (2007), **204** (1): 73 – 78
- ²⁰ <http://www.tbonline.info/posts/2011/9/9/thioacetazone/> Stand: 1.3.2015
- ²¹ <http://www.tballiance.org/newscenter/view-brief.php?id=1109> Stand: 1.3.2015
- ²² http://www.who.int/tb/challenges/mdr/mdr_tb_factsheet.pdf?ua=1 Stand: 1.3.2015
- ²³ <http://www.tballiance.org/portfolio/clinical-portfolio> Stand: 1.3.2015
- ²⁴ Bhatt, A., Molle, V., Besra, G. S., Jacobs, W. R., Kremer, L., *Mol Microbiol* (2007), **64** (6): 1442 – 1454
- ²⁵ Marrakchi, H., Laneelle, M.-A., Daffe, M., *Chemistry and Biology* (2014), **21**: 67 – 85
- ²⁶ Heath, R. J., White, S. W., Rock, C. O., *Prog Lipid Res* (2001), **40**: 467 - 497
- ²⁷ Schiebel, J., Kapilashrami, K., Fekete, A., Bommineni, G. R., Schaefer, C. M., Mueller, M. J., Tonge, P. J., Kisker, C., *J Biol Chem* (2013), **288** (47): 34190 – 34204
- ²⁸ Haapalainen, A. M., Meriläinen, G., Wierenga, R. K., *Trends Biochem Sci* (2006), **31** (1): 64 – 71
- ²⁹ Machutta, C. A., Bommineni, G. R., Luckner, S. R., Kapilashrami, K., Ruzicska, B., Simmerling, C., Kisker, C., Tonge, P. J., *J Biol Chem* (2010), **285** (9): 6161 – 6169
- ³⁰ Price, A. C., Choi, K.-H., Heath, R. J., Li, Z., White, S. W., Rocks, C. O., *J Biol Chem* (2001), **276** (9): 6551 – 6559
- ³¹ Brown, A. K., Taylor, R. C., Bhatt, A., Fütterer, K., Besra, G. S., *PLoS ONE* (2009), **4** (7), e6306
- ³² Wang, J., Soisson, S. M, Young, K., Shoop, W., Kodali, S., Galgoci, A., Painter, R., Parthasarathy, G., Tang, Y. S., Cummings, R., Ha, S., Dorso, K., Motyl, M., Jayasuriya, H., Ondeyka, J., Herath, K., Zhang, C., Hernandez, L., Allocco, J., Basilio, A., Tormo, J. R., Genilloud, O., Vicente, F., Pelaez, F., Colwell, L., Lee, S. H., Michael, B., Felcetto, T., Gill, C., Silver, L. L., Hermes, J. D., Bartizal, K., Barrett, J., Schmatz, D., Becker, J. W., Cully, D., Singh, S.B., *Nature* (2006), **441** (7091): 358 - 361
- ³³ Plesch, E., Bracher, F., Krauss, J., *Arch Pharm Chem Life Sci* (2012), **345**: 657 – 662

Bibliography

- ³⁴ Diwischek, F., Morschhäuser, J., Holzgrabe, U., *Arch Pharm Chem Life Sci* (2009), **342**: 150 – 164
- ³⁵ Luckner, S. R., Machutta, C. A., Tonge, P. J., Kisker, C., *Structure* (2009), **17** (7): 1004 – 1013
- ³⁶ Schaeffer, M. L., Agnihotri, G., Volker, C., Kallender, H., Brennan, P. J., Lonsdale, J. T., *J Biol Chem* (2001), **276** (50): 47029 – 47037
- ³⁷ Kremer, L. Douglas, J. D., Baulard, A. R., Morehouse, C., Guy, M. R., Alland, D., Dover, L. G., Lakey, J. H., Jacobs, W. R., Brennan, P. J., Minnikin, D. E., Besra, G. S., *J Biol Chem* (2000), **275** (22): 16857 – 16864
- ³⁸ Schaefer, B. Computergestützte Untersuchungen zur Inhibition und Dynamik der β -Ketoacyl-ACP-Synthase I (KasA) aus *Mycobacterium tuberculosis* (*Dissertation thesis*, 2012), University of Würzburg
- ³⁹ Topf, C., Design, Synthese und biologische Testung von KasA-Inhibitoren als potentielle Wirkstoffe gegen *Mycobacterium tuberculosis* (*Dissertation thesis*, 2013), University of Würzburg
- ⁴⁰ Ellis, G. P., *The Chemistry of Heterocyclic Compounds, Chromenes, Chromanones, and Chromones* (1977), John Wiley & Sons, ISBN: 0-471-38212-4
- ⁴¹ Devitt, P. F., Timoney, A., Vickars, M. A., *J Org Chem* (1961), **26** (12): 4941–4944
- ⁴² Nicolas, C., Verny, M., Maurizis, J.C., Payard, M., *J Labelled Comp Radiopharm* (1986), **23** (8): 837 – 844
- ⁴³ Kohlstaedt, E., Klingler, K. H., Genauck, W., Patent DE 970224 (C), 1958
- ⁴⁴ Barker, G., Ellis, G. P., *J Chem Soc* (1970), **16**: 2230 – 2233
- ⁴⁵ Williams, S. J., Woodman, O. L., Yap, S. W., Patent US 7863323 (B1), 2011
- ⁴⁶ Yap, S., Loft, K. J., Woodman, O. L., Williams, S. J., *ChemMedChem* (2008), **3** (10): 1572 – 1579
- ⁴⁷ Volodymyr, V.S., Klymchenko, A.S., de Rocquigny, H., Mely, Y, *Nucleic Acids Res* (2009), **37** (3), e25
- ⁴⁸ Guillaumel, J., Grierson, D. S., Monneret, C., *J Heterocycl Chem* (2001), **38**: 985 - 988
- ⁴⁹ Lee, L. V. , Granda B., Dean K., Tao J., Liu E., Zhang R., Peukert, S., Wattanasin S., Xie X., Ryder N. S., Tommasi R., Deng G., *Biochemistry* (2010), **49** (25): 5366 - 5376
- ⁵⁰ Gaspar, A., Silva, T., Yanez, M., Vina, D., Orallo, F., Ortuso, F., Uriarte, E., Alcaro, S., Borges, F., *J Med Chem* (2011), **54** (14): 5165 – 6173

Bibliography

- ⁵¹ Trujillo-Ferrara, J., Santillan, R., Beltran, H. I., Farfan, N., Höpfl, H., *Magn Reson Chem* (1999), **37**: 682 - 686
- ⁵² Josey, B. J., Inks, E. S., Wen, X., Chou, C. J., *J Med Chem* (2013), **56**: 1007 – 1022
- ⁵³ Gaspar, A., Cagide, F., Quezada, E., Reis, J., Uriarte, E., Borges, F., *Magn Reson Chem* (2013), **51**: 251 – 254
- ⁵⁴ Oremus, V., Smahovsky, V., Faberova, V., Kakalik, I., Schmidtova, L., Zemanek, M., Patent SK175297 (A3), 1999
- ⁵⁵ Vydzhak, R. N., Panchishin, S. Y., *Russ J Gen Chem* (2008), **78** (12): 2391 – 2397
- ⁵⁶ Gaspar, A., Reis, J., Matos, M. J., Uriarte, E., Borges, F., *Eur J Med Chem* (2012), **54**: 914 – 918
- ⁵⁷ Araki, T., Furukawa, T., Patent JP 2006069906 (A), 2006
- ⁵⁸ Davidson, D. N., Kaye, P.T., *J Chem Soc, Perkin Trans 2* (1991): 927 – 930
- ⁵⁹ Reis, J., Gaspar, A., Borges, F., Gomes, L. R., Low, J. N., *Acta Cryst* (2013), **C69**: 1527 – 1533
- ⁶⁰ Gomes, L. R., Low, J. N., Cagide, F., Gaspar, A., Reis, J., Borges, F., *Acta Cryst* (2013), **B69**: 294 – 309
- ⁶¹ Evans, P.N., *J Prakt Chem* (1893), **48**: 489
- ⁶² Wasserscheid, P., Keim, W., *Angew Chem* (2000), **39**: 3772 – 3789
- ⁶³ Larina, N. A., Lokshin, V., Berthet, J., Delbaere, S., Vermeersch, G., Khodorovsky, V., *Tetrahedron* (2010), **66**: 8291 – 8299
- ⁶⁴ Teixido, J., Borrell, J. I., Colominas, C., Deupi, X., Matallana, J. L., Falco, J. L., Martinez-Teipel, B., *J Org Chem* (2001), **66**: 192 – 199
- ⁶⁵ Joseph, J. K., Jain, S. L., Singhal, S., Sain, B., *Ind Eng Chem Res* (2011), **50**: 11463 – 11466
- ⁶⁶ Arioli, F., Borrelli, S., Colombo, F., Falchi, F., Filippi, I., Crespan, E., Naldini, A., Scalia, G., Silvani, A., Maga, G., Carraro, F., Botta, M., Passarella, D., *ChemMedChem* (2011), **6**: 2009 – 2018
- ⁶⁷ Chauhan, S. M. S., Junjappa, H., *Tetrahedron* (1976), **32**: 1911 – 1916
- ⁶⁸ Glotova, T. E., Dvorko, M. Y., Albanov, A. I., Protsuk, N. I., *Russ J Org Chem* (2007), **43** (1): 121 – 125
- ⁶⁹ Chen, H., Bai, J., Jiao, L., Guo, Z., Yin, Q., Li, X., *Bioorg Med Chem* (2009), **17** (11): 3980 – 3986
- ⁷⁰ Kreutzberger, A., Schimmelpfennig, H., *Arch Pharm* (1981), **314** (5): 391 – 394

Bibliography

- 71 Tjoeng, F.-S., Kraas, E., Stark, E., Breitmaier, E., Jung, G., *Chem Ber* (1975), **108** (3): 862 – 874
- 72 Wiley Subscription Services, Inc. (CAS Registry Number: 38675-31-9), American Chemical Society 2015
- 73 Wu, H., Chen, X., Wan, Y., Ye, L., Xin, H., Xu, H., Pang, L., Ma, R., Yue, C., *J Chem Res* (2008), **12**: 711-714
- 74 Katritzky, A.R., Agha, B.J., Awartani, R., Patel, R.C., *J Chem Soc, Perkin Trans. 1* (1983): 2617-2621
- 75 Roeterdink, F., van der Plas, H. C., *J Chem Soc, Perkin Trans 1* (1976), **11**: 1202 - 1204
- 76 Morrison, J. F., Walsh, C.T., *Adv Enzymol Relat Areas Mol Biol* (1988), **61**: 201- 301
- 77 Copeland, R. A., *Evaluation of Enzyme Inhibitors in Drug Discovery* (2005), John Wiley and Sons, ISBN: 0-471-68696-4
- 78 Topf, C., *SOP M-A4-001* (SFB 630 Protocol), University of Würzburg
- 79 Lakowicz, J. R., *Principles of Fluorescence Spectroscopy* (2006), 3. ed., Springer US, ISBN 978-0-387-46312-4
- 80 Kubista, M., Sjöback, R., Eriksson, S., Albinsson, B., *Analyst* (1994), **119**: 417 – 419
- 81 Wu, H., Chen, X., Wan, Y., Ye, L., Xin, H., Xu, H., Pang, L., Ma, R., Yue, C., *J Chem Res* (2008), **12**: 711-714
- 82 El Kimary, M. A., El-Gezawy, H.S., El-Baradie, H.Y., Issa, R.M., *Spectrochim Acta*, (2002), **58A** (3): 493-500
- 83 McFadden, J. M., Frehywot, G. L., Townsend, C. A., *Org Lett* (2002), **4**: 3859 – 3862
- 84 <http://www.mycpermcheck.aksotriffer.pharmazie.uni-wuerzburg.de/> Stand: 1.5.2015
- 85 Merget, B., Zilian, D., Müller, T., Sotriffer, C. A., *Bioinformatics* (2013), **29** (1): 62 - 68
- 86 Christoff, M., Okano, L. T., Bohne, C., *J of Photochemistry and Photobiology A: Chemistry* (2000), **134**: 169 – 176
- 87 Merck, Patent DE102004016250 (A1), 2005
- 88 Wang, Y., Qiao, X., Li, W., Zhou, Y., Jiao, Y., Yang, C., Dong, C., Inoue, Y., Shuang, S., *Anal Chim Acta* (2009), **650**: 124 - 130
- 89 Anderson, B. D., *Bulletin Technique Gattefosse* (2013), **106**: 10 – 27
- 90 Loftsson, T., Brewster, M. E., *J Pharm Sci* (1996), **85** (10): 1017 – 1025
- 91 Davis, M. E., Brewster, M. E., *Nature Reviews Drug Discovery* (2004), **3**: 1023 - 1035

Bibliography

- ⁹² Lopez-Nicolas, J. M., Bru, R., Garcia-Carmona, F., *Biochim Biophys Acta* (1997), **1347**: 140 – 150
- ⁹³ Cattaneo, M. V., Luong, J. H. T., *Anal Biochem* (1994), **223**: 313 – 320
- ⁹⁴ Higuchi, T. Connors, A. K., Phase-solubility techniques. In Reill, C. N. (ed.), *Adv Anal Chem Instr*, Wiley, New York (1965): 117 - 212
- ⁹⁵ Negi, J. S., Singh, S., *Carbohydr Polym* (2013), **92**: 1835 – 1843
- ⁹⁶ Steed, Jonathan W.; Atwood, Jerry L., *Supramolecular chemistry* (2009), 2. ed., Chichester, Wiley, ISBN: 978-0-470-51234-0
- ⁹⁷ Tronche, P.A., US 3816470 (A), 1974
- ⁹⁸ Hosseinimehr, S. J., Shafiee, A., Mozdarani, H., Akhlagpour, S., Froughizadeh, M., *J Radiat Res* (2002), **43** (3): 293-300
- ⁹⁹ Bevan, P. S., Ellis, G. P., Wilson, H. K., *J Chem Soc, Perkin Trans I* (1981), **9**: 2552 – 2556
- ¹⁰⁰ Cagide, F., Reis, J., Gaspar, A., Borges, F., *Tetrahedron lett* (2011), **52** (48): 6446 - 6449
- ¹⁰¹ Kumar, K. A., Srimannarayana, G., *Ind J Chem, Sect B* (1981), **20B** (7): 604 – 606
- ¹⁰² Josey, B. J., Inks, E. S., Wen, X., Chou, C. J., *J Med Chem* (2013), **56**: 1007 – 1022
- ¹⁰³ Gupton, J. T., Krumpe, K. E., Burnham, B. S., Dwornik, K. A., Petrich, S. A., Du, K. X., Bruce, M. A., Vu, P., Vargas, M., Keertikar, K. M., Hosein, K. N., Jones, C. R., Sikorski, J. A., *Tetrahedron* (1998), **54**: 5075 – 5088
- ¹⁰⁴ BASF, Patent GB 800006 (A), 1958
- ¹⁰⁵ Bennett, G. B., Mason, R. B., Alden, L. J., Roach, J. B., *J Med Chem* (1978), **21** (7): 623 – 628
- ¹⁰⁶ Goswami, S., Jana, S., Dey, S., Adak, A. K., *Aust J Chem* (2007), **60** (2): 120 – 123
- ¹⁰⁷ Clark, J. H., English, J. P., Winnek, P. S., Marson, H. W., Cole, Q. P., Clapp, J. W., *J Am Chem Soc* (1946), **68**: 96 – 99
- ¹⁰⁸ Miller, A., *J Org Chem* (1984), **49**: 4072 – 4074
- ¹⁰⁹ Lythgoe, B., Rayner, L.S., *J Chem Soc* (1951), 2323 – 2329
- ¹¹⁰ Abbott GmbH, Patent DE 10311065 (A1), 2004
- ¹¹¹ Heravi, M. M., Ranjbar, L., Derikvand, F., Alimadadi, B., *Mol Divers* (2008), **12**: 191 - 196
- ¹¹² Roblin, R. O., Clapp, J. W., *J Am Chem Soc* (1950), **72**: 4890 – 4892
- ¹¹³ Sheldrick, G., *Acta Cryst* (2008), **A64**, 112 – 122
- ¹¹⁴ The Cambridge Crystallographic Data Centre: www.ccdc.cam.ac.uk/data_request/cif

Bibliography

- ¹¹⁵ Muth, M., Synthese und Charakterisierung allosterer Modulatoren muscarinischer M2-Rezeptoren: Strukturvariationen der Bis(ammonium)alkan-Verbindung W84 (*Dissertation thesis*, 2004), University of Würzburg
- ¹¹⁶ Hansch, C., Leo, A., D. H. Hoekman, *Exploring QSAR.: Hydrophobic, electronic and steric constants* (1995), 4. ed., American Chemical Society, Washington DC, ISBN 08412-2993-7
- ¹¹⁷ SFB 630 SOPs:
http://www.sfb630.uni-wuerzburg.de/quality_management/qm_documents/
Stand: 13.08.2015
- ¹¹⁸ Halgren, T. A., *J Comput Chem* (1996), **17**: 490 – 519
- ¹¹⁹ Verdonk, M. L., Cole, J. C., Hartshorn, M. J., Murray, C. W., Taylor, R. D., *PROTEINS: Structure, Function, and Genetics* (2003), **52**: 609 – 623
- ¹²⁰ Jones, G., Willett, P., Glen, R. C., Leach, A. R., Taylor, R., *J Mol Biol* (1997), **267**: 727 – 748
- ¹²¹ Sotriffer, C. A., Sanschagrin, P., Matter, H., Klebe, G., *PROTEINS: Structure, Function, Bioinformatics* (2008), **73**: 395 – 419
- ¹²² Irwin, J. J., Shoichet, B. K., *J Chem Inf Comp Sci* (2004), **45**: 177 – 182
- ¹²³ Davidson, D. N., English, R. B., Kaye, P. T., *J Chem Soc, Perkin Trans 2* (1991): 1181 – 1185
- ¹²⁴ Les, A., Adamowicz, L., *J Phys Chem* (1990), **94**: 7021 – 7032
- ¹²⁵ Galvao, T. L. P., Rocha, I. M., Ribeiro da Silva, M. D. M. C., Ribeiro da Silva, M. A. V., *J Phys Chem* (2013), **117**: 12668 – 12674
- ¹²⁶ Lipinski, C. A., Lombardo, F., Dominy, B. W., Feeney, P. J., *Adv Drug Deliv Rev* (2001), **46** (1-3): 3 – 26.
- ¹²⁷ Tihanyi, K., Vastag, M., *Solubility, Delivery and ADME Problems of Drugs and Drug-Candidates* (2011), Bentham Science Publishers, ISBN: 978-1-60805-120-5
- ¹²⁸ European Pharmacopoeia 8th Edition (2015), EDQM Council of Europe, Strasbourg
- ¹²⁹ QikProp, Version 3.4, Schrodinger (2011), LLC, New York
- ¹³⁰ Markees, D. G., *J Heterocycl Chem* (1989), **26** (1): 29 – 32
- ¹³¹ Huke, J. P., Hillier, I. H., Infield, R. M., *J Chem Soc, Perkin Trans 2* (1984): 2119 – 2120
- ¹³² Glaser, J., Holzgrabe, U., *MedChemComm* (2015), **00**: 1 – 3
- ¹³³ Holder, S., Zemsanova, M., Zhang, C., Tabrizizad, M., Bremer, R., Neidigh, J. W., Lilly, M. B., *Mol Cancer Ther* (2007), **6** (1):163 – 172

Bibliography

- ¹³⁴ Iyer, K. S., Klee, W.A., *J Biol Chem* (1973), **248** (2):707 – 710
- ¹³⁵ McGovern, S. L., Caselli, E., Grigorieff, N., Shoichet, B. K., *J Med Chem* (2002), **45**:
1712 – 1722